ARCHIVES OF ACOUSTICS
18, 2, 179–181 (1993)

PROCEEDINGS OF THE CONFERENCE ON NOISE SUPPRESSION NOISE CONTROL 92

Foreword

The IX International Conference on Noise Suppression — NOISE CONTROL 92 was held from the 22-nd to the 24-th September 1992 in Cracow. The conference was organized by the Committee on Acoustics of the Polish Academy of Sciences, Polish Acoustical Society and Institute of Mechanics and Vibroacoustics of the Academy of Mining and Metallurgy, in cooperation with the Central Institute of Work Protection (Warsaw) and Repair Plant of Metallurgy (Cracow). The NOISE CONTROL 92 conference was organized under the auspices of the Ministry of Natural Resources and Forestry, and was devoted to the theme "Science and technology for silence".

The NOISE CONTROL 92 conference was organized in parallel with the XXXIX Open Seminar on Acoustics.

Both conferences were attended by 180 participants coming from 12 countries, namely from Australia, Belgium, Czechoslovakia, Denmark, France, Germany, Holland, Italy, Poland, Serbia, Switzerland, Ukraina.

On the second day of the conference, especially solemn was the session devoted to Prof. Ignacy MALECKI and Dr Per BRÜEL, the scientists of high international renown. The senior of Polish acousticians, doctor h.c. of the Academy of Mining and Metallurgy in Cracow as well as the chairman of the Scientific Committee of the NOISE CONTROL 92 Conference — Prof. Ignacy MALECKI celebrated the 80-th anniversary of his birth. The president of the Committee on Acoustics of the Polish Academy of Sciences — Prof. Leszek FILIPCZYŃSKI presented a lecture devoted the scientific activity to Prof. Ignacy MALECKI. On the occasion of the 50-th anniversary of existence of the Brüel-Kjaer Company producer of acoustical equipment, the president of the Polish Acoustical Society, Prof. Antoni ŚLIWIŃSKI, handed over the diploma of honorary membership of the Polish Acoustical Society to Dr. Per BRÜEL. Dr. Per BRÜEL presented during the session a lecture on *A new way for looking on indust hearing loss.*

The following plenary papers were presented:

1. Z. ENGEL, A. RAKOWSKI, *Prof. Stefan Czarnecki reminescence on the occasion of the 10-th anniversary of his death.*

2. I. BALLO, *Electro-pneumatic active vibration control system for driver's seat on earth moving vehicles.*

3. A. COPS, W. LAURIKS, *Characterization of sound absorbing metarials used in noise control engineering.*

4. W. MAJEWSKI, *Automatic recognition of isolated words-modern tendency.*

5. A. RAKOWSKI, *Investigations of sensorial memory of tone pitch a local method.*

6. J. SADOWSKI, B. SZUDROWICZ, J. ŻUCHOWSKA-WODNIKOWSKA, *The acoustical research in quality system of the object and building products.*

In the framework of the NOISE CONTROL 92 Conference, 18 sessions were held and 69 papers were presented, whereas during the Open Seminar on Acoustics 9 sessions were held and 59 papers were presented.

A round-table meeting was also organized the chairman of which was Prof. A. ŚLIWIŃSKI. The meeting was devoted to the role of education in noise control. A lecture initiating the discussion was presented by Prof. Z. ENGEL.

In the framework of the NOISE CONTROL 92 conference, the following sessions were organized:

1. Physical foundations,
2. Energy methods (3 sessions),
3. Measurements, diagnostics (3 sessions),
4. Machine and equipment noise (3 sessions),
5. Noise in building objects,
6. Noise and vibrations in the environment (3 sessions),
7. Effects of noise and vibrations (2 sessions).

Presentation of the state of emergency in Poland caused by noise and vibrations was not the purpose of the NOISE CONTROL 92 conference. This problem is well known from the report prepared by the Acoustical Committee in 1984 and from another report prepared by a group of specialists headed by Prof. J. SADOWSKI. In 1989, another conference on noise control was held aimed at demonstrating the possibility of reduction of the existing hazards. During this conference, the problem of bringing Poland into line with the EEC requirements was also considered.

NOISE CONTROL 92 conference has shown that there exist in Poland certain possibilities of developing extensive scientific and technological research in order to improve the acoustical environment. To this end, it is necessary to bring Polish standards and regulations into line with the international requirements, to introduce obligatory vibroacoustical certificates of machines and devices, and to support such actions financially. The last condition is of a particular importance. It should be stressed that most of the papers presented gave rise to animated discussions. The cooperation has been improved between the lawyers employed by the Polish Academy of Sciences, universities, industrial institutes, business and governmental administration (especially, by the Departments of Environment Protection of the District Offices), the cooperation being concerned with the very important and not always duly appreciated problem of noise abatement.

The subjects of the presented papers and discussions make it possible to determine the following future trends of development of scientific and technological research:

1. Development of energy methods in acoustical investigations, mainly the intensity methods.

2. Application of active methods to noise suppression and sound control.

3. Investigation of material sounds.

4. Preparation of vibroacoustic certificates of machines and devices in Polish laboratories.

5. Adaptation of Polish standards and regulations to the requirements of the European community.

6. Developing wide international cooperation.

As it was mentioned, the round-table meeting was devoted to the role of vibroacoustic education. The following conclusions can be drawn from the discussion:

1. The role of a suitable, wide public education concerning the control of noise and vibration is of great importance.

2. In Poland, the number of specialists with satisfactory education in the field of protection of the environment against noise and vibrations would be sufficient if the emigration during the last decade did not take place.

3. In spite of numerous efforts, the model of education of specialists in acoustics has not been prepared as yet; up to now, acoustics is being taught as a part of physics, mechanics, electronics etc., at different faculties of the universities.

4. The level of postgraduate studies organized in numerous schools is sufficient.

5. Several instruction courses on different levels are being organized. The number and quality of these courses are not satisfactory.

6. Some problems of protection of environment, against noise and vibrations, should be included in the public education programs.

7. The participants of the round-table meeting asked Prof. A. Śliwiński to organize a special conference devoted to the problems of acoustic education similar to the conference held in 1987.

In the framework of the NOISE CONTROL 92 conference, an exhibition was organized of measurements and materials used in the noise vibration abatement technology. It is a pity that only 10 producers participated in the exhibition.

Z. Engel

ARCHIVES OF ACOUSTICS
18, 2, 183–195 (1993)

ACTIVE VIBRATION CONTROL SYSTEMS FOR DRIVER'S SEAT OF EARTH-MOVING VEHICLES

I. BALLO

Institute of Materials and Machine Mechanics
Slovak Academy of Sciences
CS–836 06 Bratislawa Račianska str. 75. Słovakia

In the article a survey of the activity of the Institute of Materials and Machine Mechanics of the Slovak Academy of Sciences in the field of research of active vibration control systems (AVIS) is given. The contribution starts with some remarks on the vibration control properties of common passive systems. In the next part the possibilities of combination of passive and active vibration control systems (VCS) are discussed. The next topic are the results of theoretical and experimental research of electro-hydraulic and electro-pneumatic acitve VCS for driver seats in earth-moving machines. The last part of the paper deals with the problem of power consumption of the AVIS.

1. Introduction

The problem of driver's insulation from excessive mechanical vibration is an ever actual research topic. The improvement of driver's insulation from excessive vibration means not only decrease of health risk to the driver and improvement of his work comfort, but often also marked improvement in the full utilisation of the working capacity of the machine. This problem is even pronounced in earth moving machines, which operate in rough terrain. Here the main vibration control elements are the tyres and the driver's seat.

In contemporary driver's seats the most common vibration control system is a passive one, which does not need any external source of energy for his proper operation. In most systems an air spring is used as the main resilient element. The use of this structural element enables to reach rather low natural frequencies of the vibration control system. In addition, by the control of the average static pressure in the air spring, a suitable static middle position of the isolated load can be maintained, regardless of the changes in its weight. Because only the average static pressure has been changed and not the instantaneous one, such systems are often referred to as "semi-active" ones. Despite the fact that these systems require supply of compressed air, they are treated as passive ones.

2. Some limits of passive vibration control systems

For the mathematical description of the vibration control system of the driver seat (in the first approximation), a linear damped mechanical oscillator of one degree of freedom is used. The vibration control effect of passive systems is improving in line with the decrease of the system's natural frequency. In contemporary systems extremely low natural frequencies of the order of 1 Hz and below have been reached. Further decrease of the system's natural frequency brings about many technical difficulties and hence further improvement in this direction is not sought for.

Also the strive for decrease of the system's natural frequency does not bring always any marked improvement in the overall vibration control properties as the simplified basic theory would indicate. This theory is based on the assumption of stationarity of the excitation, i.e. it assumes stationary vibration of the earth-moving machine's cabin floor in the vertical direction. Any "bumps" in the excitation, i.e. transient phenomena are not covered by this theory.

The effect of a transient in the excitation is illustrated in a typical example, with results depicted in graphical form in the Fig. 1.

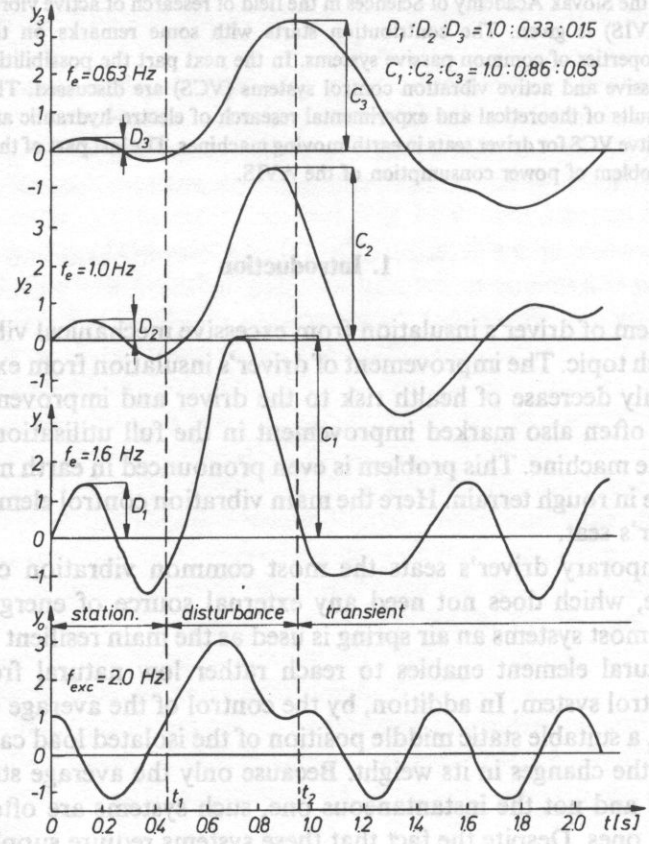

Fig. 1

In the lower part of the picture a harmonic excitation function is depicted, to which in the time interval t_1 to t_2 a disturbance is superimposed. In the upper part of the picture the reaction of three different passive vibration control systems is depicted, each of them having different natural frequency — f_e = 1.6; 1.0; 0.63 Hz in turn. The steady-state amplitudes ratio is 1; 0.33 : 0.15 in turn, but the maximal amplitudes of the transient are in the ratio of 1:0.86:0.63. From the simple example it is clearly seen that, by the decrease of the system's natural frequency from 1.6 Hz to 0.63 Hz, a 6.7-fold decrease in steady state response amplitude was reached. But the improvement in the amplitude of the transient response was only 1.6-fold.

Different reaction of the linear passive vibration control system to stationary and nonstationary excitation, as was illustrated in the picture of the previous example is also generally valid for narrow-band random excitation signals. This conclusion has an important implication for the assesment of vibration control properties of driver seats for earth-moving machines, agricultural tractors, etc. i.e. in general for any off-road vehicle operating in rough terrain. Under such conditions the non-stationary vibration of the vehicle and hence also of the cabin floor is the prevailing form of excitation. The protection of the seated driver from adverse effects of intense vibration is far less effective, as the basic theory and "perhaps" the international standards would predict.

3. Active vibration control systems

An active vibration control system is in principle a specific sort of servo-system. It uses an external source of energy. Various sources of external energy could be used. In this paper only fluids systems will be discussed, i.e. those employing the energy of compressed oil or air.

Active vibration control systems discussed in this paper consist essentially of three distinct parts:

a) Sensor or sensors of vibration. These measure the characteristic vibration time variable, which has to be controlled. In the case of driver's seat for earth-moving machines it is the cabin floor vertical vibration acceleration.

b) Electronic controller, in which appropriate control signal for the actuator is generated from the signal supplied by the sensor.

c) Actuator, which could have different fashion, depending on the energy source. In this paper two distinct actuators will be discussed.

1. An electro-hydraulic servo-cylinder, in which the input electrical signal governs the in-or outflow of hydraulic oil.

2. An air spring, in which the inflow and outflow of compressed air is controlled by governing signal.

From the point of view of control theory, the actuator can be situated in series or in parallel to the spring-damper combination of the seat suspension (Fig. 2a, b).

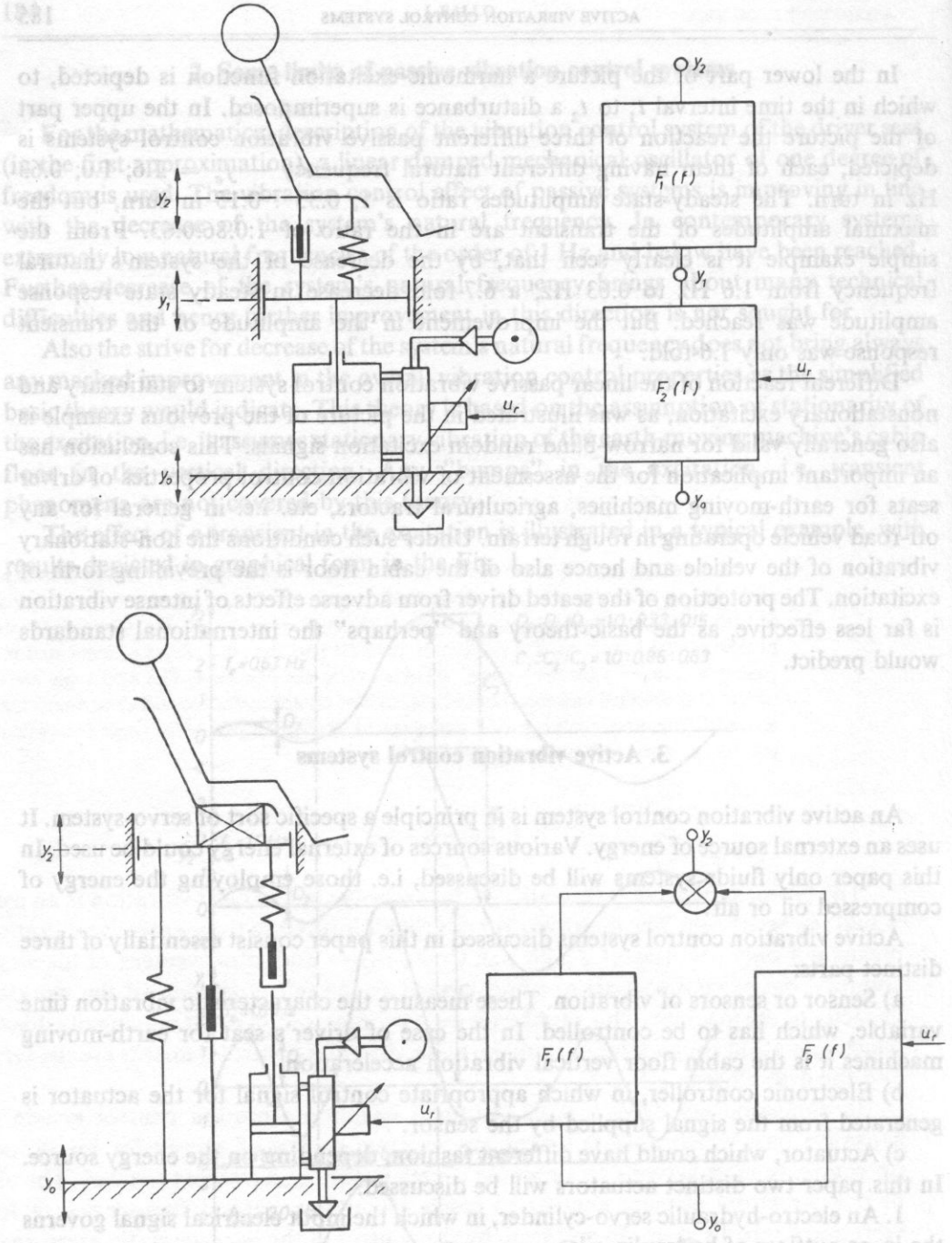

Fig. 2

The dynamic properties of the seat can be described by the transfer function $F1\,(f)$, that one of the series of active vibration control system AVIS by the transfer function $F2\,(f)$. According to the Fig. 2a the frequency response of the passive seat suspension $F1\,(f)$ can be improved by the series connection of the AVIS to the overall frequency response $F1'$:

$$\text{passive} : F1,$$
$$\text{passive} + \text{active} : F1' = F1 \cdot F2.$$

As it will be shown further, this series combination of active and passive suspension can exhibit far better vibration isolation properties than the passive suspension only.

In case of a parallel AVIS, the effect of the passive part $F1\,(f)$ is combined with the active part $F3\,(f)$ to form the resultant transfer function $F1''\,(f)$:

$$\text{passive} : F1,$$
$$\text{passive} + \text{active} : F1'' = F1 - F3.$$

This simplified approach would suggest that, under circumstances, the combined transfer function $F1''$ would tend to zero. However, it could be difficult to achieve this in practice.

As follows from the previous description, active vibration control systems are rather complicated devices in comparison to common passive ones. They need an external source of energy. The extent of energy consumption could be a sort of a burden. On the other hand, active vibration control systems have a markedly improved vibration control effect in comparison to contemporary passive ones.

4. Electro-hydraulic active vibration control system

The active vibration control system of electro-hydraulic type, which was investigated in our research laboratory, is of a series structure, Fig. 3. It consists of cylinder mounted on vehicle chassis *1*. The piston rod supports platform *3*, which can move in vertical direction only. A standard driver's seat *5* with the passive spring-damper vibration control system *4* is mounted on platform *3*. The oil flow in cylinder *2* is controlled by the servovalve or proportional flow valve *12*, which in turn is operated by the control voltage u_r (after necessary amplification in a power amplifier *11*). The control voltage u_r is generated in the electronic controller *10*. The AVIS is equipped with necessary sensors and preamplifiers, i.e. accelerometer *6* for the measurement of the chassis absolute acceleration. Also the relative displacement has to be measured by the displacement transducer *7* to maintain the static position. In our considerations it is supposed that all measuring chains are in the required frequency range linear and frequency-independent.

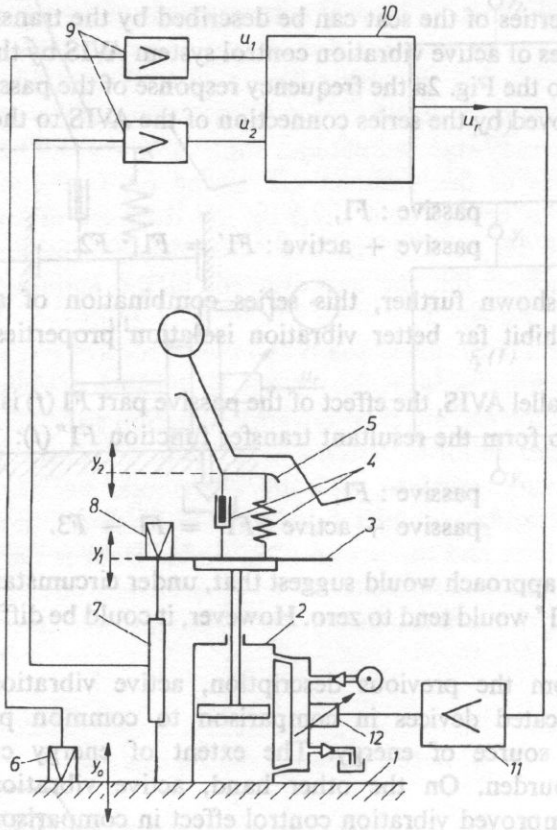

Fig. 3

In the last few years our research group undertook an extensive theoretical and experimental research of such active vibration control system.

Most interesting are the experimental results achieved with common driver seats. The seats tested together with the active system were:

1. German made driver seat of the type ZT 300, used in agricultural tractors. In this seat a torsion rod is used as the resilient element.

2. Czechoslovak made seat of type KAROSA 281.0 with an air spring and mechanico-pneumatic system for middle position control. This is a standard seat used in Czechoslovak made trucks, buses and earth moving vehicles.

For the evaluation of the vibration control properties of these systems following criteria were used:

a) Frequency response characteristics;

b) Power spectral density curves of the vertical acceleration on the seat base cabin floor and the seat cushion;

c) Assessment according to the ISO Standard 7096-82, which is a standard method for evaluation of vibration control properties of driver's seat for earth-moving machines.

d) Assessment according to the ISO Standard 2631/1-85, which describes the assessment of the vibration influence on the seated driver and states the allowed vibration level limits.

The frequency response

The amplitude-frequency response function of the seat ZT 300 alone and with the AVIS is depicted in Fig. 4. We can see, that the seat's resonant frequency is in vicinity of 1.3 Hz and the seat amplifies the vibrations in the frequency band 0.5 Hz – 2.2 Hz.

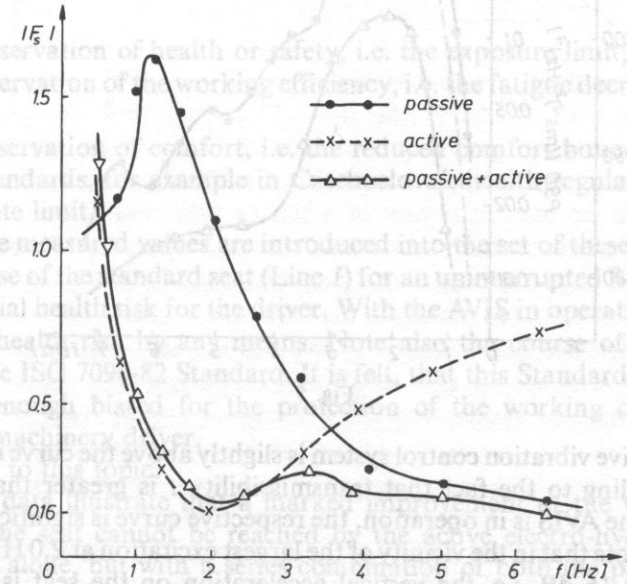

Fig. 4

On the contrary, the series combination of this seat and the AVIS suppresses the vibrations in this frequency band very well and the performance approaches the one of the passive system above 3.5 Hz. This is due to poor dynamic behaviour of the hydraulic cylinder employed. Anyhow, it practically proves that "slow" hydraulic servosystems are well suited for this task. On the other hand, there is a sharp increase below 0.5 Hz, due to chosen cut-off frequency of the electronic controller of 0.15 Hz. Note that the frequency response function of the AVIS alone has a *U*-form, in good agreement with the theoretical analysis and the simulation results.

The acceleration PSD

The acceleration PSD in the frequency range 0.5 – 20 Hz for the excitation according to the 3-rd machine class of the ISO standard 7096 was measured. Typical curves are depicted in Fig. 5. Note, that the course of the vertical acceleration PSD curve on the

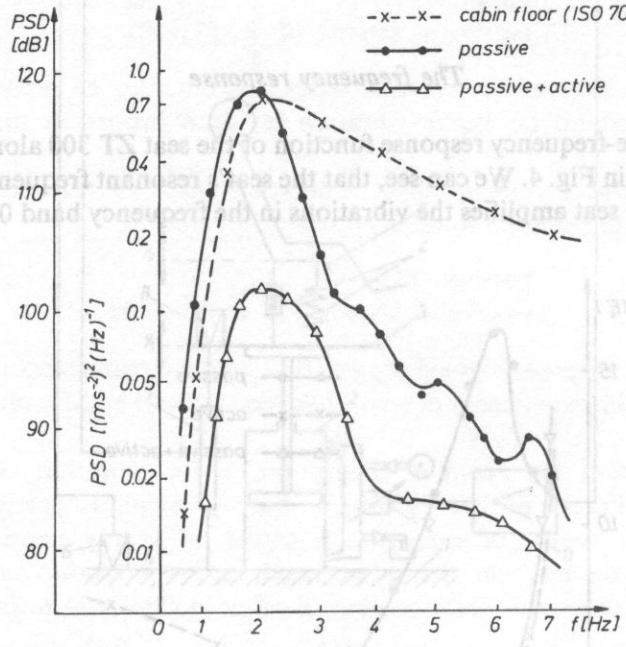

Fig. 5

seat with the passive vibration control system is slightly above the curve of the excitation PSD, corresponding to the fact that transmissibility t is greater than one. On the contrary, when the AVIS is in operation, the respective curve is significantly below the former curves. Note that in the vicinity of the largest excitation at 2.0 Hz, the difference is approximately 16 dB, i.e. the vertical acceleration on the seat is approximately 2.8-times lower than in the case of the passive vibration control system only.

Results according to the ISO 7096-82 Standard

Both seats passed the limits set down by the ISO 7096-82 Standard, even when the active part was turned off.

The permissible vibration exposure

The ISO 2631/1-85 Standard distinguishes three main criteria for the vibration influence on the human being (Fig. 6).

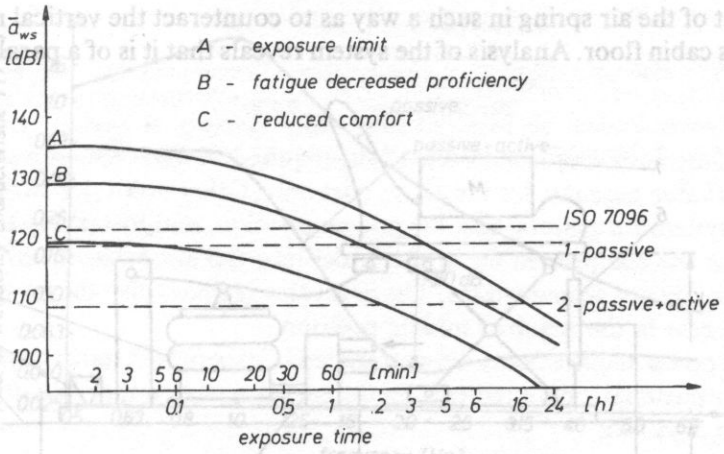

Fig. 6

A) The preservation of health or safety, i.e. the exposure limit;

B) The preservation of the working efficiency, i.e. the fatigue decreased proficiency boundary;

C) The preservation of comfort, i.e. the reduced comfort boundary.

In some standards, for example in Czechoslovak health regulations, the middle curve is absolute limit.

In Fig. 6 the measured values are introduced into the set of these curves. It can be seen, that the use of the standard seat (Line *1*) for an uninterrupted 8-hour-shift brings about a potencial health risk for the driver. With the AVIS in operation (Line *2*) there should be no health risk by any means. Note also the course of the straight line representing the ISO 7096-82 Standard. It is felt, that this Standard is a compromise criterion not enough biased for the protection of the working conditions of the earth-moving machinery driver.

Conclusion to this topic:

The above data illustrate that a marked improvement of the vibration control properties of the seat cannot be reached by the active electro-hydraulic vibration control system alone, but with a series combination of both the passive and active parts. This brings about some disadvantages, the most important being a rather complicated construction (in a real earth-moving machine there is not enough free space to build in the hydraulic cylinder in appropriate position) and also a rather large energy consumption (see later). Therefore this kind of active vibration control system for driver's seat has not found practical use till now.

5. Electro-pneumatic active vibration control system

Some disadvantages of the electro-hydraulic active vibration control system should be suppressed by the pneumatic active vibration control system. Essentially it is working on the principle of proper control of inflow and outflow of compressed air

into and out of the air spring in such a way as to counteract the vertical movement of the vehicle's cabin floor. Analysis of the system reveals that it is of a parallel structure.

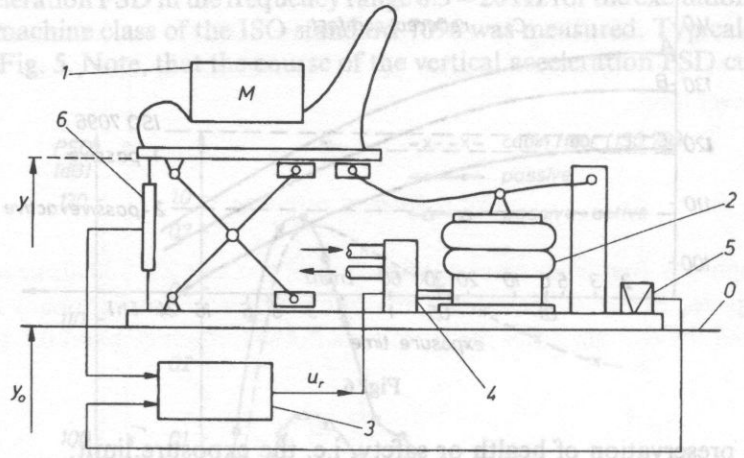

Fig. 7

The electro-pneumatic AVIS consists (Fig. 7) of an air spring *2*, acting through a lever mechanism on the upper part of a scissor type mechanism. It supports the upper part with the seat cushion and with the seated operator of mass $M(1)$, whose vibrations in the vertical direction are to be controlled. The whole system is mounted on the base *0*, which is excited mainly in the vertical direction. The air spring *2* acts as the static load bearing element, passive spring and the active part actuator, all in one structural element. The in-flow and out-flow of the compressed air into and from the air spring into atmosphere is controlled by electro-pneumatic transducer *4*, which in turn is governed by the voltage u_r, generated by the electronic controller *3*. The electro-pneumatic transducer *4* is a proportional type device with sufficiently wide frequency band which, by electrically controled changes in the orifice aperture, governs the flow of compressed air into and out of the air spring. The air spring acts as a force generator and moves through the lever mechanism the upper part with the seated operator in such a way as to conteract the vertical vibrations acting on the base *0*. The system is equipped with relative displacement sensor *6* and the accelerometer *5*.

This system was not studied in such an extent as the electro-hydraulic one. A lot of effort was spent in controller synthesis. It seems, that this crucial part of the system has to be of a rather complex structure to facilitate good vibration control properties of the active part in a suffciently broad frequency band. By theoretical analysis and measurement on a dummy system the transfer function was determined. In Fig. 8 both the whole system frequency response curve and that one of the passive part of the dummy system, obtained when the active sub-system was switched off, are depicted. The difference ilustrates improvement of the vibration control properties of the dummy seat exerted by the active part.

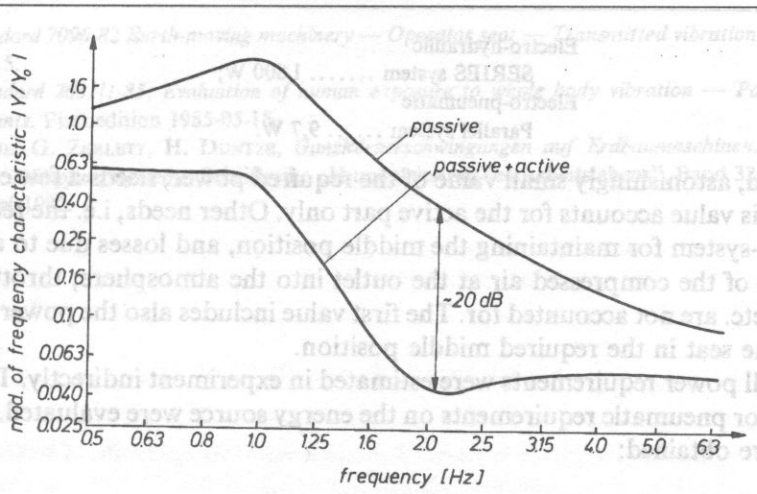

Fig. 8

It could be seen, that the theoretical improvement of the vibration control properties around the frequency of 2 Hz is nearly 20 dB. In realistic systems an improvement by 10–15 dB could be reached, depending on the excitation form and system tuning.

6. The energy consumption of the active vibration control systems

The energy consumption of the active vibration control systems plays very important role in their practical feasibility. For a linear active vibration control system subjected to a stationary random excitation, whose power spectral density is known, it is possible to estimate theoretically the average power necessary for the system's operation. The average power requirements are given by the formula:

$$\overline{P} = \int_0^\infty |H_{\Delta\dot{y}}|\,|H_f| \cos(\theta_{\Delta\dot{y}} - \theta_f)\, G_{y_0 y_0}\, d\omega\,,$$

where $|H_{\Delta\dot{y}}|$ — modulus of the frequency response function of the relative velocity of the seat cushion in respect to the seat base (cabin floor), $\theta_{\Delta\dot{y}}$ — phase angle of the above frequency response function, $|H_f|$ — modulus of the frequency response function of the force exerted by the active part only, θ_f — phase angle of the frequency response function of the force exerted by the active part, $G_{y_0 y_0}$ — power spectral density of the vertical displacement of the seat base (cabin floor), ω — frequency.

Inserting numerical values into this formula the theoretical value of the power requirements of the active part only could be estimated. When some realistic values pertinent to the systems used for experimental investigation are introduced, the following theoretical values of average power requirements could be obtained:

Electro-hydraulic
SERIES system ..... 1 800 W;
Electro-pneumatic
Parallel system ..... 9.7 W.

The second, astonishingly small value of the required power, needs a few explanatory words. This value accounts for the active part only. Other needs, i.e. the requirements of the sub-system for maintaining the middle position, and losses due to air friction, expansion of the compressed air at the outlet into the atmosphere, throttling in the actuator, etc. are not accounted for. The first value includes also the power needed for holding the seat in the required middle position.
The overall power requirements were estimated in experiment indirectly. The average hydraulic or pneumatic requirements on the energy source were evaluated. Following values were obtained:

Electro-hydraulic
Series system ..... 2400 W;
Electro-pneumatic
PARALLEL system
— for positional control .... 800 W;
— for the active part only .... 80 W.

It seems to be in relatively good agreement with the theoretical results.

7. Conclusion

In line with the successive introduction of automation means and microelectronic subsystems into the chassis of various types of vehicles, the perspectives of introduction of active vibration control means increases. These systems could markedly improve the vibration control properties of the driver's seats, and so improve the ride comfort of the driver, decrease driver's health risks and improve the utilisation of the machine.

References

[1] I. BALLO, *Active vibration control system with excitation signal compensation* (in Slovak). Proc. 2nd Conference on Theory of Machines and Mechanisms. Liberec 1976, pp. 148–156.
[2] M. GAJARSKY, *Some properties of an electro-pneumatic vibration control system* (in Slovak), Strojnicky Casopis, **35**, 1–2, 51–65 (1984).
[3] I. BALLO, *Parallel active vibration control system for operator's seat for earth-moving vehicles*, Proc. NOISE CONTROL'89 Conference, Cracow, Poland, Sept. 1988, vol. 1, pp. 31–39.
[4] G.J. STEIN, I. BALLO, *Active vibration control system for the driver's seat for off-road vehicles*, Vehicle System Dynamics, **20**, 1, pp. 57–78 (1991).
[5] G.J. STEIN, *Automated measurement and evaluation of vibration damping properties of driver's seat*, Proc. IMEKO 10th World Congress, Prague April 1985, vol. 9, pp. 102–109.

[6] *ISO Standard 7096-82 Earth-moving machinery — Operator seat — Transmitted vibration.* First edition 1982-02-15.

[7] *ISO Standard 2631/1-85, Evaluation of human exposure to whole body vibration — Part 1: General requirements.* First edition 1985-05-15.

[8] G. KÖHNE, G. ZERLETT, H. DUNTZE, *Ganzkörperschwingungen auf Erdbaumaschinen. Entwicklung geeigneter Dämpfungssysteme.* Schriftreihe „Humanisierung des Arbeitslebens", Band 32. VDI Verlag, Düsseldorf 1982.

ARCHIVES OF ACOUSTICS
18, 2, 197–207 (1993)

INFLUENCE OF REVERBERATION FIELD CONDITIONS ON SOUND POWER EVALUATION WITH THE AID OF INTENSITY METHOD

J. CIEŚLIK and R. PANUSZKA

Institute of Mechanics and Vibroacoustics Academy of Mining and Metallurgy
(30-059 Kraków, al. Mickiewicza 30)

The results of investigations presented in the article were aimed at explaining how the conditions of acoustic field described by the room absorption and reverberation time can influence the calculated sound power value determined by the sound intensity measurements. As the sound source the rigid piston in the large baffle was used. The measurements of sound intensity and sound pressure were done in the free field and diffuse field conditions. The total absorption of the room was changed.

1. Introduction

The development of the measuring technique and new tools in sound intensity measurements has enabled the elaboration of several methods for sound source localization, investigation of sound propagation paths and measurement of absorbing and insulating properties of materials. Most of the commonly used methods were based on sound pressure measurements due to ease of their application. The evaluation of acoustic parameters with the aid of sound pressure methods required the measurements to be done in conditions of free sound field or diffuse sound field. Only in these conditions the sound power could be calculated precisely. In comparison with sound intensity which was the vector value, the sound pressure gave less information about the sound energy transportation in acoustic fields. For practical application of sound intensity in investigations of sound radiation of machines, particularly important was the exactitude of sound evaluation. From the theorem that sound power can be calculated on the basis of sound intensity had no influence on the estimated value of sound power, but in practice this influence existed and was important. The disturbances of the acoustic field might be caused by waves reflected from the walls, or the acoustic field could be interfered by the waves coming from the external sound sources, e.g. the other machines working nearby. Many authors have tried to solve the problem of influence of the acoustic field conditions. The indices have been introduced, based on the difference of sound pressure level and sound

intensity level measured at the same point of the field [6, 8]. The work was the attempt to establish how the condition of acoustic field described by the room absorption and reverberation time could influence the calculated sound power value using the sound intensity. The results of comparison of sound pressure and sound intensity distribution in the field of plane piston source taken in different acoustic fields were also shown.

2. Application of sound intensity to acoustic parameter evaluation

The sound intensity methods could be used in examinations conducted in all kinds of media: gases, liquids and solids. The largest number of applications was performed in gaseous media, especially in the air. Among the main applications were estimation of sound power of the sound source, radiation efficiency, localization and sorting of sound sources in machines considering activity of their noise emission, investigations of sound propagation paths, measurement of sound absorption and specific acoustic impedance of materials and structures, and also examination of sound insulation properties, such as investigation of sound leakage in composed partitions and machine enclosures. In all the applications mentioned above the sound power was the quantity used for the acoustic parameter evaluation. Figure 1 presents the main applications of sound intensity to evaluate the acoustic parameters.

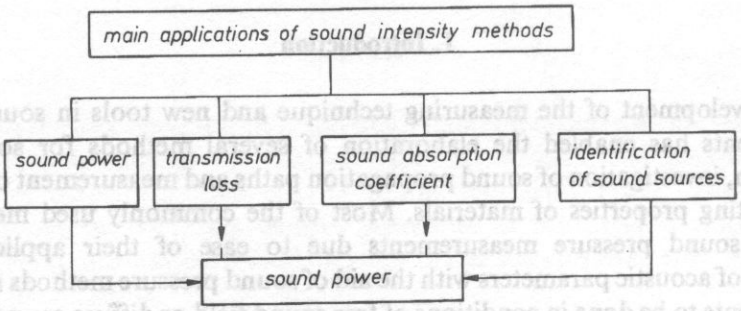

Fig. 1. Main applications of sound intensity in vibroacoustics

3. Sound power evaluation

Evaluation of sound power radiated from the sound source is based on the theorem that integral of the sound intensity normal component to the measuring surface surrounding the source is equal to the radiated sound power:

$$W = \oint_S I_n \, dS, \tag{1}$$

where S — surface surrounding the source, I_n — value of the sound intensity component normal to the surface S.

In practical cases the integral in Eq. (1) may be replaced by summation

$$W = \sum_{i=1}^{k} I_{ni} \cdot \Delta S_i, \tag{2}$$

where k — number of elementary fields into which the surface S has been divided, ΔS_i — elementary field. It has been assumed that I_{ni} was the mean value for the elementary surface ΔS_i.

Taking the same value for all elementary surfaces $\Delta S_i = \Delta S$ we obtain

$$W = \Delta S \sum_{i=1}^{k} I_{ni}. \tag{3}$$

The measurements are usually done for the array of fixed points or by sweeping method. For both methods the derived value of sound intensity is considered to be the average value for the appropriate surface element ΔS_i.

The Eq. (1) indicates that the net flow of acoustic energy integrated over the surface which does not contain sources or sinks is equal zero, even in an environment that contaminated by other sound sources. It implies that the sound power of the source inside the enclosing surface can be precisely determined. In practice, however, contaminating sources make the sound field quite reactive and cause large problems in estimating the sound power.

Statistical theory of pressure acoustic fields claimes that the reverberation fields exist in the regions of both the direct sound waves and waves reflected from the walls. The size of direct waves region for chosen sound source depended on the total room absorption. The direct waves field around the source is less reduced the lower the room absorption.

Sound power of a circular piston sound source calculated from the following formula:

$$W = \frac{1}{2} S_z \, v^2 \, Z, \tag{4}$$

where Z — acoustic radiation impedance, [kg m^{-2}s^{-1}], S_z — surface of the sound source, [m^2], v — vibration velocity of the piston surface, [ms^{-1}].

Acoustic radiation impedance of circular plane rigid piston was found from equation [1]:

$$Z = \rho c \left[1 - \frac{J_1(2ka)}{ka} + j \frac{H_1(2ka)}{ka} \right] \tag{5}$$

where ρ — density of the medium surrounding the piston source, i.e. air, [kg m^{-3}], J_1 (2ka) — Bessel function, H_1 (2ka) — Struve function, $k = \frac{2\Pi}{\lambda}$ — wave number, [m^{-1}],

a — dimension of piston, [m].

The real part of sound power was then evaluated from the equation

$$W = S_z v^2 \rho c \frac{k^2 a^2}{4} \left[1 - \frac{J_1(2ka)}{ka}\right]. \tag{6}$$

The results of calculation of sound power levels are shown in Fig. 5.

The sound power of a circular piston sound source was estimated by sound pressure measurements in a free field conditions and in a diffuse field. In the free field, in an anechoic chamber, the values of sound power levels in all examined frequencies were found from the formula

$$L_W = 10 \log \frac{p_m}{p_0} + 10 \log \frac{S}{S_0}, \tag{7}$$

where p_m — average value of sound pressure on the surface S_p, [Pa], p_0 — reference value of sound pressure, $p_0 = 2 \cdot 10^{-5}$, [Pa], S_p — area of measuring surface, [m²], $S_0 = 1$ m²,

$$p_m^2 = \frac{1}{n} \sum_{i=1}^{n} p_i^2 \tag{8}$$

where p_i — sound pressure value at point i.

In the diffuse field, in a reverberation room, the sound power value was the calculated from the formula

$$W = \frac{R}{4\rho c} p_m^2, \tag{9}$$

where $R = \frac{S_r \alpha_p}{1 - \alpha_p}$ room constant, [m²]; S_r — total area of inner room surfaces, [m²]; α_p — mean value of the sound absorption coefficient of room walls.

For very small values of $\alpha_p < 0.06$ it was possible to approximate (10) by the expression

$$R = S_r \alpha_p = A. \tag{11}$$

Then from (9) and (11) we obtained

$$L_W = 10 \log \frac{p_m}{p_0} + 10 \log \frac{A}{A_0} - 5 \tag{12}$$

where $A_0 = 2 \cdot 10^{-5}$ m².

Pressure methods for sound power evaluation in partially diffuse fields required to establish the kind of acoustic field in which the measurements were done. This establishing was based on several factors calculated from the reverberation time and total room absorption. They show the difference between the existing acoustic field and that under the free field conditions. Similar procedure was proposed for the sound

power evaluation using sound intensity measurementts in partially diffuse fields. Although the evaluation of sound power by sound intensity methods seemed to be straight — forward and simple, it had to be preceded by a complicated field control procedure to determine the appropriate parameters of the measurements. This field control was based on a number of field indicators proposed by HUBNER [5, 6]. All these procedures were given in two international standards, still in development [11, 12].

4. Description of experiment

As the sound source was used a rigid plane circular piston placed in large baffle. For that kind of sound source it was possible to calculate precisely the sound power from its theoretical model, as it was shown in Sec. 3.

The piston was forced to vibrate by the exciter with the same constant velocity of vibrations equal to 0.05 m/s for every investigated frequency in the range from 100 to 2000 Hz. A constant value of vibratio velocity was maintaned, owing to the application of a feedback with vibration control system of the vibration exciter. Investigations were conducted for harmonic signals of frequency. The piston was prepared to have a sufficient stiffness. It's wave number was equal to $ka = 1$ for the frequency of 775 Hz. To avoid the influence of noise produced by the exciter cooling ventilator, the exciter was placed in an enclosure separated from the baffle. Figure 2 presents the measuring system schema. For such chosen sound source the agreement

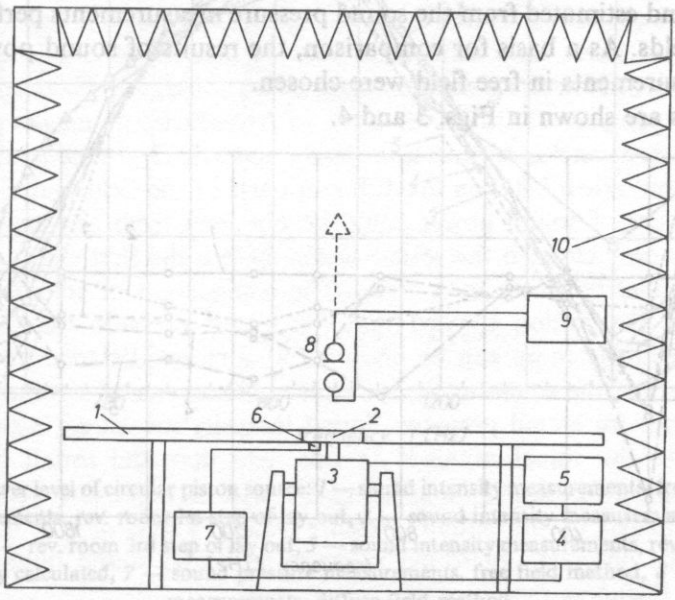

Fig. 2. Measuring system diagram: *1* — baffle, *2* — circular piston, *3* — vibration exciter, *4* — harmonic signal generator, *5* — power amplifier, *6* — accelerometer, *7* — charge amplifier, *8* — sound intensity probe, *9* — sound intensity analyzer, *10* — lay out with randomly distributed damping material.

between theoretically calculated sound power values and those evaluated from the measurements should be expected in the frequency range from 100 to 800 Hz. The investigations were also conducted for higher frequencies only to compare the results in different acoustic fields. The investigation took place in anechoic chamber and in the room with diffuse acoustic field. To obtain different acoustic conditions the total absorption of the room was changed. The changes of absorption were checked by the measurements of reverberation time in each case of layout with randomly distributed damping material. Three measuring surfaces were chosen in the form of parallelepiped. The dimension of the elementary surface ΔS for the first measuring surface were 0.1×0.1 m, and for the remaining measuring surfaces were 0.15×0.15 m. The area of the third surface was 2.72 times greater than the second one and 11.5 times than the first surface. The sound intensity component perpendicular to the measuring surface and sound pressure levels were measured.

5. Results and discussion

A. Comparison of the sound power values

The main aim of the presented investigations was the evaluation of how the acoustic field conditions influence the measured sound power of piston sound source. The results obtained allowed also to formulate the conclusions concerning the influence of the size and position of the measuring surface upon the evaluated sound power. Additionally, the sound power of the piston sound source was calculated theoretically and estimated from the sound pressure measurements performed in free and diffuse fields. As a basis for comparison, the results of sound power evaluated from the measurements in free field were chosen.

The results are shown in Figs. 3 and 4.

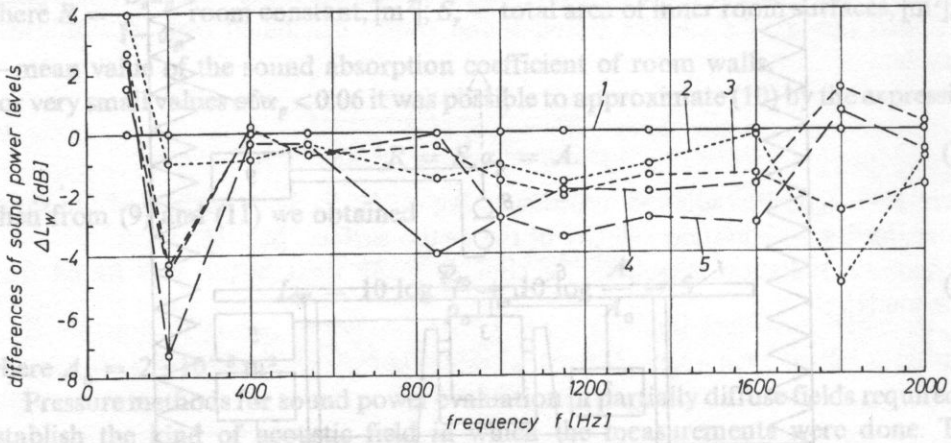

Fig. 3. Differences of sound power level values obtained from measuring surface no 1 in free field and obtained: *1* — in free field (anechoic chamber), *2* — reverberant room (1st step of lay out), *3* — reverberant room (2nd step of lay out), *4* — reverberant room (3rd step of lay out), *5* — reverberant room (with no lay out)

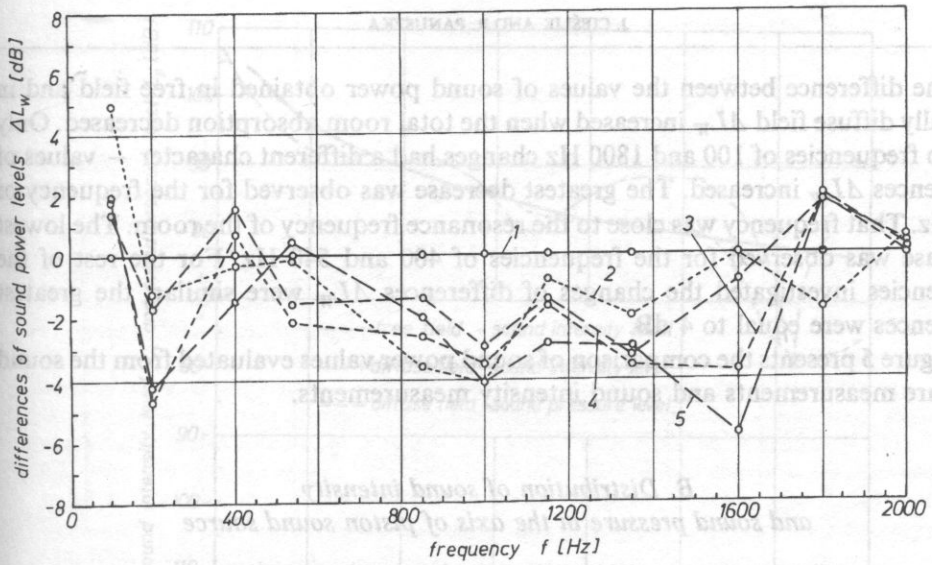

Fig. 4. Differences of sound power level values obtained from measuring surface no 2 in free field and obtained: *1* — in free field (anechoic chamber), *2* — reverberant room (1st step of lay out), *3* — reverberant room (2nd step of lay out), *4* — reverberant room (3rd step of lay out), *5* — reverberant room (with no lay out)

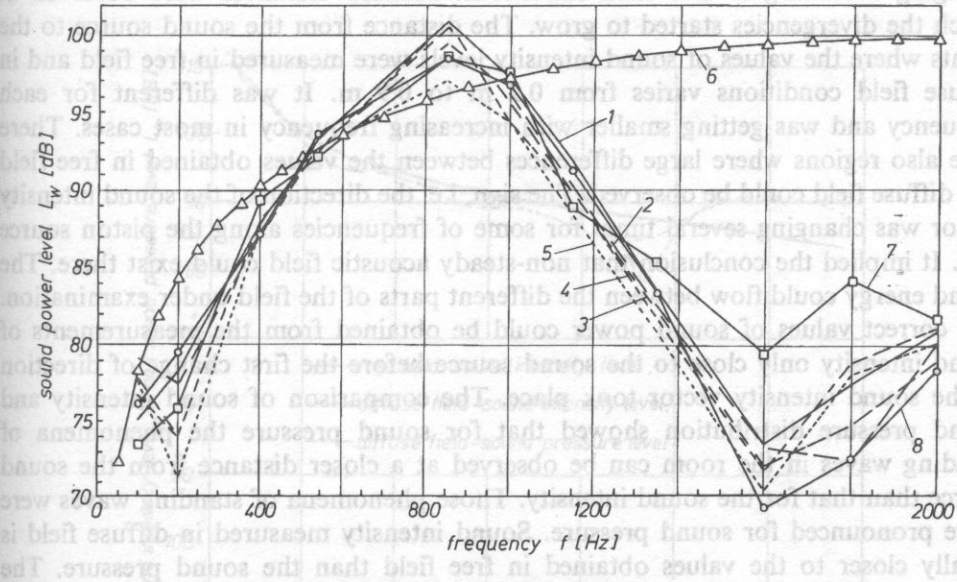

Fig. 5. Sound power level of circular piston source: *1* — sound intensity measurements, free field, *2* — sound intensity measurements, rev. room 1st step of lay out, *3* — sound intensity measurements, rev. room 2nd step of lay out, *4* — rev. room 3rd step of lay out, *5* — sound intensity measurements, rev. room no lay out, *6* — theoretically calculated, *7* — sound pressure measurements, free field method, *8* — sound pressure measurements, diffuse field method.

The difference between the values of sound power obtained in free field and in partially diffuse field ΔL_W increased when the total room absorption decreased. Only at two frequencies of 100 and 1800 Hz changes had a different character – values of differences ΔL_W increased. The greatest decrease was observed for the frequency of 200 Hz. That frequency was close to the resonance frequency of the room. The lowest decrease was observed for the frequencies of 400 and 540 Hz. For the rest of the frequencies investigated the changes of differences ΔL_W were similar; the greatest differences were equal to 4 dB.

Figure 5 presents the comparison of sound power values evaluated from the sound pressure measurements and sound intensity measurements.

B. Distribution of sound intensity and sound pressure in the axis of piston sound source

The results of distribution of sound intensity and sound pressure levels in the axis of the piston for the frequencies of 400, 540, 1000, and 1150 Hz are shown at the Fig. 6 to Fig. 9. The analysis of intensity levels distribution that for each of investigated frequencies there is the region where the values of sound intensity are changing according to free field conditions. Marked distances were observed at which the divergencies started to grow. The distance from the sound source to the points where the values of sound intensity levels were measured in free field and in diffuse field conditions varies from 0.2 m to 0.9 m. It was different for each frequency and was getting smaller with increasing frequency in most cases. There were also regions where large differences between the values obtained in free field and diffuse field could be observed. The sign, i.e. the direction of the sound intensity vector was changing several times for some of frequencies along the piston source axis. It implied the conclusion that non-steady acoustic field could exist there. The sound energy could flow between the different parts of the field under examination. The correct values of sound power could be obtained from the measurements of sound intensity only close to the sound source before the first change of direction of the sound intensity vector took place. The comparison of sound intensity and sound pressure distribution showed that for sound pressure the phenomena of standing waves in the room can be observed at a closer distance from the sound source than that for the sound intensity. Those phenomena of standing waves were more pronounced for sound pressure. Sound intensity measured in diffuse field is usually closer to the values obtained in free field than the sound pressure. The change of direction for sound intensity vector was in most cases connected with a significant change of the sound pressure value. Value of the field indicator calculated as the difference of sound pressure level and sound intensity level, $L_p - L_I$, at those distances rapidly started to increase.

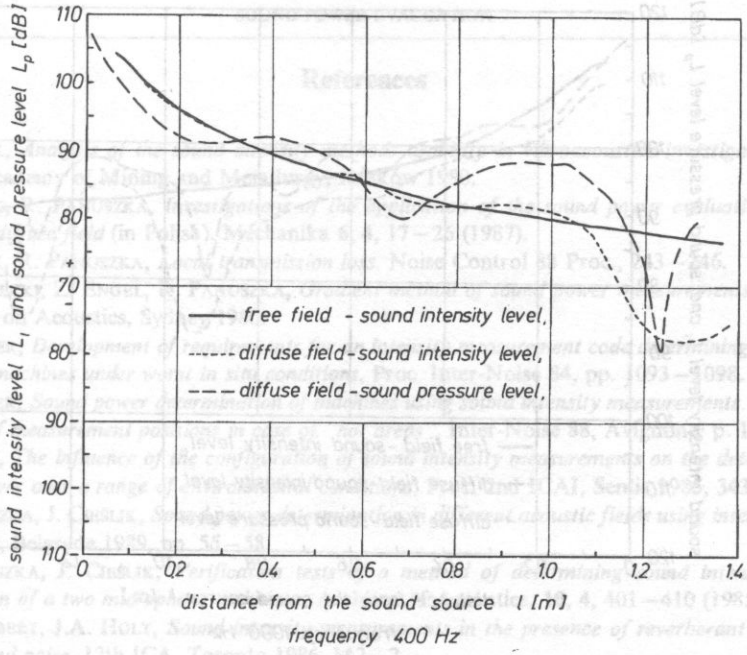

Fig. 6. Sound pressure and sound intensity distribution in the axis of circular piston sound source.

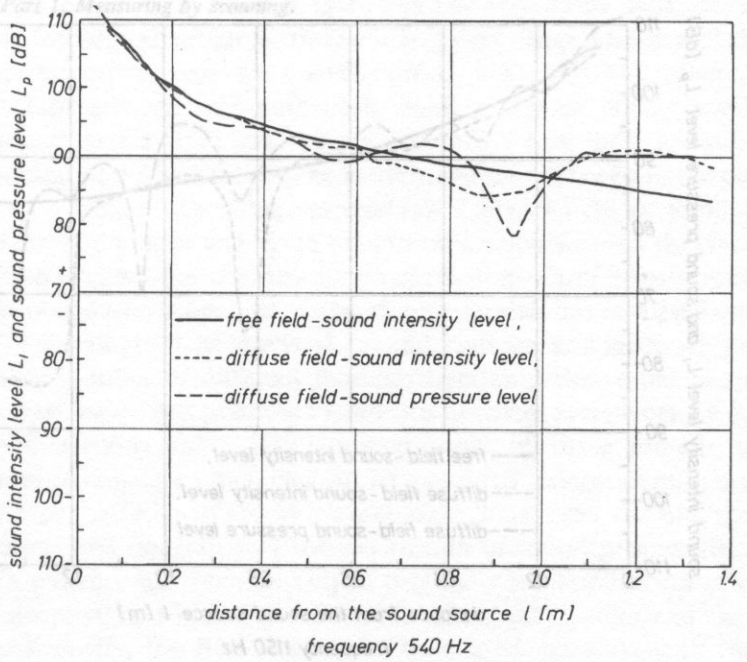

Fig. 7. Sound pressure and sound intensity distribution in the axis of circular piston sound source.

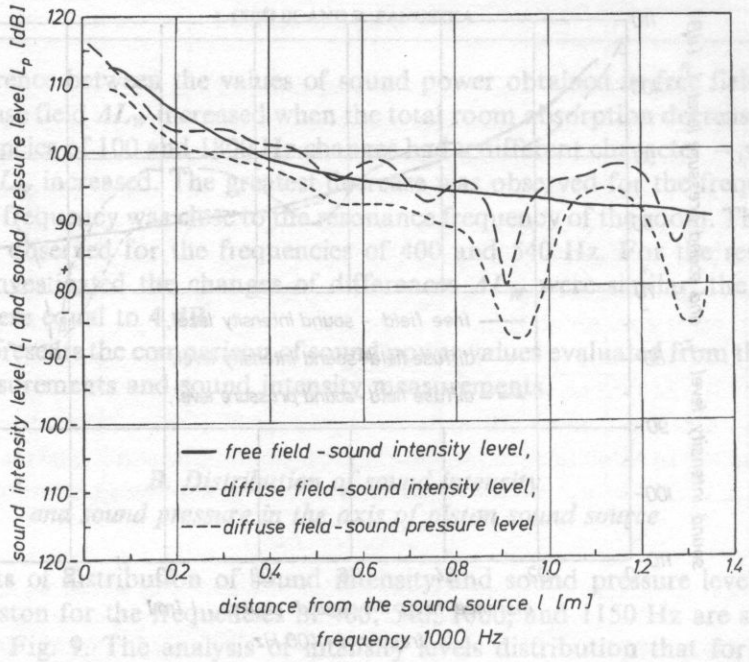

Fig. 8. Sound pressure and sound intensity distribution in the axis of circular piston sound source.

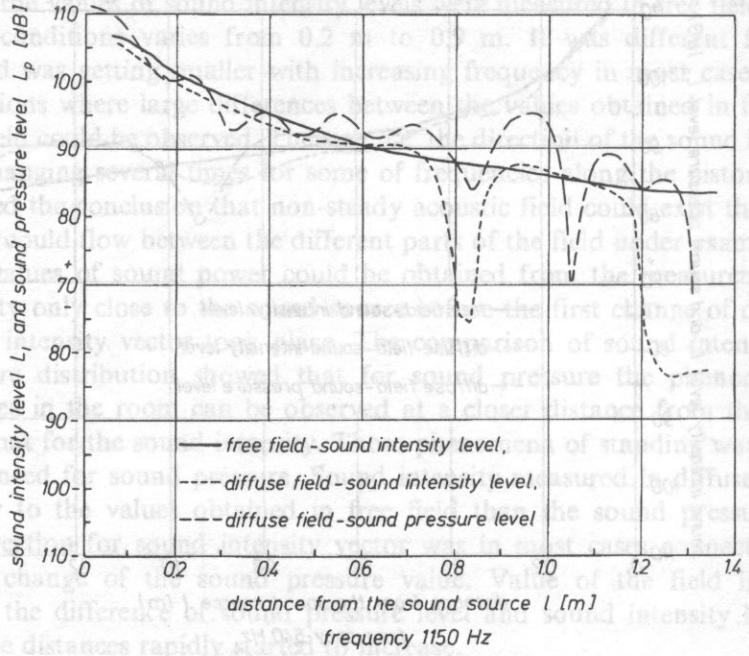

Fig. 9. Sound pressure and sound intensity distribution in the axis of circular piston sound source.

References

[1] J. CIEŚLIK, *Analysis of the sound intensity methods usability in vibroacoustics investigations*, Ph. D. Thesis Academy of Mining and Metallurgy, Kraków 1990.

[2] J. CIEŚLIK, R. PANUSZKA, *Investigations of the application of the sound power evaluation method in partially diffuse field* (in Polish). Mechanika **6**, 4, 17–26 (1987).

[3] J. CIEŚLIK, R. PANUSZKA, *Local transmission loss.* Noise Control 88 Proc., 243–246.

[4] S. CZARNECKI, Z. ENGEL, R. PANUSZKA, *Gradient method of sound power measurements in situ*, 10th Congress on Acoustics, Sydney 1980.

[5] G. HUBNER, *Development of requirements for an intensity measurement code determining sound power levels of machines under worst in situ conditions*, Proc. Inter-Noise 84, pp. 1093–1098.

[6] G. HUBNER, *Sound power determination of machines using sound intensity measurements. Reduction of number of measurement positions in case of "hot areas"*. Inter-Noise 88, Avignone, p. 1113–1116.

[7] E.L. NOE, *The influence of the configuration of sound intensity measurements on the determination of sound power over a range of environmental conditions*, Proc. 2nd ICAI, Senlis 1985, 343–348.

[8] R. PANUSZKA, J. CIEŚLIK, *Sound power determination in different acoustic fields using intensity method*, 13th ICA, Belgrade 1989, pp. 55–58.

[9] R. PANUSZKA, J. CIEŚLIK, *Verification tests of a method of determining sound intensity with the application of a two microphone technique*, Archives of Acoustics, **10**, 4, 401–410 (1985).

[10] A.F. SEYBERT, J.A. HOLT, *Sound intensity measurements in the presence of reverberant fields and/or background noise*, 12th ICA, Toronto 1986, M2–2.

[11] *Draft for ISO 9616-1, Acoustics — determination of sound power levels of noise sources using sound intensity. Part 1: Measuring at discrete points.*

[12] *Draft for ISO 9616-2. Acoustics — determination of sound power levels of noise sources using sound intensity. Part 1. Measuring by scanning.*

ARCHIVES OF ACOUSTICS
18, 2, 209–248 (1993)

CHARACTERIZATION OF SOUND ABSORBING MATERIALS USED IN NOISE CONTROL ENGINEERING

A. COPS AND W. LAURIKS*

Laboratorium voor Akoestiek en Warmtegeleiding
Department Natuurkunde, K.U. Leuven
(3001 Heverlee, Celestijnenlaan 200 D, Belgium)

1. Introduction

Sound absorbing materials are extensively used in the field of noise control engineering and architectural acoustics. Indeed they are, for an important part, responsible for the efficient sound insulation of partitions between rooms and of enclosures, for the acoustic comfort in rooms and industrial halls etc. Due to the continuing technological progress, research has been done and is still done in the motorcar, the aerospace and the manufacturing industries and others, to obtain absorbing materials who are simultaneously small in volume, have a low density, are rather cheap and have a good acoustic performance. From the other side it is often desirable to optimize the behaviour of acoustic materials for very specific purposes. To achieve highly qualified absorbing materials in a broad field of applications it is necessary to develop precise and, from time to time, sophisticated theoretical models which take into account the complex physical phenomena of acoustic materials.

The study of acoustic properties of absorbing materials has occupied scientist since the work of BERANEK [1, 2], MORSE et al. [3] and ZWIKKER and KOSTEN [4] in the early 1940's. A large number of different models, describing the sound propagation in porous materials, have been published since. An excellent review can be found in the publication of ATTENBOROUGH [5]. However most of these models require the introduction of parameters which can not be measured independently, making them inappropriate for the design of absorbing materials. Since 1956, the Biot theory allows in a very general and rigorous way the description of sound propagation in porous materials. This theory has been developed originally for application in the field of underwater geophysics, where the densities of the fluid (water) and the solids are comparable. Recently, the Biot theory has been used extensively to calculate the acoustic properties of porous materials used in noise control engineering, where the

* Senior Research Assistant N.F.W.D

fluid in the materials is air in stead of water. It has been proven that in a number of cases, the theory is indispensable to explain the acoustic behaviour of different types of acoustic materials. In this document the theory of Biot, related to the sound propagation of acoustic waves in porous materials, will be presented and adopted for different types of single and multiple layers by using matrix models for the materials. From the theory it is possible to calculate the characteristics of the material, either the specific impedance or the sound absorption coefficient.

For practical purposes also precise standardized methods, to measure acoustical parameters, are developed and still have to be developed. In this document some standardized methods will be discussed. Comparisons of theoretical predictions and measured characteristics of porous materials will be discussed.

Measuring methods

1. Measurement of sound absorption in a reverberant room

The International Standard ISO-354(6) specifies a method of measuring the sound absorption coefficient of acoustical materials used as wall or ceiling treatments, or the equivalent sound absorption area, such as furniture, persons or space absorbers, such as baffles, in a reverberation room. It is not intended for measuring the absorption characteristics of weakly damped resonators.

The results obtained can be used for comparison purposes and for design calculations with respect to room acoustics and noise control. The measuring principle is the following: Measurement of reverberation times in a reverberation room with and without the test specimen. From these times, the calculation of the equivalent sound absorption area A of the test specimen is performed. In the case of plane test specimens, the sound absorption coefficient is obtained by dividing A by its surface area S. When the test specimen comprises several identical objects, the equivalent sound absorption area of an individual object, for example a baffle, is obtained by dividing A by the number of objects.

The equivalent sound absorption area A, in square metres, of the test specimen, shall be calculated using the formula

$$A = 55.3(V/c)(1/T_2 - 1/T_1) \tag{1}$$

where V is the volume, in cubic metres, of the empty reverberation room; c is the velocity of sound in air in metres per second; for temperatures between 15°C and 30°C, the velocity of sound in air, c, can be calculated form the formula: $c = 331 + 0.6t$, where t is the air temperature, in degrees Celsius. T_1 and T_2 are respectively the reverberation times, in seconds, of the empty room and after the test specimen has been introduced.

The sound absorption coefficient α_S of a plane absorber shall be calculated using the formula:

$$\alpha_S = A/S \tag{2}$$

where A is the equivalent sound absorption area, in square metres, calculated from equation (1); S is the area, in square metres, of the test specimen.
For discrete absorbers, the result should generally be expressed as equivalent sound absorption area per object, which is determined by dividing A by the number of objects tested. For a specified array of objects, the result should be given as equivalent sound absorption area of the whole configuration.

Recently an annex has been added to the ISO 354 Standard specifying the test specimen mountings for sound absorption tests. Specific prescriptions are given for specimens mounted directly against the room surface (type A mounting), for test specimens mounted with an air space behind it (type E mounting), for test specimens, such as curtains, drapperies, window shades or window blinds, hanging parallel to the room surface (type G mounting), for spray- or towel-applied materials, such as plaster (type I mounting) and for sound absorber pads and baffles where the sound absorption per unit of rectangular unit shall be used (type J mounting).

The feature of this measuring method is that it gives the results of the sound absorption coefficient or the equivalent sound absorption area of materials for at random sound incidence, as is generally the case for practical applications. A disadvantage of this method is that no information about more fundamental parameters like the specific acoustic impedance or wave propagation constants in the material can be obtained.

2. *Sound absorbers — Rating of sound absorption*

The International Standard Document ISO/CD 11654(7) specifies a method by which the frequency dependent values of the sound absorption coefficient can be converted into a single number. Before this is done the one-third octave band values of the sound absorption coefficient measured according to ISO 354 are converted into octave bands. The sound absorption coefficient α_{pi}, for each octave band i, is calculated as the arithmetic mean value of the three one-third octave sound absorption coefficient, α_{i1}, α_{i2}, α_{i3} within the octave band:

$$\alpha_{pi} = \frac{(\alpha_{i1}+\alpha_{i2}+\alpha_{i3})}{3} \tag{3}$$

α_p has to be rounded in steps of 0.05 and maximized to 1.00, that is if α_p calculated is > 1.00 then $\alpha_p = 1.00$.
α_p is used to calculate the weighted sound absorption coefficient α_w, from the reference curve in Fig. 1 and Table 1. Shift the reference curve in steps of 0.1 towards the measured value until the sum of the unfavourable deviations is less than or equal to 0.1. An unfavourable deviation occurs at a particular frequency when the measured value is less than the value of the reference curve. Only deviaitons in the unfavourable direction shall be counted. The weighted sound absorption α_w is defined as the value of the shifted reference curve at 500 Hz.

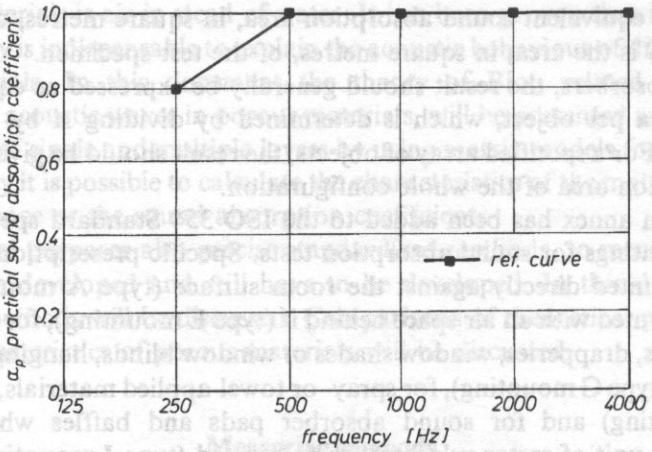

Fig. 1. Reference curve for evaluation of weighted sound absorption coefficient, α_w.

Table 1. Values of the reference curve in Fig. 1.

Frequency	250 Hz	500 Hz	1000 Hz	2000 Hz	4000 Hz
$\alpha_{pi,ref}$	0.8	1.0	1.0	1.0	1.0

If, for any octave band, $(\alpha_{pi} - \alpha_{pi,\,ref,\,shifted}) \geqslant 0.3$ then add a^* sign after α_w — value, e.g. $\alpha_w = 0.5^*$. This means that the sound absorption coefficient at one or more frequencies is considerably higher than the reference curve. An example of the calculation of α_w given in Fig. 2. Shift the reference curve in steps of 0.1 towards the measured value until the sum of the unfavourable deviations $\leqslant 0.1$. In the example the unfavourable deviations occur at 250 and 1000 Hz and the result is $\alpha_w = 0.6$.

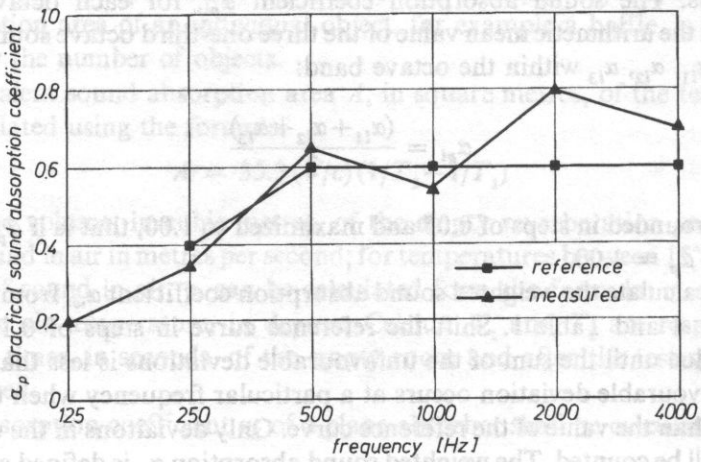

Fig. 2. Example of an α_w-calculation.

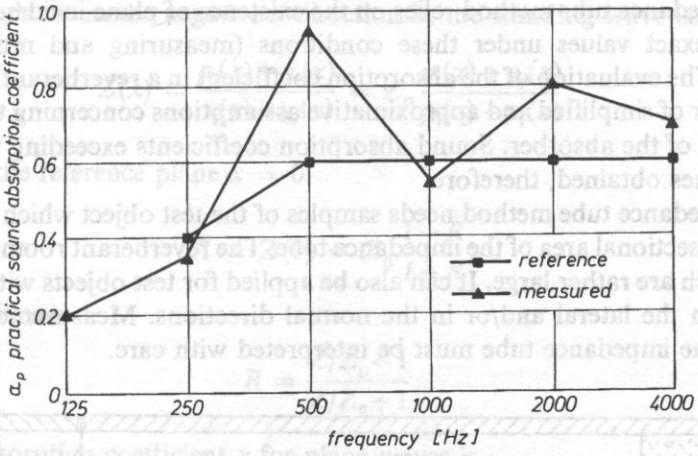

Fig. 3. Example of an $\alpha_w = 0.6^*$ calculation.

In Fig. 3 the corresponding example is shown when $(\alpha_{p,\ 500\,\mathrm{Hz}} - \alpha_{p,\ \mathrm{ref,\,shifted}}) = 0.35 \geqslant 0.30$ that is $\alpha_w = 0.6^*$.

The weighted sound absorption coefficient shall be expressed to one decimal place. This international standard is, in principle, applicable to all products for which the sound absorption coefficient has been determined according to ISO 354. It is, however, often not suitable for application on single items, such as chairs, baffles, etc.

3. Determination of the sound absorption coefficient and impedance or admittance by the impedance tube method

The International Standard Document ISO/CD. 10534 [8] describes the determination of the sound absorption coefficient, the reflection factor and the surface impedance or surface admittance of materials and objects. The values are determined for normal incidence by an evaluation of the standing wave pattern of a plane wave in a tube, which is generated by the superposition of an incident sinusoidal plane wave with the plane wave reflected from the test object. It is well suited for parameter studies and for the design absorbers, because only small samples of absorber material are needed.

There are some characteristic differences compared to the measurement of the sound absorption in a reverberant room (ISO 354). The impedance tube method can be applied for the determination of the reflection factor and the impedance or admittance, also. The sound is incident normally on the object surface. The reverberant room method will — under idealized conditions — determine the sound absorption coefficient for omnidirectional sound incidence.

The impedance tube method relies on the existence of plane incident sound waves and gives exact values under these conditions (measuring and mounting errors excluded). The evaluation of the absorption coefficient in a reverberant room is based on a number of simplified and approximative assumptions concerning the sound field and the size of the absorber. Sound absorption coefficients exceeding the values one are sometimes obtained, therefore.

The impedance tube method needs samples of the test object which are of the size of the cross-sectional area of the impedance tube. The reverberant room method needs objects which are rather large. It can also be applied for test objects with pronounced structures in the lateral and/or in the normal directions. Measurements with such objects in the impedance tube must be interpreted with care.

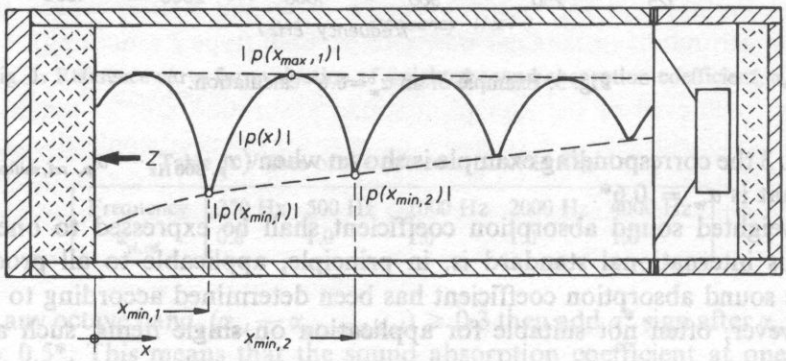

Fig. 4. Representation of the standing wave pattern in the tube.

The test object is mounted at one end of the straight, rigid smooth and tight impedance tube, see Fig. 4.

The incident sound wave p_i is assumed to be plane, harmonic in time with frequency f and angular frequency $\omega = 2\pi f$ (the time factor $e^{j\omega t}$ will be omitted in what follows), and directed along the axis of the impedance tube in the negative x-direction:

$$p_i(x) = P_0 e^{jk_0 x}; \; k_0 = \frac{\omega}{c_0} = \frac{2\pi f}{c_0}. \tag{4}$$

The amplitude P_0 is arbitrary.

The wave which is reflected from the test object having a reflection factor R is then:

$$p_i(x) = RP_0 e^{-jk_0 x}. \tag{5}$$

The particle velocities of the waves (counted positive in the negative x-direction) are respectively:

$$v_i = \frac{1}{Z_0} p_i(x); \; v_r(x) = -\frac{1}{Z_0} p_r(x). \tag{6}$$

The field impedance in the negative x-direction in the standing wave is:

$$Z(x) = \frac{p_i(x)+p_r(x)}{v_i(x)+v_r(x)} = Z_0 \frac{p_i(x)+p_r(x)}{p_i(x)-p_r(x)}. \tag{7}$$

Especially at the reference plane $x = 0$:

$$Z = Z(0) = Z_0 \frac{1+R}{1-R}, \tag{8}$$

from which follows:

$$R = \frac{Z/Z_0-1}{Z/Z_0+1}. \tag{9}$$

The sound absorption coefficient α for plane waves is

$$\alpha = 1 - |R|^2. \tag{10}$$

A pressure maximum in the standing wave is at a place where p_i and p_r are in phase

$$|p_{max}| = |P_0| \cdot (1+|R|). \tag{11}$$

A pressure minimum is at a place of opposite phase

$$|p_{min}| = |P_0| \cdot (1-|R|). \tag{12}$$

Using the standing wave ratio $s = |p_{max}| \,/\, |p_{min}|$:

$$s = \frac{1+|R|}{1-|R|} \quad \text{and} \quad |R| = \frac{s-1}{s+1}. \tag{13}$$

The sound absorption then follows from the relation (10), with $|p_{max}|$ and $|p_{min}|$ at a given frequency.

If the sound pressure in the impedance tube is measured in a logarithmic scale (in dB), and the difference in level between the pressure maximum and the pressure minimum is ΔL = dB, then:

$$s = 10^{\Delta L/20} \tag{14}$$

The sound absorption coefficient then follows from:

$$\alpha = \frac{4 \cdot 10^{\Delta L/20}}{(10^{\Delta L/20}+1)^2} \tag{15}$$

The phase angle Φ of the complex reflection factor $R = |R| e^{j\Phi}$ follows from the phase condition for a pressure minimum in the standing wave:

$$\Phi + (2n-1) \cdot \pi = 2k_0 x_{min,n} \tag{16}$$

for the n-th minimum ($n = 1, 2, ...$) in front of the reference plane (towards the sound source).
From this:

$$\phi = \pi\left(\frac{4x_{\min,n}}{\lambda_0} - 2n + 1\right), \tag{17}$$

and for the first minimum ($n = 1$):

$$\Phi = \pi\left(\frac{4x_{\min,1}}{\lambda_0} - 1\right). \tag{18}$$

The complex reflection factor is then

$$\begin{aligned} R &= R' + jR'' \\ R' &= |R|\cdot\cos\Phi;\ R'' = |R|\cdot\sin\Phi. \end{aligned} \tag{19}$$

According to Eq. (8) one obtaines the normalized impedance $z = Z/Z_0$:

$$\begin{aligned} z &= z' + jz'' \\ z' &= \frac{1-R'^2-R''^2}{(1-R')^2+R''^2};\ z'' = \frac{2R''}{(1-R')^2+R''^2}. \end{aligned} \tag{20}$$

Finally the normalized admittance is obtained as the reciprocal of the normalized impedance:

$$g = Z_0/Z = Z_0 G, \tag{21}$$

with $G = 1/Z = v/p$ the admittance, is the ratio of the sound particle velocity to the sound pressure at that point.

4. Two-microphone impedance measurement tube method

The two-microphone method (9) of measuring the acoustic absorption coefficient involves the decomposition of broad-band stationary random signal into its incident (P_i) and the reflected (P_r) components. The singal is generated by a sound source, and the incident and reflected components are determined from the relationship between the acoustic pressure measured by microphones at two locations on the wall of the tube (see Fig. 5).

From the incident and reflected components of the sound pressure at the two microphone positions, three frequency response functions are calculated; H_1 the frequency response function between the two microphone channels, and H_i the frequency response function associated with the incident component, and H_r, the frequency response function associated with the reflected component. Using these values, the complex reflection coefficient R is calculated from the following equation:

$$R = \left(\frac{H_1 - H_i}{H_r - H_1}\right) \cdot e^{j2k(1+s)} \tag{22}$$

where k is the wave number, l is the distance between the first microphone location and the front of the sample (in mm), and s is the spacing between the microphones (in mm). Using the value for the reflection coefficient, the normalized impedance z and the sound absorption coefficient α can be calculated from the equations (8) respectively (10).

For each measurement made on a sample, the following date can be calculated and displayed in the frequency range of interest from the above mentioned equations: the acoustic absorption coefficient (magnitude only); the acoustic reflection coefficient, the normalized impedance, the frequency response function or the calibration result, each displayed as magnitude, phase, real part or imaginary part.

The two-microphone theory assumes plane-wave propagation, no mean flow and no losses due to absorption at the tube wall. This absorption is kept to a minimum in the normaly used two-microphone impedance measuring tube.

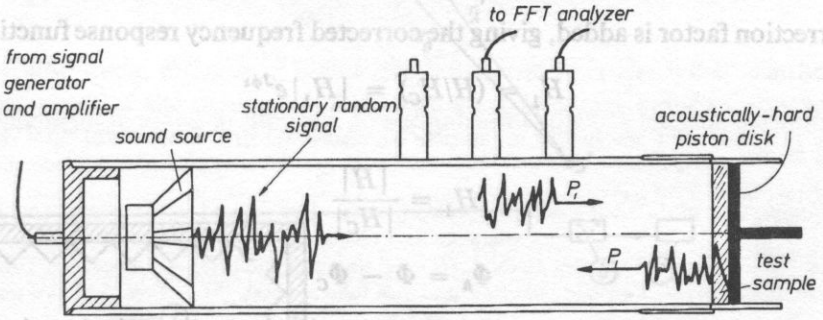

Fig. 5. Set-up of the impedance measurement tube

As described above, the frequency response function is calculated from the cross spectrum of the two microphone signals, so any phase or amplitude mismatch between these microphone channels will corrupt its calculated value. During the calibration procedure, the frequency response function is calculated with the two microphones interchanged, and then again in there initial positions. The geometric mean of these two results is a complex value which can be added to any subsequent frequency response function that is calculated using the same setup, effectively eliminating errors due to any mismatches in the microphone channels.

During the calibration procedure, the calibration frequency response functions for the microphones in the standard positions (H_{C1}) and the interchanged positions (H_{C2}) are calculated as:

$$H_{C1} = |H_{C1}|\, e^{j\Phi_1}, \tag{23}$$

and:

$$H_{C2} = |H_{C2}|\, e^{j\Phi_2}, \tag{24}$$

where Φ_1 is the phase of the calibration frequency response function H_{C1}, Φ_2 is the phase of the calibration frequency response function H_{C2} and j is $\sqrt{-1}$.

From these values, the calibration factor (H_C) is calculated as:

$$H_C = |H_C|\, e^{j\Phi_C}. \tag{25}$$

where

$$|H_C| = \sqrt{|H_{C1}|/|H_{C2}|}, \tag{26}$$

$$\phi_C = (1/2)\,(\phi_1+\phi_2). \tag{27}$$

This calibration factor can now be added to any frequency response function that is calculated using the tube set-up, giving a value that is uneffected by the amplitude or phase mismatches between the microphone channels.

For example, the following frequency response function is measured, with the microphones in the standard positions:

$$H = |H| e^{j\phi} \tag{28}$$

The correction factor is added, giving the corrected frequency response function (H_1):

$$H_1 = (H/H_C) = |H_1| e^{J\phi_1} \tag{29}$$

where

$$H_1 = \frac{|H|}{|H_C|} \tag{30}$$

$$\Phi_h = \Phi - \Phi_C \tag{31}$$

This frequency response function H_1 is the value that is used to calculate the acoustic properties of the test sample.

5. Two-microphone free field method

The two-microphone free field method [10, 11, 12] used to calculate the normalized surface impedance of a test sample involves the measurement of the Fourier transform of the pressure at the point half between the two microphones (see Fig. 6):

$$P = \frac{P_A+P_B}{2} \tag{32}$$

where P_A and P_B are the Fourier transforms of the sound pressure at the microphones A and B. The particle velocity at that point can be expressed by the Fourier transform of the pressure gradient:

$$V_z = \frac{P_A - P_B}{jw\rho\Delta z}. \tag{33}$$

For plane acoustic waves the normalized impedance at the measuring point is given by:

$$z^* = -\frac{1}{\rho c}\frac{P}{V_z} = -\frac{jw\Delta z}{2c}\frac{1+H_{AB}}{1+H_{AB}}, \tag{34}$$

with $H_{AB} = P_A/P_B$.

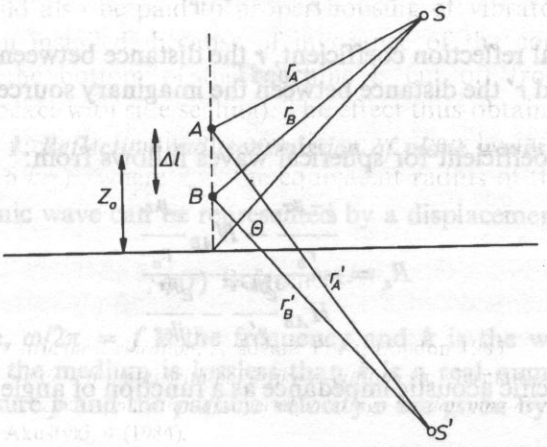

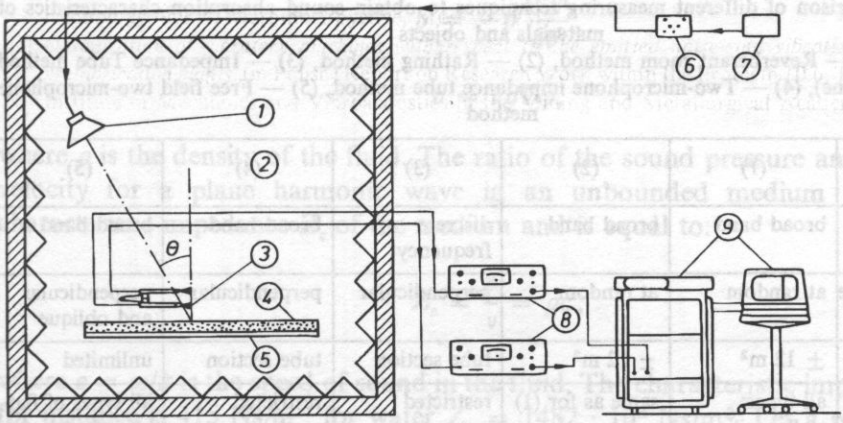

Fig. 6. Measuring set-up for impedance measurements with the two-microphone transfer function technique.

Since the impedance is measured at the point z_0 and not at the surface, a correction has to be made. It can be shown [10, 11] that the normalized specific impedance at the sample surface is given by:

$$z(\theta) = \frac{z^* + j/\cos\theta \cdot \tan(\omega z_0 \cos\theta/c)}{1 + j \cdot \cos\theta \cdot \tan(\omega z_0 \cos\theta/c)}. \tag{35}$$

Several alternatives on this two-microphone free field method have been worked out e.g. by CHUNG [13, 14] and CHU [15] for plane waves.

The most important disadvantage of the preceeding methods is the plane wave assumption. Therefore the spherical wave estimate technique has been developed [16, 17]. If the distance between the source and the measuring surface is finite, the sound pressure above the surface is approximated by:

$$p = \frac{e^{jkr}}{r} + R_s \frac{e^{jkr'}}{r'}, \tag{36}$$

with R_s the spherical reflection coefficient, r the distance between the source and the measuring point and r' the distance between the imaginary source and the measuring point.

The reflection coefficient for spherical waves follows from:

$$R_s = \frac{\dfrac{e^{-jkr_b}}{r_b} - H_{AB}\dfrac{e^{jkr_a}}{r_a}}{H_{AB}\dfrac{e^{jkr'_a}}{r'_a} - \dfrac{e^{jkr'_b}}{jkr}} \tag{37}$$

The normalized specific acoustic impedance as a function of angle of incidence can be obtained from:

Table 2. Comparison of different measuring techniques to obtain sound absorption characteristics of materials and objects

Techniques: (1) — Reverberant room method, (2) — Rathing method, (3) — Impedance Tube method (single microphone), (4) — Two-microphone impedance tube method, (5) — Free field two-microphone method

Measuring methods	(1)	(2)	(3)	(4)	(5)
Source signal	broad band	broad band	discrete frequency	broad band	broad band
Sound incidence	at random	at random	perpendicular	perpendicular	perpendicular and oblique
Sample surface	$\pm$ 12 m^2	$\pm$ 12 m^2	tube section	tube section	unlimited
Test materials	all types: walls, ceilings, furniture, persons, chairs, space absorbers etc...	same as for (1)	restricted	restricted	all types of flat absorbers, road and ground surfaces
Measuring time	fast	fast	time consuming	fast	fast
Test results	α (can be >1) A (eq.abs.area) A/test object	α (always $\leqslant 1$)	α (always $\leqslant 1$) R $z=Z/Z_0$	α (always $\leqslant 1$) R $z=Z/Z_0$	α (always $\leqslant 1$) R $z=Z/Z_0$

$$z_s(\theta) = \frac{1}{\cos\theta} \cdot \frac{1+R_s}{1-R_s} \cdot \left(1 - \frac{1}{jkr}\right) \tag{38}$$

An advantage of the spherical wave estimate technique is that measurements can be done in surroundings with background noise.

In Table 2 the features of the 5 different measuring methods to obtain absorption characteristics of sound absorbing materials are compared with each other.

Theory

1. Reflection and transmission of plane waves

A plane harmonic wave can be represented by a displacement potential:

$$\varphi(r) = Ae^{-jkr+j\omega t}, \tag{39}$$

A is the amplitude, $\omega/2\pi = f$ is the frequency and k is the wave number of the harmonic wave. If the medium is lossless than k is a real number, otherwise it is complex. The pressure p and the particle velocity v are given by:

$$p = -p\frac{\delta^2\varphi}{\delta t^2}, \tag{40}$$

$$v = i\omega\nabla\varphi, \tag{41}$$

where ρ is the density of the fluid. The ratio of the sound pressure and the particle velocity for a plane harmonic wave in an unbounded medium is called the characteristic impedance Z_c of the medium and is equal to:

$$Z_c = \frac{p}{v} = \rho c, \tag{42}$$

where $c = \omega/k$ is the speed of sound in the fluid. The characteristic impedance of air for instance is 415 Ns/m^3; for water $Z_c = 1482 \cdot 10^3$ Ns/m^3. Let a plane wave be incident on the interface between two semi-infinite fluids with a plane boundary as in Fig. 7.

The incident wave can be written as:

$$\varphi_{\text{inc}} = Ae^{-jk(x_1\sin\theta + x_3\cos\theta)+j\omega t}, \tag{43}$$

with θ the angle of incidence. The reflected plane wave can be written as:

$$\varphi_{\text{refl}} = RAe^{-jk(x_1\sin\theta + x_3\cos\theta)+j\omega t}, \tag{44}$$

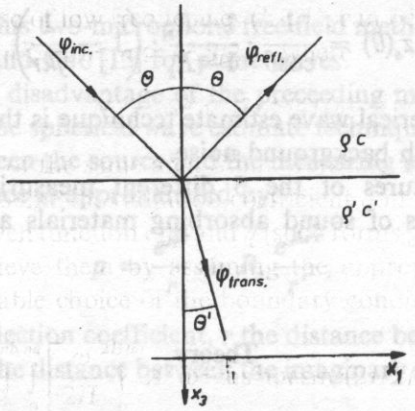

Fig. 7. A plane sound wave incident on a boundary between two semi-infinite fluids.

with R the amplitude of the reflection coefficient at the interface. In the general case, R is a complex number and consists of a magnitude and a phase: $R = |R|\, e^{j\phi}$, with $0 \leqslant |R| \leqslant 1$. The transmitted wave can be written as:

$$\varphi_{\text{trans}} = TAe^{-jk(x_1 \sin\theta + x_3 \cos\theta)}, \tag{45}$$

with T the transmission coefficient.

The ratio of the acoustic pressure and the normal component of the palocity at the interface is called the normal surface impedance Z. In general Z is a complex, frequency dependent number $Z = R + jX$.

It can be shown that:

$$Z = \frac{p}{v_3} = \frac{\rho c}{\cos\theta} \cdot \frac{1+R}{1-R}, \tag{46}$$

and

$$R = \frac{Z\cos\theta - \rho c}{Z\cos\theta + \rho c}. \tag{47}$$

In a lot of applications, the absorption coefficient α is used as a parameter:

$$\alpha = 1 - |R|^2. \tag{48}$$

Since it is a ree it is a real number, α gives less information about the acoustic behaviour of the interface than the surface impedance. Combining Eq. (47) and (48) results in:

$$\alpha = \frac{4R\cos\theta}{(R\cos\theta + 1)^2 + (X\cos\theta)^2}. \tag{49}$$

2. *Single wave propagation for materials with low flow resistivity*

Empirical relations between flow resistivity and characteristic impedance and propagation constant

A plastic foam can be considered as an elastic solid frame containing bubbles. In high porosity low density foams, the gas bubbles have approximately the shape of dodecahedra. The lines of intersection and the membranes between different cells occupy only a few percent of the total volume fraction for most materials used in noise control and architectural applications. If all the membranes are ruptured, the foam is called reticulated. For most practical purposes, the sound propagation in reticulated foams can be simplified since the viscous coupling between frame and air is weak. In a large frequency range, the sound propagation in such materials is mainly determined by a wave propagating in the air in the material. In that case, the characteristic impedance and the propagation constant (or equivalently, the speed of sound $c = \omega/k$ and the complex density $\rho = Zk/\omega$) are defined by the flow resistivity ρ of the material, which is defined as the ratio of the air pressure difference Δp accross a test specimen and the steady volumetric air flow rate Q crossing the test specimen, normalized for the cross-sectional area A and the thickness d of the test specimen:

$$\sigma = \frac{\Delta p}{Q} \cdot \frac{A}{d} \quad (\mathrm{Ns/m^4}). \tag{50}$$

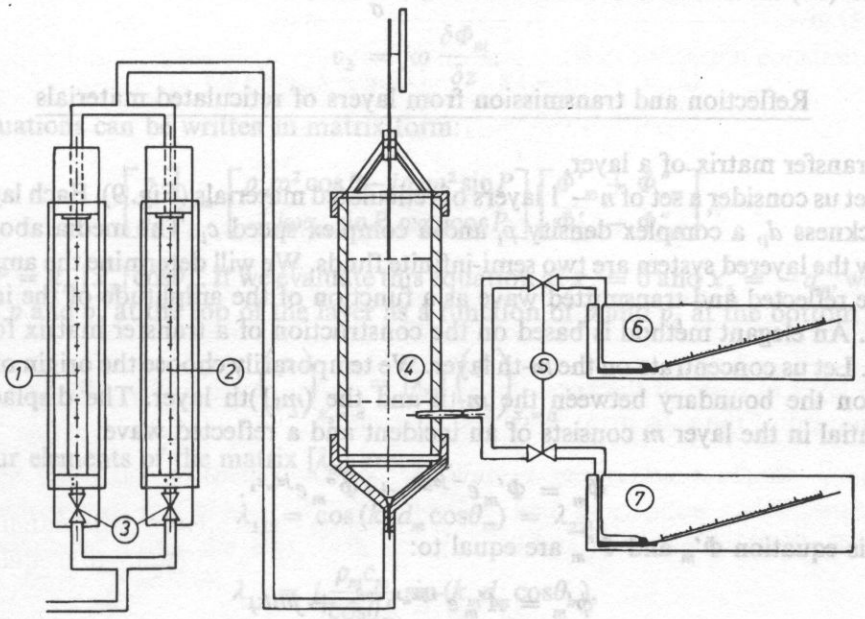

Fig. 8. Experimental set-up for the determination of the flow resistivity σ. *1* and *2* airflow meters with different range, *3* air flow control waves, *4* sample and measuring cel, *5* manometer walves, *6* and *7* oil manometers with different range.

The flow resistivity of reticulated foams varies from a few thousands Ns/m^4 to approximately 20000 Ns/m^4. The flow resistivity can be measured with the apparatus shown in Fig. 8 (18).

The relation between the flow resistivity and the acoustic properties of open cell porous materials has been determined by several authors for fibrous materials and plastic foams [19, 20, 21]. These relations are based on a number of measurements of Z_c and k as a function of σ. The results are [21]:

$$\mathrm{Re}(Z_c) = \rho_0 c_0 \left[1 + 0.1087 \left(\frac{\rho_0 f}{\sigma}\right)^{-0.6731}\right], \tag{51}$$

$$\mathrm{Im}(Z_c) = -\rho_0 c_0 \, 0.2082 \left(\frac{\rho_0 f}{\sigma}\right)^{-0.6193}, \tag{52}$$

$$\mathrm{Re}(k) = \frac{\omega}{c_0}\left[1 + 0.0608 \left(\frac{\rho_0 f}{\sigma}\right)^{-0.7173}\right], \tag{53}$$

$$\mathrm{Im}(k) = -\frac{\omega}{c_0}\left[1 + 0.1323 \left(\frac{\rho_0 f}{\sigma}\right)^{-0.6601}\right]. \tag{54}$$

In these equations ρ_0 is the density of air and c_0 is the sound speed in air. Equations (51) to (54) are considered valid if $0.01 \leqslant \dfrac{(\rho_0 f)}{\sigma} \leqslant 1$.

Reflection and transmission from layers of reticulated materials

Transfer matrix of a layer.

Let us consider a set of $n-1$ layers of reticulated materials (Fig. 9). Each layer has a thickness d_i, a complex density ρ_i and a complex speed c_i. The media above and below the layered system are two semi-infinite fluids. We will determine the amplitude of the reflected and transmitted wave as a function of the amplitude of the incident wave. An elegant method is based on the construction of a transfer matrix for each layer. Let us concentrate on the m-th layer. We temporarily choose the origin of the x_3 axis on the boundary between the m-th and the (m-1)th layer. The displacement potential in the layer m consists of an incident and a reflected wave:

$$\Phi_m = \Phi'_m e^{-j\alpha_m x_3} + \Phi''_m e^{j\alpha_m x_3}. \tag{55}$$

In this equation Φ'_m and Φ''_m are equal to:

$$\phi'_m = A'_m e^{-jk_m x_1 \sin\theta_m} + j\omega t,$$

$$\phi''_m = A''_m e^{-jk_m x_1 \sin\theta_m} + j\omega t,$$

and $\alpha_m = k_m \cos\theta_m$.

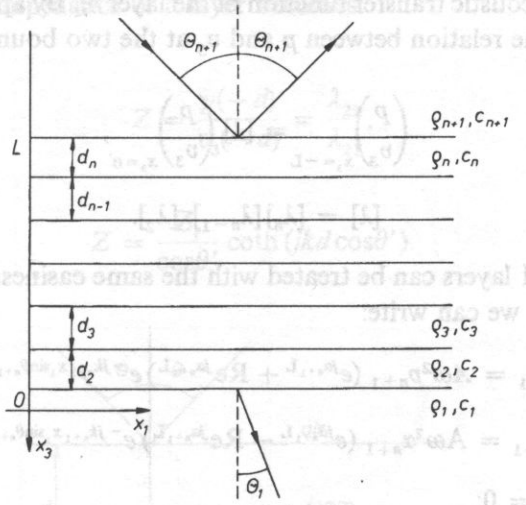

Fig. 9. A system of n-1 layers of acoustic material.

The normal component of the velocity and the sound pressure are:

$$p = -\rho \frac{\delta^2 \Phi_m}{\delta t^2}, \tag{56}$$

$$v_3 = j\omega \frac{\delta \Phi_m}{\delta z}. \tag{57}$$

The equations can be written in matrix form:

$$\begin{bmatrix} p \\ v_3 \end{bmatrix} = \begin{bmatrix} \rho_m \omega^2 \cos P - j\rho_m \omega^2 \sin P \\ -j\omega\alpha_m \sin P \;\; \omega\alpha_m \cos P \end{bmatrix} \begin{bmatrix} \Phi'_m + \Phi''_m \\ \Phi'_m - \Phi''_m \end{bmatrix}, \tag{58}$$

where $P = k_m |x_3| \cos\theta_m$. If we evaluate this equation at $x_3 = 0$ and $x_3 = -d_m$, we can express p and v_3 at the top of the layer as a function of p and v_3 at the bottom face:

$$\begin{pmatrix} p \\ v_3 \end{pmatrix}_{x_3=-d} = [\lambda_m] \begin{pmatrix} p \\ v_3 \end{pmatrix}_{x_3=0}. \tag{59}$$

The four elements of the matrix $[\lambda_m]$ are:

$$\lambda_{11} = \cos(k_m d_m \cos\theta_m) = \lambda_{22},$$

$$\lambda_{12} = j \frac{\rho_m c_m}{\cos\theta_m} \sin(k_m d_m \cos\theta_m),$$

$$\lambda_{21} = j \frac{\cos\theta_m}{\rho_m c_m} \sin(k_m d_m \cos\theta_m).$$

This matrix is the acoustic transfer function of the layer m. By application of equation (59), we can find the relation between p and v_3 at the two boundaries of the layered system:

$$\begin{pmatrix} p \\ v_3 \end{pmatrix}_{x_3=-L} = [\lambda] \begin{pmatrix} p \\ v_3 \end{pmatrix}_{x_3=0}, \tag{60}$$

$$[\lambda] = [\lambda_n][\lambda_{n-1}]..[\lambda_2].$$

The system with n-1 layers can be treated with the same easiness as for one layer. At the face $x_3 = -L$, we can write:

$$p_{n+1} = A\omega^2 p_{n+1} (e^{j\alpha_{n+1}L} + \mathrm{Re}^{j\alpha_{n+1}L}) e^{-jk_{n+1}x_1 \sin\theta_{n+1} + j\omega t}, \tag{61}$$

$$v_{3n+1} = A\omega^2 \alpha_{n+1} (e^{j\alpha_{n+1}L} - \mathrm{Re}^{j\alpha_{n+1}L}) e^{-jk_{n+1}x_1 \sin\theta_{n+1} + j\omega t}, \tag{62}$$

and at the face $x_3 = 0$:

$$p_1 = A\omega^2 \rho_1 \, \mathrm{T} e^{-jk_1 x_1 \sin\theta_1 + j\omega t}, \tag{63}$$

$$v_{31} = A\omega\alpha_1 \, \mathrm{T} e^{-jk_1 x_1 \sin\theta_1 + j\omega t}, \tag{64}$$

In these equations R is the reflection coefficient and T the transmission coefficient of the system. A is the amplitude of the incident wave. The Equations (59) to (64) give:

$$R = \frac{(\lambda_{12}\alpha_1 + \lambda_{11}\omega\rho_1)\alpha_{n+1} - (\lambda_{22}\alpha_1 + \lambda_{21}\omega\rho_1)\omega\rho_{n+1}}{(\lambda_{12}\alpha_1 + \lambda_{11}\omega\rho_1)\alpha_{n+1} + (\lambda_{22}\alpha_1 + \lambda_{21}\omega\rho_1)\omega\rho_{n+1}} e^{2j\alpha_{n+1}L}, \tag{65}$$

$$T = \frac{2\alpha_{n+1}\omega\rho_{n+1}}{(\lambda_{12}\alpha_1 + \lambda_{11}\omega\rho_1)\alpha_{n+1} + (\lambda_{22}\alpha_1 + \lambda_{21}\omega\rho_1)\omega\rho_{n+1}} e^{2j\alpha_{n+1}L}. \tag{66}$$

Application to one layer of foam, stuck on a hard backing

A layer of foam of thickness d is stuck on a hard backing (Fig. 10). The normal component of the velocity at $x_3 = 0$ is equal to:

$$v_3(0) = 0. \tag{67}$$

From Eq. (59) we obtain v_3 and p at $x_3 = -d$:

$$v_3(-d) = \lambda_{21} p(0), \tag{68}$$

$$p(-d) = \lambda_{22} p(0). \tag{69}$$

The normal surface impedance of a layer becomes:

$$Z = \frac{p(-d)}{v_3(-d)} = \frac{\lambda_{22}}{\lambda_{21}}, \tag{70}$$

or:

$$Z = \frac{Z_c}{\cos\theta'} \coth(jkd\cos\theta'). \tag{71}$$

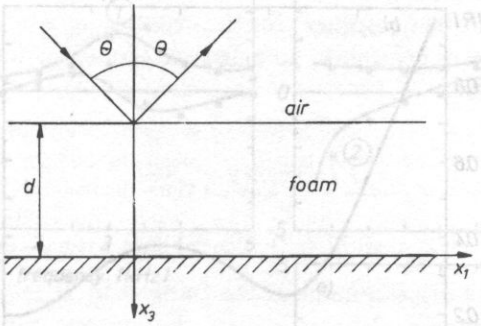

Fig. 10. One layer of foam, stuck on a hard backing.

In this equation, Z_c is the characteristic impedance, k the propagation constant. θ' is the angle of refraction and is given by Snell's law:

$$\cos\theta' = \sqrt{1 - (k_0 \sin\theta/k)^2}, \tag{72}$$

with k_0 the wave number in air and θ the angle of sound incidence.

The Figure 11 shows the normal surface impedance at normal sound incidence of a 5 cm thick foam layer, stuck on a hard floor. The low resistivity of the material is 5000 Ns/m⁴. The characteristic impedance Z_c and the propagation constant k have been calculated using the Eqs. (51) to (54) and the normal surface impedance with Eq. (71). The dots are experimental results, obtained with the free field method described in chapter measuring methods, point 5. For comparison, the values of the reflection and absorption coefficient have been calculated using the Eqs. (47) and (48). The $\lambda/2$ anti resonance at 3000 Hz can clearly be noticed.

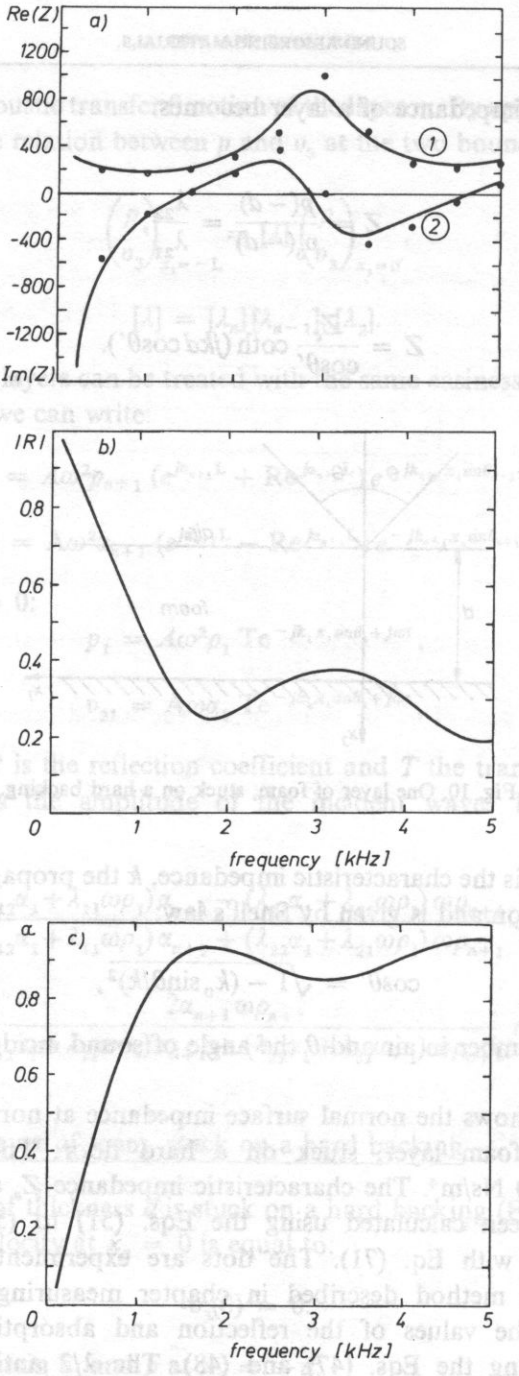

Fig. 11. a) Real (1) and imaginary (2) part of the normal surface impedance at normal sound incidence of a 5 cm thick reticulated foam, stuck on a hard backing, as a function of frequency. The foam flow resistivity is 5000 Ns/m⁴: ——— Eqs. (71) and (72) and (47) and (48). • experimental results from two-microphone technique. b) Magnitude of the reflection coefficient of the same foam layer. c) Absorption coefficient of the same foam layer.

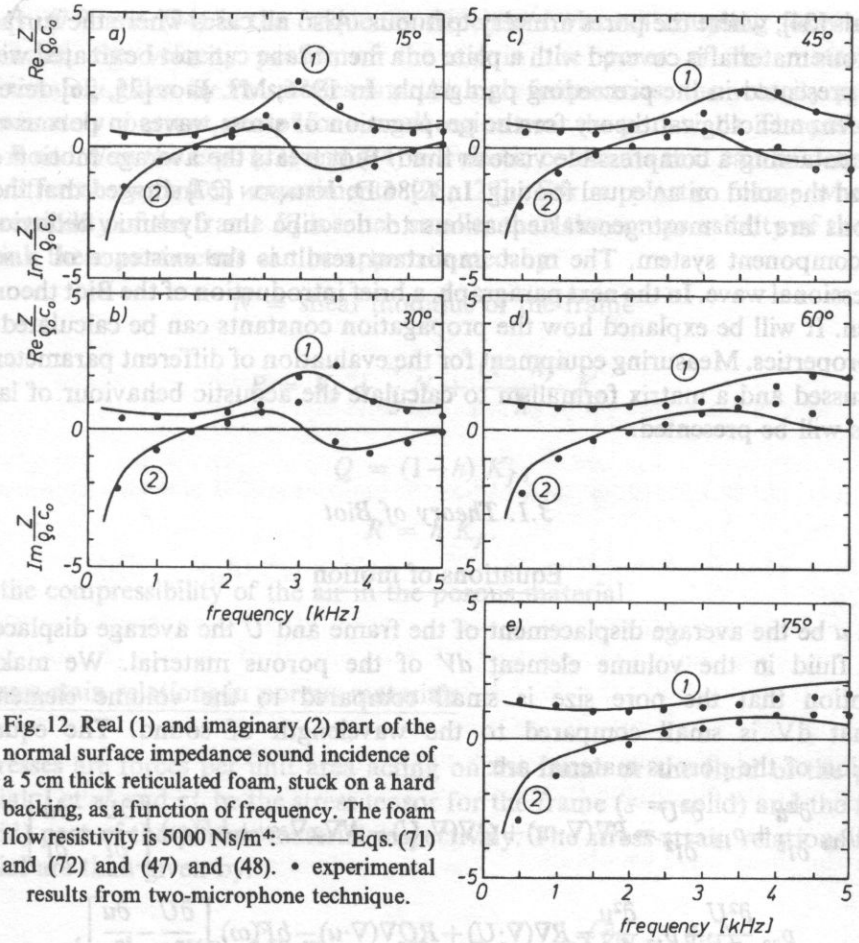

Fig. 12. Real (1) and imaginary (2) part of the normal surface impedance sound incidence of a 5 cm thick reticulated foam, stuck on a hard backing, as a function of frequency. The foam flow resistivity is 5000 Ns/m⁴: ——— Eqs. (71) and (72) and (47) and (48). • experimental results from two-microphone technique.

Figure 12 shows the normal surface impedance of the same foam layer for the angles of incidence $\theta = 15°, 30°, 45°, 60°$ and 75°.

The above described method allows for the calculation of the normal surface impedance of any combination of layers of reticulated foam including air gaps. The method is very well suited for design purposes.

3. Acoustical properties of materials with medium and high flow resistivity

The model presented in the previous paragraph allows for the calculation of the acoustic behaviour of materials with low flow resistivity. In a lot of cases, these conditions are not satisfied, and an incident sound wave will generate a movement of the air in the pores as well as a movement of the frame. This may occur for instance in materials with medium and high flow resistivity [22, 23] or partially reticulated

materials [24], where the pores are very tortuous. Also all cases where the surfaces of the porous material is covered with a plate or a membrane can not be treated with the theory presented in the preceeding paragraph. In 1956, Mr. Biot [25, 26] developed a semi-fenomenological theory for the propagation of stress waves in porous elastic solids containing a compressible viscous fluid. Biot treats the average motion of the fluid and the solid on an equal footing. In 1986 D. Johnson [27] showed that the Biot equations are the most general equations to describe the dynamic behaviour of a two-component system. The most important result is the existence of a second compressional wave. In the next paragraph, a brief introduction of the Biot theory will be given. It will be explaned how the propagation constants can be calculated from foam properties. Measuring equipment for the evaluation of different parameters will be discussed and a matrix formalism to calculate the acoustic behaviour of layered systems will be presented.

3.1. Theory of Biot

Equations of motion

Let u be the average displacement of the frame and U the average displacement of the fluid in the volume element dV of the porous material. We make the assumption that the pore size is small compared to the volume element dV and that dV is small compared to the wavelength of sound. The equations of motion of the porous material are:

$$\rho_{11}\frac{\partial^2 u}{\partial t^2}+\rho_{12}\frac{\partial^2 U}{\partial t^2}=P\nabla(\nabla\cdot u)+Q\nabla(\nabla\cdot U)-N\nabla x\nabla xu+bF(\omega)\left[\frac{\partial U}{\partial t}-\frac{\partial u}{\partial t}\right], \tag{73}$$

$$\rho_{22}\frac{\partial^2 U}{\partial t^2}+\rho_{12}\frac{\partial^2 u}{\partial t^2}=R\nabla(\nabla\cdot U)+RQ\nabla(\nabla\cdot u)-bF(\omega)\left[\frac{\partial U}{\partial t}-\frac{\partial u}{\partial t}\right], \tag{74}$$

In these equations ρ_{11}, ρ_{22} and ρ_{12} are determined as follows:

$$\rho_{11}=\rho_1+\rho_a, \tag{75}$$

$$\rho_{22}=h\rho_f+\rho_a, \tag{76}$$

$$\rho_{12}=-\rho_a, \tag{77}$$

ρ_1 and ρ_f are the densities of the frame and air respectively and ρ_a is the mass coupling term, which can be related to the structure factor k_s and the porosity h by the equation:

$$\rho_a=h\rho_f(k_s-1). \tag{78}$$

The mass coupling term allows for the force acting on one component of the porous material whenever the other component is accelerated. The coeficient $bF(\omega)$ in

the Eqs. (73) and (74) is the frequency dependent viscous coupling term. At low frequencies, the velocity profile of the air in the pores of the material are approximately given by Poisseulles law. At high frequencies, the velocity profile is approximately constant, except for a small region near the pore walls. The parameters P, Q, R and N in the Eqs. (73) and (74) are elastic constants that can be determined with different gedanken experiments [28, 29]. For a plastic foam, where the compressibility of the frame K_b is much smaller than the compressiblity of the frame material, these parameters can be approximated by:

$$N = \text{shear modulus of the frame} \tag{79}$$

$$P = K_b + \frac{4}{3} N + \frac{(1-h)^2}{h} K_f, \tag{80}$$

$$Q = (1-h) K_f, \tag{81}$$

$$R = h K_f. \tag{82}$$

K_f is the compressibility of the air in the porous material.

Stress-stain relations in porous materials

Stresses are forces per unit area acting on the frame or the fluid of the porous material. Let τ_{ij}^s and τ_{ij}^f be the stress tensor for the frame (s = solid) and the fluid (f = fluid) part of the porous material respectively. The stress-strain relations for the material are than given by:

$$\tau_{ij}^s = [(P-2N)\, \nabla \cdot u + Q \nabla \cdot U]\, \delta_{ij} + N \left(\frac{\partial u_i}{\partial x_j} + \frac{\partial u_j}{\partial x_i} \right), \tag{83}$$

$$\tau_{ij}^f = -hp\delta_{ij} = [R \nabla \cdot U + Q \nabla \cdot u]\, \delta_{ij}. \tag{84}$$

In these equations we can clearly notice the influence of a third coupling mechanism between the movement of the air and frame as a result of the term Q.

Propagation constants in an elastic porous material

The average displacement vectors of the frame and gas can be written as a function of a scalar and a vector potential [30]:

$$u = \nabla \varphi + \nabla x H, \tag{85}$$

$$U = \nabla \psi + \nabla x G \tag{86}$$

Insertion of Eqs. (85) and (86) into (73) and (74) yields two sets of equations: one for longitudinal displacements and one for transverse displacements [31, 32]. For the longitudinal displacements, assumption of harmonic time dependence results in:

$$\varphi = \varphi_1 + \varphi_2, \tag{87}$$

$$\psi = \mu_1\varphi_1 + \mu_2\varphi_2, \tag{88}$$

with:

$$(\nabla^2 + k_1^2)\,\varphi_1 = 0, \tag{89}$$

$$(\nabla^2 + k_2^2)\,\varphi_2 = 0. \tag{90}$$

In these equations, the propagation constants are:

$$k_{1,2} = \frac{\omega^2}{2(PR-Q^2)}\left[(\tilde{\rho}_{11}R + \tilde{\rho}_{22}P - 2\tilde{\rho}_{12}Q) \pm \sqrt{\Delta}\right], \tag{91}$$

$$\Delta = (\tilde{\rho}_{11}R + \tilde{\rho}_{22}P - 2\tilde{\rho}_{12}Q)^2 - 4(PR-Q^2)\,(\tilde{\rho}_{11}\tilde{\rho}_{22} - \tilde{\rho}_{12}^2). \tag{92}$$

Hence, two longitudinal waves φ_1 and φ_2, with a different propagation constant k_1 and k_2, can propagate in a porous material. They are called the slow (P_1) and the fast (P_2) wave. It can be shown that for the slow wave, frame and air move approximately in phase opposition; whereas for the fast wave they move in phase. As a consequence, the slow wave will have much higher attenuation than the fast wave. It is important to note that both the P_1 and the P_2 wave have an amplitude in the solid and in the liquid phase.

For the shear wave we obtain:

$$G = \mu_3 H, \tag{93}$$

with:

$$\nabla^2 H + k_3^2 H = 0,$$

The propagation constant is equal to:

$$k_3^2 = \frac{\omega^2}{N}\,\frac{\tilde{\rho}_{11}\tilde{\rho}_{22} - \tilde{\rho}_{12}^2}{\tilde{\rho}_{22}}. \tag{94}$$

Determination of material parameters

The porosity

In the Biot equation, the porosity h is the amount of air in the porous material that can participate to the sound propagation. For open cell reticulated foams, the porosity can be easily determined if the density ρ of the frame material is known.

$$h = 1 - m/V\rho. \tag{95}$$

In this equation, V is the volume and m is the mass of the sample. For materials containing closed cells the situation is more complicated. Since the gas in the closed cells can not be accessed from the outside, it should be considered as a part of the frame. The major influence of the closed cells is that they modify the compressibility of the frame. The acoustic porosity can be measured with a device shown in Fig. 13.

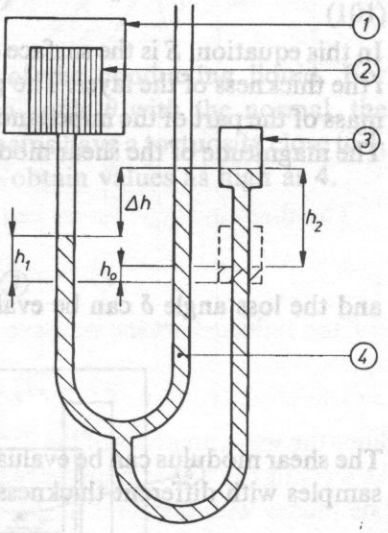

Fig. 13. Measuring set-up for the determination of the porosity *h*. *1* — sample volume, *2* — sample, *3* — controlling gas volume, *4* — manometer.

The porosity of reticulated foams is typically higher than 0.95. For most non-reticulated foams a porosity higher than 0.90 is measured, indicating that a lot of the cell membranes have been ruptured or pierced.

The shear modulus

Since losses due to the viscoelasticity of the frame have to be taken into account, the dynamic shear modulus should be used in the equation of Biot. The dynamic shear modulus can be several times higher than its static value. The shear modulus can be measured with a divice shown in Fig. 14. Two samples of equal thickness are glued

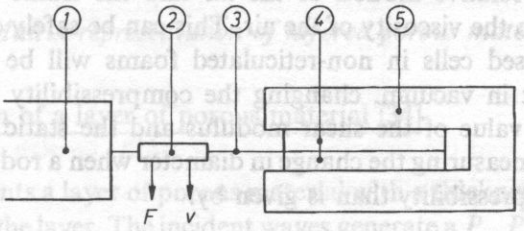

Fig. 14. Measuring set-up for the determination of the shear modulus *N*. *1* — Brüel and Kjaer 4810 shaker, *2* — Brüel and Kjaer 8001 impedance head, *3* — movable plate, *4* — sample, *5* — rigid plate.

between a solid wall and a thin movable plate. A shaker generates shear waves in the two layers. An impedance head measures the force exercised on the plate, together with the velocity of the plate. These two outputs can be fed to a two-channel FFT analyzer and the frequency response function is given by

$$\frac{F}{v} = -i\left(2S\sqrt{\rho N}\,\mathrm{cotg}\left(\sqrt{\frac{\rho}{N}}\,\omega l\right) - m\omega\right) \tag{96}$$

In this equation, S is the surface of the sample, ρ the density, N the shear modulus and l the thickness of the layer. The parameter m is the mass of the movable plate plus the mass of the part of the impedance head that participates in the movement of the plate. The magnitude of the shear modulus can be evaluated from the resonance frequency:

$$|N| = \frac{ml^2}{2S}\,\omega_{\mathrm{res}}^2 \tag{97}$$

and the loss angle δ can be evaluated from the width 2σ of the resonance peak

$$\delta = \frac{2\sigma}{\omega_{\mathrm{res}}} \tag{98}$$

The shear modulus can be evaluated as a function of frequency by measuring different samples with different thickness l.

The frame compressibility

The frame compressibility K_b can be evaluated from the shear modulus and the Young modulus E, which can be measured on a rod of porous material vibrating in longitudinally [33]

$$K_b = \frac{EN}{3\,(3N-E)} \tag{99}$$

The dynamic measurement of the Young modulus of the frame should be performed in vacuum, since the relative motion of the air and the frame influence the results considerably, due to the viscosity of the air. This can be safely done with reticulated foams, but the closed cells in non-reticulated foams will be destroyed when the material is brought in vacuum, changing the compressibility of the frame can be obtained from the value of the shear modulus and the static measurement of the Poisson ratio ν, by measuring the change in diameter when a rod of porous material is stretched. The compressibility than is given by:

$$K_b = \frac{2}{3}\,N\,\frac{1+\nu}{1-2\nu} \tag{100}$$

The tortuosity

The tortuosity k_s can be measured with a device if the frame material is an electrical insulator (Fig. 15). The air in the pores is replaced by an electrical conducting liquid, and the electrical resistivity r of the slab of the material is measured. The tortuosity is than given by:

$$k_s = h(r/r_f) \tag{101}$$

In this equation r_f is the electrical resistivity of the conducting liquid. For a material with parallel cylindrical pores making an angle θ with the normal, the tortuosity is equal to $k_s = 1/\cos^2\theta$. Most reticulated foams have a tortuosity close to 1, whereas the tortuosity of non-reticulated foams can obtain values as high as 4.

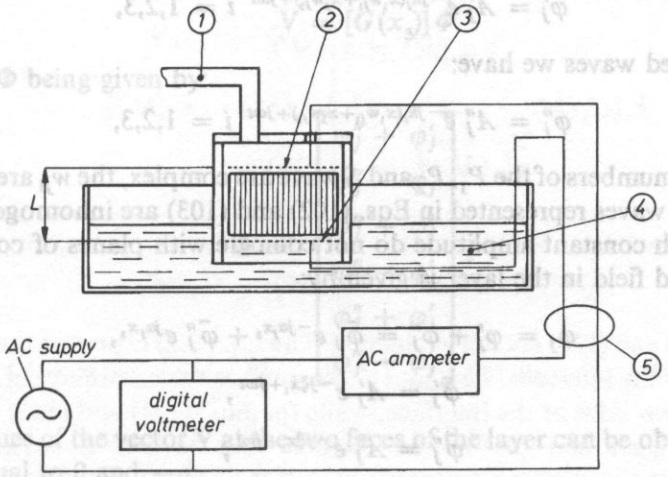

Fig. 15. Measuring set-up for the determination of the tortuosity k_s. *1* — pumping system, *2* and *3* — grid electrodes, *4* — electrolyte fluid, *5* — electric connections.

3.2 Matrix representation of layered porous materials

Matrix formalism of a layer of porous material [34]

Figure 16 represents a layer of porous material with a thickness d. A plane wave is incident from above the layer. The incident waves generate a P_1, P_2 and a S wave in the porous layer. At $x_3 = 0$ each of these waves is reflected and generates a P_1, P_2 and S wave.

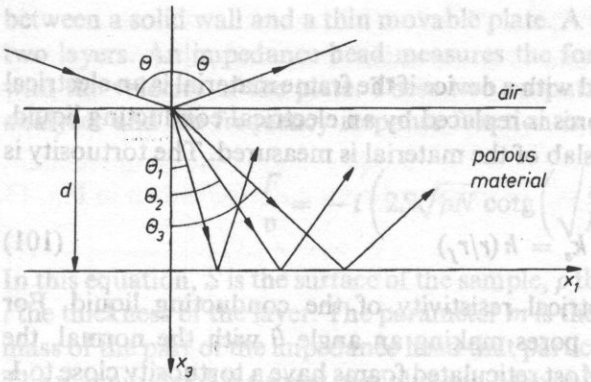

Fig. 16. A layer of foam with a thickness d, stuck on a hard backing.

The three incident waves can be represented with three displacement potentials:

$$\varphi_j' = A_j' e^{-jk_j(x_1 w_{j1} + x_3 w_{j3}) + j\omega t} \quad i = 1,2,3, \tag{102}$$

For the reflected waves we have:

$$\varphi_j'' = A_j'' e^{-jk_j(x_1 w_{j1} + x_3 w_{j3}) + j\omega t} \quad i = 1,2,3, \tag{103}$$

Since the wave numbers of the P_1, P_2 and S wave are complex, the w_{ji} are complex too. As a result the waves represented in Eqs. (102) and (103) are inhomogeneous waves. The planes with constant amplitude do not coincide with planes of constant phase. The total sound field in the layer is given by:

$$\varphi_j = \varphi_j' + \varphi_j'' = \bar{\varphi}_j' e^{-j\alpha_j x_3} + \bar{\varphi}_j'' e^{j\alpha_j x_3}, \tag{104}$$

$$\bar{\varphi}_j' = A_j' e^{-j\zeta x_1 + j\omega t}, \tag{105}$$

$$\bar{\varphi}_j'' = A_j'' e^{-j\zeta x_1 + j\omega t}, \tag{106}$$

$$\alpha_j = k_j w_{j3}, \zeta = k_j w_{j1}. \tag{107}$$

The sound field in the layer is known if the six amplitudes A_j' and A_j'' are known. The amplitudes can be calculated when six independent stresses and displacements are known at one of the two phases of the layer. The six independent stresses and displacements which have been chosen are: u_1, u_3, U_3, $\tau_{33}{}^s$ $\tau_{13}{}^s$ $\tau_{33}{}^f$.
Let **V** be the vector:

$$\mathbf{V} = [u_1, u_3, U_3, \tau_{33}^s, \tau_{13}^s, \tau_{33}^f]^T. \tag{108}$$

The displacement and the stress components can be written as a function of the potentials with the aid of the Eqs. (83) to (88).

$$u_1 = \frac{\partial \varphi_1}{\partial x_1} + \frac{\partial \varphi_2}{\partial x_1} - \frac{\partial \varphi_3}{\partial x_3}, \tag{109}$$

$$u_3 = \frac{\partial \varphi_1}{\partial x_3} + \frac{\partial \varphi_2}{\partial x_3} - \frac{\partial \varphi_3}{\partial x_1}, \tag{110}$$

$$U_3 = \mu_1 \frac{\partial \varphi_1}{\partial x_3} + \mu_2 \frac{\partial \varphi_2}{\partial x_3} - \mu_3 \frac{\partial \varphi_3}{\partial x_1}, \tag{111}$$

$$\tau^s_{33} = (P-2N)\,\nabla \cdot u + 2N \frac{\partial \mu_3}{\partial x_3}, \tag{112}$$

$$\tau^s_{12} = N\left(\frac{\partial \mu_3}{\partial x_1} + \frac{\partial \mu_1}{\partial x_3}\right), \tag{113}$$

$$\tau^f_{33} = R\nabla \cdot U + Q\nabla \cdot u. \tag{114}$$

These equations can be written in matrix form:

$$\mathbf{V} = [G(x_3)]\,\Phi \tag{115}$$

the vector Φ being given by:

$$\Phi = \begin{bmatrix} \varphi''_j + \varphi'_j \\ \varphi''_j - \varphi'_j \\ \varphi''_j + \varphi'_j \\ \varphi''_j - \varphi'_j \\ \varphi''_j + \varphi'_j \\ \varphi''_j - \varphi'_j \end{bmatrix}, \tag{116}$$

The values of the vector $\mathbf{V}$ at the two faces of the layer can be obtained by putting x_3 resp. equal to 0 and $-d$:

$$\mathbf{V}(x_3 = -d) = [G(-d)]\,\Phi \tag{117}$$

$$\mathbf{V}(x_3 = 0) = [G(0)]\,\Phi, \tag{118}$$

Inverting $[G(0)]$ gives a relation between the values V and the two faces of the layer:

$$V(x_3 = -d) = [G(-d)]\,[G(0)]^{-1}\,V(x_3 = 0). \tag{119}$$

The matrix $[\gamma] = [G(-d)]\,[G(0)]^{-1}$ is an acoustic transfer matrix for the layer.

Transfer matrix of a layered system

Figure 17 represents two layers of porous material in contact with each other. M and M' are two points in each layer, close to the interface R. In the general case,

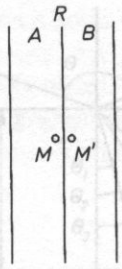

Fig. 17a. Two layers of foam in contact with each other.

characterizing the interface R requires the introduction of a coefficient of permeability for the interface [35].

However, for high porosity foams a simple transition matrix for the interface can be constructed. The continuity at the interface are:

$$u_1(M) = u_1(M'), \tag{120}$$

$$u_3(M) = u_3(M') \tag{121}$$

$$h_a[U_3(M) - u_3(M)] = h_b[U_3(M') - u_3(M')], \tag{122}$$

$$\tau^f_{33}(M)/h_a = \tau^f_{33}(M')/h_b, \tag{123}$$

$$\tau^s_{13}(M) = \tau^s_{13}(M), \tag{124}$$

$$\tau^s_{33}(M) + \tau^f_{33}(M') = \tau^f_{33}(M') + \tau^f_{33}(M'). \tag{125}$$

The Eqs. (120) and (121) are self explaining. The Eq. (122) expresses the continuity of the fluid across the interface. The Eq. (123) expresses the continuity of pressure in the pores at the two sides of the interface, while the Eqs. (124) and (125) express the continuity of the shear and total normal force at both sides of the interface. From these equations, we obtain a transfer matrix $[\gamma_{ab}]$. If the porosities of the two materials are equal, the transition matrix is unity. The transfer matrix for the layered material is given by:

$$[\gamma] = [\gamma_a]\,[\gamma_{ab}]\,[\gamma_b] \tag{126}$$

This method can be easily extended in the case of more than two layers.

3.3 Applications

One layer of foam, stuck on a hard backing

Figure 10 represents one layer of foam, stuck on a hard backing. The edge conditions at $x_3 = 0$ are:

$$u_1 = u_3 = U_3 = 0, \tag{127}$$

and at $x_3 = -d$:

$$\tau_{13}^s = 0, \tag{128}$$

$$\tau_{33}^s = -(1-h)\,p \tag{129}$$

$$\tau_{33}^f = -hp, \tag{130}$$

$$\omega\,[(1-h)\,u_3 - hU_3] = \frac{p}{Z} \tag{131}$$

p is the pressure in the air above the layer, close to the surface. The vector Eq. (108) can be written as:

$$\mathbf{V}(x_3 = -d) = \begin{bmatrix} 0 \\ 0 \\ 0 \\ \tau_{33}^s \\ \tau_{13}^s \\ \tau_{33}^f \end{bmatrix}_{x_3 = -d}. \tag{132}$$

These equations can be solved for the normal surface impedance Z:

$$Z = (\Delta_5\Delta_8 - \Delta_6\Delta_7)\times \tag{133}$$

$$\times\,[(1-h)^2\,(\Delta_2\Delta_7 - \Delta_1\Delta_8)\,h(1-h)\,(\Delta_6\Delta_1 - \Delta_2\Delta_5 - \Delta_8\Delta_3 + \Delta_4\Delta_7) + h^2(\Delta_3\Delta_6\Delta_4\Delta_5)]^{-1},$$

$$\Delta_1 = \gamma_{24}\gamma_{55} - \gamma_{25}\gamma_{54},$$

$$\Delta_2 = \gamma_{26}\gamma_{55} - \gamma_{25}\gamma_{56},$$

$$\Delta_3 = \gamma_{34}\gamma_{55} - \gamma_{35}\gamma_{54},$$

$$\Delta_4 = \gamma_{36}\gamma_{55} - \gamma_{35}\gamma_{56},$$

$$\Delta_5 = \gamma_{44}\gamma_{55} - \gamma_{45}\gamma_{54},$$

$$\Delta_6 = \gamma_{46}\gamma_{55} - \gamma_{45}\gamma_{56},$$

$$\Delta_7 = \gamma_{64}\gamma_{55} - \gamma_{65}\gamma_{54},$$

$$\Delta_8 = \gamma_{66}\gamma_{55} - \gamma_{65}\gamma_{56}.$$

Figure 17b shows the normal surface impedance of a 2 cm thick partially reticulated foam layer at different angles of sound incidence. The parameters of the layer are given in the figure caption. It must be emphasized that, since the coupling between the

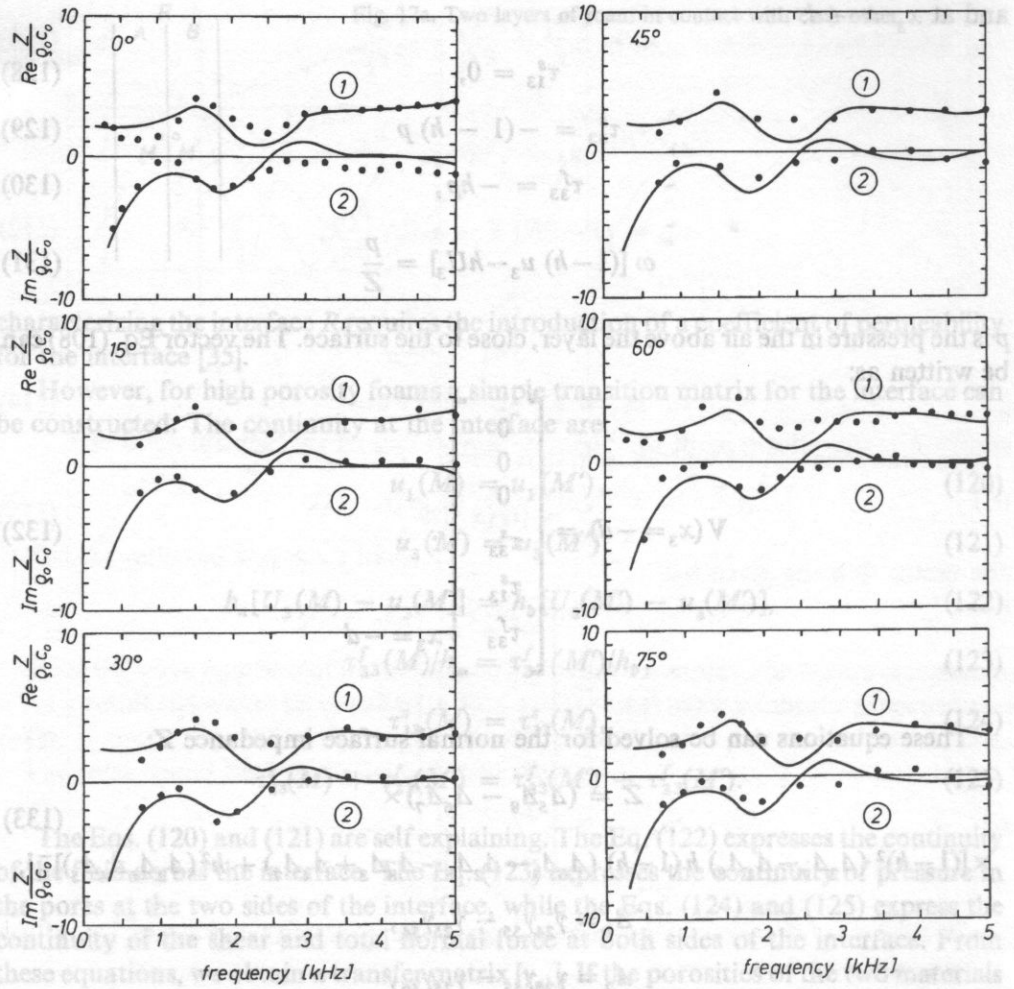

Fig. 17b. Real (1) and imaginary (2) part of the normal surface impedance of a 2 cm thick foam layer, stuck on a hard backing, as a function of frequency. ——— equation (133), • angle of incidence (experimental results), a) $\theta = 0°$, b) $\theta = 15°$, c) $\theta = 30°$, d) $\theta = 45°$, e) $\theta = 60°$, f) $\theta = 75°$. Foam parameters: $N = 4 \times 10^5$ N/m², $d = 2$ cm, $k_s = 4.5$, $h = 0.93$, $\rho_1 = 30$ kg/m³, C = 2.4, $\nu = 0.2$, $\sigma = 55000$ Ns/m⁴.

movement of the frame and the air in this material is high (large flow resistivity and high tortuosity) a one wave approximation as in paragraph 2, for the single wave propagation, is not valid.

A layer of porous material, covered with an impervious screen [36]

In a lot of applications, the foam has been covered with an impervious screen, in order to protect it from chemical agents or heat. The screen can also be applied to

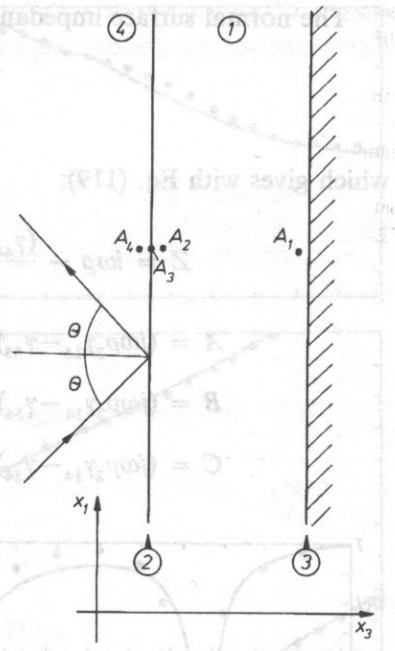

Fig. 18. A layer of foam with an impervious screen. 1) layer of foam, 2) impervious screen, 3) hard backing, 4) air.

increase the acoustic absorption in the low frequency region. Figure 18 represents a foam layer, covered with an impervious membrane. A_3 is a point of the membrane. A_4 and A_2 are points in the air above the layer and in the porous layer, close to the membrane. The equations of motion of the membrane are:

$$-\omega^2\rho_1 u_3(A_3) = \tau^s_{33}(A_2) + \tau^f_{33}(A_2) - \tau^s_{33}(A_4), \tag{134}$$

$$-\omega^2\rho_2(A_3) = \tau^s_{13}(A^2), \tag{135}$$

with:

$$\rho_1 = \rho - Tk^2\sin\theta/\omega^2 \tag{136}$$

$$\rho_2 = \rho - Sk^2\sin\theta/\omega^2 \tag{137}$$

T is the tension in the membrane and S is the stiffness of the membrane. The membrane causes the following edge conditions:

$$u_3(A_2) = U_3(A_2) = u_3(A_3) = U_3(A_4) \tag{138}$$

$$u_1(A_2) = u_1(A_3) \tag{139}$$

At A_1 we have

$$u_1(A_1) = u_3(A_1) = U_3(A_1) = 0 \tag{140}$$

The normal surface impedance is given by:

$$Z = \frac{-\tau^f_{33}(A_4)}{j\omega\, U_3(A_4)} \tag{141}$$

which gives with Eq. (119):

$$Z = i\omega\rho - \frac{(\gamma_{44}+\gamma_{64})A-(\gamma_{45}+\gamma_{65})B+(\gamma_{46}+\gamma_{66})C}{(\gamma_{24}A-\gamma_{25}B+\gamma_{26}C)} \tag{142}$$

$$A = (j\omega\rho_2\gamma_{15}-\gamma_{55})(\gamma_{26}-\gamma_{36}) - (j\omega\rho_2\gamma_{16}-\gamma_{56})(\gamma_{25}-\gamma_{35})$$

$$B = (j\omega\rho_2\gamma_{14}-\gamma_{54})(\gamma_{26}-\gamma_{36}) - (j\omega\rho_2\gamma_{16}-\gamma_{56})(\gamma_{24}-\gamma_{34})$$

$$C = (j\omega\rho_2\gamma_{14}-\gamma_{54})(\gamma_{25}-\gamma_{35}) - (j\omega\rho_2\gamma_{15}-\gamma_{55})(\gamma_{24}-\gamma_{34})$$

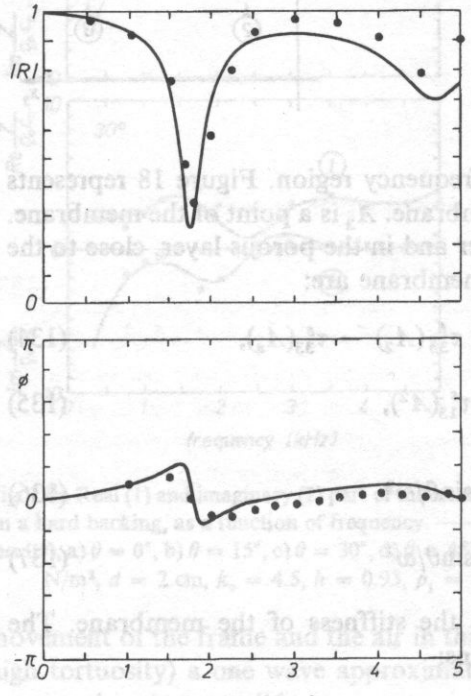

Fig. 19. Magnitude and phase of the reflection coefficient of a plastic foam, covered with an impervious screen. Material parameters: $T = S = 0$, $\rho = 0.02$ kg/m³, thickness $= 25 \times 10^{-6}$ m. ——— equations 47 and 142, • experimental results.

Figure 19 represents the reflection coefficient at normal sound incidence, calculated form the Eqs. (47) and (142), of a foam layer with an impervious screen. As a comparison Fig. 20 shows the reflection coefficient of the same foam layer without the impervious screen.

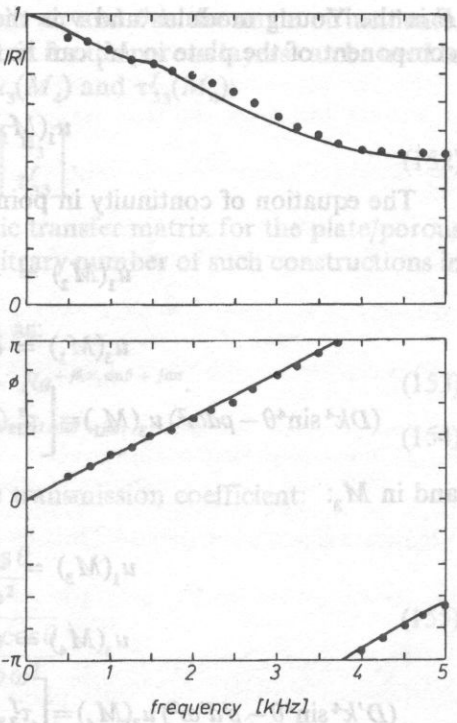

Fig. 20. Magnitude and phase of the reflection coefficient of the foam layer as in Fig. 19, but without the screen.

The acoustic transmission through layered systems

The acoustic insulation properties of foam layers, sandwiched between elastic solid plates has a wide range of application, including buildings, cars, airplanes and industrial plants. A reliable theoretical model to predict the acoustic insulation of the partitions can save a lot of development time. We can use the matrix formalism, developed in the preceding paragraph, to calculate the sound transmission through such layered systems. Figure 21 represents a plate/porous layer/plate system. Let u be the displacement of the plate and let M_1 and M_4 be two points at the left side, respectively the right side of the plates. The equation of motion of the plate, glued on a layer is given by [37]:

$$D\frac{\partial^4 u_3}{\partial x_1^4} + \rho d\frac{\partial^2 u_3}{\partial t^2} = [\tau_{33}^s(M_2)+\tau_{33}^f(M_2)-\tau_{33}^f(M_1)] + \frac{d}{2}\left[\frac{\partial \tau_{13}^s}{\partial x_1}(M_2)\right]. \quad (143)$$

In this equation, ρ is the density and d the thickness of the plate, D, the bending stiffness of the plate is given by:

$$D = \frac{Ed^2}{12(1-\nu^2)}. \quad (144)$$

E is the Young modulus and ν is the Poisson ratio of the plate material. The x_1 component of the plate in M_1 can be written as:

$$u_1(M_1) = -\frac{d}{2}\frac{\partial u_3}{\partial x_1}. \tag{145}$$

The equation of continuity in point M_1 are:

$$u_1(M_2) = -j\frac{d}{2}k\sin\theta\, u_3(M_1), \tag{146}$$

$$u_3(M_1) = u_3(M_2) = U_3(M_2), \tag{147}$$

$$(Dk^4\sin^4\theta - \rho d\omega^2)\, u_3(M_1) = \left[\tau_{33}^s(M_2) - \tau_{33}^f(M_2) - \tau_{33}^f(M_1) + \frac{d}{2}\frac{\partial \tau_{13}}{\partial x_1}(M_1)\right], \tag{148}$$

and in M_3:

$$u_1(M_3) = +j\frac{d'}{2}k\sin\theta\, u_3(M_4), \tag{149}$$

$$u_3(M_4) = u_3(M_3) = U_3(M_3), \tag{150}$$

$$(D'k^4\sin^4\theta - \rho' d'\omega^2)\, u_3(M_4) = \left[\tau_{33}^f(M_4) + \tau_{33}^f(M_3) - \tau_{33}^s(M_3) + \frac{d'}{2}\frac{\partial \tau_{13}}{\partial x_1}(M_3)\right]. \tag{151}$$

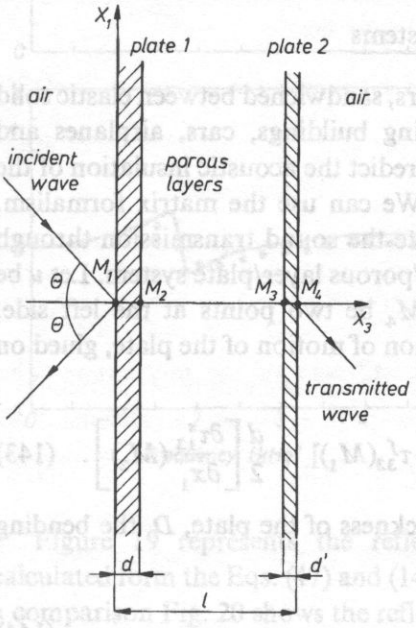

Fig. 21. A porous layer placed between two plates.

In these equations, k is the wave number in air and θ is the angle of incidence. These equations, together with the transfer matrix for the porous layers can be used to express $u_3(M_1)$ and $\tau^f_{33}(M_3)$ as a function of $u_3(M_4)$ and $\tau^f_{33}(M_4)$:

$$\begin{bmatrix} u_3 \\ \tau^f_{33} \end{bmatrix}_{M_1} = [\beta] \begin{bmatrix} u_3 \\ \tau^f_{33} \end{bmatrix}. \tag{152}$$

The matrix $[\beta]$ can be considered as an acoustic transfer matrix for the plate/porous material/plate system. The extension to an arbitrary number of such constructions in series is straightforward.

The sound field in M_1 and M_4 can be written as:

$$\varphi(M_1) = e^{+jkx_1 \sin\theta + j\omega t} + Re^{+jkx_1 \sin\theta + j\omega t}. \tag{153}$$

$$\varphi(M_4) = Te^{+jkx_1 \sin\theta - jkl\cos\theta + j\omega t}. \tag{154}$$

With the Eqs. (40) and (41) we obtain for the transmission coefficient:

$$T = \frac{2j \dfrac{k\cos\theta}{\rho\omega^2}}{X + Y \dfrac{jk\cos\theta}{\rho\omega^2}}. \tag{155}$$

$$X = \left(\beta_{11} \frac{jk\cos\theta}{\rho\omega^2} - \beta_{12}\right) e^{-jkl\cos\theta}. \tag{156}$$

$$Y = \left(\beta_{21} \frac{jk\cos\theta}{\rho\omega^2} - \beta_{22}\right) e^{-jkl\cos\theta}. \tag{157}$$

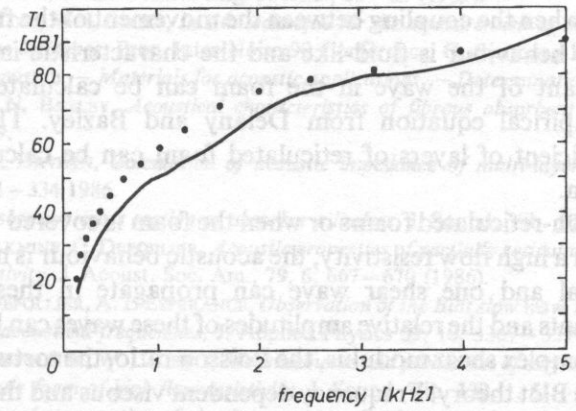

Fig. 22. Transmission loss factor of a steel plate/foam/steel plate system. Steel data: $d = 0.001$ m, $D = 16.3$ $(1+0.01j)$ Nm. Foam parameter: $d = 0.05$ m.

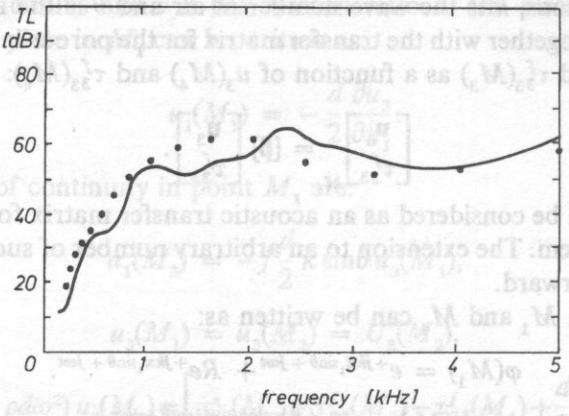

Fig. 23. Transmission loss factor of a plywood/foam/plywood system. Plywood data: $d = 0.085$ m, $D = 390$ $(1+0.04j)$ Nm. Foam parameter: $d = 0.05$ m.

The transmission loss factor TL is equal to (38):

$$TL = -10\log\left(2\int_0^{\pi/2} |T|^2 \sin\theta\cos\theta\, d\theta\right). \tag{158}$$

The Figure 22 shows the transmission loss factor of a 5 cm thick foam layer, sandwiched between two steel plates. Figure 23 shows the transmission loss of a parition made of a plywood panel, a 5 cm thick polyurethane foam layer and a second plywood panel. The plate and foam parameters are given in the figure caption.

Conclusions

The acoustic characteristics (sound absorption and transmission) of absorbing materials can be calculated from independent measurable parameters. In the case of reticulated foams, when the coupling between the movement of the frame and the air is weak, the acoustic behaviour is fluid-like and the characteristic impedance and the propagation constant of the wave in the foam can be calculated from the flow resistivity and empirical equation from Delany and Bazley. The reflection and transmission coefficient of layers of reticulated foam can be calculated easily with a matrix formalism.

In the case of non-reticulated foams or when the foam is covered with a membrane, plate of facing with a high flow resistivity, the acoustic behaviour is more complicated. Two compressional and one shear wave can propagate in these materials. The propagation constants and the relative amplitudes of these waves can be calculated from the porosity, the complex shear modulus, the Poisson ratio, the tortuosity and the flow resistivity using the Biot theory. Frequency dependent viscous and thermal effects have to be taken into account. A layer of material can be characterized acoustically with a 6×6 matrix. The matrix formalism allows for a straightforward calculation of the reflection and transmission coefficient of a variety of layered systems.

References

[1] L.L. BERANEK, *Acoustic impedance of porous materials*, J. Acoust. Soc. Am., **13**, p. 248–260 (1942).

[2] L.L. BERANEK, *Acoustical properties of homogeneous, isotropic rigid tiles and flexible blankets*, J. Acoust. Soc. Am., **19**, 4, 556–568 (1947).

[3] P.M. MORSE, R.H. BOLT, R.L. BROWN, *Acoustical impedance and sound absorption*, J. Acoust. Soc. Am., **12**, 2 (1940)

[4] C. ZWIKKER, C.W. KOSTEN, *Sound absorbing materials*, Elsevier Publ. Comp. New York 1949.

[5] K. ATTENBOROUGH, *Acoustical characteristics of porous materials*, Physics Reports, **82**, 3, 179–227 (1982)

[6] *International Standard ISO 354, Measurement of sound absorption in a reverberant room, incl. annex D, Test specimen mountings for sound absorbing tests*, 1985, 1991 (ISO/TC 43/SC 2/WG 7).

[7] *International Standard Document ISO/CD 11654 — Acoustics — Rating of sound absorption*, 1992 (ISO/TC 43/SC 2/WG 20).

[8] *International Standard Document ISO/CD 10534 — Determination of sound absorption coefficient and impedance or admittance by the impedance tube method* 1991.

[9] *Brüel and Kjaer Document, Two microphone impedance measurement tube — type* 4206, 1991.

[10] A. COPS, W. LAURIKS, *Application of new two-microphone techniques to measure the sound absorption characteristics of acoustic materials*, Proc. Second Int. Congress on Acoustic Intensity, p. 511–518, 1985.

[11] J.F. ALLARD, B. SIEBEN, *Measurement of acoustic impedance in a free field with two microphones and a spectrum analyzer*, J. Acoust. Soc. Am., **77**, 1617–1618 (1985).

[12] M. MINTEN, A. COPS, W. LAURIKS, *Absorption characteristics of an acoustic material at oblique incidence measured with the two-microphone technique*, J. Sound and Vibration, **120**, 3, 499–510 (1988).

[13] J.Y. CHUNG, D.A. BLASER, *Transfer function method of measuring induct acoustic properties, I. Theory*, J. Acoust. Soc., **68**, 3, 907–913 (1980).

[14] J.Y. CHUNG, D.A. BLASER, *Transfer function of measuring induct acoustic properties, II. Experiment*, J. Acoust. Soc. Am., **68**, 3, 914–921 (1980).

[15] W.T. CHU, *Transfer function technique for impedance and absorption measurements in an impedance tube using a single microphone*, J. Acoust. Soc. Am., **80**, 2, 555–560 (1992).

[16] J.F. ALLARD, Y. CHAMPOUX, *In situ two microphone technique for measurement of the acoustic surface impedance of materials*, Noise Control Eng. Journal, 15–23 (1989).

[17] J.F. ALLARD, A. COPS, W. LAURIKS, *In situ technique for the measurement of the surface impedance at normal and oblique incidence*, Proc. Inter-Noise 90 Conference, Gothenburg 1990.

[18] *ISO/DIS 9053 Acoustics — Materials for acoustic applications — Determination of airflow resistance.*

[19] M.E. DELANY, E.N. BAZLEY, *Acoustical characteristics of fibrous absorbent materials*, NPL Aero Report Ac37 1969.

[20] L.P. DUNN, W.A. DAVERN, *Calculation of acoustic impedance of multi-layered absorbers*, Applied Acoustics, **19**, 321–334 1986.

[21] F.P. MECHEL, *Absorption cross section of absorber cilinders*, J. Sound. Vib. **107**, 1, 131–148 (1986).

[22] J.F. ALLARD, A. AKNINE, C. DEPOLLIER, *Acoustic properties of partially reticulated foams with high and medium flow resistivity*, J. Acoust. Soc. Am., **79**, 6, 667–670 (1986).

[23] J.F. ALLARD, C. DEPOLLIER, A. L'ESPERANCE, *Observation of the Biot slow wave in a plastic foam of high flow resistance at acoustical frequencies*, J. Applied Physics **59**, 10, 3367–3370 (1986).

[24] J.F. ALLARD, C. DEPOLLIER, W. LAURIKS, *Measurements and prediction of surface impedance at oblique incidence of a plastic foam of high flow resistivity*, J. Sound. Vib. **132**, 1, 51–60 (1989).

[25] M.A. BIOT, *Theory of propagation of elastic waves in a fluid saturated porous solid, I. Low frequency range*, J. Acoust. Soc. Am., **28**, 1, 168–178 (1956).

[26] M.A. BIOT, *Theory of propagation of elastic waves in a fluid saturated porous solid, II. High frequency range*, J. Acoust. Soc. Am., **28**, 1, 179–191 (1956).

[27] D.L. JOHNSON, *Recent developments in the acoustic properties of porous media*, Proc. Int. School of Physics Enrico Fermi, Course XCIII ed. D. Sette, North Holland Phys. Pub. 1986.

[28] M.A. BIOT, D.G. WILLIS, *The elastic coefficients of the theory of consolidation*, J. Appl. Mech., 594–601 (1957).

[29] C. DEPOLLIER, J.F. ALLARD, W. LAURIKS, *Biot theory and stress-strain relations in porous sound absorbing materials*, J. Acoust. Soc. Am., **84**, 6, 2277–2279 (1988).

[30] W.M. EWING, W.S. JARDETZKY, F. PRESS, *Elastic waves in layered media*, Mc Graw–Hill Book Co New York 1957.

[31] H. DERESIEWICZ, *The effect of boundaries on wave propagation in liquid filled porous solids. I. Reflection of plane waves at a free plane boundary non-dissipative case*. Bull. Seism. Soc. Am., **50**, 4, 599–607 (1960).

[32] H. DERESIEWICZ, J.T. RICE, *The effect of boundaries on wave propagation in liquid filled porous solids. III. Reflection of plane waves at a free plane boundary general case*, Bull. Seism. Soc. Am., **52**, 3, 595–625 (1962).

[33] T. PRITZ, *Transfer function method for investigating the complex modulus of acoustic materials: rod-like specimen*, J. Sound. Vib., **81**, 3, 359–376 (1982).

[34] J.F. ALLARD, C. DEPOLLIER, P. REBILLARD, W. LAURIKS, A. COPS, *Inhomogeneous Biot waves in layered media*, J. Appl. Phys., **66**, 6, 2279–2284 (1989).

[35] H. DERESIEWICZ, R. SKALAK, *On uniqueness of dynamic poroelasticity*, Bull. Seism. Soc. Am., **52**, 4, 783–788 (1963).

[36] W. LAURIKS, A. COPS, J.F. ALLARD, C. DEPOLLIER, P. REBILLARD, *Modelization at oblique incidence of layered porous materials with impervious screens*, J. Acoust. Soc. Am., **87**, 3, 1200–1206 (1990).

[37] L. LANDAU, E. LIFCHITZ, *Théorie d'élasticité*, Edition MIR 1967.

[38] A.D. PIERCE, *Acoustics, an introduction to its physical principles and applications*, Mc Graw Hill Book Co., New York 1986.

ARCHIVES OF ACOUSTICS
18, 2, 249–260 (1993)

ANALYSIS OF PARAMETERS INFLUENCING THE NOISE EMITTED BY HIGH-VOLTAGE POWER TRANSMISSION LINES

Z. ENGEL AND T. WSZOŁEK

Institute of Mechanics and Vibroacoustics Mining and Metallurgy Academy
(30-059 Kraków, al. Mickiewicza 30)

The paper deals with the phenomena of the noise emitted by high voltage overhead power transmission lines. It contains an analysis of technical parameters of the transmission line: voltage, voltage gradient, configuration as well as technical conditions of the bundle of conductors. Test results for various weather and environmental conditions have been presented, and their influence upon the level and character of the emitted noise spectrum has been discussed. The atmospheric conditions have been pointed out which essentially influence the acoustic climate of the environment. Special attention has been paid to the noise emitted during intensive corona effect, and to the second harmonic of the power transmission line which appears then in the acoustic spectrum.

1. Introduction

The problem of noise emitted by overhead transmission lines of alternating current exists under bad atmospheric conditions only. Level of the emitted noise can then increase even by 15 dB or more and reach a value exceeding 50 dB [1]. In the noise emitted by an operating transmission line two characteristic components can be distinguished: 1) broad-band noise described alternatively as the sound of "frying" or "crackling" or "hissing" [6] and 2) a pure tone of the second harmonic of the transmission line frequency, being heard as a "hum". Broad-band noise is produced by electric discharges on the surface of the lines. Hum noise is generated by the discharge frequency of the given source. It appears in the case of regular discharges and makes the line noise arduous. Bad atmospheric conditions, such as rain, drizzle, snow and considerable humidity reduces the threshold of microdischarges.

An operating transmission line is a source of numerous nuisances for the environment (radio and television interference, ionization of air), but the most troublesome of them is noise, its effecting range being the greatest. It is now treated as the main nuisance in designing new transmission lines of alternating [7] and direct current, particularly in the countries a high degree of urbanization.

2. Sources of noise emitted by transmission line

Noise emitted by high voltage transmission lines is directly connected with the phenomenon of corona effect. When the voltage surface gradient of the line exceeds the critical value, called also "rupture gradient", random microdischarges occur. Each of them generates an acoustic wave, causes radio and television interference and loss of electric power.

According to Peek, the loss of active power due to the corona effect can be expressed by the following formula (for $f = 50$ Hz and $\delta = 1$):

$$\Delta P = 0.18 \sqrt{\frac{r}{b_{av}}} \left(U_f - U_{cr} \right)^2 .$$

In practice these losses are of the order of several kW/km to dozens kW/km in the case of the transmission lines of voltage exceeding 1.000 kV.

The critical value of the voltage gradient is strictly dependent upon the phase critical value of the line u_{cr}, which can be expressed by the following formula:

$$U_{cr} = 48.9\, m_a\, m_p\, \delta\, r \log \frac{b_{av}}{r} ,$$

where U_{cr} — critical phase voltage of the line kV, m_a — coefficient dependent upon wheather conditions, ranging within the limits from 0.8 to 1 for bad and fair weather, respectively, m_p — coefficient dependent upon the state of the surface of the conductor, δ — relative air density, r — radius of the conductor for the bundle conductors an effective radius, [cm], b_{av} — average geometrical distance between the individual conductors, [cm].

The number of the microdischarges depends upon:

— technical parameters of the line (the voltage and voltage surface gradient of the conductors, design of the bundle of conductors, surface condition, etc.),

— atmospheric conditions,

— environment conditions (dirt covering the conductor surface, impurities of air, etc.).

Technical parameters of the line determine the voltage surface gradient of the conductor, whose maximum value determines, in turn, the corona effect intensity. It can be calculated from the following relationship [3]:

$$E = \frac{U}{\sqrt{3}\; nr \ln \dfrac{b_{av}}{\sqrt[n]{rc^{n-1}}}} \left[1 + \frac{c}{r} \left[2(n-1) \sin \frac{\pi}{n} \right] \right],$$

where E — voltage surface gradient of the conductor, [kV/cm], U — line-to-line voltage, [kV], r — conductor bundle radius, [cm], n — number of the conductors in a bundle, c — distance between adjacent sub-conductors in the bundle, [cm], b_{av} — average distance between the adjacent conductors, [cm].

As it may be seen from the relationship given above, the voltage gradient depends directly upon the voltage and geometry of the bundle of sub-conductors. It increases with increasing voltage and decreases with increasing both the number of the

sub-conductors and the effective bundle radius. Formulating the calculation procedures in order to predict the noise level, the research centres assume various forms of relationships which describe the influence of the line parameters on the phenomena under study. Table 1 presents the influence of the most essential line parameters on the level of the emitted noise and the forms of the calculation procedures employed by various research centres. These empirical procedures are based on the measurement data for both the test lines and the existing lines, the first data being called the cage data.

Table 1. Comparison of calculation procedures of noise of the existing AC-lines

Method	Voltage surface gradient	Conductor diameter	Number of sub-conductor in a bundle
BPA	$130\log E/E_0$	$44\log d/d_0$	$10\log n/n_0$
Westing-house	$120\log E/E_0$	$60\log d/d_0$	$10\log n/n_0$
Ontario Hydro	$100\log E/E_0$	$40\log d/d_0$	$10\log n/n_0$
ENEL	$85\log E/E_0$	$45\log d/d_0$	$18\log n/n_0$
IREQ	$72\log E/E_0$	$48.5\log d/d_0$	$22.7\log n/n_0$
EdF	$2.5\ (E-E_0)$* $1.5\ (E-E_0)$**	$4.5\ (d-d_0)$	$15\log n/n_0$

* — $15<E<20$ kV/cm
** — $20<E<25$ kV/cm

The procedure given above are valid for rain conditions. The maximum discrepancies result from considering the voltage gradient and number of sub-conductors in a bundle. Greater influence of the gradient of electric field on the conductor surface is obtained, if the procedure based on the data for the existing lines are replaced by procedures employing the data for the test lines.

The non-uniformity of the surface of the conductors is also an important factor: at sharp curvatures of the surface one can observe a greater accumulation of electric charges being a source of micro-discharges. In the case of a perfectly smooth surface of the conductor, the discharge phenomenon does not occur during fair weather. But in practice, line conductors consist of wires with definite curvature radii and definite surface smoothness. For the existing conditions the smoothness factor is equal to about 0.75. The surface conditions of the conductors are also directly dependent upon the environment conditions, such as dirt, accumulated insects, etc., as well as on the technical conditions of both the conductors and other elements of the transmission track. On the conductor surfaces there exist often scratches, stratification caused by improper assembly (pulling the conductors). Damages of conductors, insulators and switch gear, which are caused by wear and ageing processes, can also be sources of discharges. The discharge itself damages the surface of conductors because it contributes to the creation of nitrogen compound. Under fair weather conditions the noise level is strongly dependent upon roughness of the surface of the conductors or other high voltage elements (particularly insulators). To the elements of considerable

rough surfaces belong fittings, particularly the insulators used frequently on the corner and tension poles (ON type poles) of overhead transmission lines.

For the given design data of an overhead transmission line, the noise level is dependent upon the atmospheric conditions. When the air is dry and the weather is fair, the number of microcharges is small but during rain it increases for two reasons: 1) The rain droplets result in the appearance of irregularities on the conductor surfaces, 2) the threshold at which discharge takes place (so-called "rupture gradient") is falling off. During fair weather single discharges occur at the voltage surface gradient of the order of 15 – 17 kV/cm. When the conductor is wet, the critical value of the voltage gradient is falling off to a level of about 12 kV/cm, whereas during rains it is falling off even below 10 kV/cm. According to [8], additional reduction of critical voltage gradient occurs in transmission lines with spiral vibration dampers; damping of mechanical vibration amounts to about 11 kV/cm for wet conductors and to about 8 kV/cm for rainy weather.

The number of microdischarges influences directly the level of the emitted noise. Fair weather is the weather with no rain and normal air humidity within the range of 60 to 70%. As a bad weather there will be regarded fog, drizzle, rain or snow. From the point of view of the influence of the noise of the transmission line on the environment, the most essential is the rainfall intensity, since the noise produced during heavy rain by the falling droplets is comparable with the noise generated by the transmission line itself. Also important are the conditions after the rain. The conductors are then wet, but there are no droplets on their surfaces. Such conditions exist during fog and drizzle. In foggy weather the maximum noise level is usually observed after saturation of conductors with moisture, which usually occurs after several hours.

Figure 1 [5] shows the influence of the rainfall rate on the dependence of the level of the emitted noise on the voltage surface gradient. From these investigations an

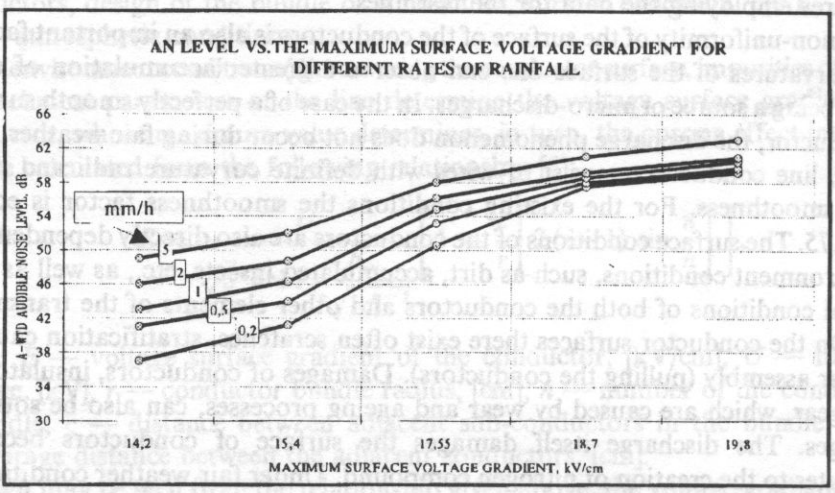

Fig. 1. Influence of power surface gradient of lines on the noise emitted by the transmission line for various rainfall rates.

essential conclusion can be drawn that sensitivity of the transmission line to the rainfall rate diminishes with increasing voltage gradient.

Noise during snow fall has a very wide range and depends upon the rate and kind of the falling snow.

Still another influence upon the noise level have the conditions of conductor surfaces connected with its age (Fig. 2 [10]). New conductors have somewhat

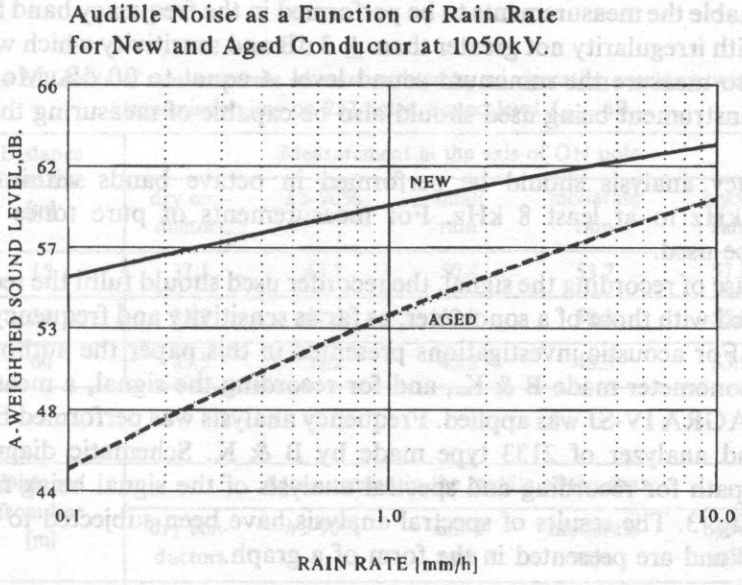

Fig. 2. Influence of the age of lines on the level of emitted noise for various rainfall rates.

greasy surface what leads to formation of drops during rain over the whole surface of the conductor. On the contrary, aged conductors have already degreassed surface like that after the use of detergents. Due to this, the drops accumulate in the bottom part of the conductor only [9], what leads to a smaller number of discharges. The age of the conductors is especially important during small rain falls drizzle and fog. The difference between the emitted noise decreases with increasing rainfall rate.

3. Result of investigations in existing conditions

Investigation of the noise produced by an operating transmission line have been carried out on a double-circuit 400 kV line on poles of series Z52 between Tarnów and Byczyna. Investigations were performed under various atmospheric conditions by a short-term method, that is for short time intervals of characteristic weather conditions.

In Poland there are now no special regulations determining the methods of investigation of the noise emitted by power transmission lines. Such measurements are performed on the basis of the existing standards relating to general measurements in natural environment. Developing the measuring methods, the authors of this paper have additionally taken into account the standards ANSI/IEEE Std 6558–1985 concerning measurements of the noise emitted by overhead transmission lines.

Main instrument used for measurements of the noise intensity was the sonometer. It should enable the measurements to be performed in the frequency band from 20 Hz to 15 Hz, with irregularity not greater than $\pm$ 3 dB and sensitivity which would make it possible to measure the minimum sound level A equal to 30 dB. Moreover, the measuring instrument being used should also be capable of measuring the levels L_{eq} and L_{min}.

Frequency analysis should be performed in octave bands within the range from 31.5 kHz to at least 8 kHz. For measurements of pure tones 1/3 octave filters can be used.

In the case of recording the signal, the recorder used should fulfil the requirements identical used with those of a sonometer, as far as sensitivity and frequency bands are concerned. For acoustic investigations presented in this paper the authors used the 2231 type sonometer made B & K., and for recording the signal, a measuring tape recorder NAGRA IV-SJ was applied. Frequency analysis was performed by means of a wide band analyzer of 2133 type made by B & K. Schematic diagram of the measuring path for recording and spectral analysis of the signal being measured is shown in Fig. 3. The results of spectral analysis have been subjected to "computer processing" and are presented in the form of a graph.

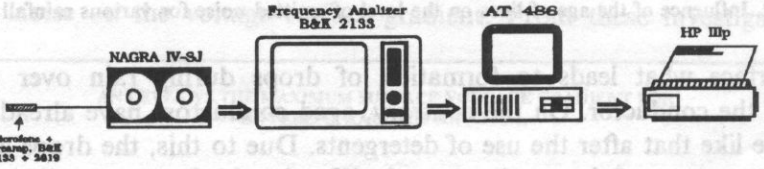

Fig. 3. Scheme of measuring channel for recording and spectral analysis of a noise signal.

Measuring points were situated at the distances of 15, 30, 60 and 120 m from the projection of the edge conductor. Measuring sections were situated in mid-span and in the axis of the pole of ON type, whereas in the case of measurements of noise distribution over the span, the measurements were performed in sections spaced 30 m from one another.

The results of investigations may be divided into two groups: 1) measurement of sound level A and 2) measurement of spectrum of 1/3 octave noise.

Measurements of the sound level A were performed mainly in order to determine the influence of acoustic phenomena on environment under various atmospheric conditions as well as the distribution of sound level along the span. Among the obtained results, five characteristic weather conditions have been distinguished:

— dry conductors (fair weather);
— considerable air humidity ($h > 90\%$),
— small rain or drizzle,
— moderate rain,
— heavy rain.

Averaged results of investigations of the sound level A for the particular atmospheric conditions for mid-span in the axis of the ON type pole are presented in Table 2.

Table 2. Results of measurements of noise emitted by an operating working two-track transmission line on 252 poles. Sound level $L_{A_{eq}}$, dB

Distance from line [m]	Measurement in the axis of ON pole				
	dry conductors	$h>90\%$	small rain	moderate rain	heavy rain
15	37.1	43.7	50.4	53.7	57.8
30	35.3	41.6	47.8	50.5	55.2
60	33.5	39.2	45.2	48.3	53.9

Distance from line [m]	Measurement in the middle of the span				
	dry conductors	$h>90\%$	small rain	moderate rain	heavy rain
15	35.1	41.4	48.5	53.5	57.5
30	33.2	39.0	46.1	51.5	55.1
60	31.4	37.1	44.1	47.2	52.7

1. Measurement results for moderate and intensive rainfalls are given in the form of average values of two series of measurements.
2. Distance is given from the projection of the edge line.

From the results presented in Table 1 the following conclusions may be drawn:
— noise level on tension pole axis (mainly the noise emitted by fittings) is slightly higher than in the middle of the span noise emitted by conductors;
— noise during intensive rainfalls is higher by about 20 dB as compared with the noise during fair weather;
— fluctuations of the level of noise emitted during rainfall change within the range of 8 to 9 dB.

Table 3 presents the results of measurements of sound level A on both sides of the transmission line in the case when the line is situated on a slops. They relate to the span 401—402 for a two-track line under good atmospheric conditions and average rain.

Table 3. Results of measurements of sound level $L_{A\,eq}$, dB for an ascending and descending slope

Distance from the line [m]	Fair weather		Moderate rainfall	
	ascending slope	descending slope	ascending slope	descending slope
15	44.3	41.9	53.9	51.2
30	41.6	40.5	51.4	48.5
60	38.6	38.0	47.7	45.8

On a descending slope noise is lower by about 2.5 dB, and this difference decreases with increasing distance from the line. A dominating factor of such a sound distribution is the distance from the source.

Figure 4 presents diagrams of sound level distribution along the span at a distance of 15.30 and 60 m from the extreme conductor for fair weather and moderate rainfall. From the presented diagrams it can be seen that during rain the transmission line is a more uniform source of noise than during fair weather. The corona effect under

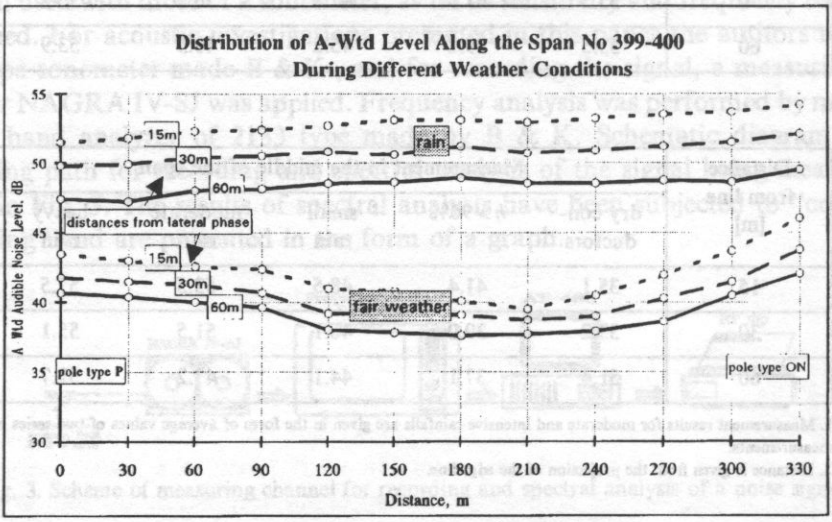

Fig. 4. Distribution of sound level A along the span at a distance of 15.30 m and 60 m from the edge line during fair and rainy weather.

these conditions is determined mainly by: 1) reducing the critical intensity level, 2) deformation of the surface by rain drops, which is of the same form on the whole line. Also visible is a higher level of the noise emitted on the axis of ON type pole.

Figure 5 shows distributions of a sound A level for various spans during fair weather. Three mutually exclusive tendencies can here be observed: raising or lowering the noise level in the middle of the span, or approaching its uniform distribution. An increase of noise in the mid-span indicates that the main sources of noise are the conductors, mainly dut to bad technical conditions of their surfaces. Such tendency was most often encountered in the transmission lines investigated by the authors.

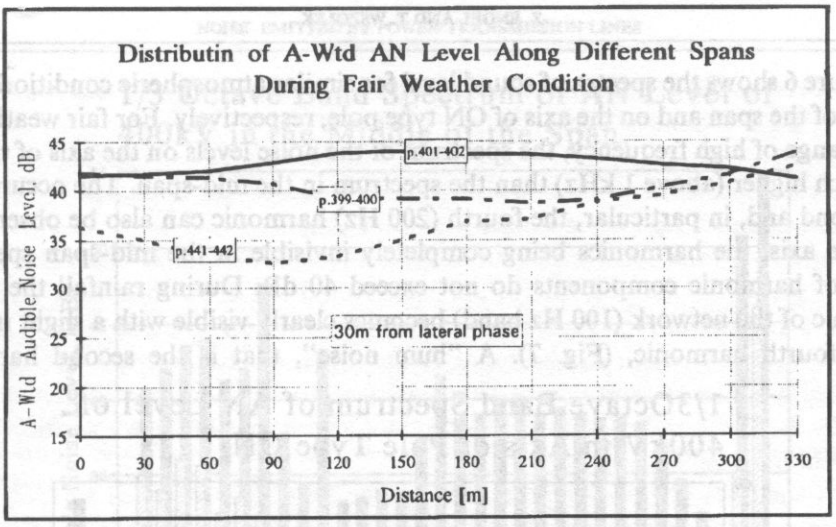

Fig. 5. Distribution of sound level *A* along various spans during fair weather. Measurements have been performed at a distance of 30 m from the edge line.

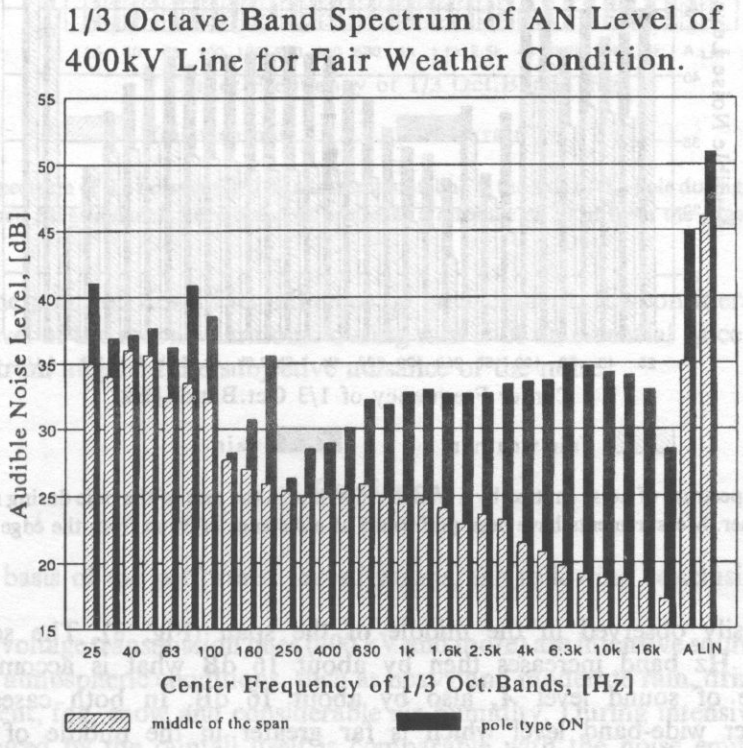

Fig. 6. Third spectrum of noise emitted by the transmission line during fair weather on axis of the ON pole and in the mid-span. Measurements have been performed at a distance of 30 m from the edge line.

Figure 6 shows the spectra of sound level for similar atmospheric conditions in the middle of the span and on the axis of ON type pole, respectively. For fair weather and in the range of high frequency, the spectrum of the noise levels on the axis of the pole are much higher (above 1 kHz) than the spectrum in the mid-span. The occurence of the second and, in particular, the fourth (200 Hz) harmonic can also be observed on the pole axis, the harmonics being completely invisible in the mid-span spectrum. Levels of harmonic components do not exceed 40 dB. During rainfall the second harmonic of the network (100 Hz band) becomes clearly visible with a slight increase of the fourth harmonic, (Fig. 7). A "hum noise", that is the second harmonic,

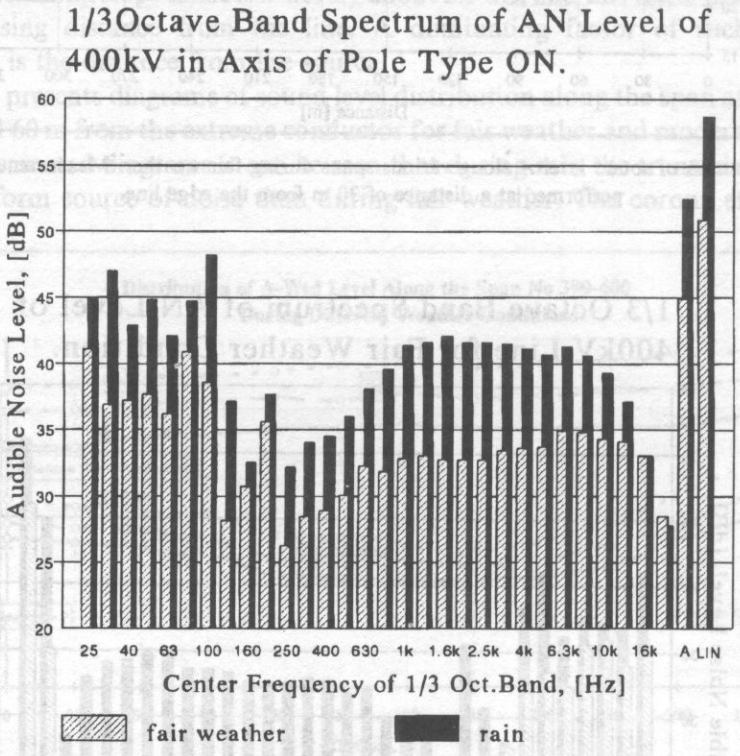

Fig. 7. Third spectrum of noise emitted by a transmission line in the axis of the pole during fair and rainy weather. Measurements have been performed at a distance of 30 m from the edge line.

is most easily observed in the middle of the span (Fig. 8). The sound level in the 100 Hz band increases then by about 16 dB what is accompanied by an increase of sound level A, also by about 16 dB. In both cases one can see a higher wide-band level which is far greater in the middle of the span. Also significant is the rise of the noise level of the fourth harmonic of the network (400 Hz). In both the cases, a rise of broad-band noise can be observed, which is considerably greater in the middle than in other points of the span.

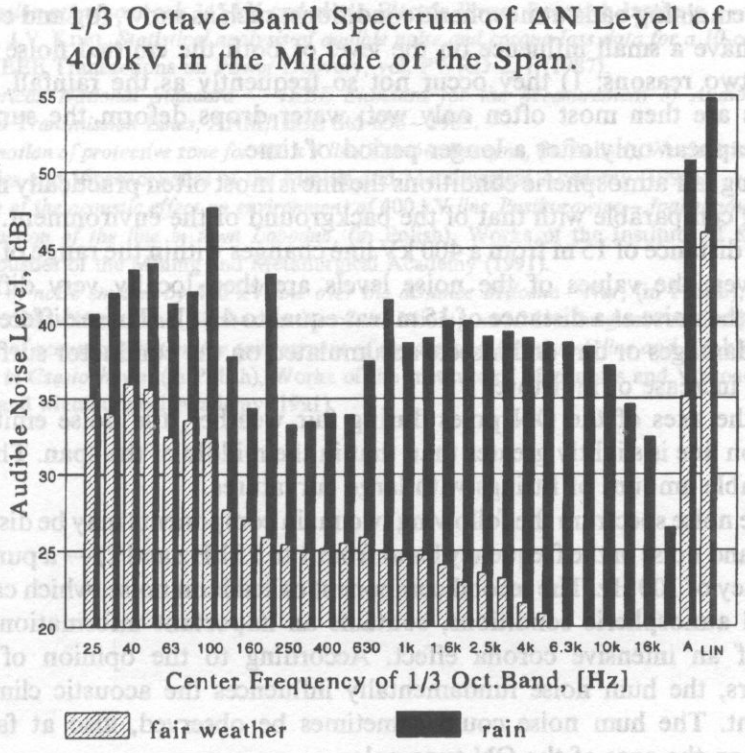

Fig. 8. Third spectrum of the noise emitted by a transmission line in the axis of the pole during fair and rainy weather. Measurements have been performed at a distance of 30 m from the edge line.

From the point of view of its influence on environment, the considerable rise of the noise level of the second harmonic during rain is of an essential since pure tones in the spectrum augment the subjective nuisance of the noise.

4. Conclusions

On the basis of the performed investigations, the following conclusions can be drawn:

1. High voltage transmission lines (400 kV and more) are intensive sources of noise during bad atmospheric conditions, such as heavy and moderate rain, drizzle and, to a lesser extent, fog, snow and considerable air humidity. During intensive rain, the noise produced by the rainfall itself is comparable with the noise emitted by the transmission already at a distance of 30 m from the lines. The level of noise of 400 kV lines at a distance of 25 m from an edge conductor during bad atmospheric conditions changes with in the range of 30 to 54 dB.

2. The remaining bada atmospheric conditions, such as snow, fog and considerable humidity, have a small influence on the level of both the emitted noise and power losses for two reasons: 1) they occur not so frequently as the rainfall, and 2) the conductors are then most often only wet; water drops deform the surface of the conductor appear only after a longer period of time.

3. During fair atmospheric conditions the line is most often practically noiseless, its noise being comparable with that of the background of the environment. The sound level A at a distance of 15 m from a 400 kV line changes within the range of 34 up to 36 dB. However, the values of the noise levels are then locally very differentiated; sometimes the noise at a distance of 15 m was equal to 45 dB. These differences can be caused by damages or dirt and insects accumulated on the conductor surface, as well as by local increase of moisture.

4. On the axes of the ON poles during fair weather, the noise emitted by the transmission line is slightly greater than that in the middle of the span. This is due to a considerable amount of fittings with large curvatures.

5. In the noise spectrum the following two main components may be distinguished: 1) broad-band noise in the frequency band from 1 to 15 kHz and 2) — a pure tone with the frequency of 100 Hz. The second component called hum noise, which can be heard during bad atmospheric conditions, contains an important information about the presence of an intensive corona effect. According to the opinion of numerous investigators, the hum noise fundamentally influences the acoustic climate of the environment. The hum noise could sometimes be observed, also at fair weather conditions on the axes of the ON type poles.

6. During bad atmospheric conditions, the noise emitted by aged lines and the induced power loss are lower than those produced by new lines.

References

[1] Z. ENGEL, T. WSZOŁEK, *Influence of atmospheric conditions on the noise emitted by high voltage power transmission lines* (in Polish), Noise Control'92, Cracow, September 1992.

[2] Z. ENGEL, T. WSZOŁEK, *Investigation of the influence of high voltage power transmission lines on the acoustic climate of environment* (in Polish), Mechanika, Scientific quarterly of the Mining and Metallurgical Academy, 2 (1992).

[3] A. HANDKE, *Power networks. Harmful effects observable during transmission and distribution of power*, PP Poznań 1987.

[4] J.J. KOWALEWSKI, J. REICHMAN, *Audible noise from an Ontario Hydro 500 kV transmission line*, International Congress on Acoustics, Toronto 1986.

[5] J. LUNDQUIST, *Methods for predicting AC transmission line audible noise by a short-term single-phase tests IEEE*, Transactions of Power Apparatuses and Systems, vol. PAS–103, 2 (1984).

[6] J. LUNDQUIST, *Results from AC transmission line. Audible noise studies at the Anneberg EHV Test Station*, IEEE Transactions on Power Delivery, 5, 1 (1990).

[7] Y. NAKANO, M. FUKUSHIMA, *Statistical audible noise performance of Shiobara HDVC line*, IEEE Transactions on Power Delivery, 5, 1 (1990).

[8] K. TANABE, *Hum noise performance of 6, 8, 10 conductor bundles for* 1000 kV *transmission lines at the Akagi Test site: A comparative study with Cage Data* — IEEE Transactions on Power Delivery, 6, 4 (1991).

[9] *Transmission reference book* 345 kV *and above*, Electric Power Research Institute.

[10] T. VINH, J.V. KING, *Statistical analysis of audible noise and corona loss data for a 10-conductor UHV bundle*, IEEE Transactions on Power Delivery, vol. PWRD-2, 1 (1987).

[11] *An American National Standard — IEEE Standard for the Measurement of Audible Noise from Overhead Transmission Lines*, ANSI/IEEE Std 656–1985.

[12] *Determination of protective zone for* 400 kV *line Tarnów-Byczyna*, (in Polish), Works of the Institute of Mechanics and Vibroacoustics of the Mining and Metallurgical Academy (1990).

[13] *Estimate of the acoustic effect on environment of* 400 kV *line Pasikurowice–Joachimów in the area of reconstruction of the line in town Lobodno*, (in Polish), Works of the Institute of Mechanics and Vibroacoustics of the Mining and Metallurgical Academy (1991).

[14] *Analysis of noise emitted by* 400 kV *line over the distance Miłosna–Nur*, (in Polish), Works of the Institute of Mechanics and Vibroacoustics of the Mining and Metallurgical Academy (1991).

[15] *Estimate of acoustic effect on the environment of the design transmission line and* 400 kV *power station Aniołów in Częstochowa*, (in Polish), Works of the Institute of Mechanics and Vibroacoustics of the Mining and Metallurgical Academy (1991).

ARCHIVES OF ACOUSTICS
18, 2, 263–279 (1993)

BAND-LIMITED NOISE INTERFERENCE IN LOUDSPEAKER SYSTEMS

T. FIDECKI

Chopin Academy of Music Laboratory of Music Acoustics
(00-368 Warszawa, ul. Okólnik 2)

It is often argued that the interference of sound from distant loudspeakers is negligible in the case of band-limited noise. Simple theory and experiment in a reflection-free environment with a pair of loudspeakers radiating a third-octave noise proves that in the case of coherent supply SPL variations are considerable. The variations disappear when non-coherent signal is applied indicating that non-coherent supply of loudspeakers is necessary wherever approximation of diffuse sound field is required.

1. Introduction

Diffuse sound field in test room is recommended in acoustic testing of hearing protectors and in some audiometric tests [1], [2]. In an ideal case the sound field has to be isotropic and homogeneous. Adequate approximation of ideal conditions of directional and spatial SPL uniformity is expected in the test site. Several loudspeakers have to be placed around the object to meet the demands of the directional distribution of the incident sound. However, the spatial uniformity of the SPL is destroyed by interference effects if the loudspeakers are fed coherently. The interference vanishes when non-coherent supply of loudspeakers is applied at the expense of increased complexity and cost of test equipment.

It has been argued in discussion of practical implementation of such measuring stand [3] that the interference effect of coherent supply of loudspeakers with third-octave noise is negligible because of stochastic phase of the signal. Investigation of that spatial phenomenon in the sound field of band-limited, constant-percentage noise is the subject of the present report.

2. Theoretical model of interference

A pair of directional, point sound sources, propagating band-limited noise of uniform spectral density W_0 is considered. The problem concerns calculation of mean-square value p^2_{rms} of the total sound pressure. The autocorrelation function $R(\tau)$ of the noise within bandwidth Δf in the frequency range $f_g - f_d$ is given by [4]:

$$R(\tau) = \frac{W_0}{\pi\tau} * \sin[\pi(f_g - f_d) * \tau] * \cos[\pi(f_g + f_d) * \tau]; \tag{1}$$

Let: $f = \sqrt{(f_g * f_d)}$ — center frequency of noise band, $a = \Delta f/f$ — constant percentage, relative bandwidth of the noise, ($a_{terc} = 0.23$, $a_{oct} = 0.707$),
then,

$$R(\tau) = W_0 * \Delta f * \frac{1}{a\pi f\tau} * \sin[a\pi f\tau] * \cos[2\pi * \sqrt{a^2/4 + 1} * f\tau]; \tag{2}$$

RMS value p_i of the sound pressure from one directional source at distance r_i equals:

$$p_i = p * \frac{\Gamma_i}{r_i}; \tag{3}$$

where: p — mean-square value of the sound pressure at 1 m on the main axis of each source, $p^2 = W_0 * \Delta f$, Γ_i — directivity function of the source,

$$\Gamma_i = p(\theta)/p(0).$$

Total sound pressure of the two distant sources at any observation point in the space takes the form:

$$p^2_{rms} = \overline{(p_1 + p_2)^2} = p^2 * \left[\frac{\Gamma_1^2}{r_1^2} + \frac{\Gamma_2^2}{r_2^2} + 2 * \frac{\Gamma_1\Gamma_2}{r_1 r_2} * \rho(kd)\right]; \tag{4}$$

The quantity $\rho(kd)$ in Eq. (4) is the normalized inter-correlation function of the two considered noise pressures at the observation point.

$$\rho(kd) = \frac{R(kd)}{R(0)} = \frac{2}{akd} * \sin\left(\frac{1}{2} akd\right) * \cos\left(\sqrt{a^2/4 + 1} * kd\right); \tag{5}$$

k — wave number, $k = 2\pi/l$, l — wavelength, d — path difference at observation point,

$$d = r_2 - r_1 \leqslant D;$$

D — distance between the two sources.

The function $\rho(kd)$ is shown in Fig. 1 for third-octave and octave noise bands.

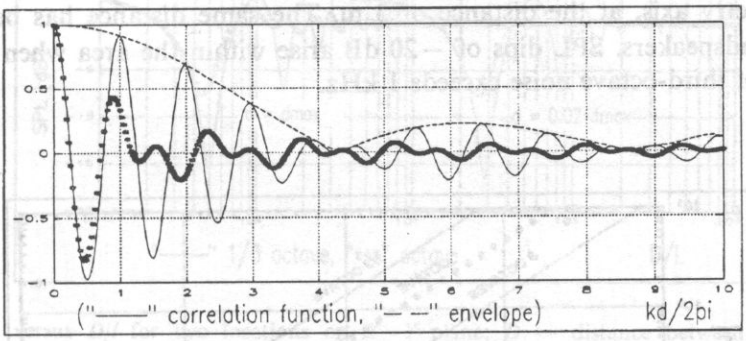

Fig. 1. Inter-correlation function of band limited noise from two sources: ———— third-octave noise, ***** octave noise.

The following may be observed from Eq. (4) and Fig. 1:

(i) Inter-correlation of band-limited noise from two coherent sources becomes negligible above some limiting value of d/l:

a) for third-octave noise, $d/l = 4$,

b) for octave noise, $d/l = 1.5$;

Corresponding SPL is approximately uniform and 3 dB higher than each component if d/l exceeds that limit.

(ii) Below the limiting value of d/l, i.e. for lower frequencies of noise, destructive interference arises with few dips and valleys of SPL. The largest SPL variations of 20 dB for third-octave noise (10 dB for octave noise) occur in the d/l range between 0.15 and 0.8.

(iii) SPL variations vanish again for $d/l < 0.15$. Here, SPL slowly falls down from the maximum to -1 dB. At maximum, which is located on symmetry axis of the loudspeaker system ($d = 0$), the 6 dB increase of SPL occurs.

The frequency dependence of interference effects is illustrated in Fig. 2 and Fig. 3.

The nature of spatial variations of SPL is similar to the frequency domain effects. In space the variable d changes from point to point in a regular manner as shown in Fig. 4. At fixed frequency SPL drops down from the maximum to the deepest minimum in close vicinity of main axis. Spatial fluctuations of SPL vanish beyond some angle corresponding to the condition (i) for d/l.

An example of SPL interference pattern on $X-Y$ plane for third-octave noise band centered at frequency $f = 1700/D$, $(D/l = 5)$, is shown in Fig. 5. As may be seen, the span of SPL variations increases proportionally with the distance from the origin of loudspeaker system along its main axis.

Another practical example is shown in Fig. 6. The diagram presents SPL variations over the small 0.3 m × 0.3 m area, which may be considered as a test site for investigation of hearing protectors. The area is located in front of two loudspeakers on

their symmetry axis, at the distance of 3 m. The same distance has been chosen between loudspeakers. SPL dips of −20 dB arise within the area when the center frequency of third-octave noise exceeds 1 kHz.

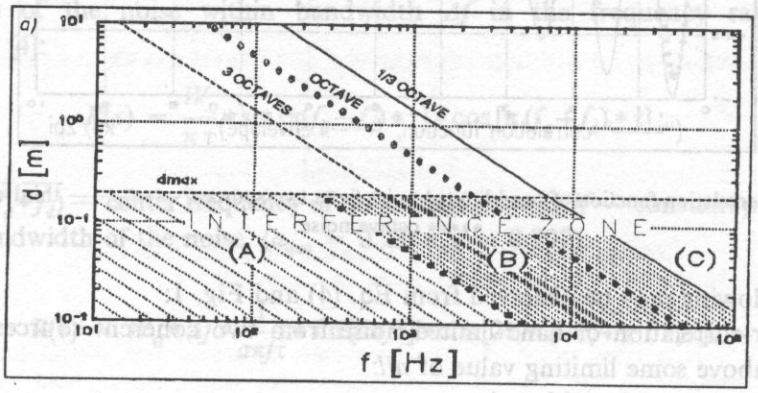

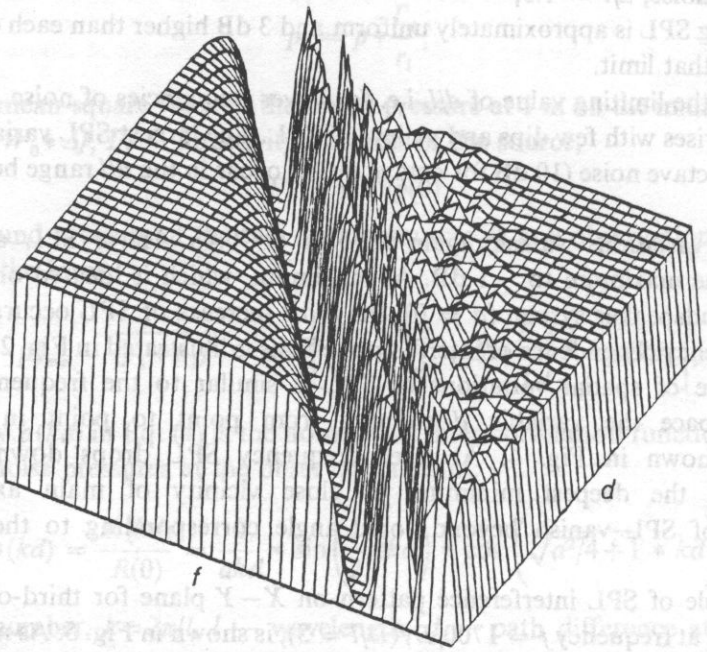

Fig. 2 a), b) Interference zones in "d–f" coordinates; a) — three zones, (A) — slow, 1 dB fall of SPL, (B) — rapid SPL variations, up to 20 dB for third-octave band and 10 dB for octave band, (C) — non-coherent contribution of each source to total SPL, b) — 3 D presentation of interference pattern.

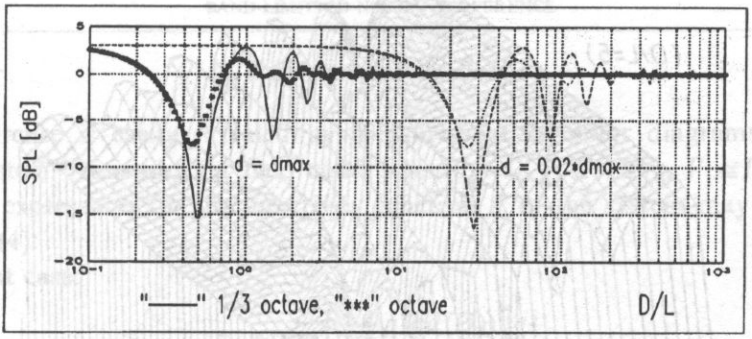

Fig. 3. SPL versus D/l for two locations on $X-Y$ plane; D — distance between loudspeakers, l — wavelength.

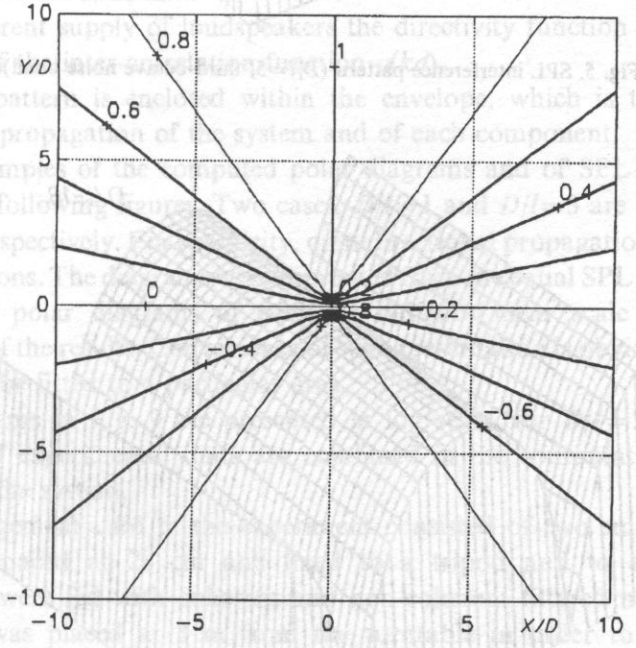

Fig. 4. Location of the path-difference d/D on $X-Y$ plane.

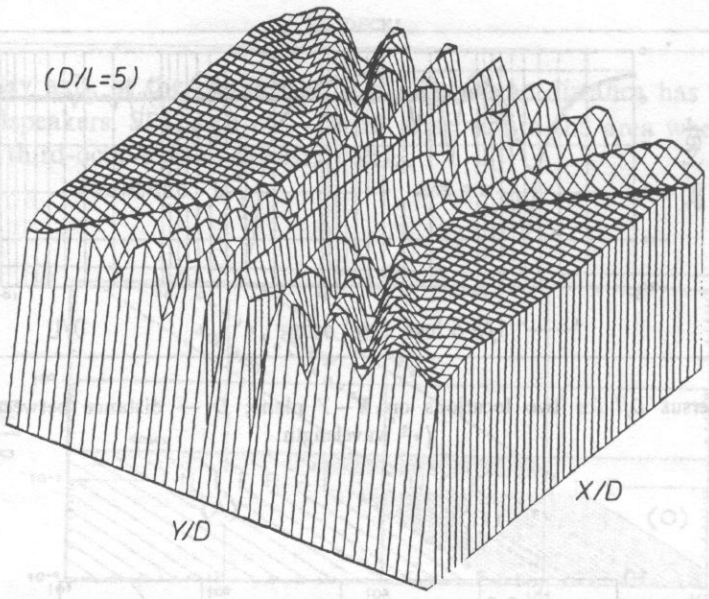

Fig. 5. SPL interference pattern ($D/l=5$, third-octave noise band).

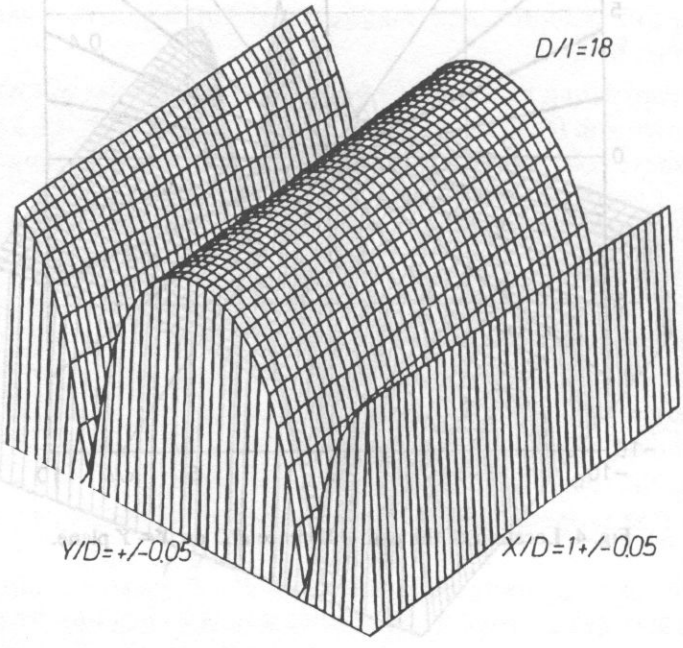

Fig. 6. SPL distribution on small area 0.3 m × 0.3 m in front of a pair of loudspeakers at the distance of 3 m. The case shown corresponds to the center frequency of 2 kHz of third-octave noise.

3. Experimental verification

Interference is easily revealed by measurement of polar diagrams of loudspeaker system. Assuming far field conditions ($r_0 \gg D$, $r_1 \cong r_2 \cong r_0$, $\Gamma_1 \cong \Gamma_2 \cong \Gamma_i$), the following expressions for the directivity function Γ of the system may be derived from Eq. (4):

a) coherent case:

$$\Gamma_c \cong \Gamma_i * \left[\frac{1+\rho(kd(\Theta))}{2}\right]^{1/2}; \tag{6}$$

b) non-coherent supply of each unit:

$$\Gamma_{nc} \cong \Gamma_i; \tag{7}$$

The conclusions are such that:

— in coherent supply of loudspeakers the directivity function Γ_c reflects initial fluctuations of the inter-correlation function $\rho(kd)$,

— polar pattern is enclosed within the envelope, which is the directivity of non-coherent propagation of the system and of each component.

A few examples of the computed polar diagrams and of SPL distributions are shown in the following figures. Two cases, $D/l=1$ and $D/l=5$ are presented in Fig. 7 and Fig. 8 respectively. For simplicity, omnidirectional propagation was assumed in the computations. The diagrams were computed from the equal SPL contours, what is equivalent to polar diagrams of constant radius. Linear scale is used for the presentation of the results. Convenience of such presentation is obvious if the contour shapes are to be fitted to a particular area.

The diagrams in Fig. 9 are presented in log scale, for $D/l=1$, 2, 3. Here the directivities of experimental units are combined in the computations of resultant directivity of the system.

The arrangement used in the experiment consisted of two small loudspeakers, which were spaced at 28 cm and fixed to a tripod and to a turntable. The loudspeakers were fed with coherent and non-coherent filtered noise signals. The microphone was placed at 3 m from the turntable in order to satisfy far field conditions. The measured polar diagrams are shown in Fig. 10. The following cases were examined:

— one unit fed with third-octave gaussian noise,

— two units fed with non-coherent third-octave noise signals from two separate generators,

— two units fed coherently from one generator.

The diagrams presented in Fig. 10 (a), (b) and (c) were taken with third-octave noise bands centered at 1250 Hz, 2500 Hz and 5000 Hz, what corresponds to D/l factors of 1, 2 and 3 respectively.

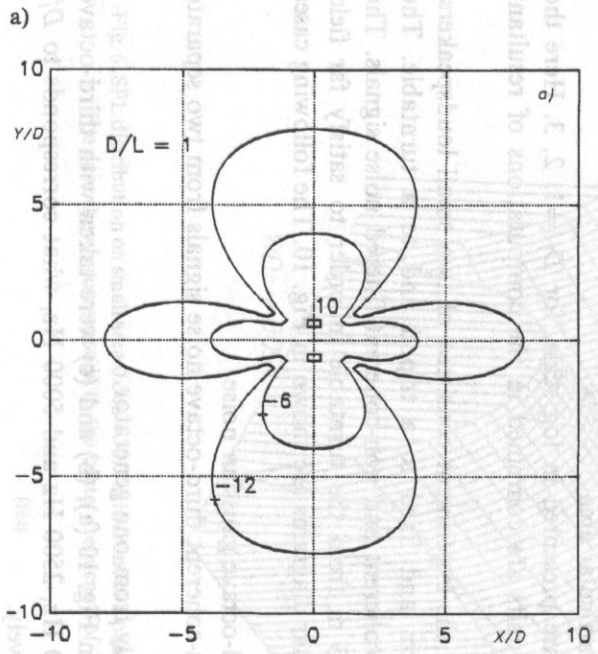
a)
10
Y/D
5
0
−5
−10
D/L = 1
a)
10
−6
−12
−10
−5
0
5
X/D
10

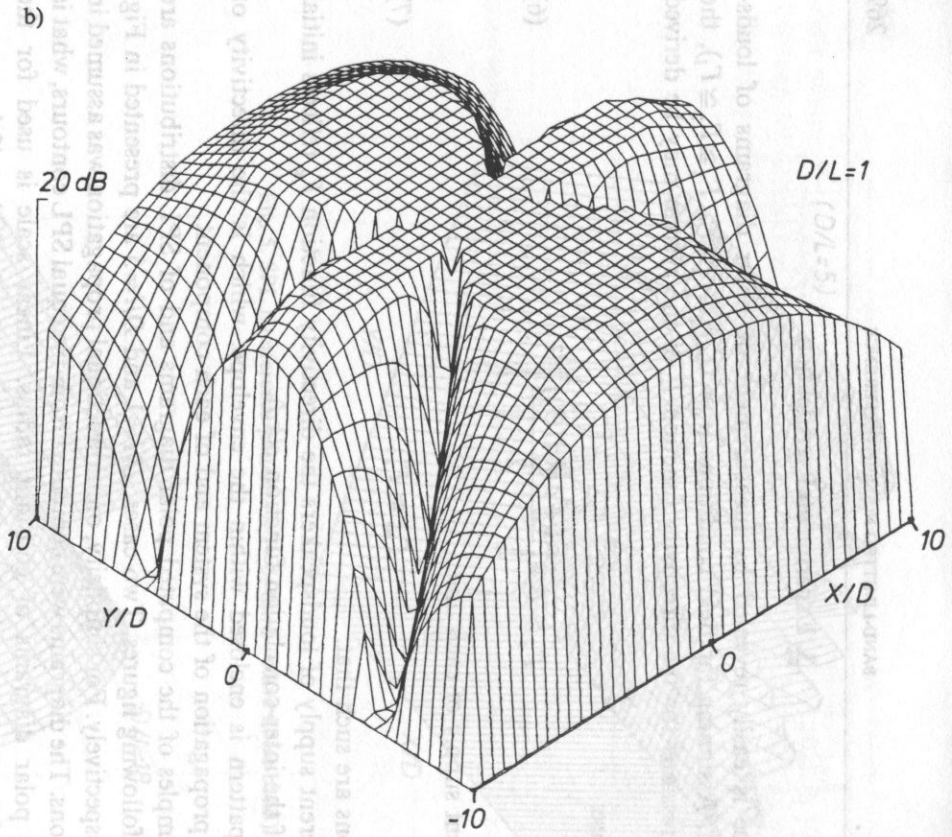
b)
20 dB
D/L=1
10
Y/D
0
-10
0
X/D
10

c)

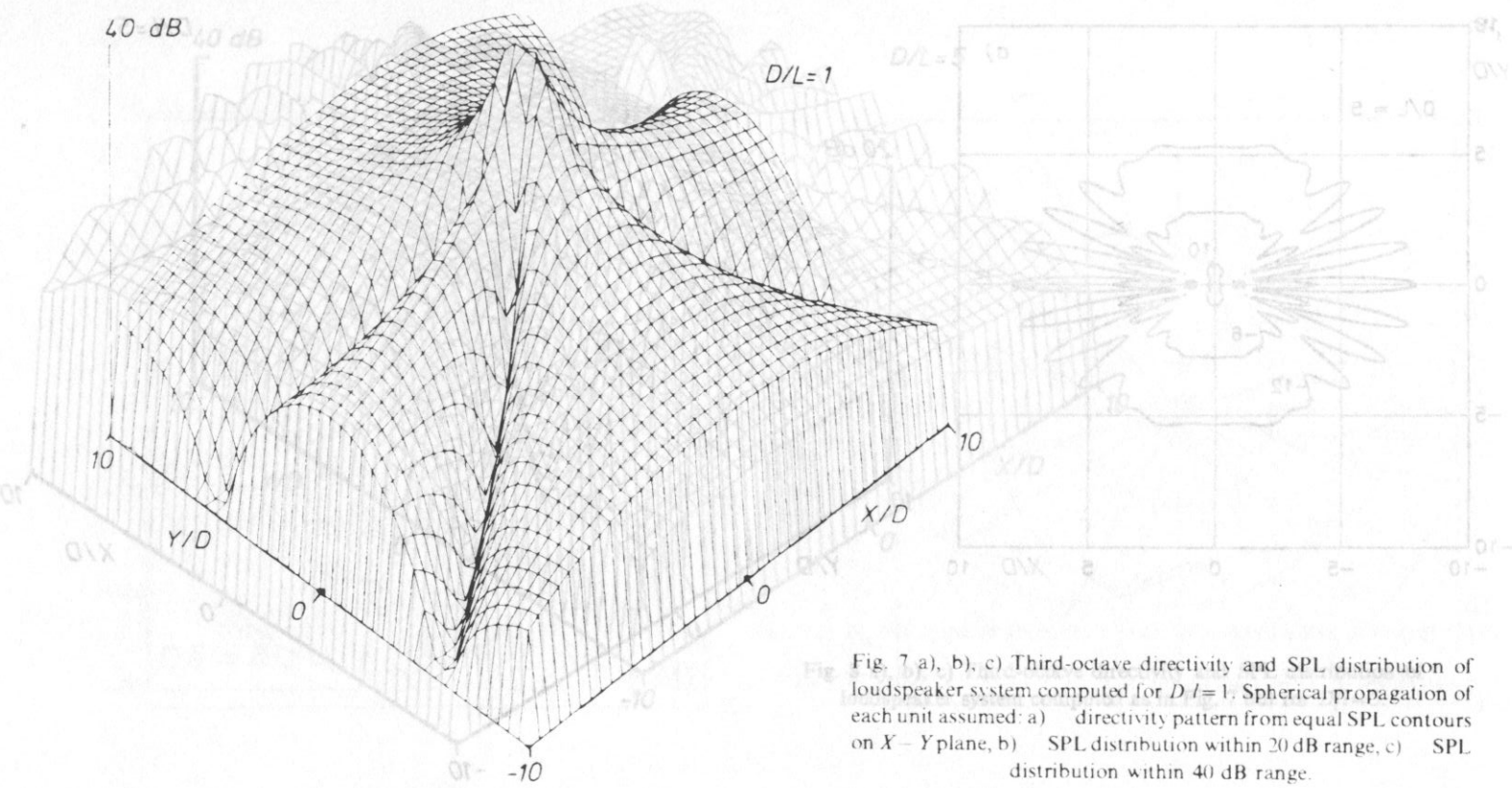

Fig. 7 a), b), c) Third-octave directivity and SPL distribution of loudspeaker system computed for $D/l = 1$. Spherical propagation of each unit assumed: a) directivity pattern from equal SPL contours on $X-Y$ plane, b) SPL distribution within 20 dB range, c) SPL distribution within 40 dB range.

a)

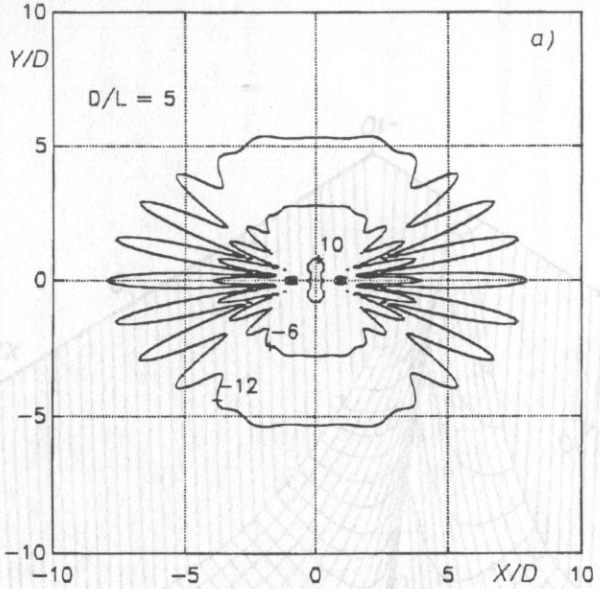

b)

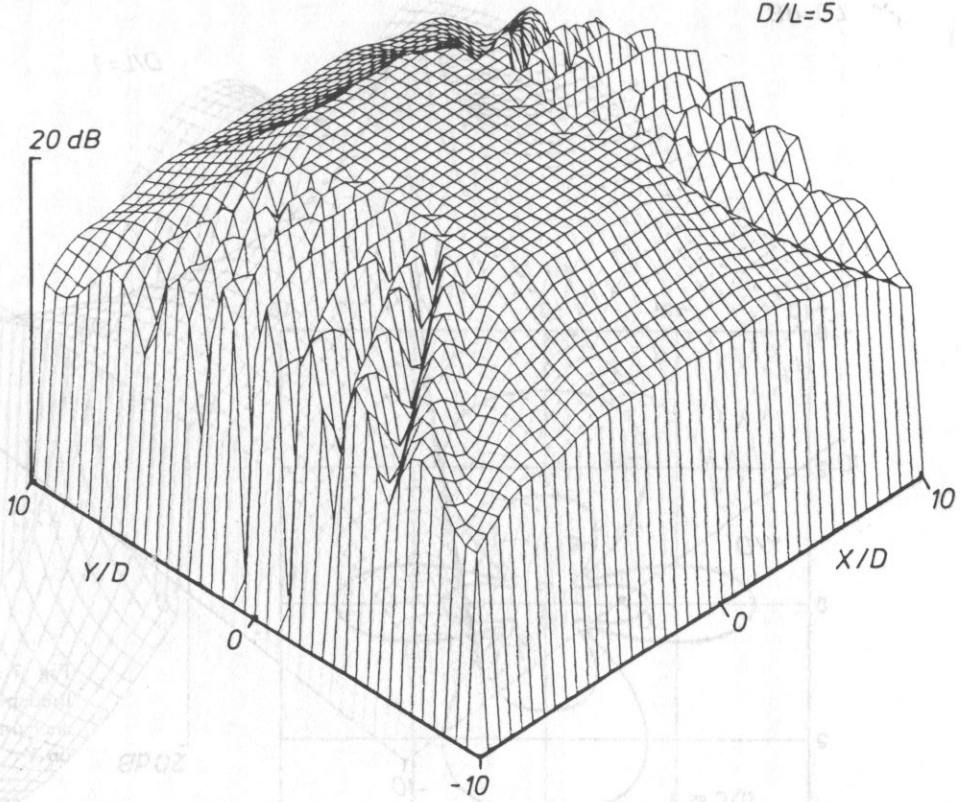

c)

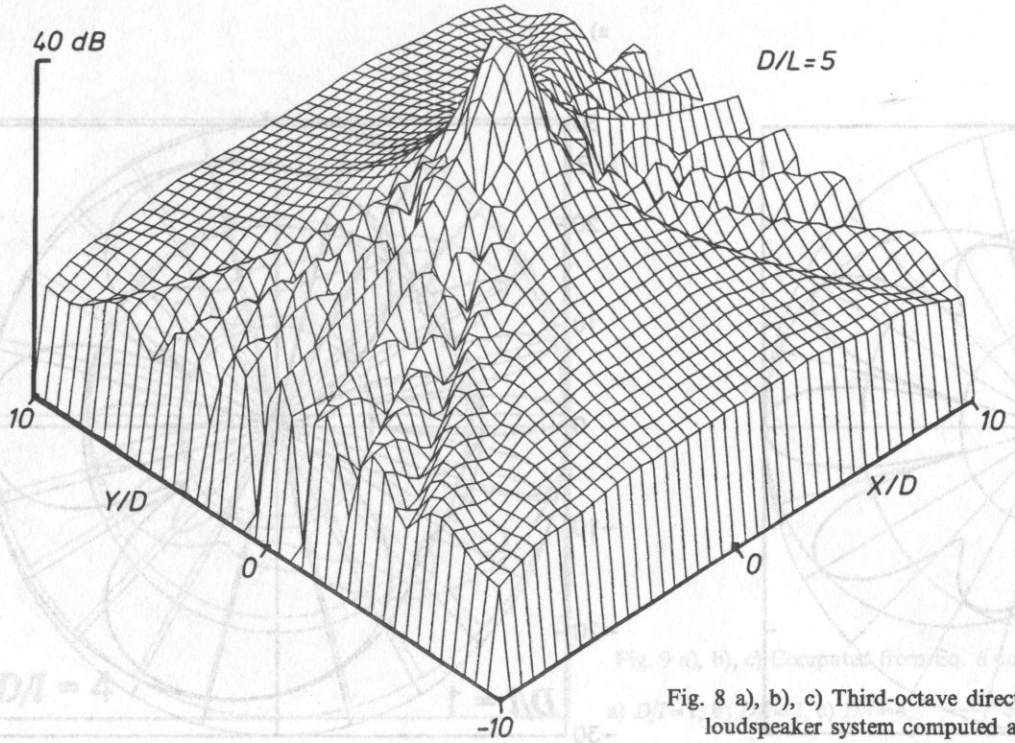

Fig. 8 a), b), c) Third-octave directivity and SPL distribution of loudspeaker system computed as in Fig. 7 but for $D/l=5$.

b)

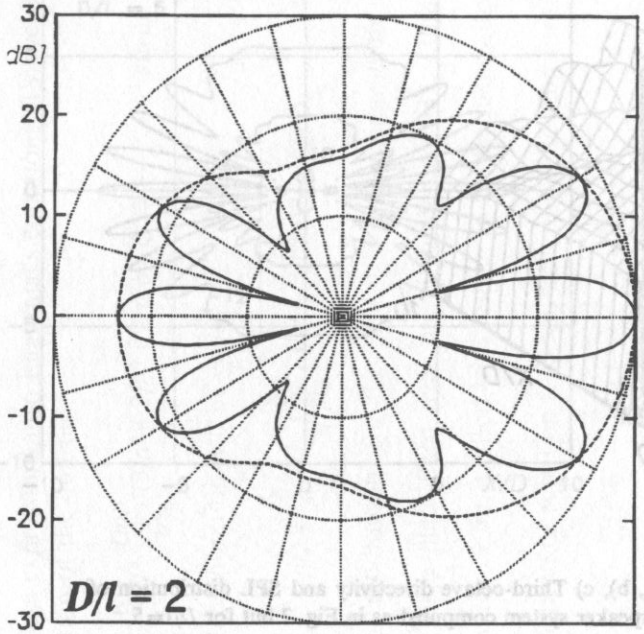

a)

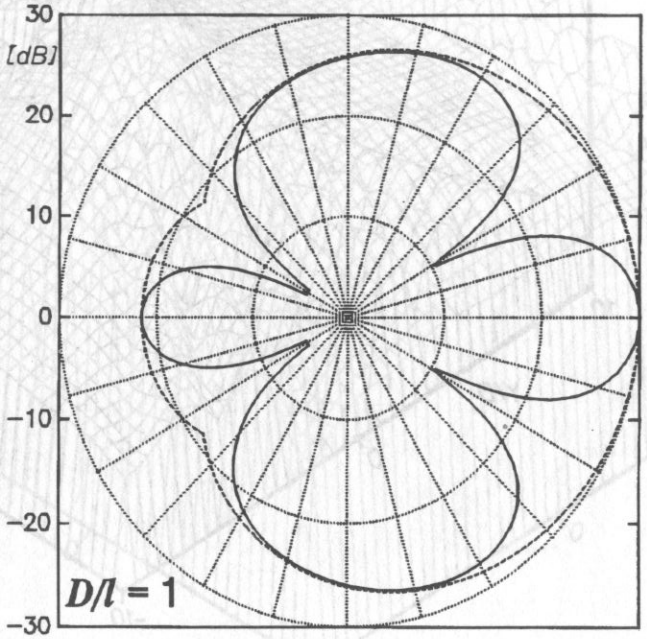

c)

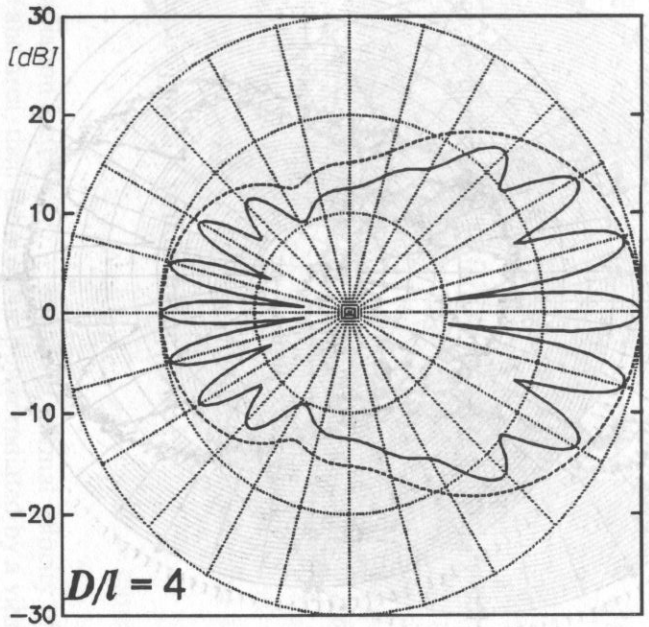

Fig. 9 a), b), c) Computed from Eq. 6 polar patterns of a pair of loudspeakers; a) $D/l=1$, b) $D/l=2$, c) $D/l=4$, " —— " coherent pair, "-----" non-coherent pair.

a)

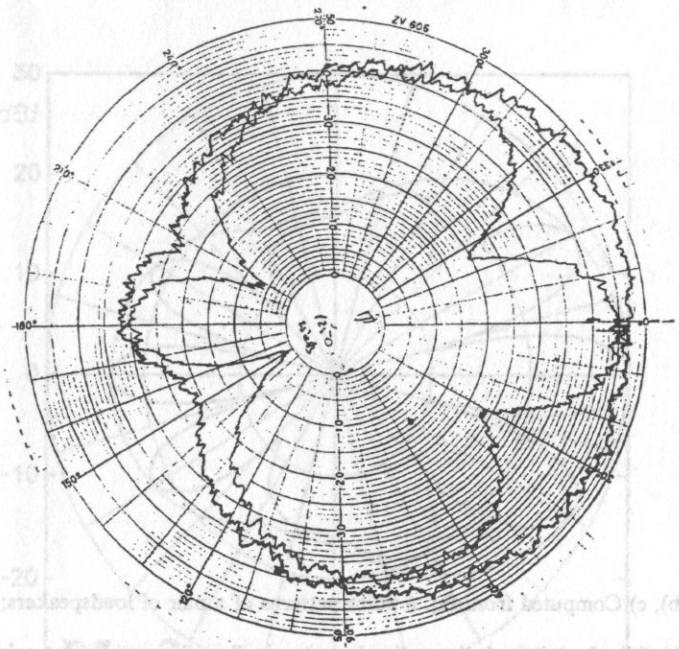

b)

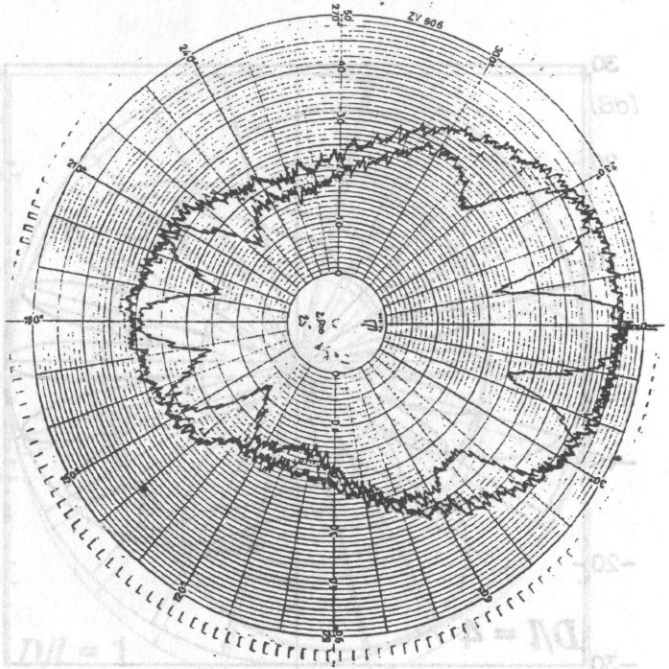

c)

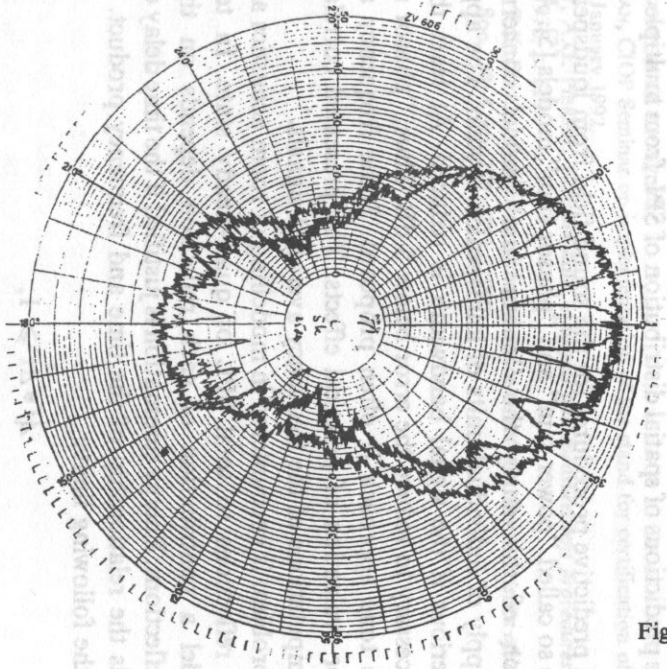

Fig. 10a), b), c) Measured with third-octave noise polar patterns of a pair of loudspeakers: a) $D/l=1$, b) $D/l=2$, c) $D/l=4$.

Comparison of the diagrams in Fig. 9 and Fig. 10 evidently confirms the predicted interference patterns in the sound pressure field of loudspeaker system radiating band-limited noise coherently. Close agreement of the experimental data with the theory confirms also the usefulness of the presented interference model for further investigation of more complex systems.

4. Final remarks

(i) Recommended conditions for acoustic testing of hearing protectors in reflection-free environments may not be fulfilled with simple, coherently fed loudspeaker system.
High level, spatial variations of SPL shall be expected at the frequency range above 1 kHz.

(ii) Promising results of the present study of stationary sound field of two sound sources may be effectively applied to extended number of sources. The most interesting applications of the correlation model are as follows:
— prediction of narrow- or wide-band directivity patterns of sophisticated loudspeaker arrays,
— more accurate predictions of spatial distribution of SPL from multiple loudspeaker arrangements,
Commonly used predictive procedures for the sound field from loudspeaker systems are based on the so called "power sum" and "phasor sum" models [5]. According to the interpretation of this study the "power sum" model concerns cases of non-coherent supply of individual units of loudspeaker system. The approximation error may be serious if the signal bandwidth is reduced. At least three octaves bandwidth is necessary to reduce the error below 5 dB. Thus, "phasor sum" model built on a pure tone approach is often proposed. Some frequency averaging is indispensable for evaluation of practical effects. The presented correlation model allows direct computations of the frequency averaged signals.

(iii) Similar problem is encountered in modelling of room acoustics and concerns contribution of reflections to total SPL of quasi-steady state. In terms of the correlation model a contribution of each reflection depends on the temporal distribution of reflections. Energy summation is justified if the time delay of successive reflections fulfills the relationship of the time and frequency product. Correlation model suggests the following limits:

$$\Delta f * \Delta \tau \geqslant 1;$$

or in frequency-spatial variables:

$$\Delta f * \Delta r \geqslant c;$$

c — sound velocity.

The delays of the order of at least ten milliseconds are necessary to satisfy the above relations in case of octave noise bands in the frequency range above 100 Hz. It means that the early reflections are the energy contributors of the summation process. Probably, such approximation may also be extended to the diffuse part of reverberation because of multiple and random phase shifts of delayed reflections.

Acknowledgments

This report was sponsored by grant No 4 4160 91 02 from the State Committee for Scientific Research. Part of the material was presented to the 39th Polish Open Seminar on Acoustics, Cracow, September 1992.

References

[1] ISO 4869-1: 1990 *Acoustics — Hearing protectors, part 1: Subjective method for the measurement of sound attenuation.*

[2] ISO/DP 8253-2: 1987 *Acoustics — Audiometric test methods, Part 2: Sound field audiometry with pure tones and narrow-band test signals.*

[3] A. LIPOWCZAN, CIOP Seminar on implementation of the stand for certification of hearing protectors, Warszawa, January 1992.

[4] J.S. BENDAT, A.G. PIERSOL, *Random data, Analysis and measurement procedures*, (in Polish), PWN, Warszawa 1976, p. 110.

[5] K.D. JACOB, T.K. BIRKLE, *Prediction of the full-space directivity characteristics of loudspeaker arrays*. J. Audio Eng. Soc., **38**, 4, pp. 250–259, (1990).

ARCHIVES OF ACOUSTICS
18, 2, 281–296 (1993)

APPLICATION OF SIMULATION METHODS TO EVALUATION OF ACOUSTIC FEATURES AND DESIGN OF ADAPTATION OF THE CONCERT HALL OF CRACOW PHILHARMONIC ORCHESTRA

A. GOŁAŚ and J. WIERZBICKI

Institute of Mechanics and Vibroacoustics Mining and Metallurgy Academy
(30-059 Kraków, Al. Mickiewicza 30)

The publication presents the problems of application of digital methods of simulation of acoustic field to the evaluation of the acoustic characteristic and adaptation of the concert hall of the Cracow Philharmonic Orchestra. The measurement method based on an advanced technique of signal processing and the results obtained have been described. The evaluation of acoustic properties of the hall was carried out according to the Beranek Scale. A geometric model of acoustic field has been presented, as well as the acoustic parameters determined. An assessment method according to Ando has been discussed. This method has been applied in order to determine the influence of the changes in stage arrangement and kind of the music performed on the hearing conditions. Directions of further research based on the experimental and digital simulation methods have been proposed.

1. Introduction

Reconstruction of the concert hall of the Cracow Philharmonic Orchestra, which was necessary after a fire, was the reason for the acoustic analysis, described in this publication. The analysis concerned an evaluation of the current state of the music hearing conditions of the hall and determination of the influence of temporary arrangement of the stage during the organ reconstruction.

The basic vibroacoustic problems of the hall of the Cracow Philharmonic Orchestra have been divided into three groups:

— traffic noise, distinctly audible during the concerts,
— floor vibrations caused by the traffic,
— acoustic characteristics of the hall.

The first two problems result from the location of the hall at the street crossing of dense traffic of motor vehicles and streetcars. Their solution is connected with radical changes in construction of the building (increasing of the insulating power of walls,

installation of sound foundation mat), which have been postponed to be realized later on. This publication concerns the acoustics of the concert hall of the Cracow Philharmonic Orchestra, and especially the attempts undertaken to assess it.

The hall of Cracow Philharmonic Orchestra has not been designed for musical purposes. Its shape is rectangular, which, according to opinion of numerous acousticians, is the best for applications of this kind. As it might be concluded from remarks of musicians, the main problem is poor mutual audibility both of them and of the conductor. No essential remarks have been made about conditions of music hearing in the auditorium (apart from the extremely annoying traffic noise and vibrations). These remarks inspired the undertaken investigation of acoustic characteristics of the hall. For the assessment of the characteristics the classical Beranek method has been applied (being criticized by numerous researchers) and, for the first time in home investigations, a method proposed by Ando. For the application of these methods it was necessary to perform acoustic measurements of the hall, and elaborate its digital model (Fig. 1). These problems will be presented in the following chapters.

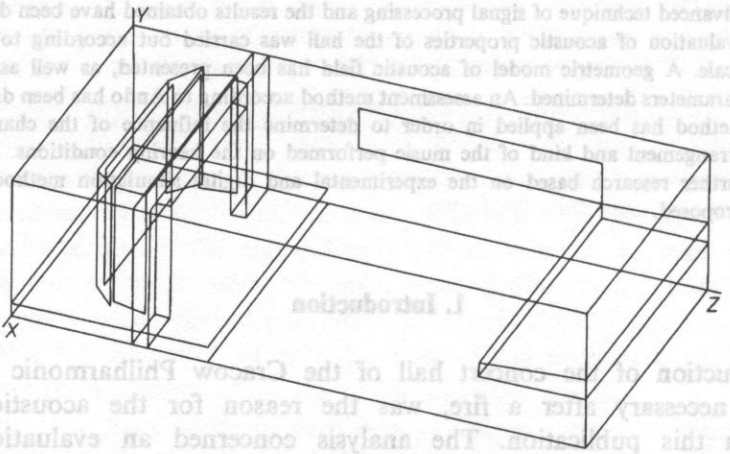

Fig. 1. Digital model of the concert hall of Cracow Philharmonic Orchestra.

2. Measurements of basic acoustic parameters

The measurements in the concert hall of Cracow Philharmonic Orchestra have been taken at points presented in Fig. 2. The applied measuring instrumentation consisted of portable microcomputer laptop Acer 1100 with signal processor card OROS AU22 type, and with professional software dB Impuls from the firm 01dB, power amplifier, and column loudspeakers (Fig. 3) [6].

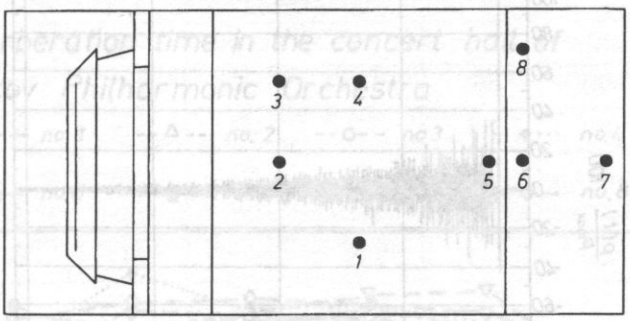

Fig. 2. Locations of measuring points (*1–5* orchestra, *6–8* balcony).

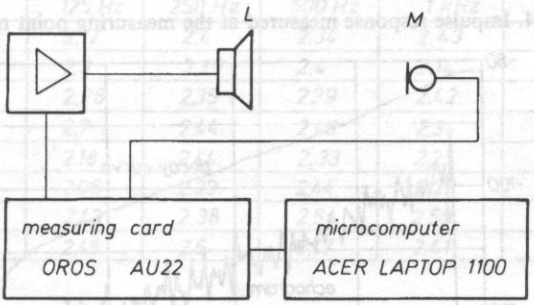

Fig. 3. Diagram of the measuring instrumentation.

The card AU22 from the firm OROS comprises signal processor TMS32OC25, two 16-bit transducers A/D, and two 16-bit transducers D/A of maximal sampling frequency 100 kHz. Storing the data in the hard disk of the microcomputer enables full elimination of magnetic recorder, while numeric computations are accelerated by the signal processor. For example, performance of spectral analysis employing FFT algorithm takes approx. 3.5 ms. Determination of acoustic parameters is realized as follows: The numerically generated white noise feeds loudspeaker *L*. The noise emitted by it is transformed into an electric signal by microphone *M*. Next, the transmittance between the two signals is determined, and after submitting it to the transformation of inverse Fourier transform the impulse response of the hall is obtained (Fig. 4). From the course of the impulse response of the hall after digital filtering a curve of acoustic pressure fading and an echograph are traced (Fig. 5), and out of them, employing the Schroeder method, the reverberation times are determined. The additional parameters determined by the dB Impuls are: early reverberation time, clarity, expressiveness, etc. The determined reverberation times for empty hall (without audience) have been shown in Fig. 6.

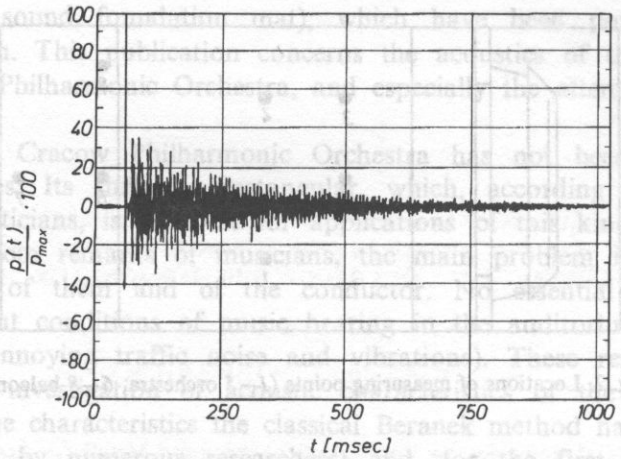

Fig. 4. Impulse response measured at the measuring point no. 6.

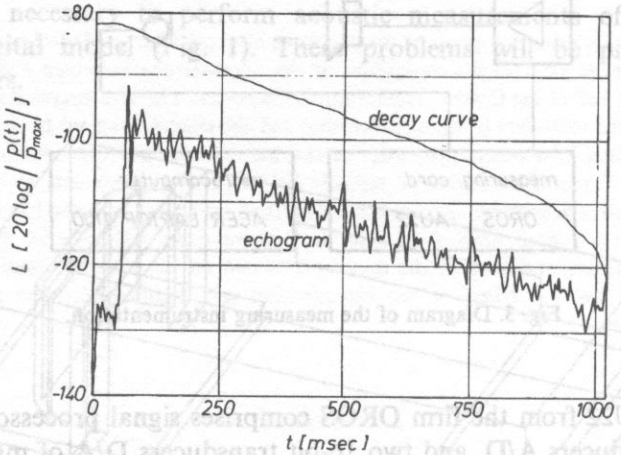

Fig. 5. Echograph and fading curve determined from the impulse responses from Fig. 4.

The maximal value of the reverberation time at the measuring point no. 4 for frequency 125 Hz results probably from the nearness of a corridor and the possibility of a rise of resonance. The results of measurements for low frequencies should be regarded as approximate, because they were constantly influenced by a low-frequency traffic noise, impossible to eliminate. For the remaining frequencies the results were repeatable. Application of this method to determination of the reverberation time in the hall with the audience seems to be troublesome because of the necessity of emitting of white noise of high level of acoustic power during the time of ten seconds. This is however a problem which concerns all presently applied methods of determination of reverberation time, and despite the attempts carried out with new measuring techniques (for instance applying a forced impulse caused by clapping hands) it has not been till now solved.

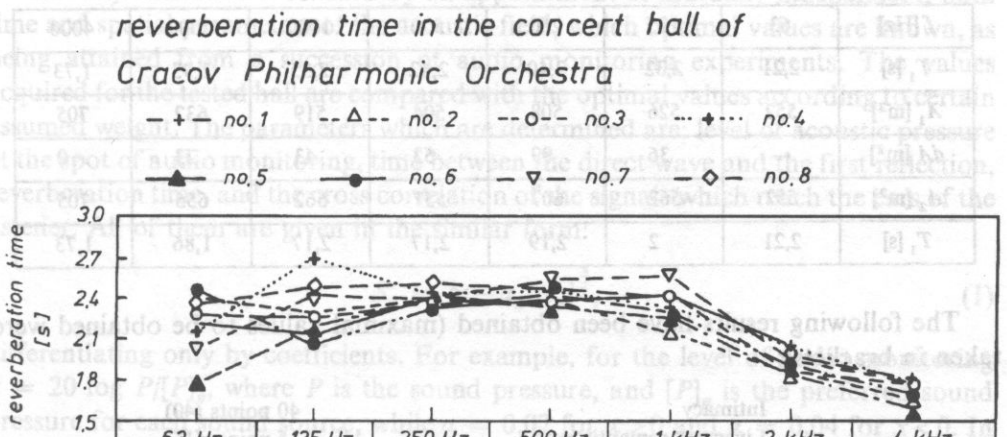

63 Hz	125 Hz	250 Hz	500 Hz	1 kHz	2 kHz	4 kHz
2.21	2.12	2.4	2.34	2.43	2.04	1.79
2.4	2.3	2.39	2.4	2.14	1.86	1.66
2.28	2.26	2.35	2.39	2.42	1.85	1.77
2.16	2.7	2.44	2.46	2.34	2.05	1.77
1.78	2.18	2.44	2.33	2.25	1.83	1.58
2.46	2.06	2.33	2.44	2.29	1.9	1.7
2.02	2.43	2.38	2.54	2.55	1.95	1.78
2.35	2.48	2.5	2.47	2.41	1.97	1.8

Fig. 6. Reverberating times in the concert hall of Cracow Philharmonic Orchestra determined according to Fig. 5.

3. Evaluation of acoustic features of the hall according to Beranek scale

In order to assess the acoustic characteristic of the hall as the first one the BERANEK method [2] was applied. The measured reverberation times refer to an empty hall (without audience), while the scale of valuations utilizes the reverberation times for filled halls. Having not at disposal such results, the times were assessed using a statistical method. Necessary data as for absorbing coefficients of empty chairs and with people have been taken from [5]. The obtained results of measurements and computations are presented in the Table 1 where T_1, A_1 are reverberation times and acoustic absorptivity of the hall without audience, while T_2, A_2 with audience (dA — estimated increment of acoustic absorptivity).

For frequency 63 Hz suitable data as for absorption coefficients were not at disposal, because of low frequency the effect of sound absorption by listeners has been neglected. It does not influence the scale of valuations, because only the reverberation times for frequencies 125 Hz, 250 Hz, 500 Hz and 1000 Hz have been utilized.

Table 1.

f [Hz]	63	125	250	500	1000	2000	4000
T_1 [s]	2,21	2,32	2,40	2,42	2,35	1,93	1,73
A_1 [m²]	552	526	508	504	519	632	705
dA [m²]	---	36	99	53	43	23	0
A_2 [m²]	552	562	607	557	562	655	705
T_1 [s]	2,21	2	2,19	2,17	2,17	1,86	1,73

The following results have been obtained (maximal values to be obtained were taken in brackets):

Intimacy		40 points (40)
Liveness:	romantic music	15 points (15)
	orchestral music	10 points (15)
	classic music	6 points (15)
	baroque music	4 points (15)
Warmth		5 points (15)
Loudness of the direct sound		8 points (10)
Loudness of the reverberant sound		0 points (6)
Diffusion		2 points (4)
Balance and blend		4 points (6)
Influence of other factors:	echo	0 points
	noise	−15 points
	tonal distortions	0 pts.

Final valuation (maximal 100 points)

Romantic music	74 pts.	B+	Orchestral music	69 pts	B
Classic music	65 pts.	B	Baroque music	63 pts.	B

Only for romantic music the hall has been given a valuation within the range: good — very good, and for the remaining kinds within the range: satisfactory — good. These valuations do not include negative points. Taking them into consideration will result in depreciation to the hall category of satisfactory quality. This method seems however not to be presently fully adequate to qualifying, because of both the influence of subjective tastes of the evaluating person, and the difference between the direct wave and the first reflection.

4. Evaluation of acoustic features of the hall according to Ando method

The mentioned ambiguity of the evaluations according to the Beranek scale was the ground of the application of a method developed by ANDO [1] to the assessment of the acoustic characteristic of the hall. The method, in comparison with the previous one, offers decidedly wider possibilities and, what is especially important, is able to an objectification of the evaluation process by operation exclusively on the numerical values, designated by a computer simulation (unlike in case of the Beranek method, there is no necessity to estimate e.g. an influence of echo).

The objectification is realized by an appointment of mutually independent, both time and spatial parameters of the acoustic field, which optimal values are known, as being attained from a succession of audio monitoring experiments. The values acquired for the tested hall are compared with the optimal values according to certain assumed weight. The parameters which are determined are: level of acoustic pressure at the spot of audio monitoring, time between the direct wave and the first reflection, reverberation time, and the cross correlation of the signals which reach the ears of the listener. All of them are given in the similar form:

$$S_n = \approx -\alpha_n |x_n|^{\frac{3}{2}}, \tag{1}$$

differentiating only by coefficients. For example, for the level of audio monitoring $x = 20 \log P/[P]_p$, where P is the sound pressure, and $[P]_p$ is the preferred sound pressure for each sound source, while $\alpha = 0.07$ for $x>0$ and $\alpha = 0.04$ for $x<0$. In analogical way the coefficients for the remaining parameters are determined. For the time difference between the direct wave and the first reflection $x = \log \Delta t/[\Delta t]_p$, for the reverberation time $x = \log T_p/[T_p]_p$, while for the function of the inter-aural cross correlation x assumes its maximal value (the index p means the preferred, optimal value). The reciprocal inter-aural correlation function, which describes the diffusion of the acoustic field in the point of audio monitoring is presented in the chapter 4.2.

The final evaluation is the sum of the component evaluations. The maximal attainable value is 0, the negative values mean deviations from the optimal conditions of audio monitoring of music.

All the parameters necessary to evaluation have been determined by means of the geometric model of acoustic field.

4.1. Geometric model of acoustic field

In order to determine the parameters used in the Ando method a digital model of acoustic field has been employed. The computer program implementing a method of image handling enables modelling of rooms of any shapes, defined by flat surfaces. To each one of these surfaces a sound attenuation coefficient is attributed as an acoustic parameter, which depends, similarly as other acoustic parameters, on frequency. The point sound sources of assignable directional characterisitcs are modelled. The results obtained for anyone of observation points inside a compartment are: passes of sound beams on the route from the sound source to the observation point (Fig. 7), levels of acoustic pressure (Fig. 8), and all the other parameters are determined by combination of the above mentioned ones. For the computations of the Ando parameters an echogram (Fig. 9) has been utilized, being a visualization of relation between the time of reaching the observation point by the wave front and its energy, as well as a sound hedgehog (Fig. 10) which in turn presents a relation between the direction of coming wave and its energy.

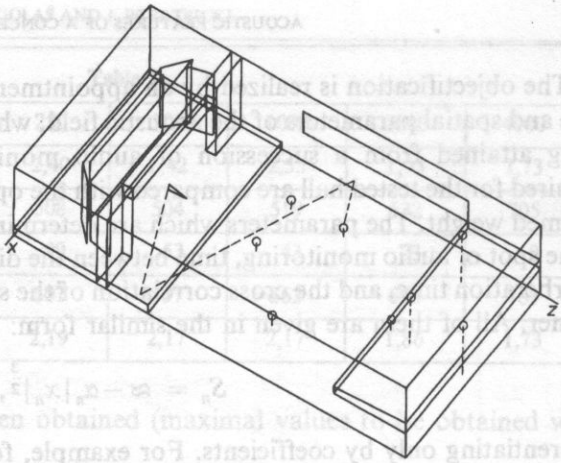

Fig. 7. Route of the sound beam.

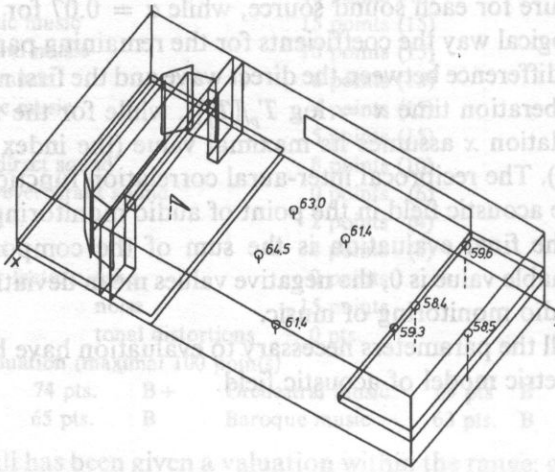

Fig. 8. Levels of acoustic pressure.

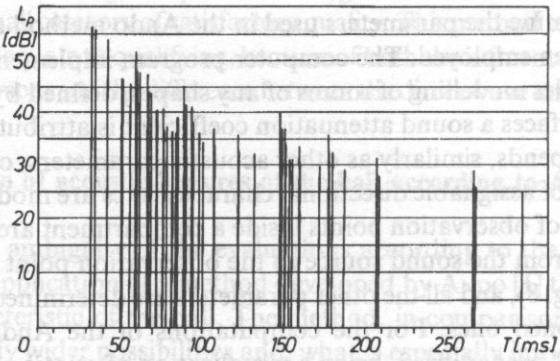

Fig. 9. Echogram at the observation point.

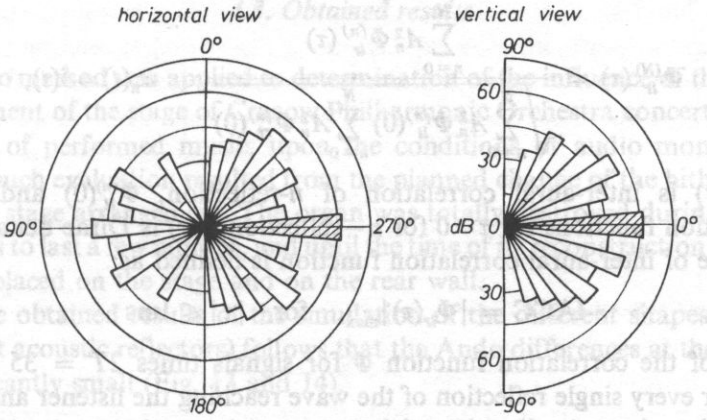

Fig. 10. Sound hedgehog at the observation point.

The model is permanently developed by both new qualitiative possibilities — as an attempt of consideration of the effects of diffraction and diffusion — as well as by quantitative ones concerning first of all the number of modelled elements and computation time.

4.2. Inter-aural cross correlation function IACC

In order to present the relations between the signals which reach the ears, it is possible to introduce a single coefficient, e.g. an inter-aural correlation between the signals $f_l'(t)$ and $f_r'(t)$, which are the acoustic pressures. The correlation becomes a significant coefficient for the determination of the degree of the field diffusion. A subjective diffusion (lack of feeling of directivity) is attained during audio monitoring in acoustic field of low correlation degree. On the other hand, well determined direction is discernable if the function has a distinct amplification for the time < 1 ms. The function depends mainly on the directions, from which the reflected waves reach the listener, and on their amplitudes. It is defined as follows:

$$\Phi_{lr}(\tau) = \lim_{T\to\infty} \frac{1}{2T} \int_{-T}^{T} f_l'(t) f_r'(t+\tau)dt, \quad |\tau| \leqslant 1\text{ms} \tag{2}$$

If the listener's face is pointed at the source of sound, the standardized inter-aural correlation function is given by the equation:

$$\Phi_{lr}^{(0)}(\tau) = \frac{\Phi_{lr}^{(0)}(\tau)}{\sqrt{\Phi_{ll}^{(0)}(0)\,\Phi_{rr}^{(0)}(0)}} \tag{3}$$

where $\Phi_{ll}^{(0)}(0)$ and $\Phi_{rr}^{(0)}(0)$ are auto-correlation functions for $\tau = 0$ for every ear. If they were added to the wave of the direct reflection the standardized inter-aural correlation is expressed by:

$$\Phi_{lr}^{(N)}(\tau) = \frac{\sum_{n=0}^{N} A_n^2 \Phi_{lr}^{(n)}(\tau)}{\sqrt{\sum_{n=0}^{N} A_n^2 \Phi_{ll}^{(n)}(0) \sum_{n=0}^{N} A_n^2 \Phi_{rr}^{(n)}(0)}}, \quad w_n(t) = \delta(t), \tag{4}$$

where $\Phi_{lr}^{(n)}(\tau)$ is inter-aural correlation of n-reflection, $\Phi_{ll}^{(n)}(0)$ and $\Phi_{rr}^{(n)}(0)$ are auto-correlation functions for $\tau = 0$ for $n-$reflection, $\delta(t)$ is Dirac delta function.

The value of inter-aural correlation function is defined as:

$$\text{IACC} = |\Phi_{lr}(\tau)|_{\max}, \quad \text{for} \quad |\tau| \leqslant 1\text{ms} \tag{5}$$

The values of the correlation function Φ for signals times $2T = 35$ s have been measured for every single reflection of the wave reaching the listener and inserted in [1]. Information about the direction of the wave coming to the monitoring point, and about the amplitude A_n of the wave are read out from the sound hedgehog (Fig. 10). Figures 11 and 12 present the determined values of the IACC function and corresponding evaluations. Great values of IACC by the stage are visible, where the influence of the direct wave is distinct, and a gradual diminishing together with the increase of the distance and nearing the walls of the compartment.

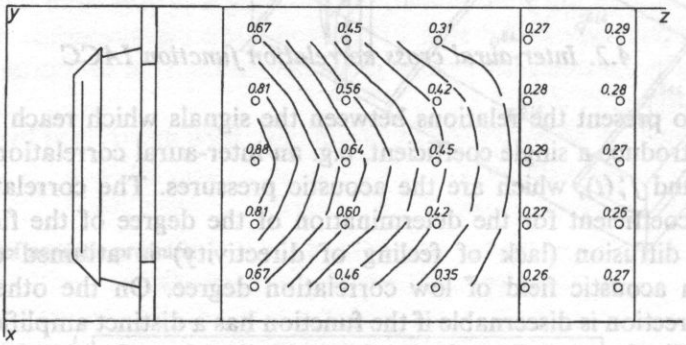

Fig. 11. Determination of IACC values.

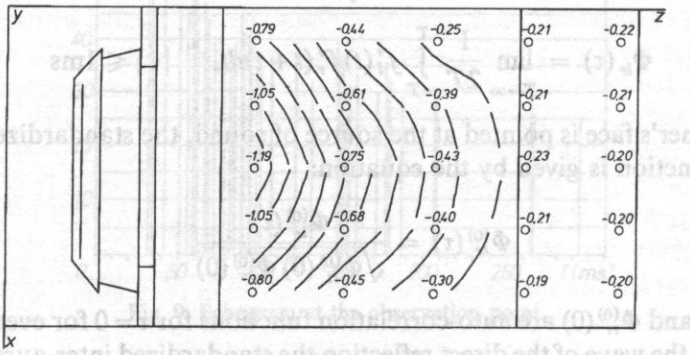

Fig. 12. Valuations according to Ando for IACC.

4.3. Obtained results

The Ando method was applied to determination of the influence of the changes in the arrangement of the stage of Cracow Philharmonic Orchestra concert hall, as well as the kind of performed music, upon the conditions of audio monitoring. The necessity of such evaluation resulted from the planned change of the hitherto existing shape of the stage arrangement. The organ was totally destroyed during the fire, its restoration is to last a few months, and until the time of its reconstruction a mockup of it has been placed on the stage and on the rear wall.

From the obtained results of the simulation of the different shapes of sceneries (being in fact acoustic reflectors) follows that the Ando differences at the auditorium are insignificantly small (Fig. 13 and 14).

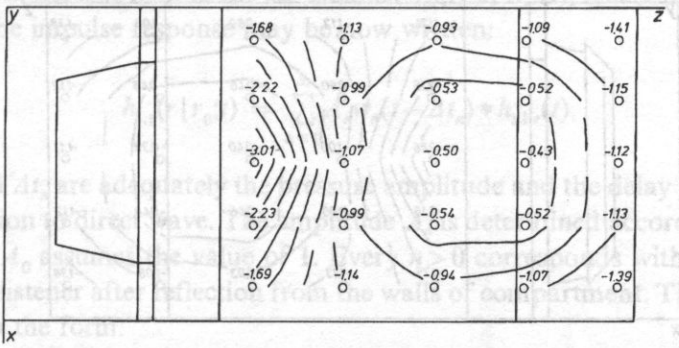

Fig. 13. Sum of valuations before modification of the hall.

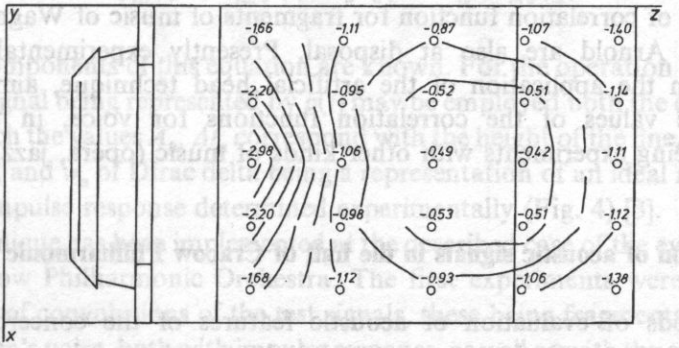

Fig. 14. Sum of valuations after modification of the hall.

For the hall of Philharmonic Orchestra the sums of evaluations of Ando parameters have been determined for different kinds of music. From the Fig. 15 and 16, which show the final evaluations adequtely to fragments of Philharmonic no. 102 of Haydn (motive C according to Ando) and Philharmonic C dur of Mozart (motive E), follows that for the last one the audio monitoring conditions are better.

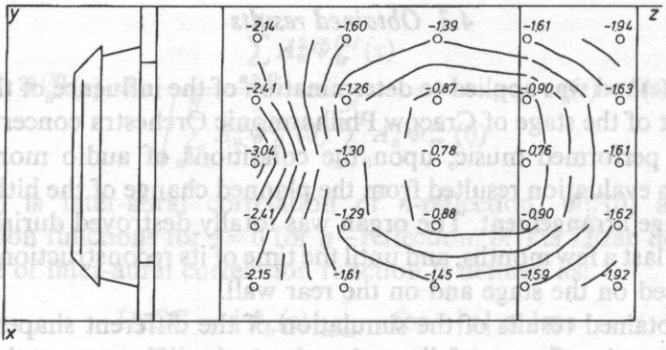

Fig. 15. Sum of valuations for Haydn music.

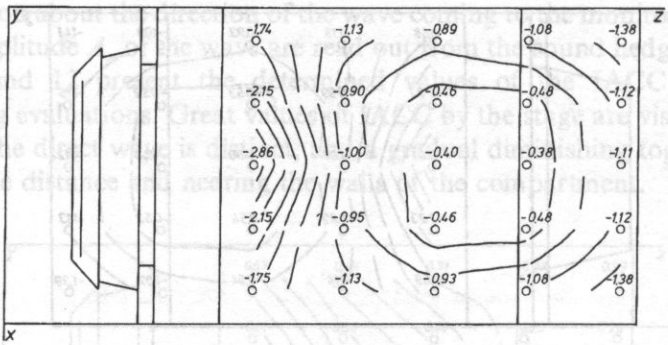

Fig. 16. Sum of valuations for Mozart music.

The values of correlation function for fragments of music of Wagner, Gibbons, and Malcolm Arnold are also at disposal. Presently experimental studies are carried out on the application of the artificial head technique, aimed to designation of the values of the correlation functions for voice, in the stage of preparation being experiments with other kinds of music (opera, jazz, rock music, etc.).

5. Simulation of acoustic signals in the hall of Cracow Philharmonic Orchestra

The methods of evaluation of acoustic features of the concert hall of the Cracow Philharmonic Orchestra presented hitherto are based on such acoustic parameters as reverberation time, inter-aural cross correlation function etc. Still the final criterion is the audio monitoring in the hall. However, exist occurrences when this monitoring is impossible, e.g. at the design stage or during considering possible changes of the shape and arrangement of halls. After all, exists a possibility of simulation of audio monitoring of the hall according to the way presented hereafter [1].

Assuming that only one source of sound exists in the stage, and that $h_l(r : r_0; t)$ and $h_r(r : r_0; t)$ are impulse responses of the pressure between the sound source located at r_0 and at the left and right ear channel of the listener (r means location of the geometric centre of the head), the acoustic pressure in the both ears, containing all the acoustic information, may be expressed by:

$$f_{lr}(t) = \int_{-\infty}^{t} p(v)h_{l,r}(t-v)dv = p(t) * h_{lr}(t), \tag{6}$$

where $p(t)$ is a signal from the source of sound, and the star means the convolution operation. The impulse response can be divided into the two components: $w_n(t)$ describing the effect of reflection from the walls of compartment and impulse responses from the free field to the ear channel $h_{nl}(t)$ or $h_{nr}(t)$, where n means a single reflection. The impulse response may be now written:

$$h_{l,r}(r \mid r_0;t) = \sum_{n=0}^{\infty} A_n w_n(t-\Delta t_n) * h_{nl,r}(t), \tag{7}$$

where A_n and Δt_n are adequately the pressure amplitude and the delay of the reflected wave in relation to direct wave. The amplitude A_n is determined according to the rule "$1/r$", while A_0 assumes the value of 1. Every $n>0$ corresponds with a single wave reaching the listener after reflection from the walls of compartment. The equation (8) assumes then the form:

$$f_{l,r}(t) = \sum_{n=0}^{\infty} p(t) * A_n w_n(t-\Delta t_n) * h_{nl,r}(t), \tag{8}$$

All the components of this equation are known. For the operation of convolution of acoustic signal being represented by $p(t)$ may be employed both the echogram (Fig. 9) — for which the values A_n, Δt_n correspond with the height of the line, and its shift in the time axis, and w_n of Dirac delta being a representation of an ideal reflection — as well as the impulse response determined experimentally (Fig. 4) [3].

This technique has been implemented at the described case of the evaluation of the hall of Cracow Philharmonic Orchestra. The first experiments were based on the performance of convolutions of the test signals, these being fragments of symphonic music and men's voice, both with impulse response, as well as with the echograph (Fig. 9). Fig. 17 presents a test signal, which has been submitted to convolution with the echogram (Fig. 9). The result of the operation is shown in Fig. 18. Audible are these changes of the signal which are relevant to appearance of reverberation. Further experiments, which have already been planned, are however necessary, as well as the verification of the results obtained e.g. by the method of cross correlation of the simulated and real signal, recorded in the hall.

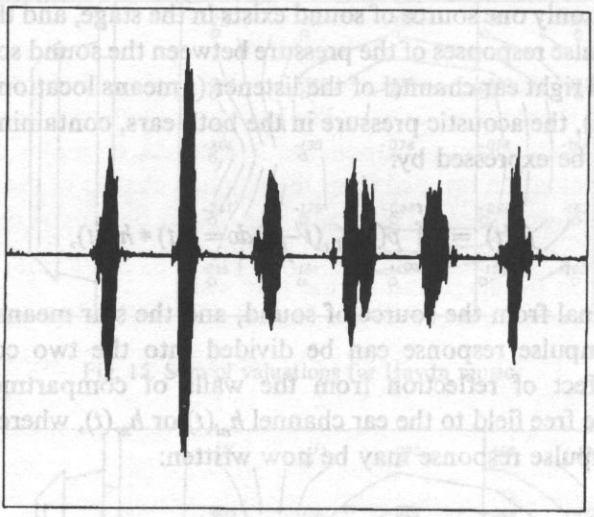

Fig. 17. Fragment of the signal from human speech.

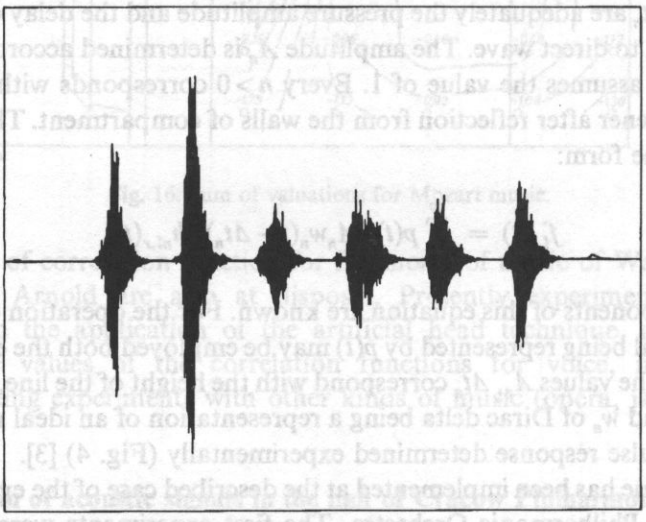

Fig. 18. The result of convolution of the signal from Fig. 17 with echogram (Fig. 9).

6. Evaluation of acoustic properties of the hall and directions of further research

The hall of the Cracow Philharmonic Orchestra has obtained the valuation within the scope of good — very good for romantic music, while for the remaining kinds satisfactory — good. After taking into account the scores for the disturbing effects, the valuation for all kinds of music lowers to satisfactory. It comes however from the

Ando method that the hall suits better to the presentation of the Mozart music than the Haydn, and the proposed changes of the stage arrangement do not cause any essential changes in the audio monitoring conditions. This method, as opposed to the Beranek method, does not enable assigning a singular valuation to the hall, and consequently, a direct comparison of different halls. The work being conducted is aimed to creation of such possibility e.g. by determination of the ratio between the zones of highest values of valuation and the entire zone of auditorium.

The results obtained hitherto demonstrated the usefulness of application of the Ando method as an essential extension of valuations according to the Beranek method. Linking the Ando method and the potentials of simulations of acoustic signals tends towards creation of a comprehensive expert system. Such system, assuring ability of modelling of acoustic field in compartments of any shape, will enable an evaluation of both current state as well as indication of applicable solutions, e.g. acoustic adaptation, etc. Being equipped with a library of absorption coefficients for different materials, directional characteristics of sources, and test acoustic signals should become a help for both acousticians and architects.

The first attempts of automatization of the process of choice and selection of arrangement of acoustic elements in a compartment have been undertaken. In the publication [4] an implementation of the method of factor analysis to choice of arrangement of sound sources has been presented, the method being able to assure a minimal level of acoustic pressure in the observation point. This method can be also applied to choice of location of musicians on the stage in order to assure the optimal hearing conditions e.g. by conductor. This subject in being developed, however not possible to a realization before modifications of the geometric model of acoustic field. The work being presently conducted are focused first of all on considering the effects of diffraction and diffusion of the sound wave. Its novelty is regarding the wave not as a sound beam; the new approach is based on determination of the degree of mutual visibility for every pair of surfaces, both between them reciprocally, as well as from direction of the sound source and the listener.

Parallel with the simulative investigations the experiments with the artificial head are carried out. Its objective is determination of the inter-aural cross correlation function for other kinds of music than the ones quoted by publications of Ando, and also to establish a basis for development of the technique of creating the virtual reality — which expands so spontaneously now — but within the domain of acoustic signals.

References

[1] Y. ANDO, *Concert hall acoustics*, Springer Verlag, Berlin, Heildelberg, New York, Tokyo 1985.
[2] L. BERANEK, *Music, acoustic and literature*, John Wiley and Sons Inc., New York, London 1962.

[3] A. Gołaś, H. Łopacz, J. Wierzbicki, *Signals simulation based on convolution of room impulse response*, AES 92 nd Convention, Vienna 1992.
[4] A. Gołaś, J. Wierzbicki, *Selection of source sound distribution with the consideration of sound pressure level in closed spaces*, Proc. Inter-Noise 90, Gothenburg 1990.
[5] H. Kuttruff, *Room acoustics*, Elsevier, London New York 1991.
[6] H. Łopacz, *Impulse methods in investigations of vibroacoustic processes*, Doctor's Thesis, Academy of Mining and Metallurgy, IMWA — Kraków.

ARCHIVES OF ACOUSTICS
18, 2, 297–309 (1993)

INFLUENCE OF THE ACOUSTIC-STRUCTURAL COUPLINGS UPON FREE VIBRATIONS OF MECHANICAL SYSTEMS

J. HORÁČEK and I. ZOLOTAREV

Institute of Thermomechanics
(182 00 Prague 8, Dolejskova 5)

The roles of acoustic-structural couplings in three entirely different aeroelastic systems are compared. The first system is a thin elastic cylindrical shell containing fluid in a coaxial annular duct, the second system is a thin plate vibrating in fluid near a rigid wall, and the third system is a simple single degree-of-freedom mechanical system, vibrating in contact with a confined volume of an acoustic medium. It is shown that the nature of the acoustic-structural coupling is identical in all the studied cases.

1. Introduction

From studies of the dynamical behaviour of cylindrical shells conveying fluid it is known that in the specific wave-number regions the strong acoustic-structural couplings exist between the vibration of a light fluid (e.g. a gas) and the shell [2, 3, 4]. Consequently, the spectrum of eigenfrequencies of the coupled shell-fluid system may be quite different from the spectra of the two separated subsystems (the shell in vacuo and the fluid in the rigid cylindrical duct).

The main idea of the paper is to point out some general and fundamental properties of coupled free vibrations of structures and acoustic media. Namely, the very similar dynamic phenomena as in the shell-fluid systems were also found for plate-fluid systems and even for systems having finite number of degrees of freedom.

2. Shell-fluid system

The natural vibration of the cylindrical shell (with the radius R and the wall thickness h) containing fluid (with the density ρ_f and characterized by the speed of sound c_0 in a coaxial duct of the radius R_d (see Fig. 1) was studied in detail in [4], and for $R_d = 0$ in [2, 3].

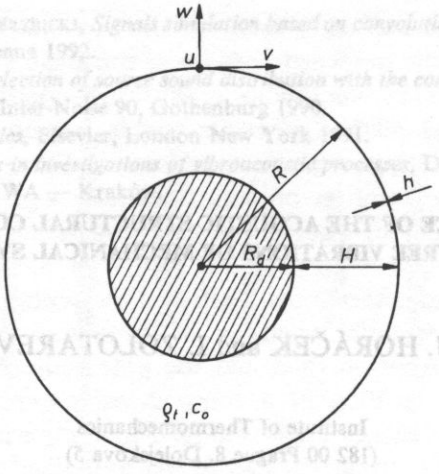

FIG. 1

The equations of motion of the thin shell can be written in the following form

$$\left[K + \frac{\rho_s R^2(1-\nu^2)}{E} I \frac{\partial^2}{\partial t^2}\right] \begin{pmatrix} u \\ v \\ w \end{pmatrix} = \frac{R^2(1-\nu^2)}{Eh} \begin{pmatrix} 0 \\ 0 \\ p \end{pmatrix}, \tag{1}$$

where K is the Goldenweizer-Novozhilov's structural operator, I is a 3×3 unit matrix; ρ_s, E and ν are the density, Young's modulus and Poisson's ratio of the shell material; u, v and w are the axial, circumferential and radial displacements of the shell, respectively; and p is the acoustic perturbation pressure.

Following closely BOLOTIN's work [1], it is possible for a structural wave of the type

$$\begin{pmatrix} u \\ v \\ w \end{pmatrix} = \begin{pmatrix} U \\ V \\ W \end{pmatrix} e^{i(\omega t - \bar{\alpha} x - n\theta)}, \tag{2}$$

to derive the perturbation pressure p for the potential flow field in the annulus in the form

$$p = \rho_t R \, \mu_n(\beta R, \beta R_d) \, \omega^2 \, W \, e^{i(\omega t - \bar{\alpha} x - n\theta)}, \tag{3}$$

where ω is the circular frequency, $\bar{\alpha}$ and n are the wave-numbers in the axial (x) and circumferential (θ) directions; U, V, W are the components of amplitude of vibration of the shell. The function μ_n, characterizes the added mass coefficient of a compressible fluid in the annulus and is given by the formula:

$$\mu_n(\beta R, \beta R_d) = \frac{1}{\beta R} \cdot \frac{{}^1\phi_n(\beta R) \; {}^2\phi_n'(\beta R_d) - {}^1\phi_n'(\beta R_d) \; {}^2\phi_n(\beta R)}{{}^1\phi_n'(\beta R) \; {}^2\phi_n'(\beta R_d) - {}^1\phi_n'(\beta R_d) \; {}^2\phi_n'(\beta R)}, \tag{4}$$

where

$$\beta = \left| \bar{\alpha}^2 - \left(\frac{\omega}{c_0}\right)^2 \right|^{1/2}, \tag{5}$$

$$^1\phi_n = I_n \quad \text{and} \quad ^2\phi_n = K_n \quad \text{for} \quad \bar{\alpha} > \frac{\omega}{c_0}, \tag{6}$$

$$^1\phi_n = J_n \quad \text{and} \quad ^2\phi_n = Y_n \quad \text{for} \quad \bar{\alpha} < \frac{\omega}{c_0}, \tag{7}$$

I_n, K_n, J_n, Y_n are the Bessel functions and the primes denote their derivatives. Substitution of the expressions (2) and (3) into Eq. (1) yields the characteristic equation for the natural frequencies of the system

$$\begin{vmatrix} f_{11}(\Omega^2) & f_{12} & f_{13} \\ f_{12} & f_{22}(\Omega^2) & f_{23} \\ f_{13} & f_{23} & f_{33}(\Omega^2) + \rho\psi\ (\Omega) \end{vmatrix} = 0, \tag{8}$$

where the following dimensionless variables were introduced

$$\Omega = \omega R\sqrt{\rho_s/E},\ \alpha = \bar{\alpha} R,\ \rho = \rho_t R/\rho_s h,\ c = c_0/\sqrt{E/\rho_s},$$
$$\xi = \beta R,\ \xi_d = \beta R_d = \xi R_d/R; \tag{9}$$

f_{ij} are functions of α, n, ν, h/R defining the vibration of the shell *in vacuo*, and ψ is the function, that defines the effects of fluid in the annulus

$$\psi = \pm(1-\nu^2)\mu_n(\xi, \xi_d)\Omega^2. \tag{10}$$

The minus sign hold for fluid inside the thin shell ($R > R_d$) and the plus sign for fluid outside ($R < R_d$).

For the shell of finite length l simply supported at both ends the wavenumber α has only discrete values $\alpha_m = m\pi R/l (m = 1, 2, ...)$, and for every studied mode of vibration, which is defined by the n waves in the circumferential direction and by the m halfwaves along the length of the shell, the Eq. (8) has an infinite number of solutions Ω.

The equation (8) can be rewritten in the form

$$[^1\phi_n'(\xi)\ ^2\phi_n'(\xi_d) - {}^1\phi_n'(\xi_d)\ ^2\phi_n'(\xi)]\ F(\Omega^2) \pm \rho(1-\nu^2)\ \Omega^2 \cdot$$
$$\cdot\ [^1\phi_n(\xi)\ ^2\phi_n'(\xi_d) - {}^1\phi_n'(\xi_d)\ ^2\phi_n(\xi)] \cdot \frac{1}{\xi}\ [f_{11}(\Omega^2) f_{22}(\Omega^2) - f_{12}^2] = 0, \tag{11}$$

where $F(\Omega^2)$ is the determinant (8) for the thin shell *in vacuo*, i.e. for $\rho = 0$.

If the dimensionless fluid density ρ equals zero, i.e., for the shell *in vacuo* ($\rho_t = 0$) or for fluid in the rigid annular duct ($h/R \to \infty$), the shell-fluid system is uncoupled and we get from Eq. (11) three natural frequencies $\Omega_{0,i}$ ($i = 1, 2, 3$) of the shell *in vacuo*, given

by the equation $F(\Omega^2)=0$, and from the first bracketed term of Eq. (11) the infinite number of acoustic resonant frequencies

$$\Omega_{a,k} = c\sqrt{\alpha^2+z_{n,k}^2} \quad (k=1, 2,...), \tag{12}$$

where $z_{n,k}$ are the positive roots of the following equation:

$$J_n'(z)\, Y_n'(z\, R_d/R) - J_n'(z\, R_d/R)\, Y_n'(z) = 0. \tag{13}$$

For $\rho>0$ the two subsystems (the shell in vacuo and the fluid in the rigid duct)

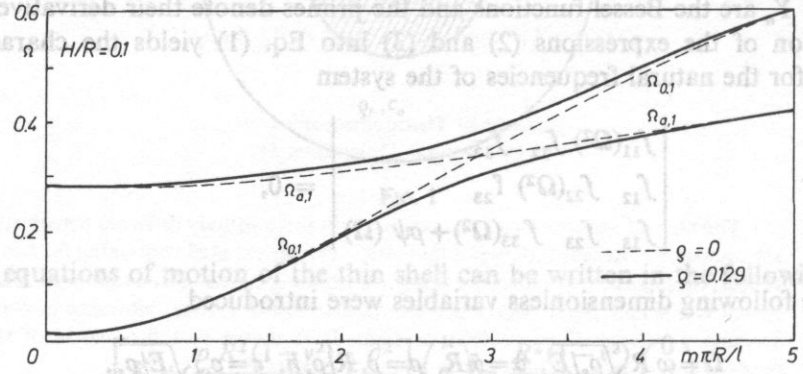

FIG. 2

are coupled, and from Eq. (11) one obtains an infinite number of frequencies Ω. The first two of them are shown, as an example, in Fig. 2 for the duralluminium shell-air system ($n=4$, $h/R=1/300$, $\nu=0.34$, $c=0.066$, $\rho=0.129$, $R_d/R=0.9$. The difference between the solutions for $\rho=0$ (dashed lines) and $\rho>0$ (solid lines), in Fig. 2 is essential near the wavenumber $m\pi R/l\approx 3$, where natural frequencies $\Omega_{0,1}$ and $\Omega_{a,1}$ of the both subsystems coincide, and where the strong acoustic-structural coupling exists. From the point of view of vibration of the shell *in vacuo* one natural frequency is here split up into the two different frequencies; the difference between them increases with the density ρ and by narrowing the annular gap width. In the regions of strong acoustic-structural coupling we cannot distinguish the acoustic modes from the structural ones. Out of this regions the vibrations are predominantly structural ($\Omega\to\Omega_{0,i}$) or acoustical ($\Omega\to\Omega_{a,k}$). The more accurate classification of the modes one gets by analysing the ratios of the perturbation flow and shell velocities [3].

3. Plate-fluid system

The second aeroelastic system studied is a thin elastic plate of thickness h, supported by an array of springs and placed near a parallel rigid wall at a distance H (see Fig. 3). Between the thin plate and the rigid wall there is an inviscid

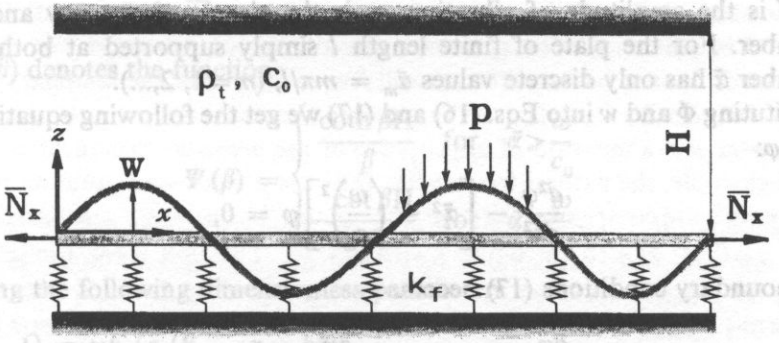

FIG. 3

compressible fluid of density ρ_t. The springs may be modelled by a continuous elastic foundatin of spring stiffness k_f per unit length of the plate. In general, the plate is subjected to a longitudinal tension $\bar{N}_x$ per unit width of the plate.

The displacement w of the plate is governed by the equation

$$D\frac{\partial^4 w}{\partial x^4} - \bar{N}_x\frac{\partial^2 w}{\partial x^2} + k_f w + \rho_s h\frac{\partial^2 w}{\partial t^2} + p = 0, \tag{14}$$

where $D = Eh^3/12\,(1-\nu^2)$ is the flexural rigidity of the plate; E and ν are, respectively, the Young's modulus and Poisson's ratio of the plate material. The perturbation acoustic pressure p acting on the vibrating plate is given according to the linear potential $2D$ flow theory by the equation

$$p = -\rho_t \cdot \left(\frac{\partial \Phi}{\partial t}\right)_{|z=0}, \tag{15}$$

where the perturbation flow velocity potential Φ must satisfy the wave equation

$$\frac{\partial^2 \Phi}{\partial x^2} + \frac{\partial^2 \Phi}{\partial z^2} = \frac{1}{c_0^2}\frac{\partial^2 \Phi}{\partial t^2}, \tag{16}$$

and the boundary conditions

$$\frac{\partial \Phi}{\partial z}\Big|_{z=0} = \frac{\partial w}{\partial t}, \quad \frac{\partial \Phi}{\partial z}\Big|_{z=H} = 0 \tag{17}$$

on the lower vibrating and upper rigid channel walls, since no fluid can pass through the surface.

Assuming a solution in the form of travelling waves, we set

$$\begin{pmatrix} w \\ \Phi \end{pmatrix} = \begin{pmatrix} W \\ \varphi(z) \end{pmatrix} \cdot e^{i(\omega t - \bar{\alpha} x)}, \tag{18}$$

where W is the amplitude of vibration, ω is the circular frequency and $\bar{\alpha}$ is the wavenumber. For the plate of finite length l simply supported at both ends the wavenumber $\bar{\alpha}$ has only discrete values $\bar{\alpha}_m = m\pi/l$, $(m=1, 2,...)$.

Substituting Φ and w into Eqs. (16) and (17) we get the following equation for the function φ:

$$\frac{d^2\varphi}{dz^2} - \left[\bar{\alpha}^2 - \left(\frac{\omega}{c_0}\right)^2\right]\varphi = 0, \tag{19}$$

and the boundary conditions (17) become

$$\frac{\partial\varphi}{\partial z}\Big|_{z=0} = i \cdot W, \quad \frac{\partial\varphi}{\partial z}\Big|_{z=H} = 0. \tag{20}$$

Denoting

$$\beta = \sqrt{\left|\bar{\alpha}^2 - \left(\frac{\omega}{c_0}\right)^2\right|}, \tag{21}$$

the general solution of Eq. (19) can be written in the form

$$\varphi = A \cdot e^{-\beta z} + B \cdot e^{+\beta z} \quad \text{for} \quad \bar{\alpha} > \frac{\omega}{c_0}; \tag{22}$$

$$\varphi = A \cdot \sin\beta z + B \cdot \cos\beta z \quad \text{for} \quad \bar{\alpha} < \frac{\omega}{c_0}. \tag{23}$$

Calculating the integration constants A and B from the boundary conditions (20) one obtains the following expression for the velocity potential:

$$\varphi = -i\frac{w}{\beta}\omega \cdot \frac{\cosh\beta(H-z)}{\sinh\beta H} \quad \text{for} \quad \bar{\alpha} > \frac{\omega}{c_0}; \tag{24}$$

$$\varphi = +i\frac{w}{\beta}\omega \cdot \frac{\cos\beta(H-z)}{\sin\beta H} \quad \text{for} \quad \bar{\alpha} < \frac{\omega}{c_0}, \tag{25}$$

and using Eqs. (18) and (15) we can write the solution for the perturbation pressure in the form

$$\begin{aligned} p &= -\rho_t\omega^2 W \cdot \frac{\coth\beta H}{\beta} \cdot e^{i(\omega t - \bar{\alpha}x)} \quad \text{for} \quad \bar{\alpha} > \frac{\omega}{c_0}; \\ p &= +\rho_t\omega^2 W \cdot \frac{\cot\beta H}{\beta} \cdot e^{i(\omega t - \bar{\alpha}x)} \quad \text{for} \quad \bar{\alpha} < \frac{\omega}{c_0}. \end{aligned} \tag{26}$$

Substituting p and w from Eqs. (26) and (18) into the equation of motion (14) we finally get the following characteristic equation for natural frequencies ω of the coupled plate-fluid system

$$D\bar{\alpha}^4 + \bar{N}_x \bar{\alpha}^2 + k_f - \rho_s h\omega^2 - \rho_t \omega^2 \cdot \Psi(\beta) = 0, \tag{27}$$

where $\Psi(\beta)$ denotes the function

$$\Psi(\beta) = \begin{cases} \dfrac{\coth \beta \mathrm{H}}{\beta} & \text{for} \quad \bar{\alpha} > \dfrac{\omega}{c_0} \\ -\dfrac{\cot \beta \mathrm{H}}{\beta} & \text{for} \quad \bar{\alpha} < \dfrac{\omega}{c_0}. \end{cases} \tag{28}$$

Introducing the following dimensionless parameters

$$\Omega = \omega h \sqrt{\rho_s / E}, \quad \alpha = h\bar{\alpha},$$
$$N_x = \bar{N}_x / Eh, \quad K = k_f h / E,$$
$$\rho = \rho_t / \rho_s, \quad c = c_0 / \sqrt{\rho_s / E}, \quad \xi = \beta h = \sqrt{\left| \alpha^2 - \left(\frac{\Omega}{c} \right)^2 \right|}, \tag{29}$$
$$\bar{H} = H/h,$$

the characteristic equation can be rewritten in the form

$$\frac{1}{\Psi(\xi)} \left[\frac{\alpha^4}{12(1-\nu^2)} + N\alpha^2 + K - \Omega^2 \right] - \rho \Omega^2 = 0, \tag{30}$$

where

$$\Psi(\xi) = \begin{cases} \dfrac{\coth \xi \bar{\mathrm{H}}}{\xi} & \text{for} \quad \alpha > \dfrac{\Omega}{c} \\ -\dfrac{\cot \xi \bar{\mathrm{H}}}{\xi} & \text{for} \quad \alpha < \dfrac{\Omega}{c}. \end{cases} \tag{31}$$

For the uncoupled plate and fluid systems ($\rho = 0$) we get from Eq. (30) the natural frequency of the plate in vacuo ($\rho_t \to 0$)

$$\Omega_0 = \sqrt{\frac{\alpha^4}{12(1-\nu^2)} + N\alpha^2 + K}, \tag{32}$$

and the infinite number of acoustic resonant frequencies for the fluid in the rigid ($\rho_s \to \infty$) channel:

$$\Omega_{a,k} = c \sqrt{\alpha^2 + \left(\frac{k\pi}{\bar{H}} \right)^2}, \qquad (k = 0, 1, 2, \ldots) \tag{33}$$

because the equation

$$\frac{1}{\Psi(\xi)} \equiv \xi \operatorname{tg} \xi \bar{H} = 0 \tag{34}$$

must be satisfied.

For the coupled plate-fluid system ($\rho > 0$) we get from Eq. (30) the infinite number of natural frequencies Ω. The greater is the dimensionless density ρ, the greater becomes the difference between the natural frequencies Ω of the coupled system and the natural frequencies Ω_0 or $\Omega_{a,k}$ of the separated acoustic and structural subsystems. The parameter ρ is a measure of importance of the acoustic-structural coupling.

An an example, the natural frequencies Ω of the pre-stressed duraluminium plate interacting with the compressed air contained in the channel were calculated ($\rho = 0.01$, $c = 0.066$, $\nu = 0.34$, $\bar{H} = 10$, $N_x = 0.5$, $K = (0.0125)^2$). The first three branches of the solution Ω for the coupled system ($\rho = 0.01$) are shown in Fig. 4a (solid lines marked by the numbers 1, 2, 3). The solutions Ω_0 and $\Omega_{a,k}$ for the uncoupled systems ($\rho = 0$) are also plotted here thin dashed lines.

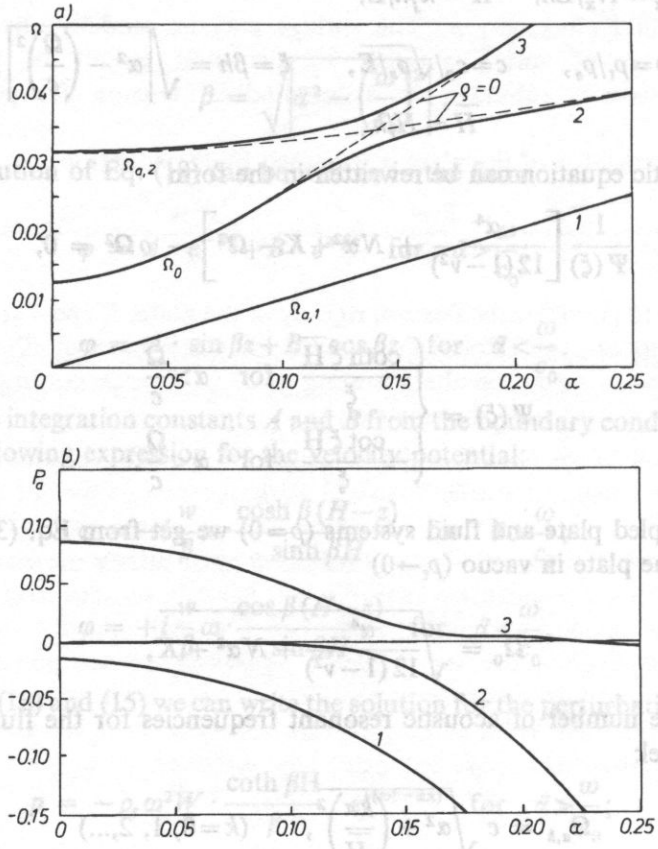

FIG. 4

The results of Figs. 2 and 4a show that the dynamical properties of the studied plate-fluid and shell-fluid systems are very close concerning the coupling of acoustic and structural natural frequencies.

The more detailed analysis of the acoustic-structural couplings gives the calculation of the amplitude p_a of the acoustic pressure on the vibrating plate surface. From Eq. (26) we get for the amplitude p_a the expression

$$p_a = -\rho E \frac{W}{h} P_a, \tag{35}$$

where $P_a = \Omega^2 \Psi(\xi)$ characterizes the ratio p_a/W of the amplitudes of the pressure and the displacement of the vibrating surface. The characteristics P_a for the studied plate-fluid system are plotted in Fig. 4b for the first three natural frequencies Ω depicted in Fig. 4a. The results displayed in Fig. 4 show, that if the mode is predominantly structural ($\Omega \to \Omega_0$) the amplitude of the pressure is very small ($P_a \to 0$) e.g. for the branch 2 and $\alpha > 0.1$. For predominantly acoustic modes ($\Omega \to \Omega_{a,k}$) the pressure P_a is much higher, e.g., for the branch 3 and $\alpha < 0.1$. If the acoustic and structural modes are strongly coupled (see the branches 2 and 3 near $\alpha = 0.14$), the pressure amplitudes P_a in absolute values for these two modes of vibration are comparable, and the difference between two modes is only in the opposite phase of the plate deflection and the pressure. We cannot distinguish the acoustic modes from the structural ones. From the point of view of free vibration of the plate *in vacuo* on mode of vibration is, in the region of strong acoustic structural coupling ($\alpha \approx 0.14$), split in the two modes, similarly as for the shell-fluid system.

4. Simplified mechanical system

The single degree-of-freedom system, with mass M and stiffness k vibrating in contact of its surface S with a fluid near a rigid wall is depicted in Fig. 5a. This mechanical system can be, e.g., a very simplified model of the shell-fluid system solved in Sec. 2 of the paper. The analogy between the two systems is illustrated in Fig. 5b, where the mode $n = 4$ for the shell is schematically plotted.

The free vibration of the mechanical system is described by the equation

$$M \ddot{w}(t) + k\, w(t) + \int_S p(x,t)\, dS = 0, \tag{36}$$

where p is a perturbation pressure on the surface $S = \bar{h} L$. For simplicity it is supposed that p is a function of time t and the coordinate x ($0 \leqslant x \leqslant L$); L and $\bar{h}$ are the length and the width of the surface of the mass M, respectively.

The pressure $p(x,t)$ is obtained from the 2D potential inviscid flow theory, as in Sec. 2 of the paper for the plate-fluid system. Equations (15), (16) and (17) for the fluid field are completed by the following boundary condition

$$\phi|_{x=0} = \phi|_{x=L} = 0 \tag{37}$$

at the free edges of the volume of fluid.

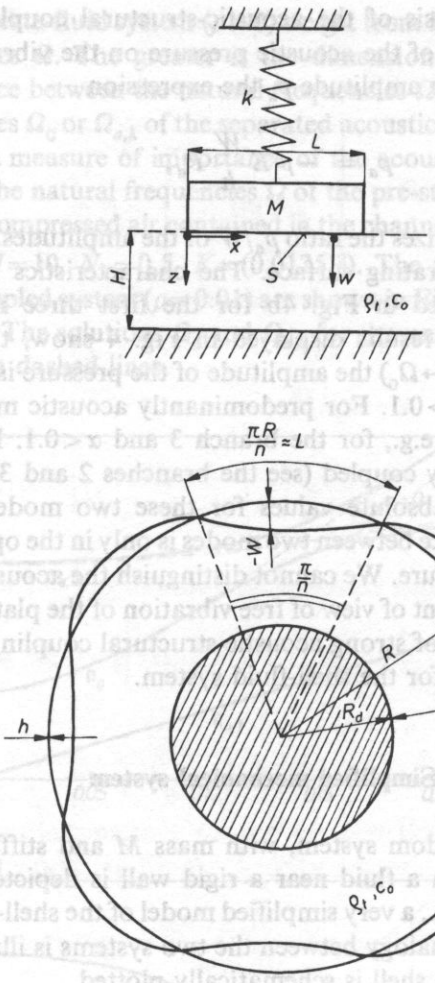

FIG. 5

The harmonic motion of mass M with frequency and an amplitude W gives

$$w = W e^{i\omega t} \quad \text{and} \quad \phi(x, z, t) = \varphi(x, z)\, e^{i\omega t}, \tag{38}$$

where the potential ϕ is the solution of Eq. (16) with the boundary conditions (17) and (37). Solving this boundary problem we get for φ the solution

$$\varphi(x, z) = \sum_{k=1}^{+\infty} \sin \kappa_k x \, (A_k \cos \beta_k z + B_k \sin \beta_k z), \tag{39}$$

where

$$\beta_k = \sqrt{(\omega/c_0)^2 - \kappa_k^2}, \quad \kappa_k = k\pi/L. \tag{40}$$

Calculating the integration constants A_k, B_k from the conditions (17) and using Eq. (15), the perturbation pressure is obtained,

$$p(x,t) = \rho_t \frac{2}{L} \omega^2 W \sum_{k=1}^{+\infty} \frac{[1-(-1)^k]}{\kappa_k \beta_k} \cot(\beta_k H) \sin(\kappa_k x)\, e^{i\omega t}. \tag{41}$$

Substitution of the integral $F(t) = \int_0^L p(x,t)\, \bar{h}\, dx$ and w in Eq. (36), yields the characteristic equation for the natural frequencies of the coupled fluid-mechanical system

$$-\bar{\Omega}^2 + \lambda^2 + \rho \bar{\Omega}^2 \frac{8}{\pi^2} \sum_{j=0}^{+\infty} \frac{1}{(2j+1)^2} \frac{\cot(\bar{H}\sqrt{\bar{\Omega}^2-(2j+1)^2})}{\pi \bar{H}\sqrt{\bar{\Omega}^2-(2j+1)^2}} = 0, \tag{42}$$

where the following dimensionless quantities were introduced:

$$\bar{\Omega} = \omega L/\pi c_0, \quad \lambda = \sqrt{k/M}\, L/\pi c_0, \quad \rho = \rho_t SH/M, \quad \bar{H} = H/L. \tag{43}$$

The modes of vibration may be characterized by the ratio of amplitudes F_A of the aerodynamic force $F(t)$ and the amplitude of vibration

$$\bar{F} \equiv \frac{F_A/(\rho_t c_0^2 S)}{W/L} = \pi^2 \frac{\bar{H}}{\rho} (\bar{\Omega}^2 - \lambda^2). \tag{44}$$

The first two natural frequencies $\bar{\Omega}$ of the coupled fluid-mechanical system with the parameters $\bar{H}=0.13$ and $\rho=0.12$ which are the equivalents of the solved shell-fluid system ($H=R-R_d$, $L=\pi R/n$, $\bar{h}=l/m$, $M=\rho_s h\pi R l/(m\cdot n)$), are depicted in Fig. 6 as

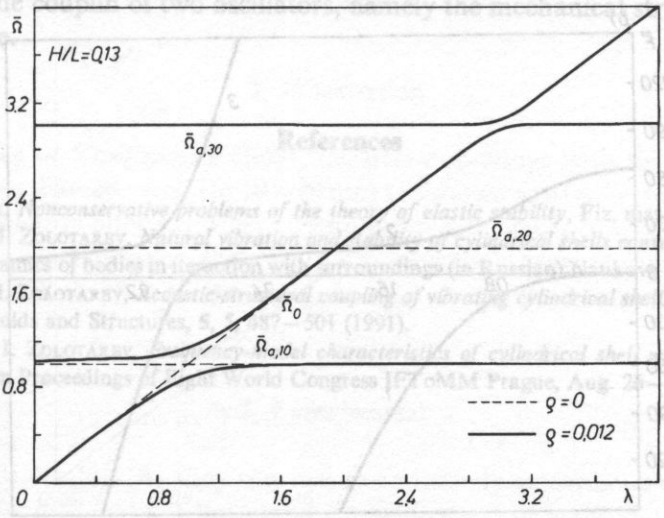

FIG. 6

functions of λ (full lines). If the dimensionless density is small ($\rho \to 0$), one obtains from Eq. (42) the natural frequency $\bar{\Omega}_0 = \lambda$ of the mechanical system *in vacuo*, and the acoustic resonant frequencies

$$\bar{\Omega}_{a,kj} = \sqrt{k^2 + (j/\bar{H})^2} \quad (k = 1, 2, \ldots; j = 0, 1, \ldots) \tag{45}$$

of the volume of fluid in the rectangular immovable slot dashed lines. Similarly to the shell-fluid system (see Fig. 2), in Fig. 6 appear the regions of λ where strong acoustic-structural couplings exist, or where the vibrations are predominantly structural ($\bar{\Omega} \to \bar{\Omega}_0$) or acoustical ($\bar{\Omega} \to \bar{\Omega}_{a,kj}$). The results of Fig. 6 are not only in

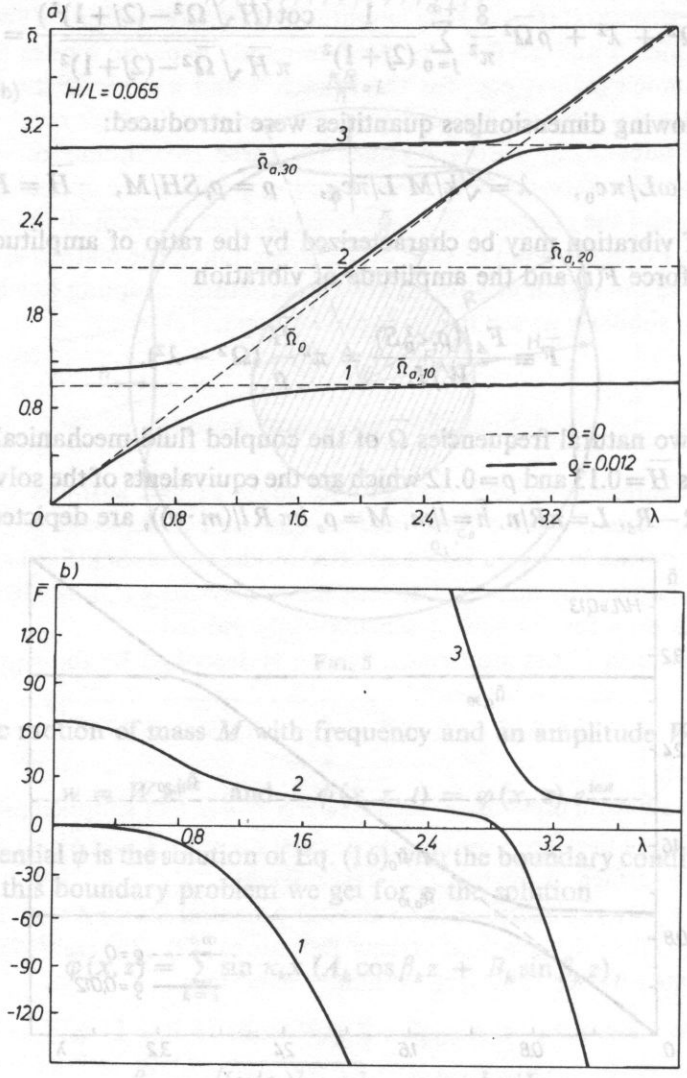

FIG. 7

qualitative agreement with the results of Fig. 2. Concerning, for example, the difference between the split natural frequencies Ω in the regions of strong coupling ($\lambda \approx 1$ in Fig. 6 and $\alpha_m = 2.8$ in Fig. 2), the difference reaches approximately 24% in both the cases studied.

By narrowing the gap width in the fluid-mechanical system (see Fig. 7a, where $\overline{H} = 0.13/2$), the regions of strong couplings substantially increase. The modes of vibration can also assorted according to the values of the force $\overline{F}$ (see Fig. 7b). If the mode is predominantly structural (see, e.g. branches 1 in Fig. 7 for $\lambda < 0.4$), then $\overline{F} \to 0$. If the mode is predominantly acoustical, then $\overline{F} \to \pm \infty$ (see, e.g., branches 1 for $\lambda > 2.4$). In the regions of strong acoustic-structural coupling (e.g. for branches 1 and 2 near $\lambda = 1$) we cannot distinguish the structural modes from the acoustic ones, because the absolute values of the aerodynamic force $\overline{F}$ for both the coupled natural frequencies Ω are practically identical.

5. Conclusion

It was shown that in fluid-elastic systems the strongest acoustic-structural couplings exist if the resonances of acoustic and mechanical subsystems are close to each other. In this case the coupled fluid-mechanical system has two different natural frequencies which are neither purely acoustic nor purely structural, and the dynamic properties of this system can not be studied separately for the structural and acoustical subsystems. Even a light medium can significantly change the spectrum of natural frequencies of a structure.

In all examples studied it was proved that the nature of the acoustic-structural couplings is the couplin of two oscillators, namely the mechanical structural and the acoustical one.

References

[1] V.V. Bolotin, *Nonconservative problems of the theory of elastic stability*, Fiz. mat., Moskva 1961.

[2] J. Horáček, I. Zolotarev, *Natural vibration and stability of cylindrical shells conveying fluid*, In A.N. Guz ed.: Dynamics of bodies in iteraction with surroundings (in Russian) Naukova dumka, Kiev 1991.

[3] J. Horáček, I. Zolotarev, *Acoustic-structural coupling of vibrating cylindrical shells with flowing fluid*, Journal of Fluids and Structures, **5**, 5, 487–501 (1991).

[4] J. Horáček, I. Zolotarev, *Frequency-model characteristics of cylindrical shell with annular flow of a light fluid*, In Proceedings of Eight World Congress IFToMM Prague, Aug. 26–31, 1991, vol. 5, p. 1503–1506.

ARCHIVES OF ACOUSTICS
18, 2, 311 – 321 (1993)

PIEZOMAGNETIC AND ULTRASONIC PROPERTIES OF THE Fe–Cu–Nb–Si–B METALLIC GLASS AFTER HEAT-TREATMENT

Z. KACZKOWSKI*, L. MAŁKIŃSKI* AND M. MÜLLER**

*Institute of Physics Polish Academy of Sciences
(02-668 Warszawa, Al. Lotników 32/46)

**Institute of Solid State and Material Research
(0-8027 Dresden, Helmholtzstr. 20, Germany)

An $Fe_{73.5}Cu_1Nb_3Si_{16.5}B_6$ alloy was cast as an initially amorphous ribbon. The samples about 50–51 mm long and 4 mm wide were cut out from the 10 mm wide and about 15 μm thick ribbon and annealed at the temperatures over 300°C (to 550°C) in the transverse magnetic field $H_\perp$ and also without magnetic field ($H=0$). Before nanocrystallization this alloy exhibits the saturation magnetostriction equal to $(20-23)\times 10^{-6}$. The annealing at the temperatures over 400°C in the transverse magnetic field increases the maximum value of the magnetomechanical coupling coefficient (k_m) from 0.10–0.15 (for as quenched state) to over 0.45. The magnetic anisotropy, introduced during the heat-treatment in the transverse magnetic field, is responsible for the predominant vector rotation mechanism which increases the magnetomechanical coupling and ΔE-effect.

1. Introduction

FINEMETs or Yoshizawa's alloys, i.e. iron-rich alloys with an ultrafine grain structure (with a diameter equal to 10–20 nm) are known as nanocrystalline materials [1–12]. These alloys after nanocrystallization are excellent soft magnetic materials, but before the crystallization they exhibit a saturation magnetostriction equal to $(20-23)\times 10^{-6}$ [1, 5–8] and they may be used as good piezomagnetic materials [9–11].

2. Experimental

An $Fe_{73.5}Cu_1Nb_3Si_{16.5}B_6$ alloy was cast as an initially amorphous ribbon [5–11]. The samples about 50–51 mm long and 4 mm wide were cut out from the 10 mm wide and about 15 μm thick ribbon and annealed at the temperatures over 300°C (to 550°C)

in the transverse magnetic field ($H_\perp$ = 650 kA/m) and also without magnetic field ($H=0$) [9–11]. In the first series the strips nos. 1–3 were annealed at the temperature of 350°C for 1/2 h in a transverse magnetic field. Next, the samples nos. 1 and 2 were annealed at a temperature of 400°C for 4 and 6 hours without magnetic field [9, 10]. In the second series these samples and the next one (i.e. nos. 1–4) were annealed at 500°C for 1/2 in $H_\perp$ and $H=0$, and at last at 550°C for 1/2 h without a magnetic field. In the third series next 11 samples (nos. 5–16) were annealed in transverse magnetic field for 1 h in the temperature range from 300 up to 500°C [11]. The characteristics of the magnetomechanical coupling coefficient (k) [13] and of the elasticity moduli at constant magnetic field (E_H) and at constant magnetic induction (E_B) versus magnetic bias field (H) were obtained using the resonance-antiresonance method [13–15]. The magnetomechanical coupling coefficient (k) was determined from the resonant (f_r) and antiresonant (f_a) frequencies of the half-wave length resonators, i.e. of the strip-shape samples [14, 15]

$$k^2 = \frac{\pi^2}{8}\frac{f_a^2 - f_r^2}{f_a^2}. \tag{1}$$

The moduli of elasticity at the constant magnetic field (E_H) and at the constant induction (E_B) were calculated also from these resonant and antiresonant frequencies, respectively, i.e.:

$$E_H = c_H^2 \rho \approx 4 l_r^2 f^2 \rho \tag{2}$$

and

$$E_B = c_B^2 \rho \approx 4 l_a^2 f^2 \rho \tag{3}$$

where l ($=\lambda/2$) is the length of the half-wave resonator ($l=50$ or 51 mm), ρ is density ($\rho=7.2$ Mg/m^3) and c_H and c_B are the ultrasound velocities at constant magnetic field H and at constant magnetic induction B respectively. The resonant frequencies were ranging from 30 to 52 kHz. The amplitude of the AC magnetic field was equal to 1–3 A/m. The characteristics of the impedance moduli are presented in Figures 1–3.

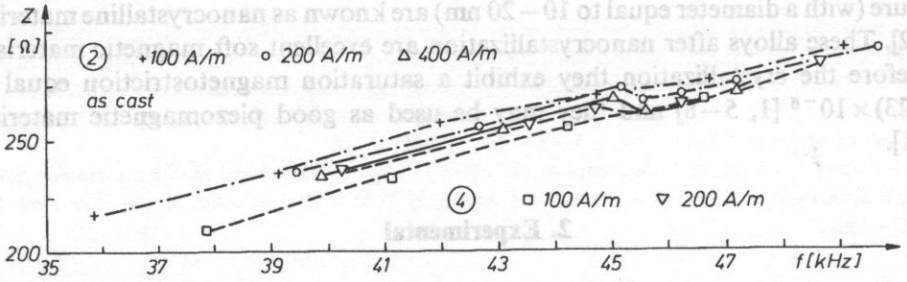

Fig. 1. Impedance (Z) vs. frequency (f) for samples no. 2 [10] and no. 4 in as-quenched state for magnetic bias field equal to 100, 200 and (400 A/m).

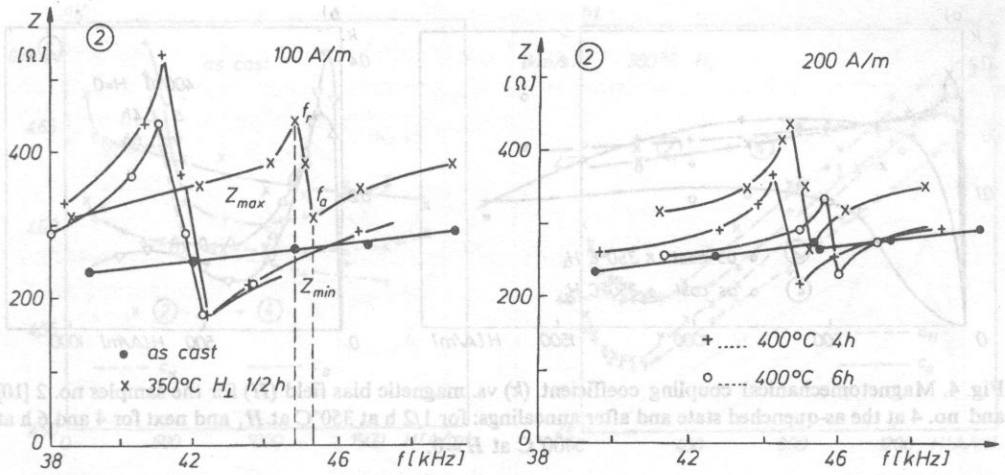

Fig. 2. Impedance (Z) vs. frequency (f) for sample no. 2 in as-quenched state and after annealing at transverse magnetic field ($H_\perp$ = 650 kA/m) for 1/2 h at 350°C and for 4 and 6 h without magnetic field at 400°C for magnetic bias field equal to 100 and 200 A/m [9].

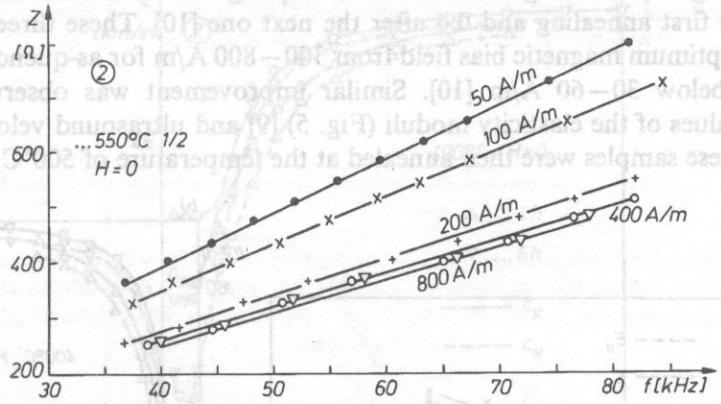

Fig. 3. Impedance (Z) vs. frequency (f) for sample no. 2 after last annealing for 1/2 h at 550°C and $H=0$.

Quasistatic hysteresis loops of magnetic induction (B) were measured and from these loops the coercive force (H_c) was determined [11]. Dynamical reversible magnetic permeability (μ) at the frequency of 10 kHz and the small amplitude of the magnetic field equal to 1A/m was measured versus quasistatic field [11].

3. Results and discussion

The annealing at the temperature of 350°C in the transverse magnetic field increases the maximum value of the magnetomechanical coupling coefficient (k) from

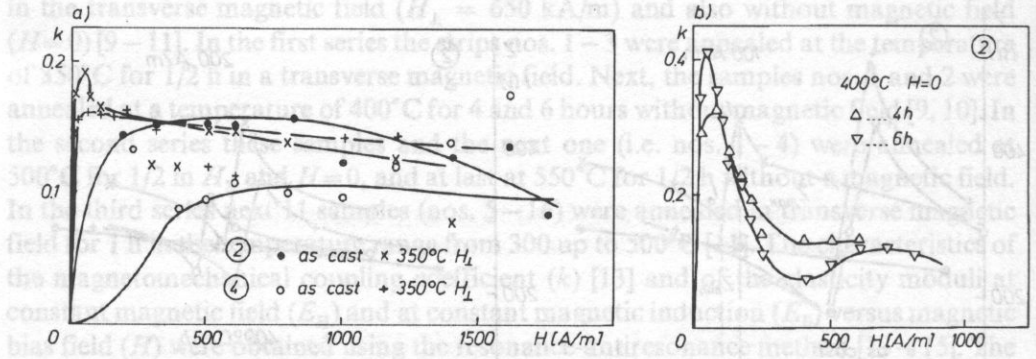

Fig. 4. Magnetomechanical coupling coefficient (k) vs. magnetic bias field (H) for the samples no. 2 [10] and no. 4 at the as-quenched state and after annealings: for 1/2 h at 350°C at $H_\perp$ and next for 4 and 6 h at 400°C at $H=0$.

0.10–0.15 to 0.15–0.19 (fig. 4a) [10]. The next annealings at the temperature of 400°C for 4 and 6 h without external magnetic field improved the piezomagnetic properties (Fig. 4b). The magnetomechanical coupling coefficient exceeds the value of 0.3 after the first annealing and 0.4 after the next one [10]. These three annealings shifted the optimum magnetic bias field from 300–800 A/m for as-quenched state to the values below 30–60 A/m [10]. Similar improvement was observed for the minimum values of the elasticity moduli (Fig. 5) [9] and ultrasound velocities (Figs. 6 and 7). These samples were then annealed at the temperature of 500°C for 1/2 h in

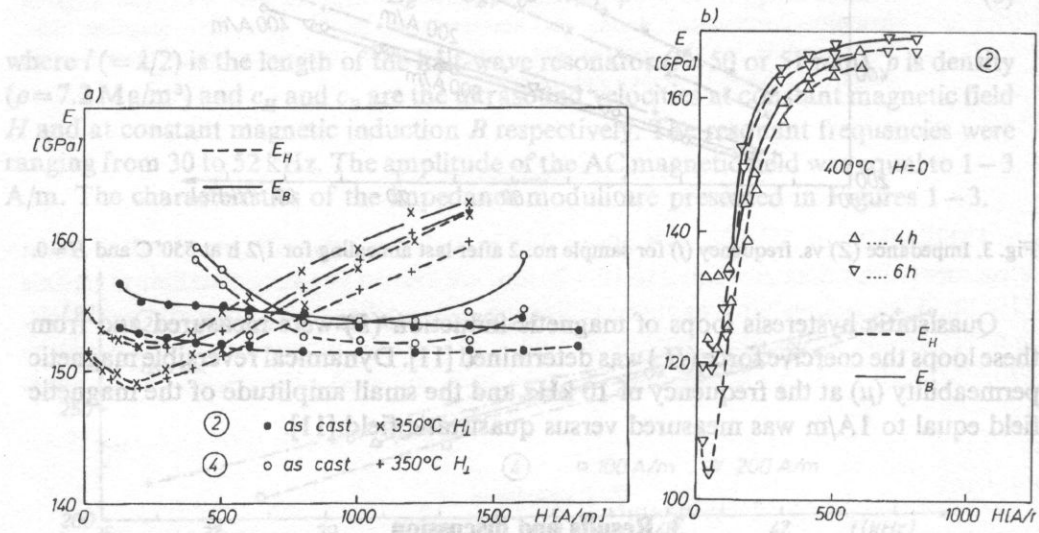

Fig. 5. Moduli of elasticity at constant magnetic field (E_H) and at constant induction (E_B) vs. magnetic bias field (H) for the as-quenched and annealed for 1/2 h at 350°C in $H_\perp$ samples (nos. 2 [9] and 4) and next annealed for 4 and 6 h at 400°C at $H=0$.

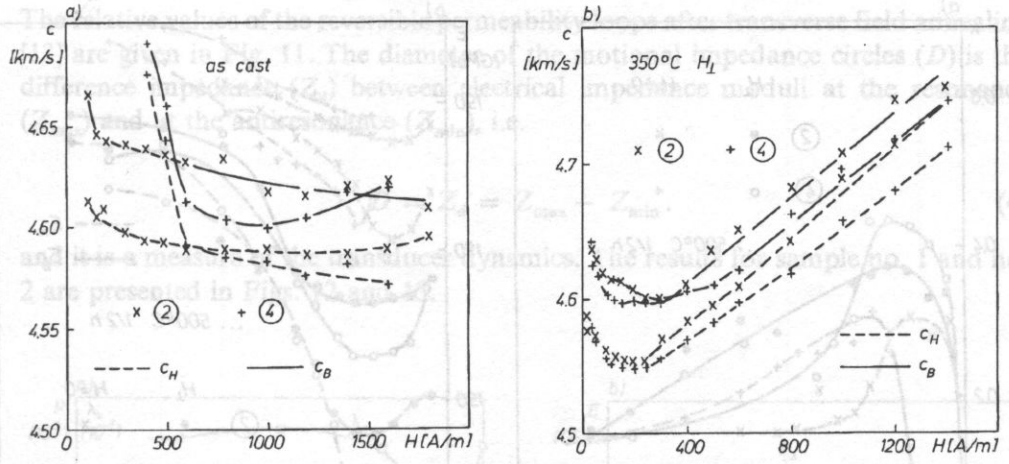

Fig. 6. Ultrasound velocities at constant magnetic field (c_H) and at constant induction (c_B) vs. magnetic bias field (H) for the as-quenched and annealed for 1/2 h at 350°C in $H_\perp$ samples nos. 2 and 4.

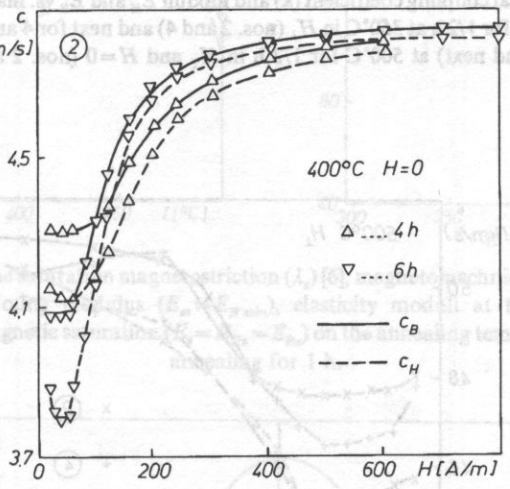

Fig. 7. Ultrasound velocities at constant magnetic field (c_H) and at constant induction (c_B) vs. magnetic bias field (H) for the as-quenched and annealed for 1/2 h at 350°C in $H_\perp$ 4 and next annealed for 4 and 6 h at 400°C at $H=0$ samples nos. 2 and 4.

the transverse magnetic field ($H_\perp$) and next without a magnetic field at 500 and 550°C for 1/2 h (Figs. 8, 9 and 3).

Summarized results from the third series of the investigations are presented in Fig. 10 [13]. The annealing temperatures starting from 300°C were increased to 320, 340, 360, 380, 400, 420, 440, 460, 480 and 500°C. An exception is the saturation magnetostriction (λ_s) for which the results were taken from the other papers [6–8].

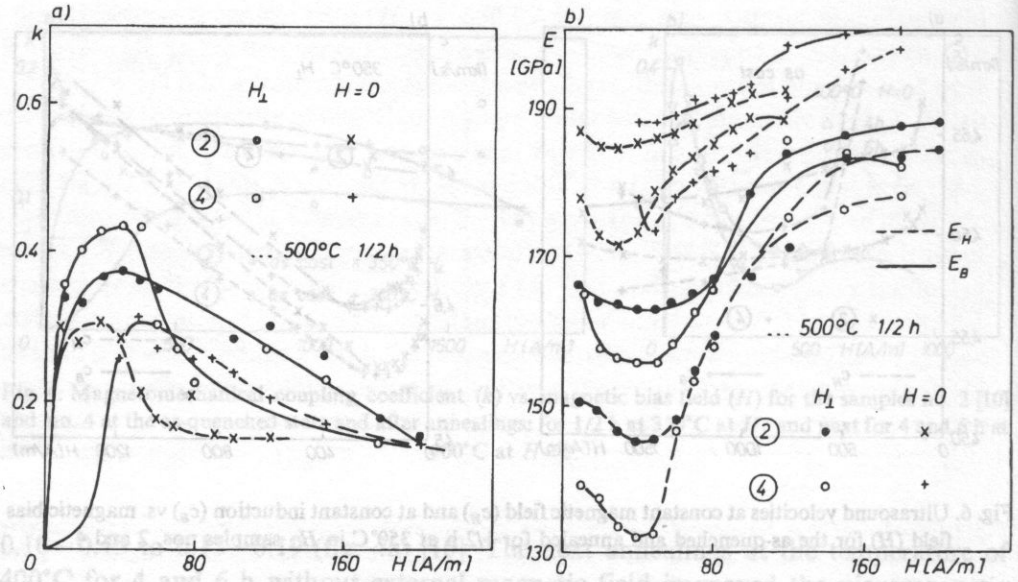

Fig. 8. Magnetomechanical coupling coefficient (k) and moduli E_H and E_B vs. magnetic bias field (H) for two samples after annealings: for 1/2 h at 350°C in $H_\perp$ (nos. 2 and 4) and next for 4 and 6 h at 400°C at $H=0$ (no. 2) and next) at 500°C for 1/2 h in $H_\perp$ and $H=0$ (nos. 2 and 4).

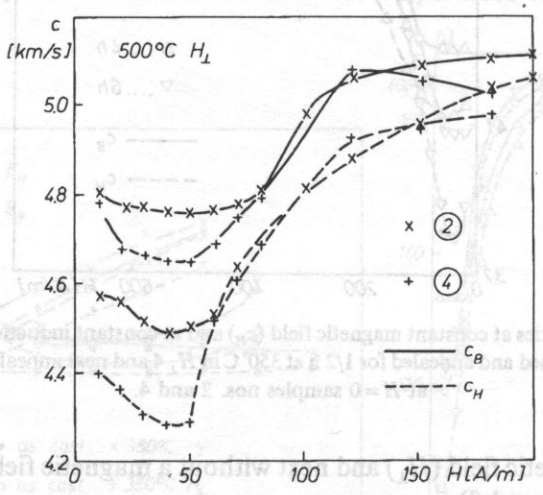

Fig. 9. Ultrasound velocities at constant magnetic field (c_H) and at constant induction (cE_B) vs. magnetic bias field (H) for two samples after annealings: for 1/2 h at 350°C in $H_\perp$ (nos. 2 and 4) and next for 4 and 6 h at 400°C at $H=0$ (no. 2) and next) at 500°C for 1/2 h in $H_\perp$ and $H=0$ (nos. 2 and 4).

The relative values of the reversible permeability loops after transverse field annealing [13] are given in Fig. 11. The diameter of the motional impedance circles (D) is the difference impedance (Z_d) between electrical impedance moduli at the resonance (Z_{max}) and at the antiresonance (Z_{min}), i.e.

$$D = Z_d = Z_{max} - Z_{min}. \tag{4}$$

and it is a measure of the transducer dynamics. The results for sample no. 1 and no. 2 are presented in Figs. 12 and 13.

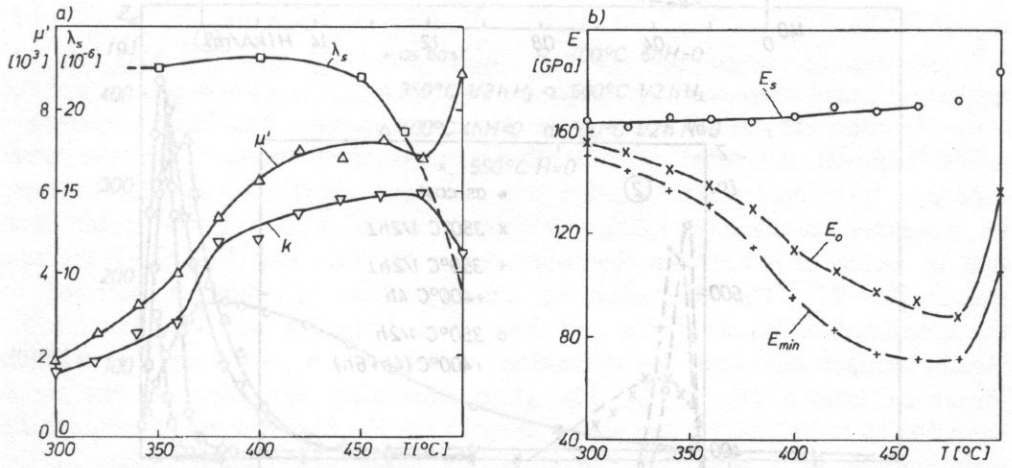

Fig. 10. Dependences of the saturation magnetostriction (λ_s) [6], magnetomechnical coupling coefficient (k), relative values of the Young modulus ($E_m = E_{H\,min}$), elasticity moduli at the demagnetization state ($E_0 = E_{H0} = E_{B0}$) and at magnetic saturation ($E_s = E_{Hs} = E_{Bs}$) on the annealing temperature of transverse field annealing for 1 h.

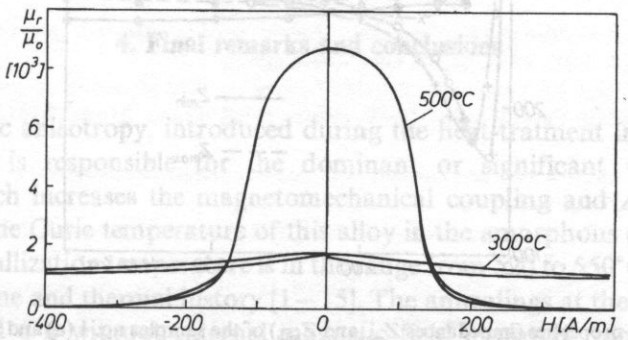

Fig. 11. Reversible ac permeability loops after transverse field annealings for 1 h at the temperature of 300 and 500°C.

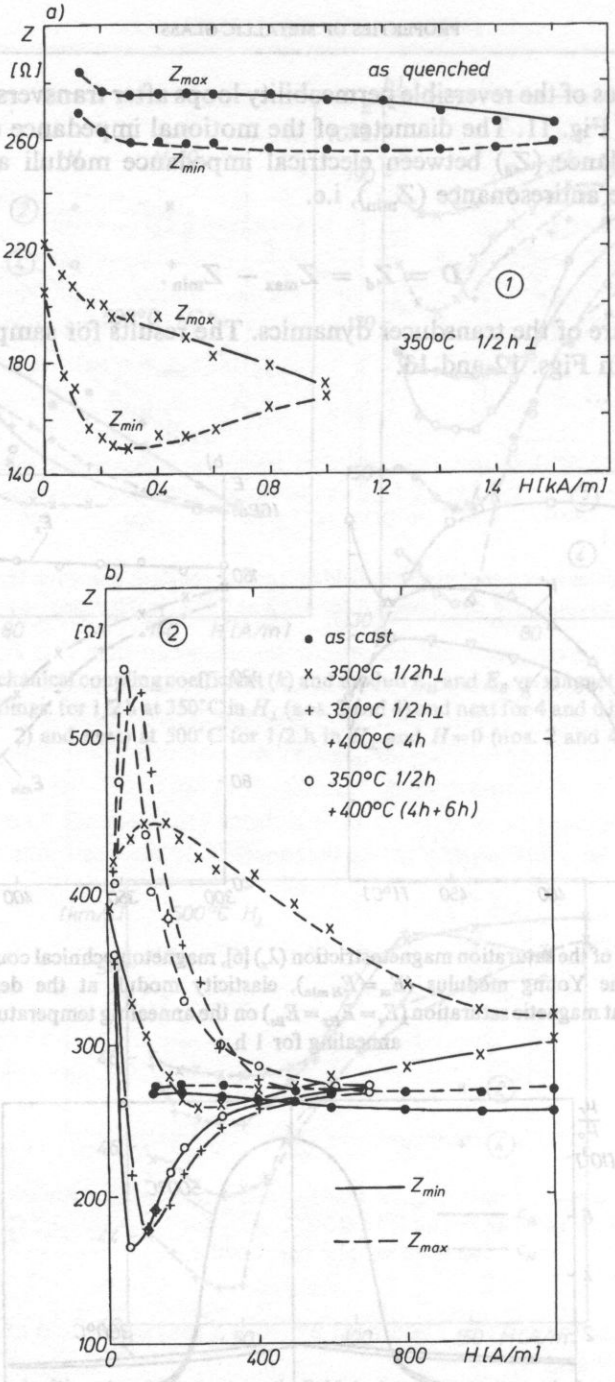

Fig. 12. Dynamical properties (impedances Z_{max} and Z_{min}) of the samples no. 1 (a) and no. 2 (b) vs. magnetic bias field (H) for as-casted state and after different heat treatment.

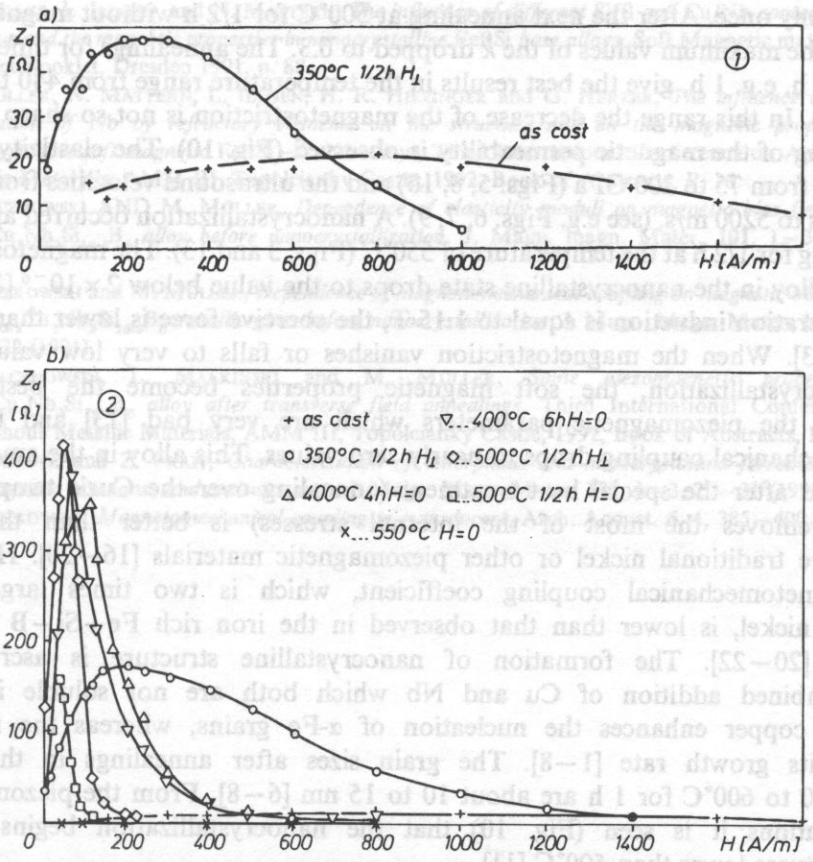

Fig. 13. Motional impedance $Z_d = Z_{max} - Z_{min}$ of the samples no. 1 (a) and no. 2 (b) vs. magnetic bias field (H) for as-casted state and after different heat treatment.

4. Final remarks and conclusions

The magnetic anisotropy, introduced during the heat-tratment in the transverse magnetic field, is responsible for the dominant or significant vector rotation mechanism which increases the magnetomechanical coupling and ΔE or Δc effect (Figs. 4–10). The Curie temperature of this alloy in the amorphous state is equal to 320°C and crystallization temperature is in the range from 520 to 550°C depending on the annealing time and thermal history [1–15]. The annealings at the temperature of 400°C for 4 and 6 h without external magnetic field improved the piezomagnetic properties (Figs. 4b, 5b and 7). After annealing at 500°C for 1/2 h in $H_\perp$ there was observed a decrease of the k coefficient for the samples with a longer thermal treatment history, and the increase of the k (up to 0.45) for the sample no. 4, annealed

before only once. After the next annealing at 500°C for 1/2 h without magnetic field ($H=0$) the maximum values of the k dropped to 0.3. The annealings for times longer than 1/2 h, e.g. 1 h, give the best results in the temperature range from 440 to 480°C (Fig. 10). In this range the decrease of the magnetostriction is not so sharp and the increasing of the magnetic permeability is observed (Fig. 10). The elasticity moduli changed from 75 to 200 GPa (Figs. 5, 8, 10) and the ultrasound velocities from about 3000 m/s to 5200 m/s, (see e.g. Figs. 6, 7, 9). A nanocrystallization occurred after next annealing for 1/2 h at the temperature of 550°C (Figs. 3 and 13). The magnetostriction in this alloy in the nanocrystalline state drops to the value below 2×10^{-6} [1, 5–8]. The saturation induction is equal to 1.15 T, the coercive force is lower than 1 A/m [1–8, 13]. When the magnetostriction vanishes or falls to very low values after thenanocrystallization, the soft magnetic properties become the best [1–8] but not the piezomagnetic parameters which are very bad [13] and the magnetomechanical coupling drops to nearly zero values. This alloy in the amorphous state and after the special heat treatment (annealing over the Curie temperature, which removes the most of the internal stresses) is better than the more expensive traditional nickel or other piezomagnetic materials [16–20]. However, its magnetomechanical coupling coefficient, which is two times larger than that of nickel, is lower than that observed in the iron rich Fe–Si–B metallic glasses [20–22]. The formation of nanocrystalline structure is ascribed to the combined addition of Cu and Nb which both are not soluble in α-Fe. Hereby copper enhances the nucleation of α-Fe grains, whereas the niobium lowers its growth rate [1–8]. The grain sizes after annealings in the range from 500 to 600°C for 1 h are about 10 to 15 nm [6–8]. From the piezomagnetic investigations it is seen (Fig. 10) that the nanocrystallization begins at the temperatures lower than 500°C [11].

References

[1] Y. YOSHIZAWA, S. OGUMA and K. YAMAUCHI, *New Fe-based soft magnetic alloys composed of ultrafine grain structure*, J. Appl. Phys. **64**, 10, 6044–6046 (1988).

[2] Y. YOSHIZAWA and K. YAMAUCHI, *Effects of magnetic field annealing on magnetic properties in ultrafine crystalline* Fe–Cu–Nb–Si–B *alloys*, IEEE Trans. Magn. **MAG-25**, 5, 3324–3326 (1989).

[3] G. HERZER, *Grain structure and magnetism of nanocrystalline ferromagnetics*, IEEE Trans. Magn. **MAG-25**, 5, 3327–3330 (1989).

[4] H.R. HILZINGER, *Recent advances in rapidly solidified soft magnetic materials*, J. Magn. Magn. Mater. **83**, 1–3, 370–374 (1990).

[5] M. MÜLLER, L. ILLGEN, E. KOHLER, M. BARTH and H. GRAHL, *Nanocrystalline Fe–B–Si-base soft magnetic alloys*, Int. Symp. MASHTEC'90, Dresden, Collected Abstracts, vol. 2, p. 345 (1990).

[6] M. MÜLLER, L. ILLGEN, E. KOHLER, M. BARTH and N. MATTERN, *The influence of the composition of nanocrystalline* FeBSi/CuNb *soft magnetic alloys*, European Magnetic materials and Applications Conference, EMMA, Digest Booklet, Dresden 1991, pp 69–70.

[7] M. MÜLLER, L. ILLGEN, and N. MATTERN, *The influence of different* Si/B *and* Cu/Nb *contents on the structrue and the magnetic properties in nanocrystalline* FeBSi *base alloys*, Soft Magnetic materials 10, Abstract Booklet, Dresden 1991, p. 88.

[8] M. MÜLLER, N. MATTERN, L. ILLGEN, H. R. HILZINGER and G. HERZER, *The influence of partial substitution of* Nb *by refractory elements on the structure and on the magnetic properties in nanocrystalline soft magnetic* FeBSi–CuNb *alloys*, Third International Conference on Amorphous Metallic Materials, AMM III, Topolcianky Castle, 1992, Book of Abstracts, P. 16.

[9] Z. KACZKOWSKI AND M. MÜLLER, *Dependence of elasticity moduli on magnetic bias field of the* $Fe_{73.5}Cu_1Nb_3Si_{16.5}B_6$ *alloy before nanocrystallization*, J. Magn. magn. Mater. **101**, 1–3, 21–23 (1991).

[10] Z. KACZKOWSKI and M. MÜLLER, *Dependence of magnetomechanical coupling on magnetic bias field in the* $Fe_{73.5}Cu_1Nb_3Si_{16.5}B_6$ *metallic glass before nanocrystallization*, J. Magn. Magn. Mater. **112**, 1–2, 320–322 (1991).

[11] Z. KACZKOWSKI, L. MAŁKIŃSKI and M. MÜLLER, *Some piezomagnetic properties of* $Fe_{73.5}Cu_1Nb_3Si_{16.5}B_6$ *alloy after transverse field annealings*, Third International Conference on Amorphous Metallic Materials, AMM III, Topolcianky Castle, 1992, Book of Abstracts, P 40.

[12] D. FRAITOVA and Z. FRAIT, *Characterization of amorphous and nanocrystalline ferromagnets by ferromagnetic resonanse and antiresonance*, J. Magn. Magn. Mater. **101**, 1–3, 29–31 (1991).

[13] Z. KACZKOWSKI, *Magnetomechanical coupling in transducers*, Arch. Acoust. **6**, 4, 385–400 (1981).

ARCHIVES OF ACOUSTICS
18, 2, 323–335 (1993)

OVERSAMPLING ANALOG TO DIGITAL CONVERSION IN ACOUSTIC MEASUREMENTS

P. KLECZKOWSKI

Institute of Mechanics and Vibroacoustics
Academy of Mining and Metallurgy
(30-059 Kraków, al. Mickiewicza 30)

The new method of analog to digital conversion known as "oversampling" or "delta-sigma", is inherently more suitable for acoustics measurements than the traditional method was. The theoretical background of this new method is presented. Both methods of conversion are compared with reference to their use in acoustics. The tests of parameters important in processing of acoustics signals performed on monolithic "delta-sigma" converters are reported. A digital procedure for evaluating the THD+N parameter is proposed.

1. Introduction

Contemporary means of digital processing of acoustic signals are very powerful. This power comes from developments in hardware (monolithic digital signal processors) and from developments in the theory of signal processing. Wide access to theoretically unlimited precision of digital processing evokes the need for inexpensive analog to digital conversion systems introducing low error.

The recent developments in microelectronic technology made possible a large scale production of integrated circuits performing the task of analog to digital (A/D) and digital to analog (D/A) conversion according to the so-called "delta-sigma" conversion technique, known also as "sigma-delta" or "one-bit" conversion. This technique is the most popular version of a larger defined method of "oversampling" conversion. The actual method is not new. It stems from the patent of C. Cutler (filed in 1954), describing a multibit implementation in vacuum-tube technology [6]. The first presentation of the one-bit version of this method comes from 1962 [7]. The authors called their method "delta-sigma modulation".

The delta-sigma conversion technique applies very well to monolithic implementation in CMOS technology, which is substantial for low cost mass production. However, such production has become practicable only recently.

Oversampling A/D converters supersede the systems with "classical" A/D converters in most of the applications requiring high resolution of 16 bits or more. Achieving

the parameters of monolithic delta-sigma conversion systems with „classical" method is possible but much more expensive.

2. The classical data acquisition system

This system results from the function performed by a "classical" A/D converter. Any circuit, converting an isolated analog sample into a digital code representing its value will be meant under this term. Such converters are in fact quantizers. A full A/D interface must usually include also a low-pass antialiasing filter and a sample-and-hold (S/H) circuit (Fig. 1) [3, 5].

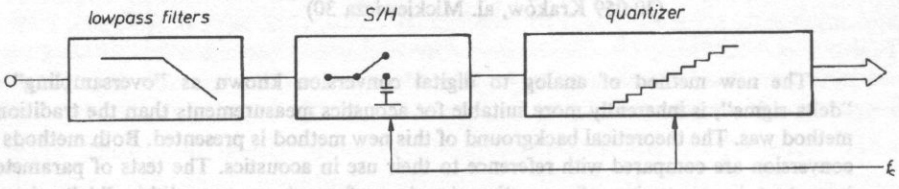

Fig. 1. "Classical" data acquisition system.

The systems performing all three tasks of Fig. 1 will be called data acquisition systems.

The realization of a lowpass filter of Fig. 1 is not easy. It must have sharp cut-off slope (as required to reduce sampling frequency) and very flat passband characteristics. It should not introduce phase and harmonic distortion and generate noise. It is very difficult to obtain a filter with such characteristics in monolithic technology.

The S/H circuit can be a source of nonlinear distortion or sampling jitter.

In classical quantizers it is not easy to exceed the resolution of 16 bits, because of the 2^N factor (where N is the number of bits), magnifying technological difficulties (and hence costs). This factor is present in all three basic methods of traditional A/D quantization. In successive approximation method it is the precision of components to the order of one part in 2^N, in flash conversion it is the number of elements and in integrating quantizers it is the speed of conversion that must increase with the 2^N factor.

Oversampling method eliminates the filter and 2^N factor from the implementation technology of the quantizer. It also makes the sample and hold circuit easy to realize.

3. Oversampling data acquisition systems

The term "oversampling" denotes sampling an analog signal at frequency deliberately above the rate resulting from the sampling theorem for that signal. The ratio of actual sampling frequency to the frequency given by the sampling theorem will be denoted by D.

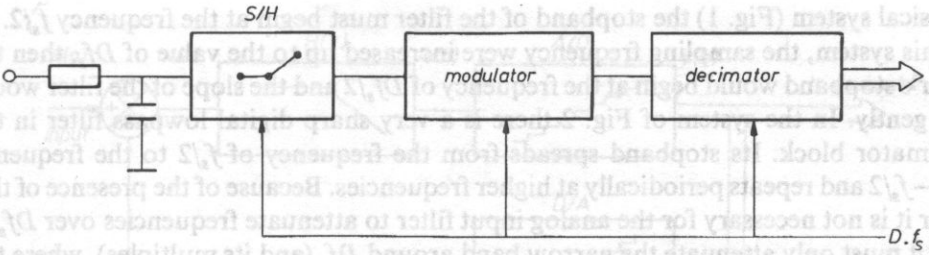

Fig. 2. Oversampling data acquisition system.

In oversampling method of A/D conversion the three separate tasks shown in Fig. 1 are performed in a different way. They can be seen to be redisposed to other three blocks, two of them specific to this method: a S/H circuit, a modulator and a decimator (Fig. 2).

In the bibliography the S/H circuit is usually not separated (because of its trivial implementation at relatively high sampling frequencies). It is included as a part of a modulator instead. In Fig. 2 it was shown, because of the method of analysis of the system used.

In such a system the task of antialiasing filtering is performed by an RC network at the input and the decimator, while the process of quantization should be assigned to both modulator and decimator. The modulator will be discussed below. The decimator is a low-pass digital filter which yields on its output the data stream at a rate reduced D times, that is at a rate close to that resulting from the sampling theorem. An important feature of the digital filter in the decimator is that it is a finite impulse response filter, hence it has linear phase characteristics despite very sharp slope in the transition band.

4. Oversampling

Oversampling is used in a system from Fig. 2 to achieve two different goals at the same time: to facilitate low-pass filtering and to increase the resolution of quantization.

Fig. 3 shows the spectrum of the signal of interest (up to f_B) together with some energy over the band of interest, at the input of any signal acquisition system. In the

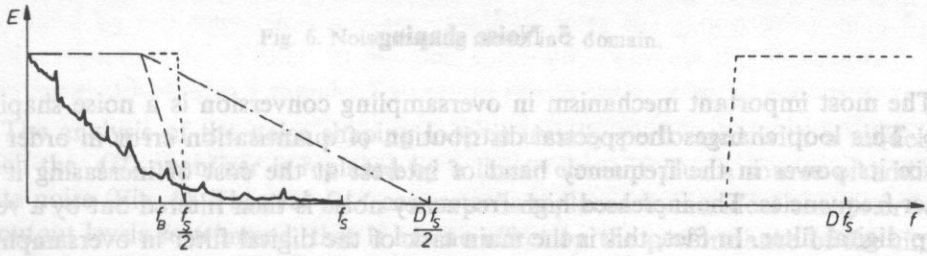

Fig. 3. Antialiasing in data acquisition system.

classical system (Fig. 1) the stopband of the filter must begin at the frequency $f_s/2$. If, in this system, the sampling frequency were increased up to the value of Df_s, then the filter's stopband would begin at the frequency of $Df_s/2$ and the slope of the filter would fall gently. In the system of Fig. 2 there is a very sharp digital lowpass filter in the decimator block. Its stopband spreads from the frequency of $f_s/2$ to the frequency $Df_s - f_s/2$ and repeats periodically at higher frequencies. Because of the presence of this filter it is not necessary for the analog input filter to attenuate frequencies over $Df_s/2$, and it must only attenuate the narrow band around Df_s (and its multiples), where the digital filter has its passband. In practice this task is performed well enough by a simple RC two-termination network.

The other task of oversampling is to increase the resolution of the quantization process. If the classical quantizer has on its input a signal of moderate amplitude (i.e. well above the value of a least significant bit and below the saturation limit) and of a band not too narrow, then the quantization error introduced resembles additive white noise. The spectrum of signal on the output of the quantizer can be, under such condition shown as in Fig. 4.

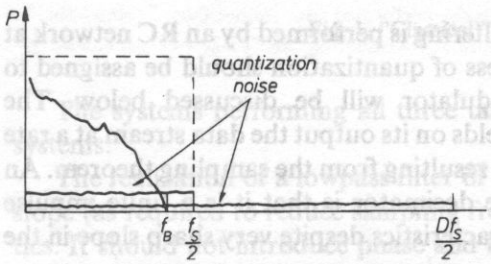

Fig. 4. Effect of oversampling on increasing the resolution of conversion

The power of the quantization noise corresponds to the resolution of the quantizer, but is independent of the sampling frequency so that at higher sampling rates this power will be distributed over a wider range of frequencies. Hence, if all spectral components over $f_s/2$ were filtered out, the power of quantization noise in the band of interest up to $f_s/2$ would be reduced by a factor of D. It can be shown [6] that the increase in resolution attained for octave of oversampling (D) is 0.5 bit, so it is not attractive enough for practical use.

5. Noise shaping

The most important mechanism in oversampling conversion is a noise shaping loop. This loop changes the spectral distribution of quantisation error in order to reduce its power in the frequency band of interest at the cost of increasing it at higher frequencies. The increased high-frequency noise is then filtered out by a very sharp digital filter. In fact, this is the main task of the digital filter in oversampling systems.

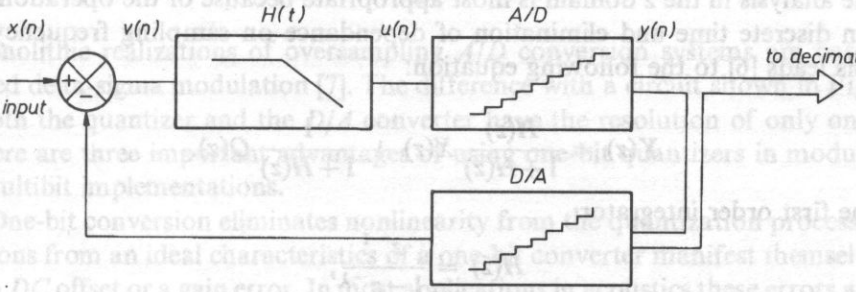

Fig. 5. Modulator

The diagram of modulator (from Fig. 2), where this process takes place, is shown in Fig. 5. The input of this circuit receives samples from the S/H circuit in discrete time, at the rate of Df_s. The discrete-time integrator (an analog accumulator) is described in the time domain by the following equation:

$$v(n+1) = v(n) + u(n). \tag{1}$$

The sequence of analog input samples $x(n)$ change their values slowly, because the input signal has been oversampled. The sequence $u(n)$ represents the approximation of quantization error of the N-bit A/D quantizer. This error varies strongly from sample to sample, while its long-term average is zero. The values of $y(n)$ represent a coarse approximation of $x(n)$, that oscillates over neighbouring values on the quantizer's scale around the slowly changing value of $x(n)$. The digital filter in a decimator block (Fig. 2) averages out the oscillation of $y(n)$, yielding a fine approximation of $x(n)$ [6, 12].

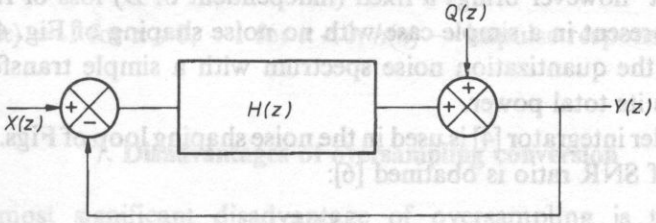

Fig. 6. Noise shaping model in z domain.

The analysis of the noise shaping loop is usually performed with a model, in which the A/D quantizer is replaced by a linear element plus a source of additive white noise (Fig. 6). The real D/A converter is replaced by an ideal converter with its output levels so trimmed, that it has no effect on the performance of the circuit and can be eliminated from the model. It should be emphasized, that the validity of such a model is limited by the character of the real quantization noise.

The analysis in the z domain is most appropriate because of the operation of the loop in discrete time and elimination of dependance on sampling frequency. This analysis leads [6] to the following equation:

$$Y(z) = \frac{H(z)}{1+H(z)} X(z) + \frac{1}{1+H(z)} Q(z). \tag{2}$$

For the first order integrator:

$$H(z) = \frac{z^{-1}}{1-z^{-1}}, \tag{3}$$

The comparison of power spectral density functions of the signal and the quantization noise in the passband of the decimator (Fig. 2) gives the following result [6]:

$$\text{SNR} = \left[\frac{P_x}{P_q}\right] \frac{\frac{\pi}{2}}{\frac{\pi}{D} - \sin\left(\frac{\pi}{D}\right)}, \tag{4}$$

where: SNR — the ratio of power of signal to the power of noise, $\frac{P_x}{P_q}$ — the SNR of the quantizer itself, operating on the same input signal $x(n)$ with no oversampling and noise shaping loop.

For $D \gg \pi$ it can be assumed, that

$$\text{SNR} = \frac{3D^3}{\pi^2} \tag{5}$$

It can be shown [6], that the increase of resolution per octave of oversampling is 1.5 bits. The term $3/\pi^2$ however brings a fixed (independent of D) loss of resolution of about 1 bit, not present in a simple case with no noise shaping of Fig. 4. This is an effect of altering the quantization noise spectrum with a simple transfer function, which also boosts its total power.

If a second order integrator [4] is used in the noise shaping loop of Figs. 5 and 6, the following value of SNR ratio is obatined [6]:

$$\text{SNR} = \frac{5D^5}{\pi^4}. \tag{6}$$

This corresponds to the increase of resolution of 2.5 bits per octave of oversampling with the fixed loss of resolution of about 2 bits.

Implementation of higher order loops is difficult because of their potential instability. Instead, more complex transfer functions are used, which exhibit a high order low-pass characteristics at low frequencies and more gentle response at higher frequencies, where the gain exceeds unity and a phase shift of π would cause oscillation [1]. Another solution are multistage noise shaping loops, called MASH [11].

6. The delta-sigma modulator

Monolithic realizations of oversampling A/D conversion systems are based on so-called delta-sigma modulation [7]. The difference with a circuit shown in Fig. 5 is that both the quantizer and the D/A converter have the resolution of only one bit.

There are three important advantages of using one-bit quantizers in modulators over multibit implementations.

1. One-bit conversion eliminates nonlinearity from the quantization process. Any deviations from an ideal characteristics of a one-bit converter manifest themselves as either a DC offset or a gain error. In most applications in acoustics these errors are not harmful and can be easily compensated. This elimination of nonlinearity opens way to very high potential resolution of this technique.

2. It is much easier to implement one-bit converters in monolithic technology.

3. One-bit signal on the decimator's input substantially simplifies the digital filter arithmetics and hence its monolithic implementation.

The obvious drawback is that higher order noise shaping loops or higher oversampling rates must be used to obtain the same resolution as those with multibit realizations.

The analysis of a delta-sigma modulator is difficult, because in the same circuit there are: a linear filter (integrator) and a strong nonlinearity — comparator (one-bit quantizer). If the model of Fig. 6 and (abstracted) equations (2−4) were used with one-bit quantizer, then the result obtained for the second order loop case would overestimate the SNR ratio by about 14 dB, as verified in near-ideal circuits and by careful simulation [6]. This model is also inappropriate, because the additive white quantization noise assumption is more likely to be not fulfilled in the one-bit case [6].

With an ideal D/A converter, the following nonlinear equation describes the performance of the one-bit loop in the time domain:

$$y(n+1) = \operatorname{sgn}\,[h(n) * [x(n)-y(n)]] \tag{7}$$

where: $\operatorname{sgn}(x) = 1$ for $x \geqslant 0$, -1 for $x<0$; $h(n)$ — impulse response function of the integrator.

7. Disadvantages of oversampling conversion

1. The most significant disadvantage of oversampling is the latency time introduced by the conversion process, resulting from the group delay of a finite impulse response digital filter. In practical monolithic circuits this latency is in the order of milliseconds and rises with lowering the sampling rate.

2. In classical conversion systems a maximum quantization error is comparable to the average quantization error. In oversampling conversion an error at individual samples can occasionally be noticeably higher than the average error, due to the stochastic nature of the conversion process.

3. An oversampling system must work with a fixed sample rate. It is not possible to acquire individual samples at arbitrary times.

4. The digital filter with very sharp cut-off slope generate oscillations when processing impulses. In classical conversion method of Fig. 1 this problem can be alleviated by increasing the system's sampling rate and using a filter with more gentle characteristics.

8. Basic tests of a monolithic delta-sigma converter

A monolithic implementation chosen for testing was a 16-bit two-channel converter from Crystal Semiconductor Co., type CS5336KP.

This particular integrated circuit was at the time of writing the only one that allowed for effective sampling rates to be as low as 1 kHz, kwhich is particularly useful in some acoustic research. The oversampling factor D in this circuit equals 64 and the manufacturer did not specify the type (order) of noise shaping loop used [13].

Out of many A/D converter parameters that can be specified [9], the author decided to measure and report only those having practical consequences in acoustic measurements, that is dynamic performance parameters.

Traditionally, such three basic parameters were: signal to noise ratio (SNR), total harmonic distortion (THD) and intermodulation distortion (IMD). In classical conversion methods nonlinear distortion introduced higher errors than quantization noise (except at low amplitudes of input signal). Excellent linearity of delta-sigma conversion reduces the THD and IMD errors to the level close to quantization noise. Therefore another, global parameter is usually used to assess these converters: total harmonic distortion + noise (THD+N). This parameter can be considered a measure of global dynamic error of a converter.

The author developed the following procedure for THD+N measurement: a spectrally pure sinusoid is presented to a converter and the output signal from the converter is compared to the ideal digitally generated sinusoid. The parameters of the ideal sinusoid are derived from the converter's output signal, by a least-squares method.

The following function was minimized:

$$E = \sum_{i=1}^{I} (c + a \cdot \cos(x \cdot i + \phi)) - s_i)^2, \tag{8}$$

where: I — the number of samples taken for this measurement (the band of analysis assumed was from 10 Hz to 22 kHz; this correspond to 4800 samples at 48 kHz sampling rate), c — the value of the DC component, a — amplitude, x — frequency, ϕ — phase, s_i — at value of the i-th sample of the signal at converter's output.

Having found the minimum of E function the THD+N coefficient was computed:

$$\text{THD+N} = 20 \log \left(\frac{A}{\sqrt{\frac{E_{\min}}{I}}} \right) \tag{9}$$

The constant A is the RMS value of full-scale sinusoid at the input, in the case of 16-bit long words it is 23170.

The initial values of parameters were derived by observation of digitally stored waveform. Then the minimum of E was found by a semi-automatic software procedure, which minimized E as a function of one of the parameters, fixing the remaining three. All four parameters were optimized in turn, and such iteration procedure was repeated three times, until E was minimized to the precision of three decimal digits, which corresponded to 0.02 dB of the final result of THD+N.

The practical measurement was difficult because of lack of the source of highly pure sinusoid. The purest sinusoidal signal that was available (from B&K 1022 oscillator) analysed with B&K 2134 analyser showed a noise floor of about -80 dB. Therefore the author decided to measure THD+N for a sinusoidal input signal that guaranteed to have all its distortion and noise components well below those of the converter, that is a -30 dB (related to full scale) signal.

An important advantage of oversampling converters is the lack of inherent sources of specific nonlinear distortion that can manifest strongly at low input signals [3], where quantization noise does not fulfill the assumptions of additive white noise. Therefore it was decided to test the converter's performance also at low amplitude (-80 dB) input signals.

The "idle channel noise" parameter (ICHN) was also measured, with input of the converter grounded. The computation algorithm was similar to the one shown in Eqs. (8) and (9), with a in (8) equal to zero.

The measurement setup was a special system interfacing two such monolithic double channel converters to the IBM PC AT computer, constructed by the author [8].

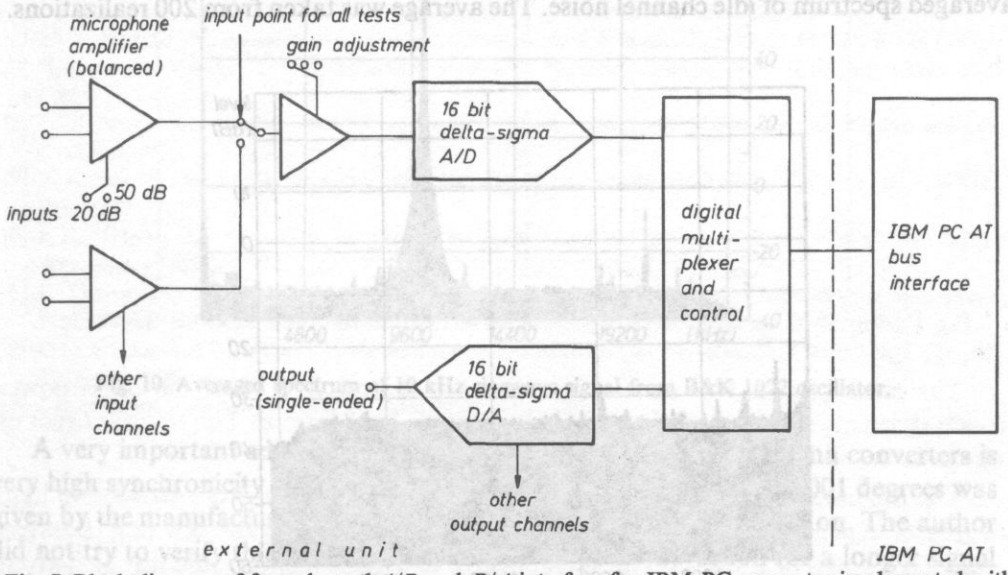

Fig. 7. Block diagram of four channel A/D and D/A interface for IBM PC computer implemented with delta-sigma technology.

This interface can receive four channels of simultaneously sampled analog signals and record them on computer hard disk. It can also reproduce analog signals through four *D/A* channels, using the similar (but inverted) delta-sigma method for *D/A* conversion. The block diagram of this interface is shown in Fig. 7. Input signal in all tests was from the B&K oscillator type 1022.

The tests were performed for three frequencies: 100 Hz, 1 kHz and 10 kHz. The results of tests [dB]:

	THD+N/−40 dB			THD+N/−80 dB			ICHN
Frequency [kHz]	0.1:	1:	10:	0.1:	1:	10:	–
Left channel	92.16	92.39	91.42	92.87	93.12	92.20	94.02
Right channel	93.71	93.53	92.88	93.27	93.45	93.04	94.11

The ICHN test was more representative statistically, as the results were averaged for three integrated circuits (ICs), each one of different manufacturing series. Ten realizations were taken on each IC. The results obtained in the ICHN test are better, probably because of shorter signal path in this case (direct grounding of the input pin on the IC instead of passing through a buffer operational amplifier).

In research of vibration it is often necessary to analyse a narrow band of low frequencies. The manufacturer's specification [13] gave 1 kHz as the lowest limit of effective sampling frequency. It was found that the converter still worked at the frequency of 187.5 Hz. The THD+N with a 30 Hz sinewave input signal and ICHN results were still at similar level.

The 1024-point FFT analysis was also performed. Fig. 8 shows a typical plot of the averaged spectrum of idle channel noise. The average was taken from 200 realizations.

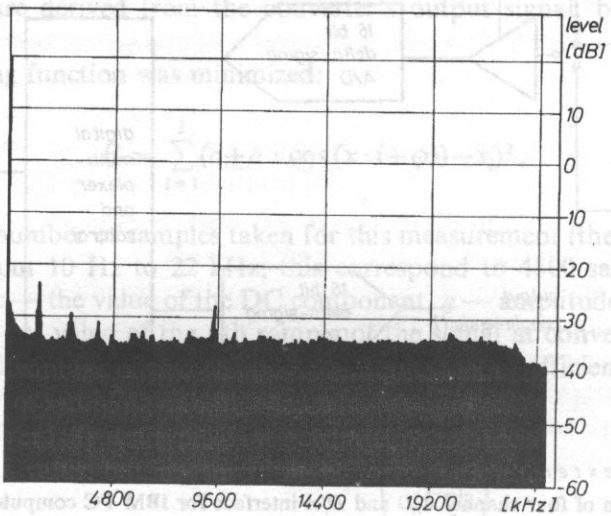

Fig. 8. Typical plot of the averaged spectrum of idle channel noise.

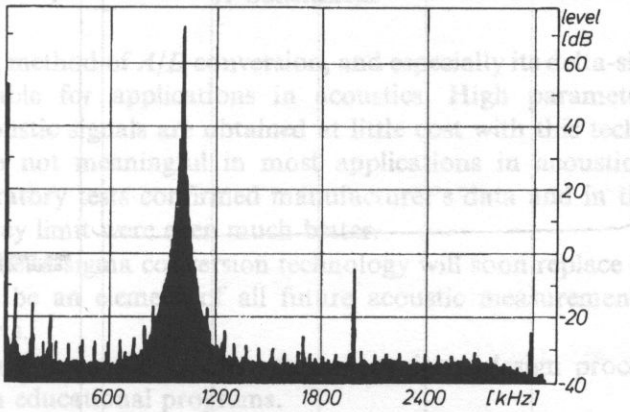

Fig. 9. Averaged spectrum of 1 kHz sinewave signal from B&K 1022 oscillator.

Fig. 9 shows the plot of averaged spectrum of a 1 kHz sinusoidal signal (from B&K 1022 oscillator). The sampling frequency for this case was 6 kHz (instead of 48 kHz for all other tests) and cosine window was used. The level of the input signal was deliberatery chosen so that its second and third harmonics can be seen but its noise floor does not exceed the noise floor of the conversion system (except for some disturbing peaks). A similar plot for 10 kHz sinewave is shown in Fig. 10.

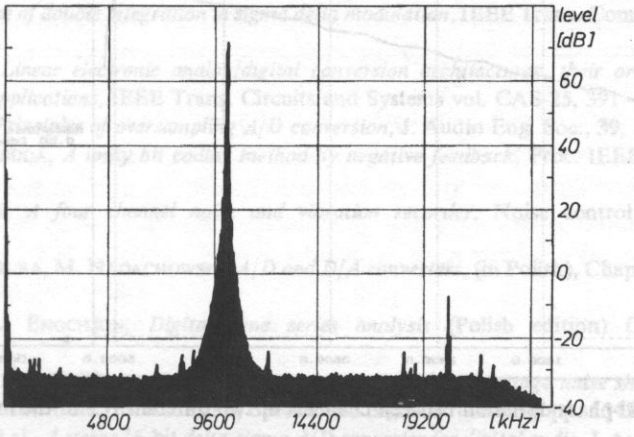

Fig. 10. Averaged spectrum of 10 kHz sinewave signal from B&K 1022 oscillator.

A very important advantage of two-channel monolithic delta-sigma converters is very high synchronicity of sampling in both channels. A figure of 0.0001 degrees was given by the manufacturer [13] as a typical interchannel phase deviation. The author did not try to verify this value, but measured the phase deviation for a longer signal path, including a buffer operational amplifier. The amplifier was a Motorola MC33078, optimised for audio signal processing, in standard inverting configuration.

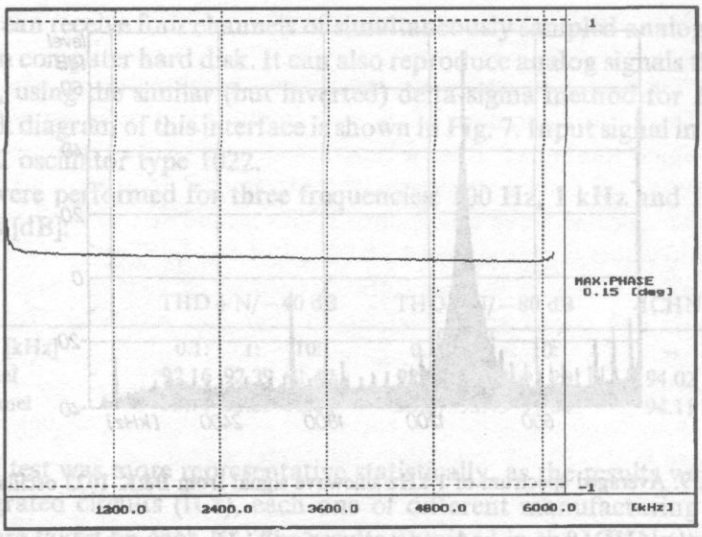

Fig. 11. Typical phase deviation between a pair of channels of the same IC.

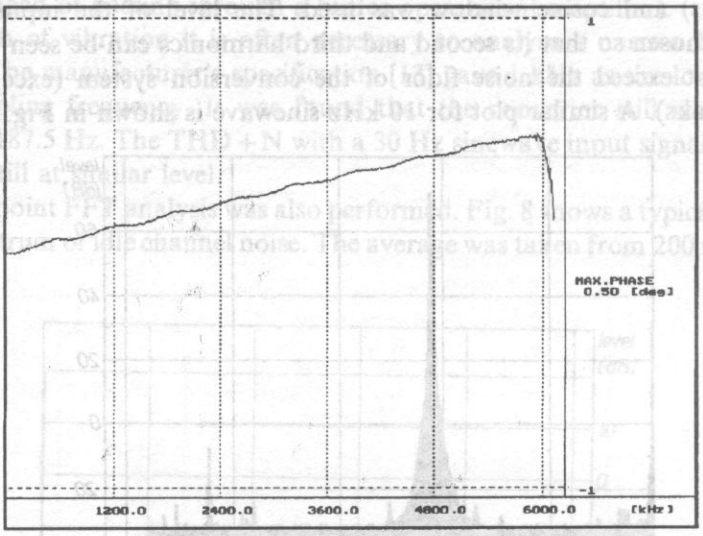

Fig. 12. Typical phase deviation between channels of two different ICs in the interface of Fig. 7.

The measurement was carried according to the method based on cross power spectral density spectrum [2, 10], with white signal on the input. The resultant plot of phase deviation versus frequency is shown in Fig. 11.

The architecture of the interface of Fig. 7 was designed in order to achieve high degree of synchronicity between channels belonging to different ICs (e.g. between channels 2 and 3 or 2 and 4). The actual degree of synchronicity could not be derived during the design stage from manufacturer's data. The results of measurement are shown in Fig. 12 and are good enough to consider all four channels as simultaneously sampling.

7. Conclusions

Oversampling method of A/D conversion, and especially its delta-sigma version is particularly suitable for applications in acoustics. High parameters needed in processing of acoustic signals are obtained at little cost with this technology. Their shortcomings are not meaningful in most applications in acoustics. The values obtained in laboratory tests confirmed manufacturer's data and in the case of low sampling frequency limit were even much better.

It seems that delta-sigma conversion technology will soon replace the traditional method and will be an element of all future acoustic measurement systems and consumer products.

This fact should be considered in research projects, design procedures of new equipment and in educational programs.

References

[1] R.W. ADAMS, P.E. FERGUSON, A. GANESAN, *Design of single-bit noise-shaping loops with higher-order loop filters*, J. Audio Eng. Soc., **38**, 871–872 (1990).

[2] J.S. BENDAT, A.G. PIERSOL, *Random data: analysis and measurement procedures*, Chapt. 1, Polish edition PWN, Warszawa 1976.

[3] B.A. BLESSER, *Digitization of audio: A comprehensive examination of theory, implementation and current practice*, J. Audio Eng. Soc., **26**, 739–771 (1978).

[4] J.C. CANDY, *A use of double integration in sigma delta modulation*, IEEE Trans. Comm., vol. **COM-33**, 249–258 (1985).

[5] B.M. GORDON, *Linear electronic analog/digital conversion architectures, their origins, parameters, limitations and applications*, IEEE Trans. Circuits and Systems vol. CAS-25, 391–418 (1978).

[6] M.W. HAUSER, *Principles of oversampling A/D conversion*, J. Audio Eng. Soc., **39**, 1/2, 3–26 (1991).

[7] H. INOSE, Y. YASUDA, *A unity bit coding method by negative feedback*, Proc. IEEE, **51**, 1524–1535 (1963).

[8] P. KLECZKOWSKI, *A four channel noise and vibration recorder*, Noise control 92 Proceedings, Kraków 1992.

[9] Z. KULKA, A. LIBURA, M. NADACHOWSKI, *A/D and D/A converters*, (in Polish), Chapt. 6 and 7, WKiŁ, Warszawa 1987.

[10] R.K. OTNES, L. ENOCHSON, *Digital time series analysis* (Polish edition) Chapt. 6, WNT, Warszawa 1978.

[11] K. UCHIMURA et. al., VLSI *A to D and D to A converters with multi-stage noise shaping modulators*, Proc. 1986 IEEE Int. Conf. on Acoustics, Speech and Signal Processing, pp. 1545–1548.

[12] D.R. WELLAND et al., *A stereo* 16-bit *delta-sigma A/D converter for digital audio*, J. Audio Eng. Soc., **37**, 476–486 (1989).

[13] *Crystal Semiconductor Corporation Data Book* vol. 1, 1990.

ARCHIVES OF ACOUSTICS
18, 2, 337–349 (1993)

NOISE REDUCTION PROBLEMS OF VIBRATORY MACHINES

J. MICHALCZYK

Institute of Mechanics and Vibroacoustics Academy of Mining and Metallurgy
(30-059 Kraków, al. Mickiewicza 30)

Several new methods of reduction of the noise produced by vibratory machines, such as conveyors, vibratory tables and sieves, shakeout grates etc. are proposed. Special attention is devoted to the problems of optimization of vibration parameters in the machines mentioned above, with restrictions imposed by the required production output and quality of the manufacturing process. The methods consisting in modification of the character of vibration of housing elements and application of low-tuned coverings in machines are outlined.

1. Introduction

Vibratory machines used in various branches of industry for compaction and moulding of precast concrete members, screening, grinding and transportation of loose materials, for knocking-out of the castings, crushing and other technological operations are often nuisant and reduction of noise emitted from such sources is often extremely difficult. Noise emitted from these sources often reaches 110 to 120 dB (for instance during compaction of ceiling members in concrete prefabrication plants or for knocking-out of the castings), which can lead to a permanent demaging of hearing ability in the case of 30 to 50% workers who have been working for a period of time longer than about five years.

Reduction of the noise emitted by those machines, achieved by means of traditional methods is especially difficult, since their operation is connected with generation of intensive mechanical vibration, whereas the passive methods of reduction of emission and propagation of acoustic waves meet serious difficulties. So, for instance, possible use of housings of various types and sound absorbing and silencing cabins is very limited, since numerous vibration processes (for instance moulding of concrete members) require incessant manipulations by the operators. A usually short duration of technological operations of an order of several minutes causes also that auxiliary times connected with opening and closing of doors and flaps lead to a major prolongation of the production cycle. Similarly, acoustic screens are also not so effective in the case of reduction of propagation of the noise emitted by machines. Because of a strong sound component, of an order or several scores of

cycles per second, their effectiveness is limited by a strong diffraction at the screen edges, by reduction of the area of the acoustic shadow and necessity of application of large-size screens. Large dimensions of production rooms and the necessary presence of operators in immediate vicinity of the machines reduce, in turn, the effectiveness of acoustic adaptation as a method of reduction of noise at the work stands. Hence, new noise reduction methods must be devised. Some of them have been presented in this paper.

2. Method of optimization of vibration parameters

Let us consider a machine as a translating rigid body vibrating with frequency ω and vibration amplitude A in the direction normal to the main exterior surface of machine body and emitting sound as a vibrating piston. A major reduction of vibration parameters is in the case impossible, because of the required production capacity. Hence, we should search for such a combination of parameters which ensure, on the one hand, the required production capacity and the desired quality of the production process and, on the other hand, reduction of the sound level. To cope with those demands we should construct two models of the phenomenon under consideration, taking into account the vibration parameters, and namely:

model of the production output and

model of the acoustic emission.

Moreover, information must be available (usually in the form of constraints imposed on the range of variability of the vibration parameters) concerning the effect of those vibration parameters on the quality of the technological process. The information will enable us to determine the curves of constant productivity in the space of vibration parameters, within the parameter variability range allowable from the point of view of quality, and then to find the point of minimum acoustic emission at those curves. Consider the example of parameter optimization of the vibratory table used for compaction of the concrete mix.

In the case under consideration it has been assumed that the vibration intensity described by the following expression

$$N_B = A^2 \omega^3 \tag{1}$$

can be assumed as a measure of productivity and, because of the required quality of the compaction process, we can usually assume that $2 < N_B < 7.5$ m^2/s^3, $0.2 < A < 1.2$ mm, $25 < \omega < 75$ c/s.

For machines with a flat body installed above the floor level, the model of vibrating piston without an acoustic baffle may be assumed, and for $k < 1$ (what is valid for medium-size machines) the noise level on the surface of the measuring sphere may be assumed as a measure of the acoustic emission:

$$L_A = 10 \lg \frac{4\rho S^3 A^2 \omega^6}{27\pi^4 c^3 I_0 S_0} - \Delta L_A(\omega) \tag{2}$$

where ρ, c — density and speed of sound in air, S — area of the vibrating surface, S_0 — area of the surface of a sphere on which we evaluate measure the sound level (S_0 for a 1 m radius has been assumed hereinafter), I_0 — reference sound intensity, $I_0 = 10^{-12}$ W/m², $\Delta L_A(\omega)$ — scale correction factor A according to IEC 123 and 179, k — wave number, a — characteristic dimension of the machine.

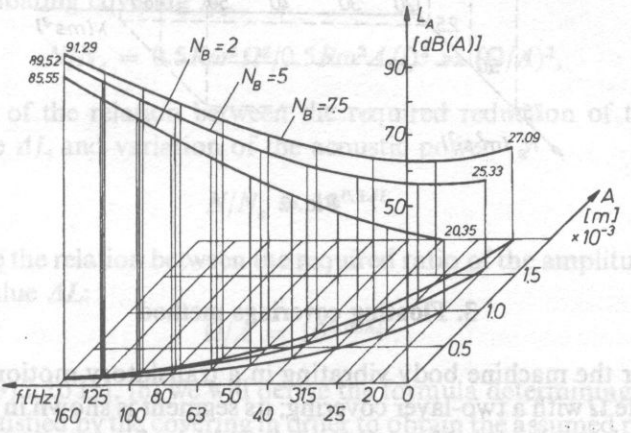

FIG. 1

Figure 1 presents curves of constant productivity in the plane of vibration parameters A, ω for $N_B = 2$, 5 and 7.5 m²/s², and the corresponding curves of the sound level. As it can be seen from these curves, in order to reduce of the sound level it is advisable to reduce the frequency of vibration to a level allowed by the quality of the compaction process and to compensate this reduction by the respective increasing of the amplitude of vibration according to relation (1).

When the procedure described above is used attention must be paid whether the translatory vibration of the machine body is really the main reason for the acoustic emission of the machine. So, for instance, in the case of compaction of concrete mix on a vibrating table which is not provided with a fixture for fastening the mould to the table, high-frequency bending vibration due to periodical pulling out of the mould from the table usually produces greater noise emission than the translatory vibration of the mould.

Model of acoustic emission will then differ from that described by the relationship (2). Taking advantage of ZABOROV estimate [4] of variation of the level of acoustic power due to the change of relative collision velocity and the interval between collisions, and relating the collision velocity to the vibration period of the machine, one may state [5] that in this case it is slightly better to reduce the amplitude and to increase the frequency; however, the results obtained do not exceed several decibels. The curve illustrating this relationship in coordinates N_B, λ (where $\lambda = A\omega^2$ is the vibration acceleration) is shown in Fig. 2.

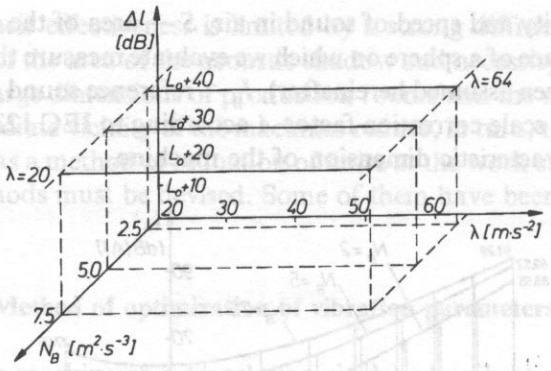

FIG. 2

3. Floating coverings method

Let us cover the machine body vibrating in a translatory motion with frequency ω and amplitude Ω with a two-layer covering; its segment is shown in Fig. 3. Layer 1 is made of a material with a low Young's modulus which, due to a considerable rigidity, will be considered to be undeformable and possess high density ρ and mass per unit

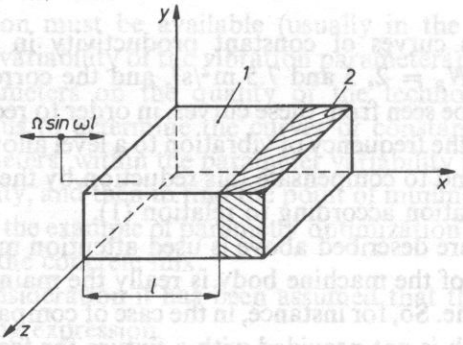

FIG. 3

area m. The equation of the motion of the system may then be written in the form [4, 5] as follows

$$\frac{\delta^2 w}{\delta t^2} = \frac{E^* \delta^2 w}{\rho \delta x^2}, \quad \text{where } E^* = (1-\nu) E/1(1-\nu-2\nu^2), \tag{3}$$

$$w(0,t) = \Omega \sin \omega t, \tag{4}$$

$$\frac{\delta w(l,t)}{\delta x} E^* = -m \frac{\delta^2 w}{dt^2}(l,t). \tag{5}$$

Hence, the amplitude of vibration of the outer layer is

$$A(l) = \Omega/[\cos(\omega\sqrt{\rho l/E^*}) - (m\omega/\sqrt{E^*\rho})\sin(\omega\sqrt{\rho l/E^*})]. \tag{6}$$

Taking into consideration the relation between the average active acoustic powers in the case of absence of the covering N and in the case when the outer surface is covered with a floating covering N_c,

$$N/N_c = 0.5R\omega^2\Omega^2/0.5R\omega^2 A(l)^2 = (\Omega/A)^2, \tag{7}$$

and making use of the relation between the required reduction of the level of the acoustic pressure ΔL and variation of the acoustic power

$$N/N_c = 10^{0.1\Delta L}, \tag{8}$$

we can determine the relation between the required ratio of the amplitude of vibration to the desired value ΔL:

$$\Omega/A = 10^{0.05\Delta L}. \tag{9}$$

Subsituting (9) into Eq. (6) we will derive the formula determining the conditions which must be satisfied by the covering in order to obtain the assumed reduction of the level of the acoustic pressure

$$|\cos(\omega\sqrt{\rho l/E^*}) - m\omega/\sqrt{\rho E^*}\sin(\omega\sqrt{\rho l/E^*})| >= 10^{0.05\Delta L}. \tag{10}$$

It should be emphasized that, in spite of the fact that on the axis ω there is an numerable series of intervals where condition (10) can be satisfied, the covering for which the first frequency of free vibration is lower and the second frequency of free vibration is higher than the excitation frequency ω, is the most feasible one.

4. Method of flexural coverings

As early as in 1959, HECKL [2] proposed the plates subjected to kinematically induced vibrations by assuming the boundary conditions in the form of the assumed harmonic vibration to support at some points only. This leads in effect to excitation of vibration being the sum of translation and bending vibration, wherein sound radiation coefficient is slightly reduced.

The author of this paper has proposed such boundary conditions of plates with kinematically induced vibrations (for instance, covering plates of vibratory machine bodies) to obtain pure bending vibration of the plate, containing notranslation component, in spite of the assumed formula of the motion of the edge. This contributes to a mutual compensation of sound radiated by the regions of the plate vibrating in counterphase and enables us to use Wallace's integer [1] for optimization of parameters of the system on the basis of the condition of minimum of the radiation coefficient.

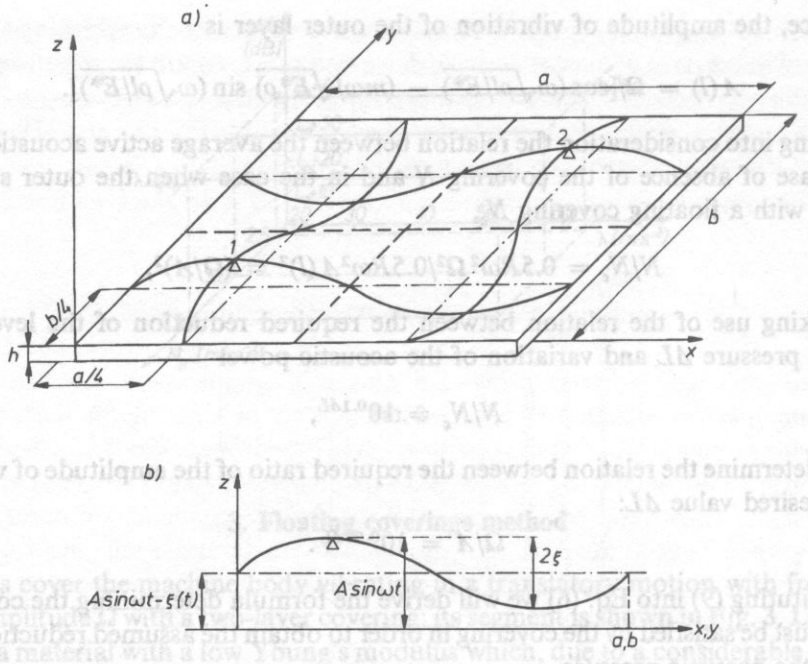

FIG. 4

In order to illustrate the proposed approach consider the case of a rectangular isotropic plate of constant thickness. We assume the boundary conditions as shown in Fig. 4. It shows a unit segment that is a "module" of the plate supported at two points situated on a diagonal and representing centers of two out of the four identical quarters into which the module can be divided. The mentioned points of support vibrate along the z-axis according to the formula

$$z_i = A \sin \omega t, \qquad i=1, 2. \tag{11}$$

Let us assume that the steady state forced motion can be presented as a sum of a translatory convection motion $z_u\ (x, y, t)$ and flexural vibrations in the form analogical to the case of free vibration of an element freely supported at the edges. The equation of vibration of the plate will then have the form

$$\frac{\delta^4 z}{\delta x^4} + 2\frac{\delta^4 z}{\delta_z^2 \delta_y^2} + \frac{\delta^4 z}{dy^4} + \frac{\rho h}{D} + \frac{\delta^2 z}{dt^2} = 0, \qquad D = Eh^3/12\,(1-\nu^2), \tag{12}$$

and in the case of a simply supported member the following formula holds:

$$z(0,y,t)=0, \quad z(x,0,t)=0, \quad z(a,y,t)=0, \quad z(x,b,t)=0$$
$$\frac{\delta^2 z}{\delta x^2}(0,y,t)=0, \quad \frac{\delta^2 z}{\delta y^2}(x,0,t)=0, \quad \frac{\delta^2 z}{\delta x^2}(a,y,t)=0, \quad \frac{\delta^2 z}{\delta y^2}(x,b,t)=0. \tag{13}$$

The form of free vibration of order 2.2 for the boundary conditions (13) has the form

$$z_g(x,y,t) = \xi \cdot \sin(2\Pi x/a) \cdot \sin(2\Pi y/b), \tag{14}$$

Let us note (see Fig. 4b) that in the case when the amplitude of vibration of points 1, 2 is equal to the amplitude of flexural vibration of the plate around a plane being in translatory motion, the resultant motion of the plate will then have the character of pure flexural vibration with respect to motionless a reference plane. In such a case the boundary conditions represent, in view of the neighbourhood of identical modules, a simply supported member (13). This confirms the validity of the formula describing the forced vibration as a sum $z(x,y,z) = z_u(t) + z_g(x,y,t)$, in conformity with Fig. 4b.

$$z(x,y,t) = A \sin \omega t + \xi(t) [\sin(2\Pi x/a) \sin(2\Pi y/b) - 1], \tag{15}$$

where $\xi = \xi(t)$ is now a generalized coordinate.

Analyse now the conditions which must be satisfied in order to ensure similarity of the form of forced vibration (15) of the plate of the form of flexural vibration of a plate with boundary conditions (13), that is to ensure the absence of a convection component in the plate motion. The equations of motion of the plate excited by vibration of the supports will be found by means of the Lagrange method.

Kinetic energy of the system is equal to

$$E = \int_0^{ba}\int_0^{ba} \frac{1}{2} \rho h v^2(x,y,t)\, dx\, dy =$$

$$= \frac{1}{2} \rho h \int_0^{ba}\int_0^{ba} \{A^2\omega^2 \cos^2\omega t + 2A\omega \cos\omega t\, \dot{\xi} [\sin(2\Pi x/a) \sin(2\Pi y/b) - 1] + \tag{16}$$

$$+ \dot{\xi}^2 [\sin(2\Pi x/a) \sin(2\Pi y/b) - 1]^2\}\, dx\, dy =$$

$$= \frac{1}{2} m \left(A^2\omega^2 \cos^2\omega t - 2A\omega\dot{\xi} \cos\omega t + \frac{5}{4} \dot{\xi}^2 \right).$$

Potential energy is expressed by the equation

$$U = \int_0^{ba}\int_0^{ba} \frac{D}{2} \left[\left(\frac{\delta^2 z}{\delta x^2}\right)^2 + \left(\frac{\delta^2 z}{\delta y^2}\right)^2 + 2\nu \frac{\delta^2 z}{\delta x^2} \cdot \frac{\delta^2 z}{\delta y^2} + 2(1-\nu) \left(\frac{\delta^2 z}{\delta x \delta y}\right) \right] dx\, dy =$$

$$= D/2 \int_0^{ba}\int_0^{ba} [\xi^2 (2\Pi/a)^4 \sin^2(2\Pi x/a) \sin^2(2\Pi y/b) + \xi^2 (2\Pi/b)^4 \sin^2(2\Pi x/a) \cdot \tag{17}$$

$$\cdot \sin^2(2\Pi y/b) + 2\nu\xi^2 (2\Pi/a)^2 (2\Pi/b)^2 \sin^2(2\Pi x/a) \sin^2(2\Pi y/b) + 2(1-\nu) \cdot$$

$$\cdot \xi^2 (2\Pi/a)^2 (2\Pi/b)^2 \sin^2(2\Pi x/a) \sin^2(2\Pi y/b)]\, dx\, dy =$$

$$= 2\Pi^4 Dab\xi^2 (1/a^2 + 1/b^2)^2.$$

Substituting this relation into Lagrange's equations

$$\frac{d}{dt}\frac{\delta(E-v)}{\delta\dot{\xi}} - \frac{\delta(E-v)}{\delta\xi} = 0, \tag{18}$$

we obtain the equation of forced vibration of the plate

$$\ddot{\xi} + \frac{16}{5}\Pi^4\frac{Dab}{m}(1/a^2+1/b^2)^2\xi = -\frac{4}{5}A\omega^2\sin\omega t \tag{19}$$

Denoting by ω_n the frequency of free undamped vibration of the system described by the equation (19)

$$\omega_n = \sqrt{\frac{Dab}{5m}[(2\Pi/a)^2+(2\Pi/b)^2]^2}, \tag{20}$$

we can write the solution of the Eq. (19) in the following form

$$\xi(t) = -\frac{4}{5}A\frac{1}{(\omega_n/\omega)^2-1}\sin\cdot\omega t = \xi_0\sin\omega t \tag{21}$$

In order to determine the vibrations of the plate, corresponding (as far as their form, not frequency, is concerned) to free vibrations of order 2.2. of a plate of dimensions *axb*, simply supported at the edges we must satisfy the condition

$$\xi_0 = A. \tag{22}$$

This leads to the condition (23) which corresponds to the free vibration frequency of order 2.2 of the plate *axb* freely supported at the edges.

$$\omega = \omega_n\sqrt{5} \tag{23}$$

Hence, by supporting each of the "modules" of the plate at two points undergoing a harmonic motion with frequency ω and amplitude A we can obtain vibration of the module in the form corresponding to the vibration of order 2.2 of plate *axb* simply supported along the stationary edge. However the dimensions (for instance thickness) and material of the plate must be properly chosen: its frequency of order 2.2 in the case of a simply supported member should be equal to that of free vibration ω of that member.

Prior to proceeding to evaluate the variation of the radiated acoustic power, which can be achieved by the selection of the boundary conditions given above, considered now the caase frequently encountered in practice of a plate, which is a housing of the machine body, fastened for instance by welding to a framework vibrating together with the machine body (see Fig. 5a). Thick dashed lines show the location of that bracing framework. Cross-section through one of the quarters is shown in Fig. 5b.

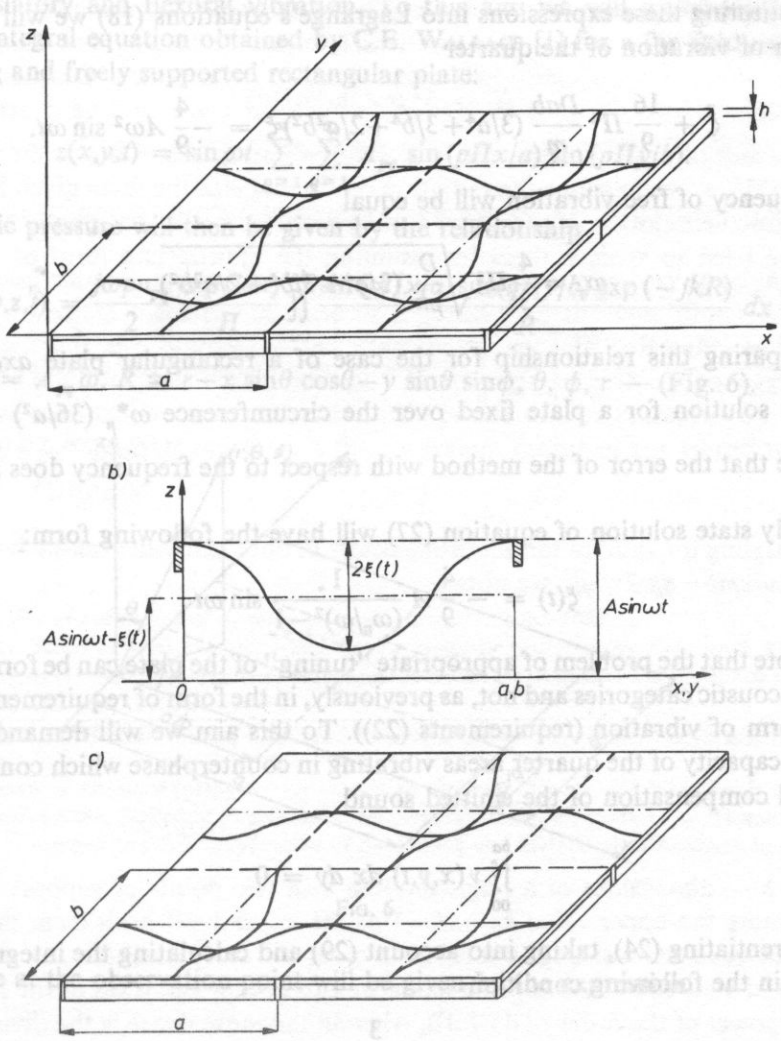

FIG. 5

For each of the quarters modules we have assumed the form of forced vibration

$$z(x,y,t) = A \sin \omega t - \xi(t) \left[\cos (2\Pi x/a) - 1\right] \left[\cos (2\Pi y/b) - 1\right]. \tag{24}$$

Calculating the kinetic and potential energy similarly as before from the relationships (16) and (17), we will obtain

$$E = \frac{1}{2} m \left[A^2\omega^2 \cos^2\omega t - 2A\omega\dot{\xi}(t) \cos \omega t + \frac{9}{4} \dot{\xi}^2(t)\right]. \tag{25}$$

$$U = 2\Pi^4 abD\xi^2(3/a^2 + 3/b^2 + 2/a^2b^2). \tag{26}$$

Substituting these expressions into Lagrange's equations (18) we will obtain the equation of vibration of the quarter

$$\ddot{\xi} + \frac{16}{9}\Pi^4 \frac{Dab}{m}(3/a^4+3/b^4+2/a^2b^2)\xi = -\frac{4}{9}A\omega^2 \sin\omega t. \tag{27}$$

Frequency of free vibration will be equal

$$\omega_n = \frac{4}{3}\Pi^2 \sqrt{\frac{D}{\rho h}(3/a^4+3/b^4+2/a^2b^2)}. \tag{28}$$

Comparing this relationship for the case of a rectangular plate axa with the accurate solution for a plate fixed over the circumference $\omega^*_n (36/a^2)\frac{D}{\rho h}$ we can conclude that the error of the method with respect to the frequency does not exceed 3.39%.

Steady state solution of equation (27) will have the following form:

$$\xi(t) = -\frac{4}{9}A\frac{1}{(\omega_n/\omega)^2-1}\sin\omega t. \tag{29}$$

Let us note that the problem of appropriate "tuning" of the plate can be formulated at once in acoustic categories and not, as previously, in the form of requirements relating to the form of vibration (requirements (22)). To this aim we will demand the same acoustic capacity of the quarter areas vibrating in counterphase which contributes to a mutual compensation of the emitted sound

$$\int_0^b \int_0^a v(x,y,t)\,dx\,dy = 0 \tag{30}$$

Differentiating (24), taking into account (29) and calculating the integral (30) we will obtain the following condition

$$\omega = \frac{3}{\sqrt{5}}\omega_n, \tag{31}$$

$$\xi(t) = A\sin\omega t \tag{32}$$

It is seen that the condition of an "acoustic" type leads similarly to the condition (22), to the requirement of equal relative amplitude vibration in steady-state ξ_0 and the vibration amplitude of edge A, which takes place for ω_n determined by the relationship (31). The value ω_n can be adjusted again to the existing requirements by assuming proper elastic and inertia properties of the plate.

Let us now proceed to estimate the emission limit which may be obtained if a plate of dimensions $naxmb$ (n, m— natural numbers, a, b — dimensions of a single module) vibrating like a piston in an acoustic baffle is replaced by a plate subject simultaneous-

ly to translatory and flexural vibration. To this aim we will use the solution of Rayleigh integral equation obtained by C.E. WALLACE [1] for a far field emitted by a vibrating and freely supported rectangular plate:

$$z(x,y,t) = \sin \omega t \sum_{p=1}^{\infty} \sum_{q=1}^{\infty} A_{pq} \sin(p\Pi x/a) \sin(p\Pi y/b). \tag{33}$$

Acoustic pressure will then be given by the relationship

$$p(x,y,z,t) = \frac{j\omega\rho v_{pq}}{2} \frac{\exp(j\omega t)}{\Pi} \int_{00}^{ab} \frac{\sin(p\Pi x/a) \sin(q\Pi y/b) \exp(-jkR)}{R} dx\, dy \tag{34}$$

where: $v_{pq} = A_{pq}\omega$, $R \cong r - x \sin\theta \cos\theta - y \sin\theta \sin\phi$, θ, ϕ, r — (Fig. 6).

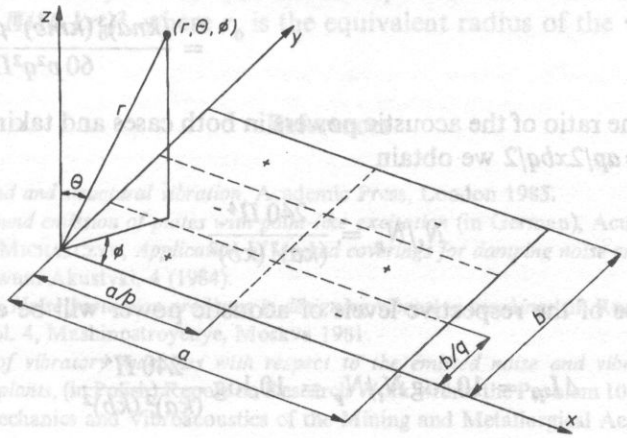

FIG. 6

Pressure at the observation point will be given by the expression

$$p(r,\theta,\phi) = jv_{pq} k\rho c \frac{\exp(-jkr)\, ab}{2\Pi^3 rpq} \left[\frac{(-1)^p \exp(-j\alpha) - 1}{(\alpha/p\Pi)^2 - 1}\right] \left[\frac{(-1)^q \exp(-j\beta) - 1}{(\beta/q\Pi)^2 - 1}\right] \tag{35}$$

$$\alpha = ka \sin\theta \cos\phi,$$

$$\beta = kb \sin\theta \sin\phi.$$

If the acoustic power is written in the form

$$N = \sigma\rho c S \langle \bar{v}^2 \rangle \tag{36}$$

where σ — radiation factor, $\langle \bar{v}^2 \rangle$ — square of normal velocity of the plate averaged over the time and area, then the acoustic power radiated by a vibrating plate, treated

as a rigid body in the case of low frequencies ($k<1$), can be calculated by substituting in the expression (36) $\langle \bar{v}^2 \rangle = v^2$, $\sigma \cong k^2 S/2\Pi$, where

$$N_t = S^2 \rho c A^2 \omega^4 / 4\Pi c^2 \tag{37}$$

In the case of a plat of the same area S but vibrating according to the expression (15) and (21), we will assume the radiation coefficient σ in the form given by Wallace for vibration being an even function of p and q (such forms give the minimum of σ and, hence, we tried to achieve them by assuming the appropriate form of the forced vibration and by a suitable choice of the boundary conditions

$$N_p \cong \frac{2(kna)^2(kmb)^3}{15p^2q^2\Pi^5} \rho c \int_0^{mb} \int_0^{na} \left[\frac{\omega}{2\Pi} \int_0^{2\Pi/\omega} A^2 \omega^2 \cos^2 \omega t \sin^2(2\Pi x/a) \sin^2(2\Pi y/b)\, dt \right] dx\, dy = \tag{38}$$

$$= \frac{(kna)^3 (kmb)^3 \rho c A^2 \omega^2 S}{60 p^2 q^2 \Pi^5}$$

Calculating the ratio of the acoustic powers in both cases and taking into account that $S = naxmb = ap/2xbq/2$ we obtain

$$N_t / N_p = \frac{240\,\Pi^4}{(ka)^2 (kb)^2} \tag{39}$$

and the difference of the respective levels of acoustic power will be equal

$$\Delta L_N = 10 \log N_t / N_p = 10 \log \frac{240\,\Pi^4}{(ka)^2 (kb)^2}. \tag{40}$$

where a, b — dimensions of a single module with two points of support.

Assuming the upper value $ka = kb = 1$ as the upper limit both from the point of view of the practical working conditions of most vibratory machines, as well as from the point of view of the assumption made we can obtain variation of the level of the acoustic power of the order of 43.7 dB, wherein the more dense is the division of the plate, the larger values of ΔL_N are obtained.

5. Conclusions

The proposed methods which principally are to be used for reduction of the sound level radiated by the surfaces of vibratory machine bodies in translatory motion do not exhaust all the possibilities of reduction of noise of such machines. There exist numerous traditional methods, which can be used simulatneously with the methods described above. The following methods should be mentioned:

— rationalization of the time of vibration for instance, in the case of the machines for compaction of concrete mix, a delayed engagement of the vibrating drive at

a moment when the mould has already been partly filled: such procedure ensures a considerable lowering of the emitted noise level,

— elimination of the sources of impact noise (for instance by fixing the moulds to the support beams in the vibrating tables, application of tension and support counterflexure of sieves in vibrating sieves, fixing of loose elements, such as washers and cotter pins,

— maintenance of proper technical condition of the equipment, particularly vibrators.

Attention should also be paid to proper housing of vibratory machines. These machines are often installed, because of ingorance of the conditions of acoustic emission so that the bottom of the machine is cut off from the environment (foundation in a socket with side sealing). The effect thus obtained is contrary to the desired one and namely the emitted acoustic power can be increased by the value $L=10 \log (27\ \Pi/16\ kr_0)^2$, where r_0 is the equivalent radius of the vibrating surface.

References

[1] F. Fahy, *Sound and structural vibration*, Academic Press, London 1985.

[2] M. Heckl, *Sound emission of plates with point-like excitation* (in German), Acustica 9, 5, (1969).

[3] A. Łopata, J. Michalczyk, *Application of layered coverings for damping noise emitted by machines* (in Polish), Archiwum Akustyki, 4 (1984).

[4] W.I. Zaborov, *Noise protection problems in designing vibratory machines* (in Russian) in: Vibration in technology, vol. 4, Mashinostroyenye, Moskva 1981.

[5] *Optimization of vibratory machines with respect to the emitted noise and vibration in the concrete prefabrication plants*, (in Polish) Report on Research Work within the Problem 10.6, Theme 05.03 of the Institute of Mechanics and Vibroacoustics of the Mining and Metallurgical Academy in Kraków.

ARCHIVES OF ACOUSTICS
18, 2, 351–357 (1993)

SHORT-TERM MEMORY FOR PITCH INVESTIGATED WITH VOCAL MATCHINGS

A. RAKOWSKI (WARSZAWA)

Chopin Academy of Music
(00-368 Okólnik 2, Warszawa)

Three musicians not possessing absolute pitch repeated vocally five standard tones played on the guitar. The repetition was completed over various periods of delay ranging from 10 seconds to 6 minutes. Periods of delay were: a) silent, b) filled with cognitive activity (counting backward in threes) or c) filled with interfering tonal stimuli (an endless, ascending chromatic scale). The frequencies of tones sung by the subjects were measured and compared to those of standard tones. Standard deviations of the sets of frequency differences were taken as measures of the inaccuracy of pitch memory trace. The obtained "forgetting curves" show that at concentrated attention subjects could retain the memory for pitch of a standard with accuracy better than a quartertone for three minutes. With cognitive interference the same was possible for two minutes, and with tonal interference for thirty seconds. Conclusions may be drawn concerning the hypothetical time constant for short-term auditory memory.

1. Introduction

Pitch is that attribute of sound sensation which enables the ordering of sounds into a scale from low to high. Distances between discrete values of pitch form the most important part of the code used in music: the set of musical intervals. Musical intervals can be taught and permanently remembered, in particular as elements constituting melodies. However this is not so with absolute values of pitch. A limited number of such discrete absolute values can be fixed in the memory of only a limited number of people: those having the so-called "absolute pitch" (RAKOWSKI and MORAWSKA-BUNGELER [7]). People not having absolute pitch cannot remember the exact values of pitch permanently and recognize only broad pitch registers (POLLACK [4]). However most people can easily and very accurately remember absolute values of pitch for short time periods, e.g. repeating vocally a given note or performing tests of frequency discrimination (RAKOWSKI [5]). A question arises whether there exists a constant time value limiting the operation of exact memory for pitch.

The notion of pitch should be specified more exactly before an answer to the above question can be given. It was found by music psychologists, in reference to music, that the sensation of pitch has two separate components: tone height and tone chroma

(REVESZ [8]). Tone chroma refers to twelve within-octave categories or localized pitch classes having the musical names C, C sharp, D, etc. Tone height refers to a non-categorized sensation which may be used for ordering sounds from very low to very high and which changes continuously. The present investigation concerns exclusively this second aspect of pitch sensation, namely tone height.

The transition between the "very exact" (at short time distance) and "very inaccurate" (at longer time delays) mode of memory for pitch has much to do with one of the most important problems within the theory of human memory. It concerns the controversy between the unitary and dualistic theories of memory. The proponents of dualistic theory, like HEBB [3] tried to find the evidence for the existance of two qualitatively different types of memory in various sensory modalities. The existence of a specific sensory mode of auditory memory, a "precategorical" one, was propounded by CROWDER and MORTON [1] and several others. DEUTSCH [2] summarised comprehensive studies on the short-term memory of categorized pitch classes. However very few investigators turned their attention towards the memory of the uncategorized form of pitch: the tone height.

Investigating short-term memory for tone height, as specified by RAKOWSKI [6], may be fruitful for two reasons. Firsty, this form of memory is not loaded with verbal descriptions. Second, the sensation is unidimensional and strength of its memory trace can be easily measured.

In the present experiment sensory memory for tone height is investigated with the use of vocal emission. Three musicians, a man and two women not possessing absolute pitch, participated as subjects.

2. Preliminary experiment

2.1. Training the Subjects

Each subject was given two-hour training in according to the following experimental design. One of the tones of the equally tempered chromatic scale within the subject's convenient vocal range was played on a guitar. The quitar was very accurately tuned and tone frequencies controlled with the automatic tuner ZEN-ON, Chromatina 331, with the accuracy of 1 cent (one hundredth part of a semitone). Subjects tried to repeat the tone as accurately as possible. The sequence was repeated until the matching was within the error of $+/-$ 2 cents. The tones were sung at a moderately low level, using any vowel that the subject wanted to chose. The training lasted 2 hours altogether and was performed within 3 or (in the case of one subject) 4 days.

2.2. Measuring Precision of Vocal Intonation

In all the subsequent parts of the experiment five standard tones were used: F♯, G, G♯, A and A♯ For the male subject these tones were taken from the third octave and

had the frequencies: 185.0; 195.9; 207.7; 220.0; and 233.1 Hz. For the female subjects the tones were taken from the fourth octave and had the frequencies: 370.0; 391.9; 415.3; 440.0; and 466.2 Hz.

Each subject's task was to listen to a tone played on the quitar, to sing a note with the same pitch and, if not correct, keep repeating until its accuracy was within +/− 2 cents of a standard. After that, responding to a signal, the subject repeated the note once again trying to make kit exactly the same. The difference in cents between frequencies of these two last tones was noted as raw data. After that, next tone chosen randomly from the set of remaining tones was played and the procedure repeated until each of the five standard tones had been worked on 12 times. The whole task was usually completed within 2 to 3 sesssions. Standard deviations were taken as measures of inaccuracy. They were computed for each tone and averaged for each subject. The results for the man and two women were: 0.07, 0.08 and 0.10 semitones.

2.3. Measuring accuracy of Long-Term Memory

At the begining of each experimental session, or as a separate measurement performed at least 15 minutes after any other singing activity, listeners were asked to sing one randomly chosen note from the set of 5 notes used in the experiment. The frequency of this note was measured. After 12 results for each note had been collected, the mean value for all standard deviations was computed and presented in Fig. 1 over the sign LTM.

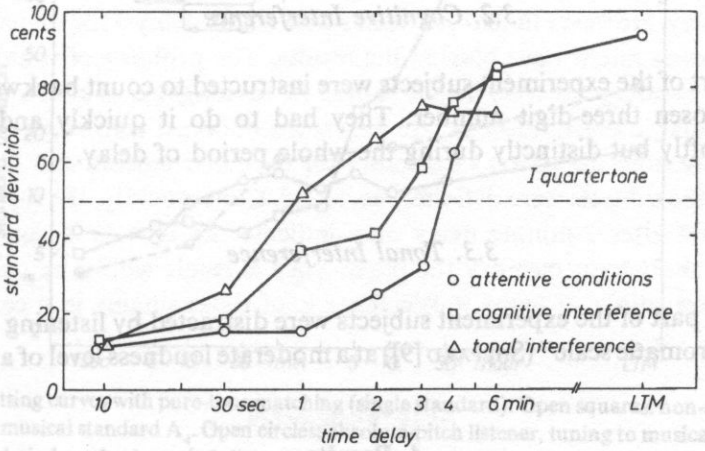

Fig. 1. Pitch forgetting curves with vocal matching. (Averaged results for tuning to five standards: F♯ G, G♯ A and A♯.

3. The main experiment

The procedure adopted in the main experiment was as follows: Subjects listened to a single note played two times on a very exactly tuned quitar and repeated the note by singing it twice under the control of an automatic tuner. The frequency of this second repetition was taken as the standard for the delayed matching. After a randomly chosen delay of 10, 30, 60 seconds and 2, 3, 4 or 6 minutes subjects repeated the standard note as exactly as possible. The frequency level difference between the standard and the matched tone was noted and the next matching started. The order of matchings was randomized within five standard pitches and seven times of delay.

For each one of the three listening conditions specified below subjects performed the same number of matchings. Two of the subjects (a man and a woman) performed 12 matchings and the third subject performed 6 matchings at every pitch and at each delay. Measurements were performed in a sound-isolated room, during individual sessions lasting no more than one hour with several short intermissions. Subjects were allowed to control timing and were warned just before the end of each delay time.

3.1. Attentive Conditions

In the first part of the main experiment subjects were instructed to concentrate their full attention on the standard pitch. However they were not allowed to hum the remembered tone and were told not to keep the larynx muscles in tension.

3.2. Cognitive Interference

In this part of the experiment subjects were instructed to count backward in threes from any chosen three-digit number. They had to do it quickly and accurately, whispering softly but distinctly during the whole period of delay.

3.3. Tonal Interference

In the last part of the experiment subjects were distracted by listening to the rising "unending chromatic scale" (SHEPARD [9]) at a moderate loudness level of about 60 dB.

4. Results

The results of the experiment are presented in Fig. 1 as "pitch forgetting curves". They show averaged values of standard deviations calculated under each experimental condition. Each measuring point represents data from 150 individual matchings.

Pitch forgetting curves show the growth of dispertion within sets of matchings performed at consecutively increasing time delays. The dispersion, represented by numerical value of the standard deviation may be taken as a measure of inaccuracy of the memory trace of a standard.

5. Discussion

There may be some doubts concerning the credibility of the method used in the present investigations. It may be argued that in spite of the instruction subjects tried to use a non-specific kind of memory (memory for muscular tension in the throat) to solve the auditory tasks. However, even if such an effect existed in some isolated cases, it must have been excluded in the conditions of cognitive interference when subjects had to whisper numbers.

The pitch forgetting curve for the attentive conditions shows a rapid increase in forgetting after a time delay of 3 minutes. This is in full agreement with the results of similar investigation with subjects who tuned the pure-tone oscillator to a standard pitch 440 Hz after varying time delays (RAKOWSKI, MORAWSKA-BUNGELER [7]). The results obtained in that experiment are shown in Fig. 2. They represent the pitch-forgetting curves produced by two subjects. One of subjects had the so-called "absolute pitch", or the ability to preserve in a long-term memory the set of standard musical pitches. The other one did not possess this ability.

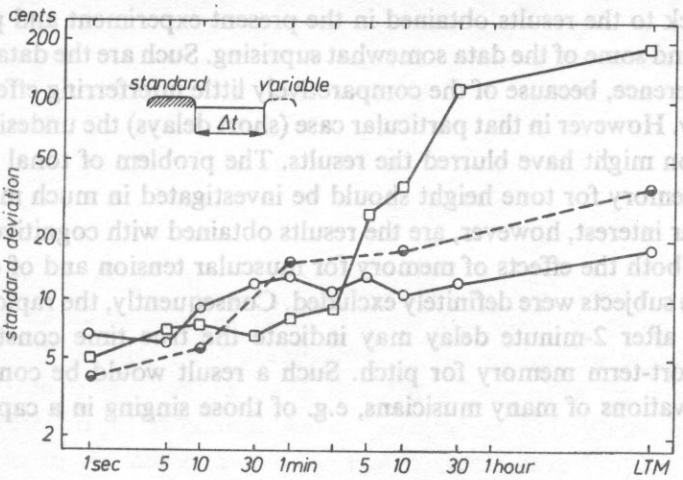

Fig. 2. Pitch forgetting curves with pure-tone matching (single standard). Open squares: non-absolute-pitch listener, tuning to musical standard A_4. Open circles: absolute-pitch listener, tuning to musical standard A_4. Semi-filled circles: absolute-pitch listener, tuning to non-musical standard A_4+66 cents.

The results of the second listener, a non-possessor of absolute pitch, are shown in Fig. 2 as open squares (standard deviations of twenty frequency settings at delayed tunings to the standard tone $A_4=440$ Hz). The conditions of performing that

experiment were very similar to the "attentive conditions" of the present investigation. The listener was placed in a sound-proof booth in silence and had to concentrate his whole attention on the pitch of the standard exposed at the beginning of each trial. No humming was allowed. After the delay time the variable-tone oscillator was heard, producing a very high or very low tone. The subject's task was to regulate its frequency to obtain equal pitch with the remembered standard. That tuning process lasted on average about three seconds.

As can be seen in Fig. 2 the results obtained by the non-absolute-pitch listener of RAKOWSKI and MORAWSKA-BUNGELER [7] are very similar to those obtained in the present investigation at attentive conditions. It seems that in both experiments the time delay of about 3 minutes marked a significant change in the salience of a preserved memory trace of a standard. The generally better accuracy of tuning obtained with the oscilator may be partly due to the fact that standard frequency there was always the same — 440 Hz.

Interesting comparisons may be made while looking at the results obtained by the absolute-pitch listener. In Fig. 2 those results are marked by circles. The open circles represent tuning to the exact musical standard 440 Hz (A_4). The semi-filled circles concern tuning to a non-musical standard 457 Hz (A_4+66 cents). At longer time delays tuning to the musical standard is superior to that performed with the non-musical standard. However at longer time delays in both cases, the performance of the absolute-pitch possessor is superior to that of the non-absolute-pitch listener.

Coming back to the results obtained in the present experiment and presented in Fig. 1 we may find some of the data somewhat suprising. Such are the data concerning the tonal interference, because of the compare tively little interferring effect up to the 30-second delay. However in that particular case (short delays) the undesired effect of muscular tension might have blurred the results. The problem of tonal interference with sensory memory for tone height should be investigated in much more detail.

Of particular interest, however, are the results obtained with cognitive interference. In this case both the effects of memory for muscular tension and of covert pitch rehearsal by the subjects were definitely excluded. Consequently, the rapid increase of forgetting rate after 2-minute delay may indicate the true time constant for the existance of short-term memory for pitch. Such a result would be consistent with everyday observations of many musicians, e.g. of those singing in a capella choirs.

Acknowledgments

This paper was sponsored by grant No 4 4160 91 02 from the State Committee for Scientific Research. Parts of the material were presented at the International Seminar on Music Acoustics, Tokyo, August 1992, and at the 39th Polish Open Seminar on Acoustics, Cracow, September 1992.

References

[1] R.G. CROWDER, J. MORTON, *Precategorical acoustic storage (PAS)*, Perception and Psychophysics, **5**, 365–373 (1969).

[2] D. DEUTSCH, *The organization of short-term memory for a single acoustic attribute*, In: D. Deutsch and J.A. Deutsch (Eds.), Short-Term Memory, Academic Press, New York–San Francisco–London 1975, pp. 107–151.

[3] D.O. HEBB, *The organisation of behaviour*, Wiley, New York (1948).

[4] I. POLLACK, *The information of elementary auditory displays*, J. Acoust. Soc. Am. **24**, 245–249 (1952).

[5] A. RAKOWSKI, *Pitch discrimination at the threshold of hearing*, Proc. 7th International Congress on Acoustics, Budapest, 20–H–6 (1971).

[6] A. RAKOWSKI, *Memory for pitch in music*, Proc. of the First International Conference on Music Perception and Cognition, Kyoto, pp. 137–140 (1989).

[7] A. RAKOWSKI, M. MORAWSKA-BUNGELER, *In search for the criteria of absolute pitch*, Archives of Acoustics, **12**, 75–87 (1987).

[8] G. REVESZ, *Zur Grundlagen der Tonspychologie*, Veit, Leipzig 1913.

[9] R.N. SHEPARD, *Circularity in judgments of relative pitch*, J. Acoust. Soc. Am. **36**, 2346–53 (1964).

ARCHIVES OF ACOUSTICS
18, 2, 359–368 (1993)

RADIATION EFFICIENCY CHARACTERISTICS ESTIMATED BY SOUND INTENSITY METHOD

S. WEYNA

Faculty of Maritime Technology
Technical University of Szczecin

Radiation efficiency factor is determined conventionally by a very complicated method and may be carried out only in laboratory condition. Using SI techniques, precise measurements can be made even under in-situ conditions, saving a lot of time in comparison to the classical method. The article presents the application of SI to measure radiation efficiency characteristics for ship cabin partitions (bulkheads, floors and ceilings). Tests carried out with SI techniques using scanning method to measure are compared with those made by conventional method. Based on the near-field acoustic intensity measurements with the fixed point method, the spatial intensity vectors in a plane close to the ship partitions. As a result of such investigation, a three-dimensional flow map of active intensity vectors, together with paths of energy streamlines, is graphically illustrated for one of the partitions.

1. Introduction

The noise is penetrating to the cabins as airborne noise and structure-borne noise. The airborne noise is radiated from the main working machines and is exciting the deck above and transmitted to the region on which possible cabins may be placed. The structure borne sound is generated in the steel structure at all solid connections as structural waves penetrating hull plate and pillars to the upper decks in the accommodation. The flexural wave motion of the deck will also cause flexural wave motion of the bulkheads, because of their strong coupling with the vibrating deck. The sound radiated, however, because of this effect contributes considerably to the several noise in the cabin, especially at low frequencies, where the commonly used bulkheads are generally stronger sound radiators than is the deck. The excited vibrational movements of the accommodation elements (result of structure borne noise cause the sound to be radiated to the enclosed cabin.

For a ship accommodation system one must determine the acoustic parameters wanted as input data for sound transmission prediction methods or for construction information during product development work as well as for ship designers. Because of the complicated ship structures and coupling involved, the determination of acoustic characteristics must be done experimentally. Acoustic investigation carried out directly on board gives rise to a number of technological and organizational problems which practically exclude a possibility of complex studies.

Therefore it is a usual practice that the vibroacoustic properties of the accommodation partitions are tested experimentally using model or mock-up system, that is as near the real ones as possible. From a number of tests it follows that the most effective are the investigations of real size cabins with complete equipment. The tests carried out on real construction make it possible to determine the effect of each partition of cabin on the noise level permeating inside. From the analysis of the phenomena occurring inside the cabin it follows that the noise results from the acoustic radiation transferred by the vibrating floor, bulheads and ceiling (structure borne noise).

The amount of airborne sound, due to structure borne sound transmission, obtained in a cabin depends on the vibrating levels of the lining surfaces, usually expressed as velocity levels, and the radiation properties of the lining, usually expressed as radiation efficiences "σ". When radiation efficiency is used, the radiated sound power from a surface with the area "S" can be expressed as

$$P = \rho_0 c_0 \sigma S \langle v^2 \rangle \quad [\mathrm{W}], \tag{1}$$

where $\langle v^2 \rangle$ — the mean square velocity over the surface and over sufficiently long time, and $\rho_0 c_0$ — characteristic impedance of the surrounding medium air.

The power can also be expressed as a function of the resulting pressure squared and the equivalent absorption area in the room, i.e.:

$$P = \frac{\langle p^2 \rangle A}{4 \rho_0 c_0} \quad [\mathrm{W}]. \tag{2}$$

According to the Eqs. (1) and (2), radiation efficiency described as level value $10 \log \sigma$ may be determined from the formula

$$10 \log \sigma = L_p - L_v + 10 \log \frac{A}{4S} \quad [\mathrm{dB}]. \tag{3}$$

The radiation factor can be calculated for rigid and homogeneous plates [2, 5], but in the present ship practice (soft and sandwich constructions of partitions) the only possibility is an experimental procedure.

It is well known from the existing theory that the radiation from a finite homogeneous, isotropic plate, excited to free bending vibrations, is partly due to contribution for resonant modes and, partly, a contribution from the forced motion of the plate areas around the excitation points or lines [3]. The measurements should therefore use an excitation method that produces a resonant bending wave field, sufficiently independent of the choice of excitation point or lines. However, when complicated constructions are used, such as the sandwich-type bulkheads or ceiling with a mineral wool core, the theoretical formulas are no longer applicable. For the ship accommodation partitions, in lack of theoretical estimates, experimental procedures have to be developed to measure the radiation efficiency according the formula (3). Until now, this measurement method has been called conventional and the details of the excitation as well as the details of attachments and edge conditions for all investigated partitions are described in [7] and [8].

Recently new measurement techniques have been developed. The sound power radiated by the structure can be done by intensity measurement, and the surface velocity may be measured with accelerometer, optical or ultrasonic transducers, or sound intensity probe. According to the Eqs. (1) the radiation ratio can be now expressed as

$$10 \log \sigma = L_I - L_v \quad [\text{dB}], \tag{4}$$

where the L_I is the sound intensity level calculated the mean value of scanning of the intensity probe just behind the investigated partition.

By using the SI method to measure the radiated sound power directly, it should also be possible to determine the amount of radiated sound power from different parts of the test partition. The scope of this research is experimental determination of the radiation for the same set of different types of bulkheads, ceiling and ship floors, using a conventional method of measurement and sound intensity technique.

2. Description of tests and results

As the conventional method of radiation efficiency measurement is commonly known [1], it will suffice to describe only the sound intensity measurement technique. One should underline, however, that the measurement conditions and excitation methods remain the same for both techniques.

The sound intensity measurements were made with NORSONIC Sound Intensity Analyzing System type RTA-830 together with "$p-v$" type intensity probe. Measuring frequency range covered the range from 63 Hz to 4000 Hz.

The first test was carried out for the total acoustic power radiated by each partition. The scanning method was used, moving the probe over the investigated surface. The scan plane being 0.1 m from the partitions, each partition was divided

into sub-areas about 1 m², scanning speed was 0.2 m/s with a distance between scanning lines of 0.1 m. The distance between the probe and the partition has been not critical, so scanning the probe at nearly constant distance is preferred to the measurements at different sub-areas. With the scanning method, the measurement time is shorter than with the conventional method.

When scanning the sample to measure the radiated energy it is important to determine the level of precision of sound intensity measure. Therefore, the measurement condition must be chosen after the introductory measurement and analysis of the *"pI"* field idicators according to description in NORDTEST [6] and ISO Recommendation described in DP-9614 [4].

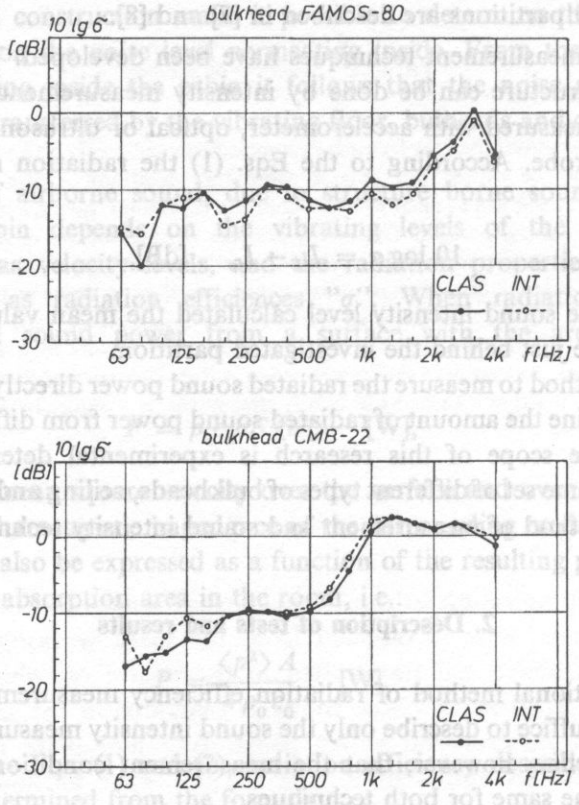

Fig. 1. Comparison of the results for the 80 mm thick, light bulkhead type FAMOS-80 and hard-core, 22 mm bulkhead type CMB-22.

Figures 1, 2 and 3 show the comparative results between both measuring techniques for six different ship accommodation partitions. It must be noticed that, except at lower frequencies, where SI gives higher values, the agreement between the results obtained by

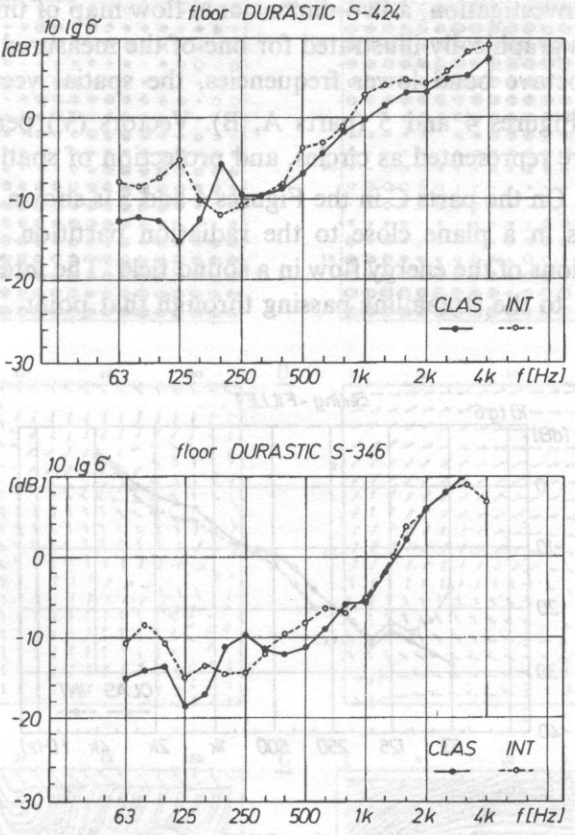

Fig. 2. Comparison of the results for the floating floor type Durastic S—424 on top of Rockwool 200/40 and S—346 on top of Rockwool 150/50.

both methods is good. The agreement is very satisfying over the frequency 250 Hz. Differences at lower frequency could be attributed to the Waterhause correction which should be made on the sound pressure measurements in the classical method.

Recognition of the vectorial nature of acoustic intensity provides very useful information in the study of phenomena of the acoustic field; in further investigation we try to explain the differences between both methods of measurements. In the second test with the intensity technique, the point measurement method was using for a more detailed analysis of the acoustic field in vicinity of the radiated structures. In the point measurements the probe is rotated to measure the intensity vector in tree directions: horizontal ($\overline{H}$) and vertical ($\overline{L}$) parallel to the partition, and normal ($\overline{V}$) to the partition. During this rotation, the acoustical and geometrical center of motion is kept in the same position. The measured grid is 22 by 18 points, with 0.1 m distance between points and 0.1 m from the partition.

As a result of investigation, a two-dimensional flow map of time-averaged active intensity vectors is graphically illustrated for one of the measured partition. For the four chosen 1/3 octave band lower frequencies, the spatial vector distribution is demonstrated in Figures 4 and 5 (parts A, B). Vectors $(\overline{V})$ perpendicular to the measured plane are represented as circles, and projection of spatial vector on plane $(\overline{H}+\overline{L})$ as arrows. On the parts C in the Figures 4 and 5 is shown the distribution of energy streamlines in a plane close to the radiation partition. These streamlines indicate the directions of the energy flow in a sound field. The intensity vector at any point is tangential to the streamline passing through that point.

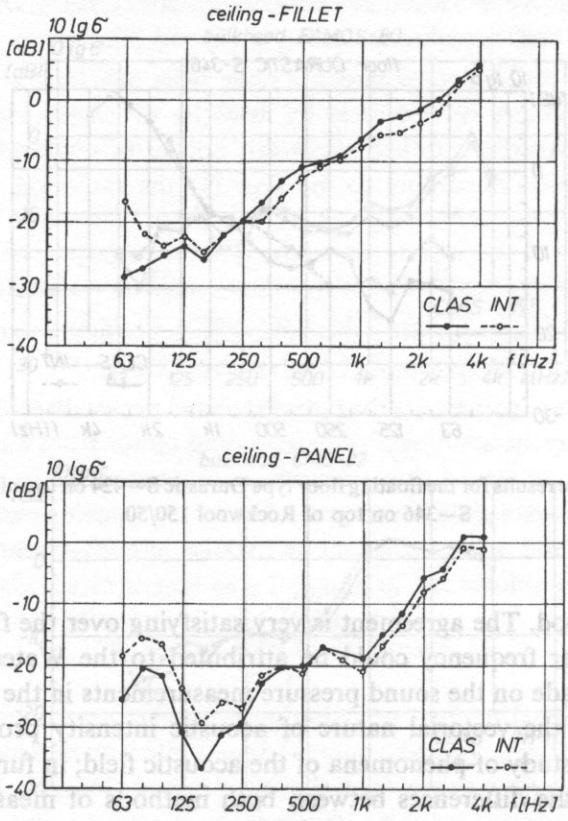

Fig. 3. Comparison of the results for the ship lightweight fillet ceiling and steel, panel ceiling.

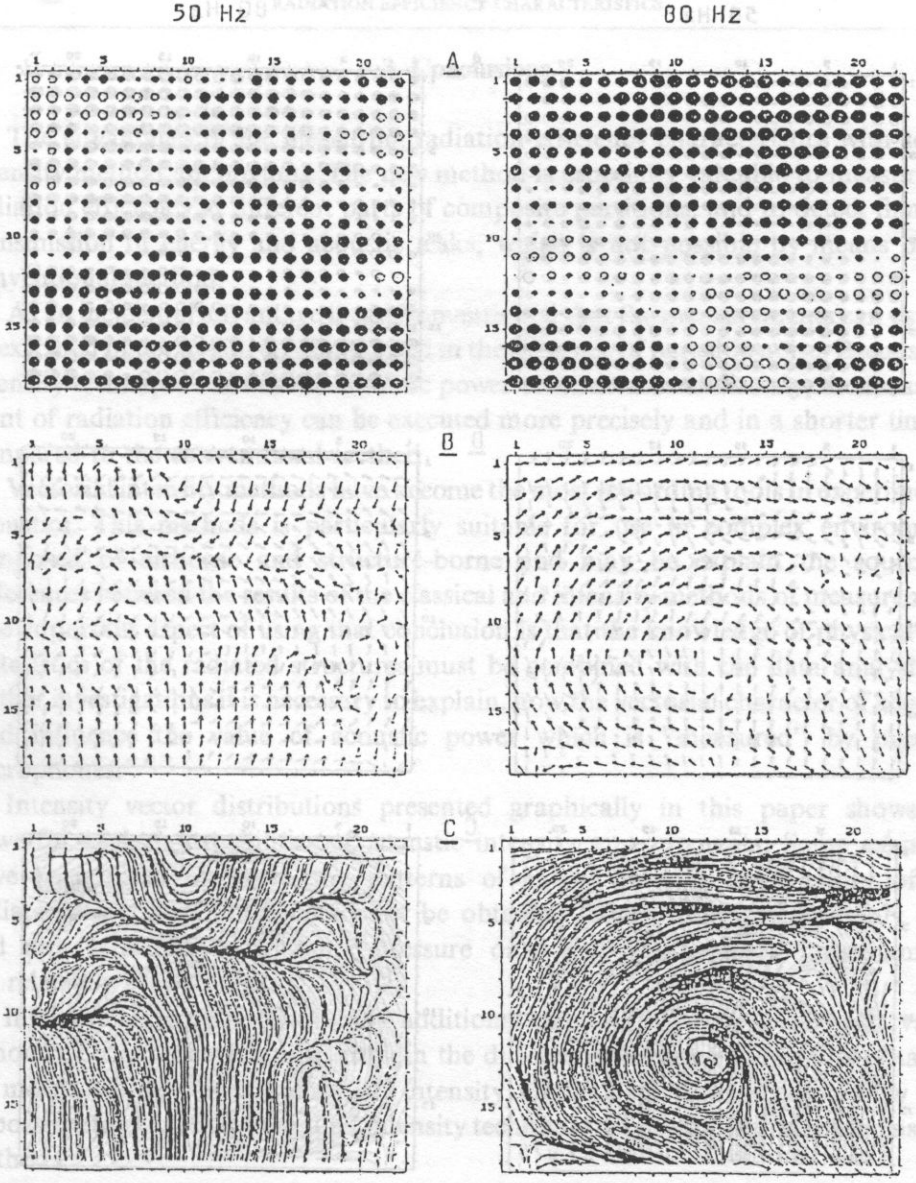

Fig. 4. Intensity vector distribution in vicinity of vibrating floor for 1/3 octave band 50 Hz and 80 Hz. A — vector V, B — vector H + L, C — energy streamlines.

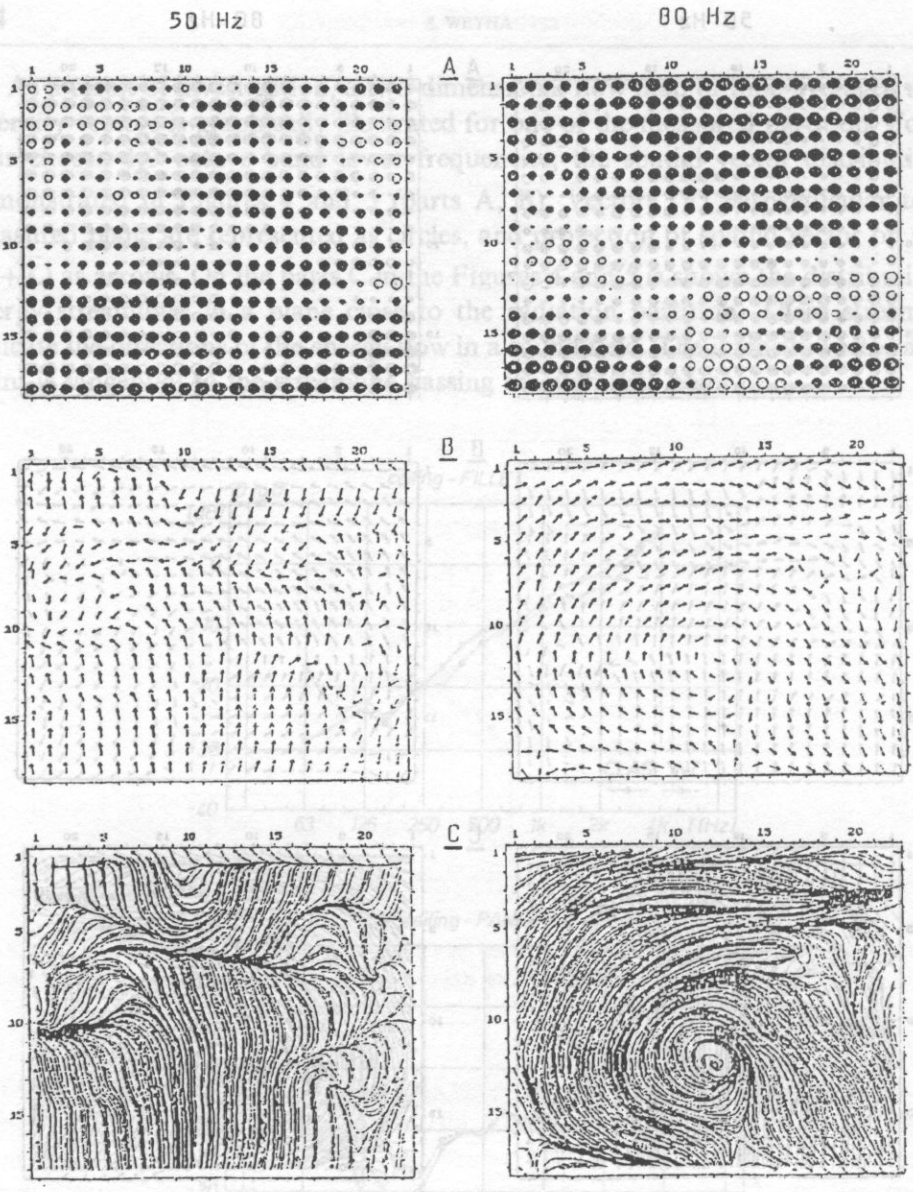

Fig. 5. Intensity vector distribution in vicinity of vibrating floor for 1/3 octave band 125 Hz and 315 Hz. A — vector V, B — vector H + L, C — energy streamlines.

3. Conclusions

The advantages of the measuring radiation efficiency characteristics with sound intensity method are obvious. The new method is especially valuable to measure the radiation efficiency at different parts of composite partitions, and to detect flanking transmission of energy and acoustic leaks, which is not possible by means of the conventional method.

As an incidental advantage it can be mentioned that the measurements can usually be executed under in-situ conditions and in the presence of parasitic noise. Because the intensity technique enables the acoustic power to be measured directly, the measurement of radiation efficiency can be executed more precisely and in a shorter time as compared to the conventional method.

Vectorial intensity methods have become the most rewarding tools in experimental acoustics. This methods is particularly suitable for use in complex environment composed of airborne and structure-borne and may be explain the source of differences between the results of the classical and intensity methods of measurement. One important aspect of using that conclusion is that the knowledge of physical characteristics of the radiated structures must be combined with the data analysis. In further investigations it is necessary to explain, how the vectorial character of acoustic field influence the value of acoustic power which is "measured" by pressure microphones.

Intensity vector distributions presented graphically in this paper shows the powerful analysis capabilities of acoustic intensity measurements. Some examples have been given of interesting patterns of energy flow in the vicinity of the radiated structures, which could not be obtained from the more commonly used and measured data concerning pressure only however pressure measurements are relatively easy to make.

Intensity measurements provide additional data which may be of great value, although further research must explain the differences between the results obtained by means of the conventional and intensity methods of measurement; now it is impossible to claim that the sound intensity technique may totally replace the classical methods.

References

[1] L. CREMER, M. HECKL, *Structure-borne sound — structural vibrations and sound radiation at audio frequencies* (Second Ed.), Springer Verlag, Berlin 1988, pp. 491–564.

[2] F. FAHY, *Sound and structural vibration — radiation, transmission and response*, Academic Press, London, New York 1985, pp. 53–111.

[3] M. HECKL, *Schallabstrahlung von Platten bei Punktformiriger Anregung*, Acustica **9**, 371–380 (1959).

[4] *ISO/DP-9614 — Determination of the sound power levels of noise sources using sound intensity measurement*, Draft Proposal, Montreal 1990.

[5] G. MAIDANIK, *Response of ribbed panels to reverberate acoustic fields*, J. Acoust. Soc. Am., **34**, pp. 809–826, (1962).

[6] *NORDTEST Pr. 558–85, The determination of radiated sound power using intensity measurement in-situ*, Trondhaim University 1985.

[7] S. WEYNA, *Vibroacoustic abatement of crew cabins*, Proc. "Theory and Practice of Shipbuildings" Pula 1986, pp. 168–177.

[8] S. WEYNA, *Measurements of acoustic power radiated by cabin partitions in-situ using SI method*, Proc. Noise-Control'88 Kraków 1988, pp. 413–416.

Notes for authors

ARCHIVES of ACOUSTICS is a quarterly journal in which original papers, both theoretical and experimental, concerning problems in acoustics its application are published.

Each paper submitted to the Editorial Office is reviewed and the decision to accept is for publication is taken by the Editorial Board. The period from submission of the paper to its publication is usually not shorter than 6 months but can be minimized if intending authors will prepare their typescripts according to the following notes:

1. The papers should be typed on one side of size A4 paper, with double spacing, a margin of 4 cm at the left side and with serial numbering of the pages. Two copies should be submitted.

2. The author's first name and surname, the name of his place of work and its location should be typed under the title of the paper.

3. The paper should be divided into numbered sections, which should be given appropriate brief subheadings.

4. Enclosed with the paper, on a separate page of typescript, there should be a summary of up to 20 lines. It should contain information about the paper's purpose, the research methods applied and about the basic results. It is a good practise not to cite any references in the summary.

5. At the end to the paper it is necessary to state on a separate sheet the cited references, numbered and in alphabetical order, according to the following sequence:

(a) Papers appearing in journals and regular publications: author's initials and surname, full title of the paper, title of the publication or its abbreviation, volume number (underlined), number of publication, first and last pages of the paper, and year of publication in brackets.

For example: [7] A.S. Śliwiński, A.E. Brown, Ultrasonic light diffraction patterns in ethylene in the critical region, Acoustica, **16**, 5, 312–323 (1965/66).

(b) Books: author's initials and surname, chapter title (in collective works), book title, editor, publisher, place of publications, year of publication, pages.

For instance: [5] W.P. Mason, Piezoelectric crystals and their application to ultrasonics, Van Nostrand, New York 1960, p. 30.

In the text of the paper's reference should be cited by enclosing the appropriate number in square brackets.

6. Formulae and designation should be inscribed manually, very legibly, using only Latin and Greek letters. Indices should be written down distinctly and with particular care. All symbols occuring in the formulae should be explained in the text at the place where they appear for the first time. The formulae should be numbered at the right-hand side of the typescript page by numbers in round brackets. Formulae which can be easily found in the literature not be derived — it is sufficient to cite appropriate reference.

7. The International System of Units (SI) should be used throughout.

8. All drawings, diagrams and photos should be referred to in the text as figures (Fig.). They should be made on separate sheets (not smaller than A5) and at the very bottom (in the case of photos overleaf) the number on separate sheets (not smaller than A5) and at the very bottom (in the case of photos overleaf) the number of the figure, the author's name and the title of paper should be written. The figure number should be inscribed in the margin of the typescript at the place where the drawing should be included. The captions of the illustrations should be listed on separate sheets. Final execution of figures in undertaken by the Editorial Office.

9. Photos should be printed on high contrast gloss paper.

10. All tables, as figures, should be made on separate sheets and numbered in succession with Arabic numbers. At the top of each table an explanatory title should be given. A list of table captions should be enclosed on a separate sheet.

Authors are entitled to 25 free reprints. Additional copies can be ordered at their own expense.

The author of a paper accepted for publication will receive one proof should be corrected and returned within five days to the Editorial Office.